

VOL. 693 NO. 2 24 FEBRUARY 1995

THIS ISSUE COMPLETES VOL. 693

JOURNAL OF

CHROMATOGRAPHY A

INCLUDING ELECTROPHORESIS AND OTHER SEPARATION METHODS

EDITORS

U.A.Th. Brinkman (Amsterdam)
R.W. Giese (Boston, MA)
J.K. Haken (Kensington, N.S.W.)
C.F. Poole (London)
L.R. Snyder (Orinda, CA)
S. Terabe (Hyogo)

EDITORS, SYMPOSIUM VOLUMES,
E. Heftmann (Orinda, CA), Z. Deyl (Prague)

EDITORIAL BOARD

D.W. Armstrong (Rolla, MO)
W.A. Aue (Halifax)
P. Boček (Brno)
P.W. Carr (Minneapolis, MN)
J. Crommen (Liège)
V.A. Davankov (Moscow)
G.J. de Jong (Weesp)
Z. Deyl (Prague)
S. Dilli (Kensington, N.S.W.)
Z. El Rassi (Stillwater, OK)
H. Engelhardt (Saarbrücken)
M.B. Evans (Hatfield)
S. Fanali (Rome)
G.A. Guiochon (Knoxville, TN)
P.R. Haddad (Hobart, Tasmania)
I.M. Hais (Hradec Králové)
W.S. Hancock (Palo Alto, CA)
S. Hjertén (Uppsala)
S. Honda (Higashi-Osaka)
Cs. Horváth (New Haven, CT)
J.F.K. Huber (Vienna)
J. Janák (Brno)
P. Jandera (Pardubice)
B.L. Karger (Boston, MA)
J.J. Kirkland (Newport, DE)
E. sz. Kováts (Lausanne)
C.S. Lee (Ames, IA)
K. Macek (Prague)
A.J.P. Martin (Cambridge)
E.D. Morgan (Keele)
H. Poppe (Amsterdam)
P.G. Righetti (Milan)
P. Schoenmakers (Amsterdam)
R. Schwarzenbach (Dübendorf)
R.E. Shoup (West Lafayette, IN)
R.P. Singhal (Wichita, KS)
A.M. Siouffi (Marseille)
D.J. Strydom (Boston, MA)
T. Takagi (Osaka)
N. Tanaka (Kyoto)
K.K. Unger (Mainz)
P. van Zoonen (Bilthoven)
R. Verpoorte (Leiden)
Gy. Vigh (College Station, TX)
J.T. Watson (East Lansing, MI)
B.D. Westerlund (Uppsala)

EDITORS, BIBLIOGRAPHY SECTION

Z. Deyl (Prague), J. Janák (Brno), V. Schwarz (Prague)

ELSEVIER

JOURNAL OF CHROMATOGRAPHY A

INCLUDING ELECTROPHORESIS AND OTHER SEPARATION METHODS

Scope. The *Journal of Chromatography A* publishes papers on all aspects of **chromatography, electrophoresis** and related methods. Contributions consist mainly of research papers dealing with chromatographic theory, instrumental developments and their applications. In the *Symposium volumes*, which are under separate editorship, proceedings of symposia on chromatography, electrophoresis and related methods are published. *Journal of Chromatography B: Biomedical Applications*—This journal, which is under separate editorship, deals with the following aspects: developments in and applications of chromatographic and electrophoretic techniques related to clinical diagnosis or alterations during medical treatment; screening and profiling of body fluids or tissues related to the analysis of active substances and to metabolic disorders; drug level monitoring and pharmacokinetic studies; clinical toxicology; forensic medicine; veterinary medicine; occupational medicine; results from basic medical research with direct consequences in clinical practice.

Submission of Papers. The preferred medium of submission is on disk with accompanying manuscript (see *Electronic manuscripts* in the Instructions to Authors, which can be obtained from the publisher, Elsevier Science B.V., P.O. Box 330, 1000 AH Amsterdam, Netherlands). Manuscripts (in English; *four* copies are required) should be submitted to: Editorial Office of *Journal of Chromatography A*, P.O. Box 681, 1000 AR Amsterdam, Netherlands, Telefax (+31-20) 485 2304, or to: The Editor of *Journal of Chromatography B: Biomedical Applications*, P.O. Box 681, 1000 AR Amsterdam, Netherlands. Review articles are invited or proposed in writing to the Editors who welcome suggestions for subjects. An outline of the proposed review should first be forwarded to the Editors for preliminary discussion prior to preparation. Submission of an article is understood to imply that the article is original and unpublished and is not being considered for publication elsewhere. For copyright regulations, see below.

Publication information. *Journal of Chromatography A* (ISSN 0021-9673): for 1995 Vols. 683–714 are scheduled for publication. *Journal of Chromatography B: Biomedical Applications* (ISSN 0378-4347): for 1995 Vols. 663–674 are scheduled for publication. Subscription prices for *Journal of Chromatography A*, *Journal of Chromatography B: Biomedical Applications* or a combined subscription are available upon request from the publisher. Subscriptions are accepted on a prepaid basis only and are entered on a calendar year basis. Issues are sent by surface mail except to the following countries where air delivery via SAL is ensured: Argentina, Australia, Brazil, Canada, China, Hong Kong, India, Israel, Japan, Malaysia, Mexico, New Zealand, Pakistan, Singapore, South Africa, South Korea, Taiwan, Thailand, USA. For all other countries airmail rates are available upon request. Claims for missing issues must be made within six months of our publication (mailing) date. Please address all your requests regarding orders and subscription queries to: Elsevier Science B.V., Journal Department, P.O. Box 211, 1000 AE Amsterdam, Netherlands. Tel.: (+31-20) 485 3642; Fax: (+31-20) 485 3598. Customers in the USA and Canada wishing information on this and other Elsevier journals, please contact Journal Information Center, Elsevier Science Inc., 655 Avenue of the Americas, New York, NY 10010, USA, Tel. (+1-212) 633 3750, Telefax (+1-212) 633 3764.

Abstracts/Contents Lists published in Analytical Abstracts, Biochemical Abstracts, Biological Abstracts, Chemical Abstracts, Chemical Titles, Chromatography Abstracts, Current Awareness in Biological Sciences (CABS), Current Contents/Life Sciences, Current Contents/Physical, Chemical & Earth Sciences, Deep-Sea Research/Part B: Oceanographic Literature Review, Excerpta Medica, Index Medicus, Mass Spectrometry Bulletin, PASCAL-CNRS, Referativnyi Zhurnal, Research Alert and Science Citation Index.

US Mailing Notice. *Journal of Chromatography A* (ISSN 0021-9673) is published weekly (total 52 issues) by Elsevier Science B.V., (Sara Burgerhartstraat 25, P.O. Box 211, 1000 AE Amsterdam, Netherlands). Annual subscription price in the USA US\$ 5389.00 (US\$ price valid in North, Central and South America only) including air speed delivery. Second class postage paid at Jamaica, NY 11431. **USA POSTMASTERS:** Send address changes to *Journal of Chromatography A*, Publications Expediting, Inc., 200 Meacham Avenue, Elmont, NY 11003. Airfreight and mailing in the USA by Publications Expediting.

See inside back cover for Publication Schedule, Information for Authors and information on Advertisements.

© 1995 ELSEVIER SCIENCE B.V. All rights reserved.

0021-9673/95/\$09.50

No part of this publication may be reproduced, stored in a retrieval system or transmitted in any form or by any means, electronic, mechanical, photocopying, recording or otherwise, without the prior written permission of the publisher, Elsevier Science B.V., Copyright and Permissions Department, P.O. Box 521, 1000 AM Amsterdam, Netherlands.

Upon acceptance of an article by the journal, the author(s) will be asked to transfer copyright of the article to the publisher. The transfer will ensure the widest possible dissemination of information.

Special regulations for readers in the USA—This journal has been registered with the Copyright Clearance Center, Inc. Consent is given for copying of articles for personal or internal use, or for the personal use of specific clients. This consent is given on the condition that the copier pays through the Center the per-copy fee stated in the code on the first page of each article for copying beyond that permitted by Sections 107 or 108 of the US Copyright Law. The appropriate fee should be forwarded with a copy of the first page of the article to the Copyright Clearance Center, Inc., 222 Rosewood Drive, Danvers, MA 01923, USA. If no code appears in an article, the author has not given broad consent to copy and permission to copy must be obtained directly from the author. The fee indicated on the first page of an article in this issue will apply retroactively to all articles published in the journal, regardless of the year of publication. This consent does not extend to other kinds of copying, such as for general distribution, resale, advertising and promotion purposes, or for creating new collective works. Special written permission must be obtained from the publisher for such copying.

No responsibility is assumed by the Publisher for any injury and/or damage to persons or property as a matter of products liability, negligence or otherwise, or from any use or operation of any methods, products, instructions or ideas contained in the materials herein. Because of rapid advances in the medical sciences, the Publisher recommends that independent verification of diagnosis and drug dosages should be made.

Although all advertising material is expected to conform to ethical (medical) standards, inclusion in this publication does not constitute a guarantee or endorsement of the quality or value of such product or of the claims made of it by its manufacturer.

⊙ The paper used in this publication meets the requirements of ANSI/NISO Z39.48-1992 (Permanence of Paper).

Printed in the Netherlands

CONTENTS

(Abstracts/Contents Lists published in Analytical Abstracts, Biochemical Abstracts, Biological Abstracts, Chemical Abstracts, Chemical Titles, Chromatography Abstracts, Current Awareness in Biological Sciences (CABS), Current Contents/Life Sciences, Current Contents/Physical, Chemical & Earth Sciences, Deep-Sea Research/Part B: Oceanographic Literature Review, Excerpta Medica, Index Medicus, Mass Spectrometry Bulletin, PASCAL-CNRS, Referativnyi Zhurnal, Research Alert and Science Citation Index)

REGULAR PAPERS

Column Liquid Chromatography

- Investigation of displacer equilibrium properties and mobile phase operating conditions in ion-exchange displacement chromatography
by C.A. Brooks and S.M. Cramer (Troy, NY, USA) (Received 19 September 1994) 187
- Adsorptive interaction of Ficoll standards with porous glass size-exclusion chromatography columns
by G. Shah and P.L. Dubin (Indianapolis, IN, USA) (Received 11 October 1994) 197
- Slow change in the electrical potential at glass and silica surfaces due to Na⁺ sorption in the hydrated layer
by D.M. Vermeulen and F.F. Cantwell (Edmonton, Canada) (Received 17 October 1994) 205
- A simple method for the determination of capacity factor on solid-phase extraction cartridges. I
by A. Gelencsér, G. Kiss, Z. Krivácsy, Z. Varga-Puchony and J. Hlavay (Veszprém, Hungary) (Received 9 November 1994) 217
- The role of capacity factor in method development for solid-phase extraction of phenolic compounds. II
by A. Gelencsér, G. Kiss, Z. Krivácsy, Z. Varga-Puchony and J. Hlavay (Veszprém, Hungary) (Received 9 November 1994) 227
- Silver ion high-performance liquid chromatography of esters of isomeric octadecenoic fatty acids with short-chain monounsaturated alcohols
by B. Nikolova-Damyanova and W.W. Christie (Dundee, UK) and B. Herslöf (Stockholm, Sweden) (Received 1 December 1994) 235
- Simple and highly sensitive high-performance liquid chromatographic method for separating enantiomeric diacylglycerols by direct derivatization with a fluorescent chiral agent, (*S*)-(+)-2-*tert*-butyl-2-methyl-1,3-benzodioxole-4-carboxylic acid
by J.-H. Kim, Y. Nishida, H. Ohruji and H. Meguro (Sendai, Japan) (Received 11 October 1994) 241
- Ionic strength dependence of protein retention on Superose 12 in SEC-IEC mixed mode chromatography
by C.-h. Cai, V.A. Romano and P.L. Dubin (Indianapolis, IN, USA) (Received 21 October 1994) 251
- High-performance liquid chromatography with chemiluminescence detection of derivatized microcystins
by H. Murata, H. Shoji, M. Oshikata, K.-I. Harada, M. Suzuki and F. Kondo, (Nagoya, Japan) and H. Goto (Tokyo, Japan) (Received 1 November 1994) 263
- Separation of geometrical retinol isomers in food samples by using narrow-bore high-performance liquid chromatography
by E. Brinkmann, L. Dehne, H.B. Oei, R. Tiebach and W. Baltes (Berlin, Germany) (Received 26 October 1994) 271
- HPLC separation and determination of naphtho[2,3-*b*]furan-4,9-diones and related compounds in extracts of *Tabebuia avellanedae* (Bignoniaceae)
by J. Steinert, H. Khalaf and M. Rimpler (Hannover, Germany) (Received 17 October 1994) 281
- HPLC of basic drugs and quaternary ammonium compounds on microparticulate strong cation-exchange materials using methanolic or aqueous methanol eluents containing an ionic modifier
by K. Croes, P.T. McCarthy and R.J. Flanagan (London, UK) (Received 11 November 1994) 289
- Cation-exchange high-performance liquid chromatographic assay of piperazine in some pharmaceutical formulations
by H.S.I. Tan, J. Xu and Y. Zheng (Cincinnati, OH, USA) (Received 24 October 1994) 307
- Gas Chromatography*
- Elimination of adsorption effects of polarity parameters determined by inverse gas chromatography
by A. Voelkel and J. Janas (Poznań, Poland) (Received 18 October 1994) 315
- Polycyclic aromatic sulfur heterocycles. IV. Determination of polycyclic aromatic compounds in a shale oil with the atomic emission detector
by J.T. Andersson and B. Schmid (Ulm, Germany) (Received 7 November 1994) 325

(Continued overleaf)

Contents (continued)

- Solid-phase extraction on C₁₈ in the trace determination of selected polychlorinated biphenyls in milk
by Y. Picó, M.J. Redondo, G. Font and J. Mañes (València, Spain) (Received 10 October 1994) 339

Electrophoresis

- Calculation of the composition of sample zones in capillary zone electrophoresis. I. Mathematical model
by J.L. Beckers (Eindhoven, Netherlands) (Received 25 October 1994) 347
- Influence of buffer electrolyte pH on the migration behavior of phenolic compounds in co-electroosmotic capillary
electrophoresis
by S.M. Masselter and A.J. Zemann (Innsbruck, Austria) (Received 26 October 1994) 359

SHORT COMMUNICATIONS

Column Liquid Chromatography

- Chiral metal complexes. XLII Reversed-phase high-performance liquid chromatographic separation of racemic dipeptides as
their ternary Co(III) complexes with a chiral triamine
by J.R. Aldrich-Wright (Campbelltown, Australia), P.D. Newman (Cardiff, UK), K.R.N. Rao (Hengoed, UK) and
R.S. Vagg and P.A. Williams (Kingswood, Australia) (Received 16 November 1994) 366
- Determination of Methocel A15-LV cellulose ether in blends with microcrystalline cellulose
by S.S. Cutié and C.G. Smith (Midland, MI, USA) (Received 21 September 1994) 371

Gas Chromatography

- Quantitative analysis by gas chromatography of volatile carbonyl compounds in cigarette smoke
by T. Miyake and T. Shibamoto (Davis, CA, USA) (Received 28 November 1994) 376

Electrophoresis

- Capillary electrophoresis of plant starches as the iodine complexes
by J.D. Brewster and M.L. Fishman (Philadelphia, PA, USA) (Received 15 November 1994) 382

- AUTHOR INDEX 388

Investigation of displacer equilibrium properties and mobile phase operating conditions in ion-exchange displacement chromatography

Clayton A. Brooks¹, Steven M. Cramer*

Howard P. Isermann Department of Chemical Engineering, Rensselaer Polytechnic Institute, Troy, NY 12180-3590, USA

First received 18 April 1994; revised manuscript received 19 September 1994

Abstract

One of the major advantages of displacement chromatography is the simultaneous concentration and purification that can be effected during the process. The steric mass-action model of non-linear ion-exchange chromatography is employed to investigate the affects of mobile phase salt concentration and displacer equilibrium properties on the concentration of proteins in isotachic displacement zones. The results indicate that the salt microenvironment in displacement zones plays a major role in determining the concentration of the displaced proteins. The parameters which affect the salt microenvironment are both the initial salt concentration in the carrier as well as the induced gradient produced during the displacement process. For a given breakthrough volume, the induced gradient is determined by the ratio of the steric factor to the characteristic charge of the displacer. These results indicate that the use of relatively low salt concentrations in the carrier along with displacers with relatively high steric factor to characteristic charge ratios will produce significant concentration of the proteins during the purification process.

1. Introduction

Ion-exchange displacement chromatography provides an attractive method for overcoming the deleterious effects of peak tailing encountered in conventional overloaded and gradient elution chromatography of proteins. Separations performed in the displacement mode offer the ability to both concentrate and purify solutes in a single chromatographic operation. In addition, under appropriate conditions displacement chro-

matography can offer an improvement in the selectivity achieved under conventional elution modes of chromatography. While these advantages are clearly well suited for the purification of biopharmaceuticals, the displacement mode of chromatography is seldom considered as a viable option in the pharmaceutical and biotechnology industries. A major reason for this inertia is the lack of understanding of simple cause and effect relationships between the choice of various displacers and chromatographic operating conditions and the outcome of displacement separations.

Operationally, displacement chromatography is performed in a manner similar to elution chromatography where the column is subjected

* Corresponding author.

¹ Present address: Purification Development Department, Immunex Manufacturing Corporation, Seattle, WA 98101, USA.

to sequential step changes in the inlet conditions. In ion-exchange displacement chromatography the column is initially equilibrated with a carrier solution at constant pH and ionic strength. The feed mixture is then introduced onto the column and immediately followed by a solution containing the displacer. The displacer is chosen such that its affinity for the stationary phase is greater than any of the components in the feed. Under appropriate conditions the displacer forces the desorption of the feed components which develop into adjacent “square wave” zones of homogeneous material. If the column is long enough the system will reach an isotachic state moving at the velocity of the displacer; the least strongly adsorbed feed component appearing first in the displacement train.

Experimentally, ion-exchange displacement chromatography has been employed for the purification of proteins by a number of researchers [1–8]. To date, the development of these separations has relied on trial and error experimental procedures and common rules of thumb. In general, when a displacement separation is not fully developed (i.e., the displacement train is not comprised of homogeneous “square wave” zones), a more completely developed separation can be effected by: increasing the length of column, decreasing the amount of feed, or modifying the mobile phase operating conditions to an environment where the feed components are more strongly retained (i.e., lower salt conditions).

These rules of thumbs, however, address the attainment of the fully development isotachic displacement train. The steric mass-action (SMA) model of non-linear ion-exchange chromatography [9] is able to accurately predict induced salt gradients and complex behavior in protein displacement systems [6–8]. Equilibrium in the model is characterized by three independent parameters for each solute: the characteristic charge, the equilibrium constant and the steric factor. In order to design effective displacers for protein purification, it is critical to understand what displacer properties are required to give sufficient affinity and to minimize induced salt gradients. An analytical solution developed

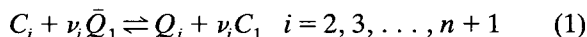
for ideal ion-exchange displacement chromatography [9] provides a simple and rapid method for addressing this question. In this paper we examine how properties of the displacer as well as the prevailing mobile phase salt conditions effect the final isotachic displacement profile.

2. Theoretical background

2.1. SMA ion-exchange equilibrium

The analytical solution to ideal ion-exchange displacement chromatography based on the SMA ion-exchange equilibrium formalism has been reported elsewhere [9]. An abbreviated form of the ideal SMA displacement model is presented here.

Consider an ion-exchange resin with a total capacity, Λ , equilibrated with a carrier solution containing salt counterions. Upon adsorption, the protein interacts with ν_i stationary phase sites, displacing an equal number of monovalent salt counterions. The adsorption of the protein also results in the steric hindrance of σ_i salt counterions. These *sterically* hindered salt counterions are *unavailable* for exchange with the protein in free solution. For a system of n polyelectrolytes and a single mobile phase modifying salt, n expressions can be written to represent the stoichiometric exchange of each individual protein with the salt.



where C and Q are the mobile and stationary phase concentrations, and the subscripts i and 1 refer to the protein and salt, respectively. The overbar, $\bar{}$, denotes bound salt counterions *available* for exchange with the protein. The equilibrium constants, K_{1i} , for the ion-exchange process is defined as:

$$K_{1i} \equiv \left(\frac{Q_i}{C_i} \right) \cdot \left(\frac{C_1}{Q_1} \right)^{\nu_i} \quad i = 2, 3, \dots, n + 1 \quad (2)$$

Electroneutrality on the stationary phase requires:

$$\Lambda \equiv \bar{Q}_1 + \sum_{i=2}^{n+1} (\nu_i + \sigma_i) Q_i \quad (3)$$

For a single protein, substituting Eq. 3 into Eq. 2 and rearranging yields the following implicit isotherm.

$$Q_i = K_i C_i \cdot \left(\frac{\Lambda - (\nu_i + \sigma_i) Q_i}{C_1} \right)^{\nu_i} \quad (4)$$

The equilibrium stationary phase concentration of the protein, Q_i , is implicitly defined in terms of its mobile phase concentration and the concentration of the salt. Thus, once the SMA equilibrium parameters of the protein are determined [10], the isotherm of the protein can be constructed at any mobile phase salt condition. In addition, Eqs. 2 and 3 provide $n + 1$ equations which implicitly define the multicomponent equilibrium for n proteins and a single salt counterion.

In ion-exchange displacement chromatography, adsorption of the displacer produces an induced salt gradient which travels ahead of the displacer. This increase in salt concentration is *seen* by the feed components traveling in front of the displacer and results in a depression of the feed component isotherms. Thus, the traditional Tiselian treatment of displacement, using a displacer operating line and single component isotherms, first requires the determination of the local salt microenvironment *seen* by each of the

feed components since the initial carrier salt conditions do not apply to the feed components. A schematic of an SMA ion-exchange displacement separation of a binary ($n = 2$) feed mixture under ideal isotachic conditions is depicted in Fig. 1 [9].

The breakthrough volume of the displacer is given by:

$$V_{Bd} = V_f + V_0(1 + \beta\Delta) \quad (5)$$

where the slope of the displacer operating line, $\Delta = Q_d/C_d$, is calculated using the displacer's single-component SMA isotherm.

$$\Delta = \frac{Q_d}{C_d} = K_{1d} \cdot \left(\frac{\nu - (\nu_d + \sigma_d) Q_d}{(C_1)_d} \right)^{\nu_d} \quad (6)$$

and $(C_1)_d$ is the concentration of salt the displacer *sees* (i.e., the carrier salt concentration, C_1^0).

The local concentration of salt in the isotachic zone of pure feed component i , under the induced salt gradient conditions is given by:

$$(C_1)_i = \frac{\Lambda - (C_1^0 + \nu_d C_{fd}) \cdot \frac{\Delta}{\Omega}}{\frac{1}{\lambda} - \frac{\Delta}{\Omega}} \quad (7)$$

and the concentration of feed component i in the zone is given by:

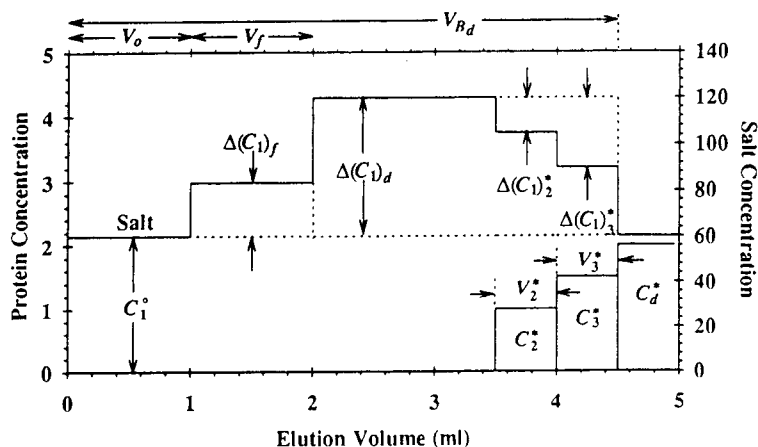


Fig. 1. Ideal SMA ion-exchange displacement separation of a binary feed mixture. From Ref. [9].

Table 1
SMA parameters for proteins and displacers

Protein/ displacer	Characteristic charge (ν)	Steric factor (σ)	σ/ν	Equilibrium constant (K)
α -Chymotryp-sinogen A	4.8	49.2	10.3	$9.2 \cdot 10^{-3}$
Cytochrome <i>c</i>	6.0	53.6	8.9	$1.1 \cdot 10^{-2}$
Lysozyme	5.3	34.0	6.4	$1.8 \cdot 10^{-1}$
Protamine	17.5	11	0.6	$1.0 \cdot 10^9$
M_r 10 000 DEAE-dextran	21	32	1.5	$6.3 \cdot 10^{-3}$
M_r 40 000 DEAE-dextran	64	130	2.0	$5.5 \cdot 10^{44}$

Chromatographic conditions: SCX column (bed capacity, $\Lambda = 561$ mM), sodium phosphate buffer, pH 6.0.

$$C_i \equiv \frac{\Lambda - (C_1^0 + \nu_d C_{fd}) \cdot \frac{1}{\lambda}}{-\nu_i \left(\frac{1}{\lambda} - \frac{\Delta}{\Omega} \right)} \quad (8)$$

where the parameters Ω and Λ are defined as:

$$\Omega = \left(\frac{\nu_i}{\nu_i + \sigma_i} \right) \quad \lambda = \sqrt[3]{\frac{K_{fi}}{\Delta}} \quad (9)$$

The parameters Ω and λ characterize the non-linear and linear adsorption behavior of the proteins, respectively. The volume (i.e., width) of the isotachic displacement zone, V_i , is determined from a mass balance to be

$$V_i = V_f \cdot \left(\frac{C_{fi}}{C_i} \right) \quad (10)$$

The parameter λ also characterizes the “dynamic affinity” of the proteins under these displacement conditions [11]. Thus, the order of the feed components in the isotachic displacement train is given by

$$\lambda_i < \lambda_j < \dots < \lambda_n \quad (11)$$

where component i is the first component in the displacement train and component n is the last (note: the order of the feed components in all displacement simulations presented in this manuscript is α -chymotrypsinogen A, cytochrome *c* and lysozyme).

Thus, once the slope of the displacer operating

line is determined (Eq. 6), the breakthrough volume can be calculated from Eq. 5. The local salt *microenvironment* for each feed component can then be calculated from Eq. 7. The concentrations and widths of the isotachic zones are determined using Eqs. 8 and 10, respectively. Finally, the order of the feed components are determined from Eq. 11.

3. Results and discussion

The technique described above for calculating isotachic displacement profiles is employed to study the effects of mobile phase salt concentration and displacer equilibrium properties on the concentration of proteins and induced salt gradients in the displacement zones.

3.1. Effect of mobile phase salt concentration

The operating variable which provides the greatest flexibility in the development of ion-exchange displacement separations is the prevailing mobile phase salt concentration. Typically displacement separations are performed with mobile phase salt concentrations in the range of 25 to 150 mM. Within this range, the concentrations and widths of the fully developed displacement zones can vary considerably. In order to examine the effect of this operating variable, displacement separations were simulated for the

separation of a three-component feed mixture (containing the proteins α -chymotrypsinogen A, cytochrome *c* and lysozyme) employing mobile phase salt concentrations of 25, 50 and 75 mM. In each of the simulations depicted in Fig. 2, the feed consisted of 1.0 ml of the three feed components at a concentration of 0.75 mM each. The simulations correspond to a column with a void volume of 1.0 ml (i.e., $V_0 = 1.0$ ml). The displacer equilibrium parameters were: $K = 6.31 \cdot 10^{-3}$, $\nu = 21$ and $\sigma = 32$. In addition, in order to compare the various separations, the breakthrough volume of the displacer was fixed

at 5.5 ml. As seen in the figure, the separation performed at 25 mM resulted in the highest concentrations of feed components (note: the order of proteins in all isotachic displacement profiles in this paper was α -chymotrypsinogen A, cytochrome *c* and lysozyme). A major advantage of displacement chromatography is the ability to *concentrate* the feed components while also achieving their separation. Clearly, as seen in the figure, the lower the concentration of salt in the carrier the greater the isotachic concentrations of the feed components.

The separations depicted in Fig. 2 all have the

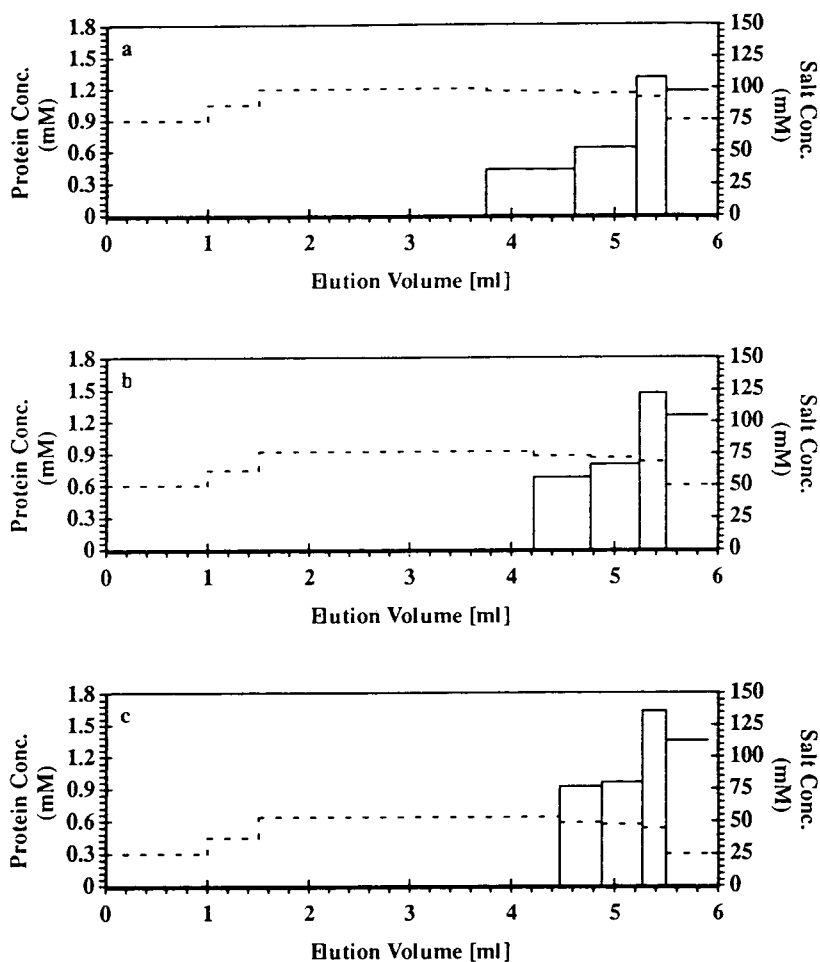


Fig. 2. Effect of mobile phase salt concentration on displacement separations; (a) 75 mM; (b) 50 mM; (c) 25 mM. Displacer: *M*, 10 000 DEAE-dextran; feed: α -chymotrypsinogen A, cytochrome *c* and lysozyme, 0.5 ml of 1.0 mM each (equilibrium parameters presented in Table 1).

same throughput since the feed amount and separation time are the same. In comparing the separations at 75 and 25 mM, however, it is clear that the 75 mM separation has further approached the maximum feed loading of the column as compared to the 25 mM separation. Thus, the feed mass could be significantly increased in the 25 mM separation; whereas increasing the feed loading at 75 mM would probably result in non-development. In terms of separation performance, this increased feed loading at the lower salt concentration corresponds to greater overall throughput. In general, performing displacement separations at lower mobile phase salt concentrations yields greater throughputs and more concentrated products, each of these a major objective in displacement separations. One caveat with respect to this point is that, as the salt microenvironment of the protein bands decrease in magnitude, the kinetics of desorption may adversely affect the separation. It has been observed that the displacement boundaries can become less sharp at extremely low salt concentrations. Furthermore, at very low salt concentrations the elevated protein concentrations may result in precipitation of the purified product. In general, the carrier salt concentration should be decreased until kinetics or precipitation become a problem.

3.2. Effect of displacer equilibrium parameters

Of fundamental importance in displacement chromatography is the design and/or selection of the displacer. It is critical to establish rules of thumb about the effects of displacer SMA parameters on their performance as protein displacers. As defined by Eq. 11, the dynamic affinity of solutes in displacement systems is defined by the magnitude of affinity parameter λ . Thus, the ability of a compound to act as a displacer for a given feed mixture is dictated by this affinity parameter which defines the constraints on the displacer's characteristic charge and equilibrium constant. In this section we will examine the effect of these parameters on the final isotachic displacement profiles. Assuming that the affinity parameter of the displacer is greater than that of any of the feed components,

we then have the freedom to employ or design displacers with various combinations of characteristic charge, equilibrium constant and steric factor.

The effect of the displacer's characteristic charge on the final isotachic displacement profile is depicted in Fig. 3. The feed consists of three proteins in 1.0 ml mobile phase at a concentration of 1.0 mM each; the displacer concentration is chosen such that the breakthrough volume is constant at 5.5 ml. The initial mobile phase salt concentration remains constant at 50 mM and the displacer's equilibrium constant and steric factor are $6.31 \cdot 10^{-3}$ and 32, respectively. As seen in the figure, increasing the displacer's characteristic charge results in wider, less concentrated displacement zones. In addition, a higher induced salt gradient results from an increased characteristic charge. In fact, it is the elevated salt concentration in the displaced protein zones, produced by the induced salt gradient, which is responsible for the wider less concentrated zones. Thus, as long as the affinity constraint is satisfied, it may be advantageous to employ a displacer with minimal characteristic charge. This will result in more concentrated displacement zones, higher throughputs, and may also facilitate column regeneration.

The effect of the displacer's steric factor on the final isotachic displacement profile is presented in Fig. 4. The conditions are the same as those in Fig. 3 except that the displacer's steric factor is now allowed to vary from 16 to 64. The equilibrium constant and characteristic charge are constant at $6.31 \cdot 10^{-3}$ and 21, respectively. As seen in the figure, increasing the displacer's steric factor results in narrower, more concentrated displacement zones. Again, the reason for this is the increased induced salt gradient. This is not surprising since an increase in the displacer's steric factor corresponds to a decrease in the overall number of interactions with the stationary phase under non-linear adsorption conditions (thus, less induced salt gradient).

Figs. 3 and 4 indicate that the induced salt gradient can be minimized by increasing the displacer's steric factor and decreasing its characteristic charge. Thus, increasing the ratio of the displacer's steric factor to characteristic charge

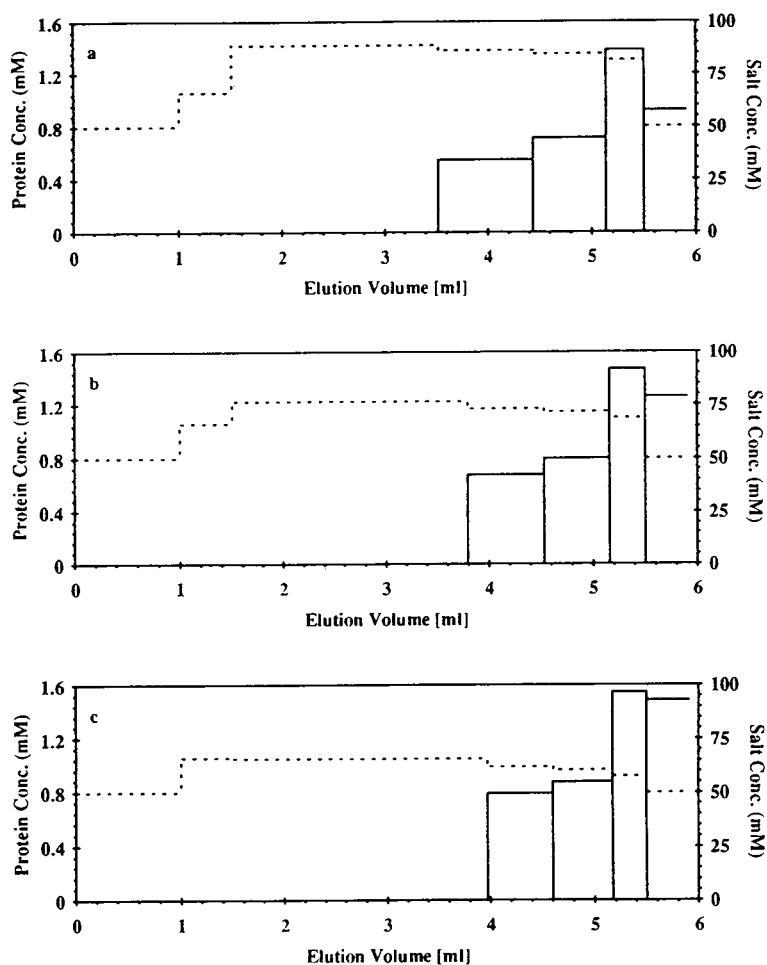


Fig. 3. Effect of displacer characteristic charge on displacement separations; (a) $\nu = 42$; (b) $\nu = 21$; (c) $\nu = 10.5$. Displacer $\sigma = 32$ and $K = 6.31 \cdot 10^{-3}$. (Feed as in Fig. 2).

should increase the performance of the displacement separation. In fact, this ratio has important implications for displacer design. Consider the displacers protamine, M_r 10 000 DEAE-dextran and M_r 40 000 DEAE-dextran; the σ/ν ratios for these cation-exchange displacers are 0.63, 1.52 and 2.03, respectively [6,10]. Thus, from these σ/ν ratios, we would expect the largest induced salt gradient from protamine and the least induced salt gradient from M_r 40 000 DEAE-dextran. Fig. 5 depicts displacement separations employing the σ/ν ratios of these displacers. The feed conditions as well as the displacer breakthrough volumes are the same as in the previous

examples. As seen in the figure, the induced salt gradient caused by the protamine front is greater than that of the DEAE-dextran displacers. As already established, this increased induced salt gradient results in broader, less concentrated displacement zones.

In addition to the effect on the final displacement zones, a relatively small value for the σ/ν ratio also restricts the practical operating range of salt in which to perform the displacement separation. The significant induced salt gradient caused by protamine results in a smaller effective window of working salt concentrations in which displacement actually occurs. In fact, operation

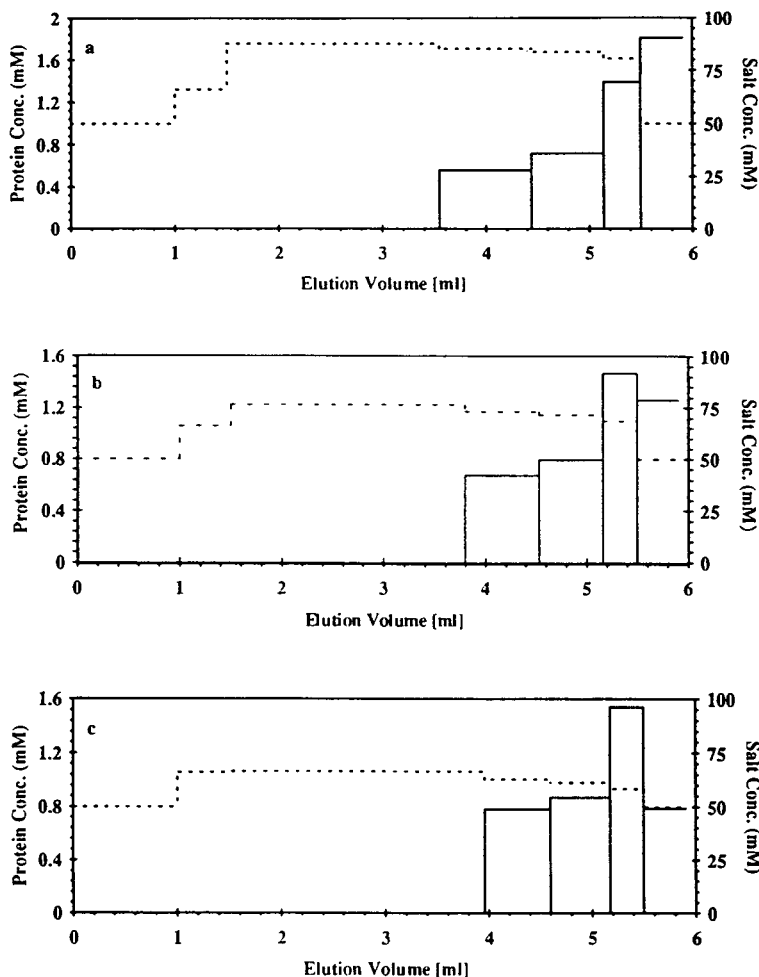


Fig. 4. Effect of displacer steric factor on displacement separations; (a) $\sigma = 16$; (b) $\sigma = 32$; (c) $\sigma = 64$. Displacer $\nu = 21$ and $K = 6.31 \cdot 10^{-3}$. (Feed as in Fig. 2).

outside of this window substantially depresses the feed component isotherms and can result in the elution of the least retained feed component ahead of the displacement train [6].

4. Conclusions

A significant factor affecting the final isotachic displacement profile is the local salt microenvironment *seen* by the feed components. Clearly,

in order to achieve the most concentrated displacement zones, the concentration of salt in the zones must be minimized (allowing for less depression of the feed component isotherms). From the above examples, two effects predominate: the initial carrier salt conditions and the additional induced salt gradient. Thus, it is advantageous to minimize the initial concentration of salt and to choose the displacer which results in the least induced salt gradient (i.e., the highest σ/ν ratio).

It is also important to realize that two displac-

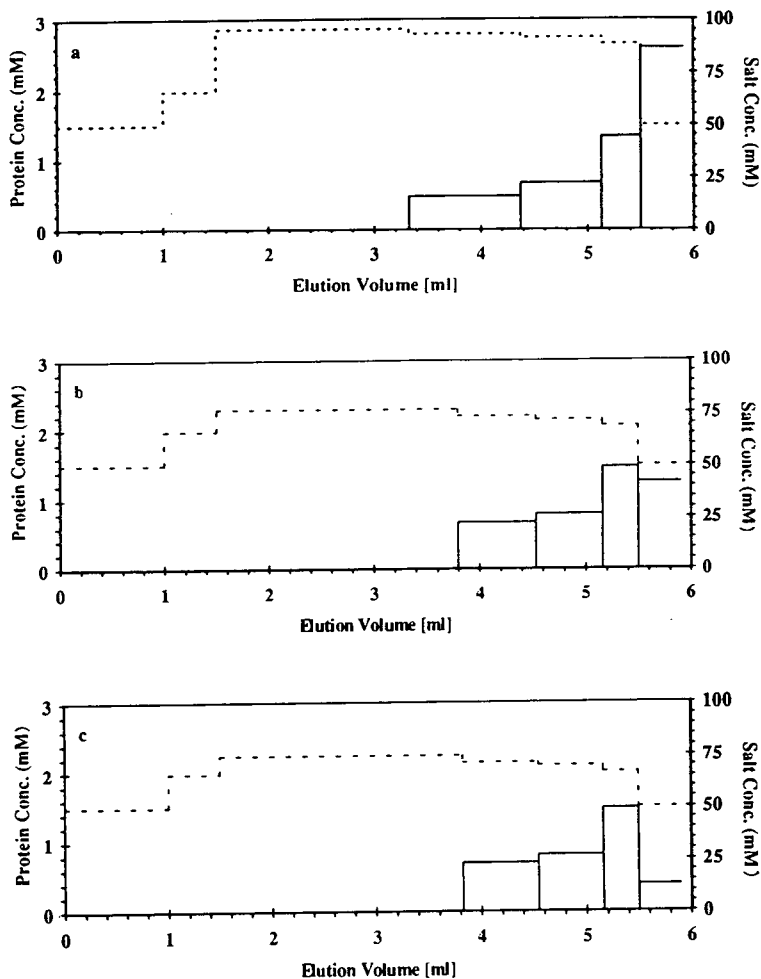


Fig. 5. Effect of displacer steric factor to characteristic charge ratio on displacement separations. (a) Protamine sulfate, $\sigma/\nu = 0.63$; (b) M_r 10 000 DEAE-dextran, $\sigma/\nu = 1.52$; (c) M_r 40 000 DEAE-dextran, $\sigma/\nu = 2.03$. Equilibrium parameters as defined in Table 1. (Feed as in Fig. 2).

ers with significantly different characteristic charges can effect the same induced salt gradient if the σ/ν ratios and the breakthrough volumes are identical. Thus, a highly charged high affinity polymer does not necessarily act as a better displacer than a low-molecular-mass displacer, providing it has sufficient affinity [12]. A detailed analysis of the effect of displacer properties on the transient behavior of ion-exchange displacement chromatography is currently being carried out using both rigorous computer simulations

and experiments and will be the subject of a future report.

Symbols

C	mobile phase concentration, mM
$\Delta(C_1)$	change in salt concentration due to a front, mM
K	equilibrium constant, dimensionless

Q stationary phase concentration (per volume SP), mM
 V volume, ml

ν characteristic change, dimensionless
 σ steric factor, dimensionless
 Ω adsorption parameter (Eq. 9), dimensionless

Subscripts and Superscripts

– sterically non-hindered
 * unit selectivity
 0 initial (*i.e.*, carrier)
 0 unretained solute
 1 salt
 a solute a
 B breakthrough
 d displacer
 f feed
 i solute i
 n solute n

Greek letters

β column phase ratio, $(1 - \epsilon_t)/\epsilon_t$, dimensionless
 Δ slope of displacer operating line, dimensionless
 ϵ_t total porosity (*i.e.*, inter- and inter-particle), dimensionless
 λ isotachic affinity parameter (Eq. 9), dimensionless
 Λ stationary phase capacity (monovalent salt counterions), mM

References

- [1] E.A. Peterson, *Anal. Biochem.*, 90 (1978) 767.
- [2] E.A. Peterson and A.R. Torres, *Anal. Biochem.*, 130 (1983) 271.
- [3] A.W. Liao, Z. El Rassi, D.M. LeMaster and Cs. Horváth, *Chromatographia*, 24 (1987) 881.
- [4] G. Subramanian and S.M. Cramer, *Biotechnol. Prog.*, 5 (1989) 92.
- [5] S.C.D. Jen and N.G. Pinto, *J. Chromatogr. Sci.*, 29 (1991) 478.
- [6] J.A. Gerstner and S.M. Cramer, *Biotechnol. Prog.*, 8 (1992) 540.
- [7] J.A. Gerstner and S.M. Cramer, *BioPharm.*, 5 (1992) 42.
- [8] G. Jayaraman, S.D. Gadham and S.M. Cramer, *J. Chromatogr.*, 630 (1993) 53.
- [9] C.A. Brooks and S.M. Cramer, *AIChE J.*, 38 (1992) 1969.
- [10] S.D. Gadham, G. Jayaraman and S.M. Cramer, *J. Chromatogr.*, 630 (1993) 37.
- [11] C.A. Brooks and S.M. Cramer, *Chem. Eng. Sci.*, (1994) in press.
- [12] G. Jayaraman, Y.F. Li, J.A. Moore and S. M. Cramer, *J. Chromatogr. A*, in press.

Adsorptive interaction of Ficoll standards with porous glass size-exclusion chromatography columns

Gita Shah, Paul L. Dubin*

Department of Chemistry, Indiana University–Purdue University, Indianapolis, IN 46202-3274, USA

First received 8 July 1994; revised manuscript received 11 October 1994; accepted 26 October 1994

Abstract

Ficoll, a densely branched non-ionic polysaccharide, whose hydrodynamic properties resemble those expected for compact spheres, is an interesting material for fundamental studies of permeation in chromatographic and porous media. Calibrating porous glass size-exclusion chromatography columns with Ficoll, we found unexpected retention of this solute in salt solution, but normal behavior in nearly pure water (0.003 M, pH 7.0 sodium phosphate buffer). These chromatographic results, along with the findings of adsorption studies and viscometric measurements, can be best explained on the basis of sodium ion binding to Ficoll and consequent adsorption of the transient pseudo-polycation thus formed.

1. Introduction

A wide variety of packing materials are currently available for aqueous size-exclusion chromatography (SEC), and many of them provide satisfactory attributes in the four categories of mechanical properties, pore size range, chromatographic efficiency, and low affinity for adsorbing solutes such as proteins [1–4]. Porous glass, initially developed by Haller [5] and commercialized first by Corning (hence the term “CPG”), and then by Electronucleonics and recently also Schott, performs well in the first two categories but not in the third and fourth. Consequently, its practical use is restricted. Nevertheless, the facts that its pore structure can be well defined by porosimetry and microscopy

and that the composition is very well known (in contrast to other commercial packings) make it quite well suited for fundamental studies [6–11]. In such investigations, it is commonplace to employ neutral polysaccharide as model polymers; their elution on this and on all other SEC packings are always observed or assumed to be “ideal”, i.e. controlled by steric repulsion alone, and no other form of interaction [12]. While the principal polysaccharides so employed have been dextrans, and subsequently pullulan [13], an additional solute of interest is Ficoll [14–16], a densely branched polysaccharide that more nearly approximates a compact sphere [17]. Because of its well-defined geometry, Ficoll has been extensively used in studies of permeation of both synthetic membranes and biological media [18–22]. Our investigation of Ficoll on CPG disclosed unexpected adsorption behavior in the presence

* Corresponding author.

Table 1
Characteristics of pullulan standards

Sample	M^a	$\overline{M}_w/\overline{M}_n^a$	$[\eta]$ (cm ³ /g) ^b	R_η (Å) ^c	$[\eta]$ (cm ³ /g) ^d	R_η (Å) ^e
P-800	853 000	1.14	187.0	294	171	285
P-200	186 000	1.13	70.4	128	55	118
P-100	100 000	1.10	45.9	90	39.8	86
P-50	48 000	1.09	28.6	60	23.4	56
P-20	23 700	1.07	18.1	41	15.5	39
P-10	12 200	1.06	11.9	28	9.7	27
P-5	5 800	1.07	7.9	19	6.3	18

\overline{M}_w = Weight-average molecular mass; \overline{M}_n = number-average molecular mass.

^a Supplied by the manufacturer.

^b In water, at 25°C (supplied by the manufacturer).

^c From columns 2 and 4, via Eq. 1.

^d From Ref. [24], in 0.2 M sodium phosphate buffer (pH 7.0) at 25°C.

^e From columns 2 and 6, via Eq. 1.

of added electrolyte, which is the subject of this communication.

2. Experimental

2.1. Materials

Pullulan standards (Shodex Standard P-82) with polydispersity of about 1.1 were obtained from Shodex (New York, NY, USA). Ficoll fractions were obtained from Dr. K. Granath of Kabi Pharmacia (Uppsala, Sweden), and were characterized at Uppsala by a combination of

light scattering and SEC on Sepharose 4B (fractions 9, 12, 15 and 20) and Sephadex G-200 Superfine (fractions 2 and 11). The characteristics for pullulan and Ficoll are described in Tables 1 and 2, respectively. Reagents were ACS grade. The water used throughout was deionized water from a Millipore system.

2.2. Methods

Viscometry

Intrinsic viscosities were measured with a Schott Geräte AVS-400 equipped with a 2-ml capacity capillary viscometer (capillary

Table 2
Characteristics of Ficoll fractions

Fraction	M_r^a	$[\eta]$ (cm ³ /g) ^b	R_η (Å) ^c	$[\eta]$ (cm ³ /g) ^d	R_η (Å) ^e
T1800, fraction 9	714 000	20.0	131	23.9	139
T1800, fraction 12	461 000	17.5	109	20.8	115
T1800, fraction 15	321 000	16.2	94	17.5	96
T1800, fraction 20	132 000	12.6	64	13.4	65
T2580-IVB, fraction 2	71 800	9.9	48	10.9	50
T2580-IVB, fraction 11	21 800	7.0	29	7.8	30

^a From supplier.

^b In water at 25°C.

^c From columns 2 and 3, via Eq. 1.

^d In 0.2 M sodium phosphate buffer (pH 4.5) at 25°C.

^e From columns 2 and 5, via Eq. 1.

constant = 0.008352) at $25.0 \pm 0.02^\circ\text{C}$. Ficoll was dissolved in water or ionic strength 0.2 M, pH 4.5 sodium phosphate buffer, at concentrations ranging from 10 to 24 mg/ml, and filtered through 0.45- μm Gelman filters. The average efflux times for solvents were in the range of 100–120 s with a precision of ± 0.02 s. The intrinsic viscosity $[\eta]$ was obtained from the intercept of the plot of the reduced specific viscosity, $\eta_{\text{sp}}/\text{concentration}$, vs. concentration (cm^3/g), and the viscosity radius R_η (cm) from the following equation [23]

$$R_\eta = \left[\frac{3[\eta]M_r}{10\pi N_A} \right]^{1/3} \quad (1)$$

where M_r is the molecular mass of the polymer and N_A is Avogadro's number.

Separate measurements for intrinsic viscosity were carried out with a Schott Geräte AVS-300 equipped with a dilution viscometer (capillary constant ca. 0.01) at 25.0°C for pullulan-1600 K (Shodex P-82) and Ficoll fraction 9 in different solvents. The average solvent efflux times were in the range of 90–98 s and the Hagenbach kinetic correction was applied to all measured efflux times as recommended by the manufacturer of the capillary viscometer.

Chromatography

A stainless-steel column (50 cm \times 5.5 mm I.D.) was dry packed with Bioran-CPG, pore diameter 330 \AA , 30–60 μm grain size, and 86 m^2/g surface area, from Schott Geräte (Mainz, Germany). The number of theoretical plates, 800, was obtained by injecting 10% $^2\text{H}_2\text{O}$ in water as a mobile phase. The chromatography system consisted of a Mini Pump from Milton Roy (St. Petersburg, FL, USA). A 75- μl injecting loop from Valco (Houston, TX, USA), differential refractometer R401 from Waters (Milford, MA, USA), and Omniscrite Recorder from Houston Instruments (Austin, TX, USA).

Mobile phases were prepared to the required ionic strength and pH from (1) NaH_2PO_4 and Na_2HPO_4 , (2) CH_3COOH and CH_3COONa and (3) H_3PO_4 and Li_3PO_4 , and filtered through a 0.45- μm filter. All chromatograms were ob-

tained by injecting 3 to 5 mg/ml of polymer solution at a flow-rate of 0.8 to 0.9 ml/min. Flow-rate and chart speed were measured periodically by weighing the column eluent, and by measuring the chart paper for about 20 to 25 min. respectively. Total volume (V_t) and void volume (V_0) were obtained by injecting $^2\text{H}_2\text{O}$ and pullulan-800K, respectively.

Adsorption experiments

TLC standard-grade silica gel with an average particle size 2–25 μm , pore diameter 60 \AA , and surface area ca. 500 m^2/g was from Aldrich. Small-particle-size silica was removed by settling in water and discarding the supernatant. The remaining silica was dried at 80°C overnight. A 5 mg/ml polymer solution was prepared in the required buffer and divided into two equal parts. To one part, 20% (w/w) of dried silica gel was added. A separate polymer-free solution of 20% (w/w) of silica gel in buffer served as a blank. All three solutions were tumbled for two days, centrifuged, filtered (0.45 μm), and injected onto the column in the same buffer as the mobile phase. Comparisons of the peak areas of the chromatograms indicated the magnitude of the adsorption effect.

3. Results

The partition coefficient, K_{SEC} , is given by

$$K_{\text{SEC}} = \frac{V_e - V_0}{V_t - V_0} \quad (2)$$

where V_e is the solute elution volume, V_0 is the interstitial volume or void volume and V_t is the total mobile phase volume.

Fig. 1 shows the "universal calibration" [25] plot of $\log [\eta]M_r$ vs. V_e for pullulan and Ficoll fractions in sodium phosphate buffer of different ionic strength, I , and pH. Both polymers conform to a single plot at $I = 0.003$ M, pH 7.0, but late elution is observed in $I = 0.2$ M, pH 7.0 buffer. This anomalous retention is significantly higher for Ficoll fractions than for pullulan, suggesting some interaction between CPG and Ficoll. This interaction is also evident from the

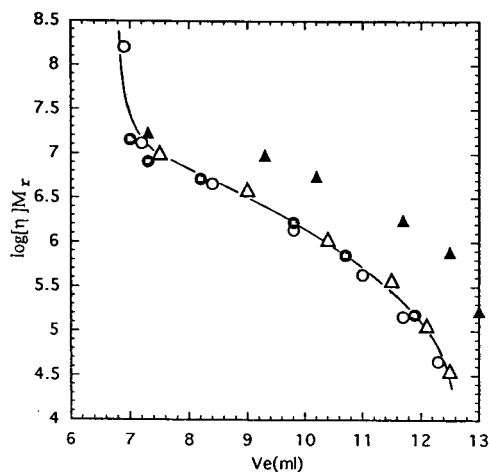


Fig. 1. Universal calibration plot for pullulan (open symbols) and Ficoll (filled symbols) on CPG in $I=0.003$, pH 7.0 phosphate buffer (\circ, \bullet), and in $I=0.2$, pH 4.5 phosphate buffer (Δ, \blacktriangle).

tailing of the peaks of Ficoll fractions 9 and 12 in $I=0.2 \text{ M}$, pH 4.5 buffer.

The partition coefficient, K_{SEC} , is given by

$$K_{\text{SEC}} = \frac{V_e - V_0}{V_t - V_0} \quad (3)$$

K_{SEC} for spherical solutes in pores of well defined geometry [26] is given by

$$K_{\text{SEC}} = \left(\frac{r_p - R}{r_p} \right)^\lambda \quad (4)$$

where $\lambda=1, 2$ or 3 for slab, cylindrical or spherical geometry of the pore, r_p is pore radius, and R is solute radius. If the plot of $K^{1/2}$ vs. R ($R=R_\eta$) gives a straight line with an intercept of 1, then the value of λ is 2 and the pores behave as if they were cylindrical. The slope of this plot is $1/r_p$. The value of r_p so obtained from the upper part of Fig. 2 was around 190 \AA , in close agreement with the mercury porosimetry data, supplied by the manufacturer, which yield 199 \AA . For the present work, the principal value of Eq. 4 is the linearization of the data which simplifies comparisons between pullulan and Ficoll, and also among the different mobile phases studied.

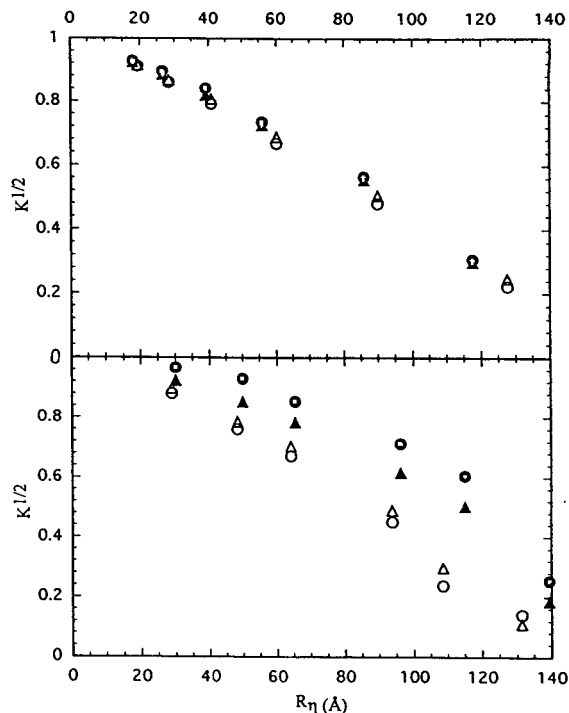


Fig. 2. Dependence of K_{SEC} on solute radius for pullulan (upper) and Ficoll (lower) in sodium phosphate buffers: (\circ) $I=0.003$, pH 7.0; (\bullet) $I=0.2$, pH 4.5; (Δ) $I=0.003$, pH 4.5; and (\blacktriangle) $I=0.2$, pH 7.0.

Fig. 2 shows $K^{1/2}$ vs. R_η for pullulan and Ficoll fractions in sodium phosphate buffer of different ionic strengths and pH. From Tables 1 and 2 we observe that the effect of salt on the dimensions of pullulan and Ficoll is negligible on the scale of Fig. 2; therefore, R_η was calculated using the values of $[\eta]$ measured in pure water for all 0.003 ionic strength buffers. Similarly, $[\eta]$ measured for pullulan and Ficoll in $I=0.2$, pH 4.5 buffer was used to calculate R_η in all high-ionic-strength buffers, regardless of pH. Plots of $K^{1/2}$ vs. R for Ficoll fractions are seen to show strong deviations from Eq. 3 especially at high ionic strength. The effect of ionic strength is larger at pH 4.5 than at pH 7.0, and the effect of pH is larger at high ionic strength (0.2 M) than at low ionic strength (0.003 M). That is, the anomalous retention is strongest at high ionic strength and lower pH. These correspond to the conditions

under which peak tailing was most clearly observed.

Fig. 3 shows the effect of the buffer anion on the dependence of $K^{1/2}$ on R for both polymers in phosphate and acetate buffers of different ionic strength and pH. Relatively little effect is seen for pullulan. For Ficoll, 0.003 *M* ionic strength phosphate buffers give nearly normal behavior at both pH 4.5 and 7.0. Anomalous retention appears for low-ionic-strength acetate buffer, high-ionic-strength phosphate at pH 7.0, or high-ionic-strength acetate at pH 4.5. The most striking effects are observed for high-ionic-strength pH 4.5 sodium phosphate.

The effect of cation is shown in Fig. 4. There is no measurable difference between lithium and sodium phosphate for pullulan at different ionic strengths and pH. For Ficoll, however, K_{SEC} is

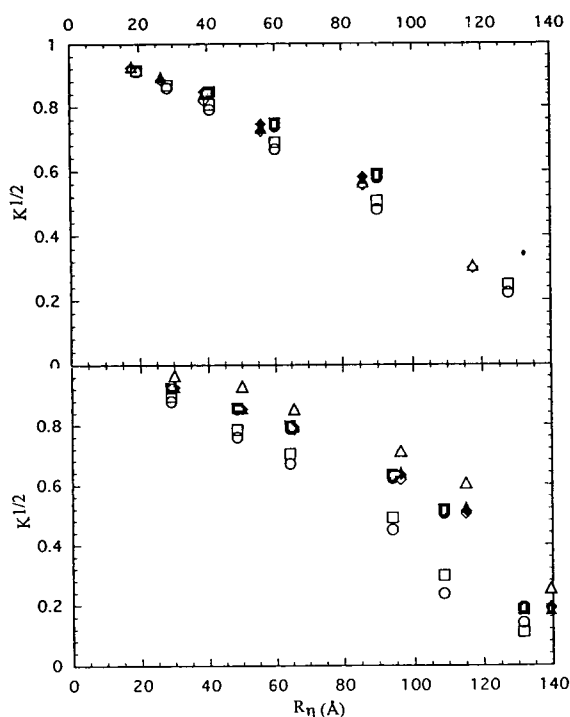


Fig. 3. Dependence of K_{SEC} on solute radius for pullulan (upper) and Ficoll (lower) in mobile phase buffers of (\circ, \bullet) $I = 0.003$, pH 7.0; ($\triangle, \blacktriangle$) $I = 0.2$, pH 4.5; (\square, \blacksquare) $I = 0.003$, pH 4.5; (\diamond, \blacklozenge) $I = 0.2$, pH 7.0. Open symbols for phosphate buffer, filled symbols for acetate buffer.

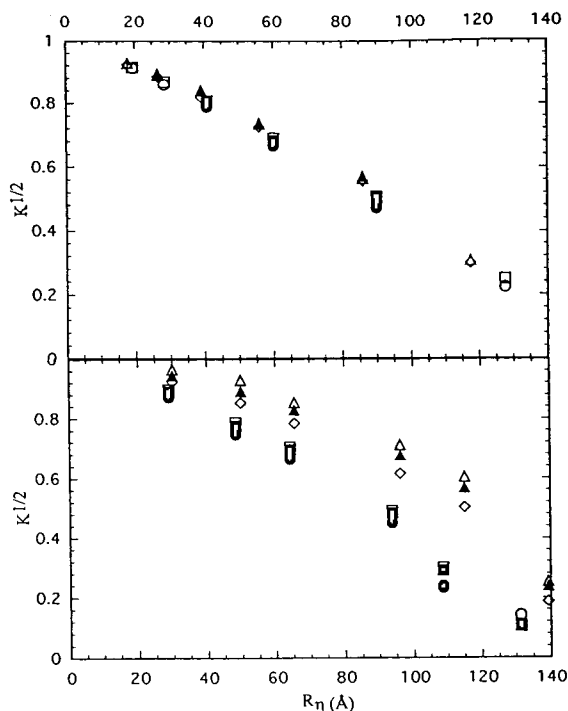


Fig. 4. Dependence of K_{SEC} on solute radius for pullulan (upper) and Ficoll (lower) in sodium phosphate buffer and lithium phosphate buffer. Open symbols as in Fig. 3; filled symbols are for lithium phosphate buffer of same ionic strength and pH as corresponding open symbols.

observed to increase when 0.2 *M*, pH 4.5 lithium phosphate is replaced by 0.2 *M*, pH 4.5 sodium phosphate.

The adsorption of Ficoll was studied using Ficoll-400 instead of the more precious Ficoll fractions. No adsorption could be observed on CPG glass, but a strong effect could be seen using silica gel as a model siliceous packing. Ficoll-400 was tumbled in sodium phosphate buffer of $I = 0.2$ *M*, pH 4.5 with and without silica gel. Both samples were centrifuged, filtered and injected onto the analytical column. Fig. 5 shows the resulting chromatograms. The peak area for Ficoll-400 after tumbling with silica is less than for the control sample, showing adsorption of the sample on silica. Equilibration with silica had no effect on peak shape or area for pullulan-100 in this buffer, or for either

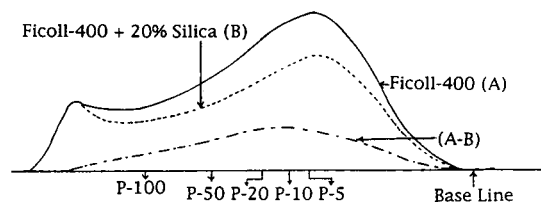


Fig. 5. Chromatograms of Ficoll-400: (A) untreated polymer; (B) polymer after equilibration with silica (supernatant). The difference (A – B) corresponds to the amount of Ficoll adsorbed. The horizontal axis corresponds to elution volumes, here parametrized using the elution volumes of pullulan standards (shown by vertical arrows).

pullulan or Ficoll at $I = 0.003 M$, pH 7.0. Thus adsorption was seen only for Ficoll in high-ionic-strength, pH 4.5 phosphate buffer, which corresponds to the conditions for anomalous retention as seen in Figs. 2 and 3.

Table 3 shows the intrinsic viscosity of pullulan-1600K and Ficoll fraction 9 in deionized water sodium phosphate buffer and tetramethylammonium chloride (TMACl). Despite its compact configuration, Ficoll exhibits the largest viscosity effect: a 15% increase upon addition of 0.1 M sodium phosphate at pH 4.0. On the other hand, no change in $[\eta]$ is observed upon addition of TMACl. The increase in viscosity of pullulan upon addition of salt is smaller, about 3% and not counterion-specific.

4. Discussion

Marked deviations from universal calibration are seen for Ficoll on CPG, particularly in the presence of added salt. These effects are not

exhibited by pullulan. The results of the adsorption measurements with silica gel as shown in Fig. 5 suggest that, while adsorption on CPG is clearly not as strong as on silica gel, it could account for the observed chromatographic effects. Some aspects of these observations are readily explained. In general, silica is more adsorptive towards hydrophilic solutes than glass, because of its higher surface density of silanol groups. We can also account for the enhanced adsorption of the lower- M_r Ficoll fractions observed in both the chromatography and the equilibrium experiments, by the greater access of smaller molecules to any porous surface. On the other hand, neutral polysaccharides in general do not display adsorption on SEC packings, and it is furthermore difficult to understand why Ficoll should be unique in this regard. A possible explanation could be that Ficoll might interact with cations like Na^+ leading to a transient polycation which then adsorbs onto the negatively charged surface of CPG. Although the nature of this interaction is not fully understood, the metal ion could be weakly coordinated to the ether and hydroxyl groups in Ficoll. Johansson [27] has in fact observed the formation of weak complexes between dextran and Na^+ and K^+ .

The intrinsic viscosity, a very sensitive measure of intramolecular expansion, increases by 15% for Ficoll fraction 9 upon addition of sodium phosphate as seen in Table 3. The absence of any viscosity change in tetramethylammonium chloride is consistent with a specific Na^+ ion interaction. Despite the fact that densely branched Ficoll should be more resistant

Table 3
Intrinsic viscosities of pullulan-1600K and Ficoll fraction 9

Solvent	$[\eta]$ (cm^3/g) (at 25°C)	
	Pullulan-1600K	Ficoll fraction 9
Deionized water	262	2.4
Sodium phosphate buffer, $I = 0.1$, pH 4.0	270	2.8
Tetramethylammonium chloride, 0.1 M	279	2.4

to conformational change than pullulan, the relative influence of salt on Ficoll viscosity is much larger. We suggest that transient binding of Na^+ to Ficoll to produce a pseudo-polycation results in intramolecular repulsion which leads to the observed intrinsic viscosity change.

We believe that the unusual effects of salt on both Ficoll adsorption and Ficoll viscosity are related, and that both arise from specific interactions between macromolecules and cation. While Johansson [27] has referred to weak complexation of this type for dextran, the effects seems to be stronger for Ficoll. Perhaps the closer proximity of saccharide units in densely branched Ficoll might facilitate intramolecular coordination of Na^+ with a saccharide residue.

Acknowledgement

This work was supported by Grant CHE-9021484 from the National Science Foundation.

References

- [1] K.K. Unger and J.N. Kinkel, in P.L. Dubin (Editor), *Aqueous Size-Exclusion Chromatography*, Elsevier, Amsterdam, 1988, Ch. 8.
- [2] K. Makino and H. Hatano, in P.L. Dubin (Editor), *Aqueous Size-Exclusion Chromatography*, Elsevier, Amsterdam, 1988, Ch. 9.
- [3] P.L. Dubin, *Adv. Chromatogr.*, 31 (1992) 122.
- [4] R.W.A. Oliver (Editor), *HPLC of Macromolecules*, IRL Press, Oxford, 1989.
- [5] W. Haller *Nature*, 206 (1965) 693.
- [6] W. Haller, A.M. Basedow and B. Konig, *J. Chromatogr.*, 132 (1977) 387.
- [7] C. Rochas, A. Domard and M. Rinaudo, *Eur. Polym. J.*, 16 (1980) 135.
- [8] M.G. Styring, C.J. Davison, C. Price and C. Booth, *J. Chem. Soc., Faraday Trans. 1*, 80 (1984) 3051.
- [9] H. Waldmann-Meyer, *J. Chromatogr.*, 350 (1985) 1.
- [10] P.L. Dubin, C.M. Speck and J.I. Kaplan, *Anal. Chem.*, 60 (1988) 895.
- [11] P.L. Dubin, R.M. Larter, C.J. Wu and J.I. Kaplan, *J. Phys. Chem.*, 94 (1990) 94.
- [12] P.L. Dubin, *Carbohydr. Polymers*, in press.
- [13] T. Kato, T.O. Kamoto, T. Tokuya and A. Takahashi, *Biopolymers*, 21 (1982) 1623.
- [14] H. Holter and K.M. Møller, *Exptl. Cell Res.*, 15 (1956) 631.
- [15] T.C. Laurent and K.A. Granath, *Biochim. Biophys. Acta*, 136 (1967) 191.
- [16] T.C. Laurent, *Biochim. Biophys. Acta*, 136 (1967) 199.
- [17] P.N. Lavrenko, O.I. Mikryukova and S.A. Didenko, *Polymer Sci. USSR*, 28 (1986) 576.
- [18] W.M. Deen, M.P. Bohrer and N.B. Epstein, *AIChE J.*, 27 (1981) 952.
- [19] M.P. Bohrer, G.D. Patterson and P.J. Carroll, *Macromolecules*, 17 (1984) 1170.
- [20] M.G. Davidson and W.M. Deen, *Macromolecules*, 21 (1988) 3474.
- [21] K. Luby-Phelps, D.L. Taylor and F. Lanni, *J. Cell. Biol.*, 102 (1986) 2015.
- [22] K. Luby-Phelps, P.E. Castle, D.L. Taylor and F. Lanni, *Proc. Natl. Acad. Sci. U.S.A.*, 84 (1987) 4910.
- [23] P.J. Flory, *Principles of Polymer Chemistry*, Cornell Univ. Press, Ithaca, NY, 1953, p. 606.
- [24] P.L. Dubin, S.L. Edwards and M.S. Mehta, *J. Chromatogr.*, 635 (1993) 51–60.
- [25] Z. Grubisic, P. Rempp and H. Benoit, *J. Polym. Sci., Part B*, 5 (1967) 753.
- [26] E.F. Casassa and Y. Tagami, *Macromolecules*, 2 (1969) 14.
- [27] G. Johansson, *Acta Chem. Scand., Ser. B*, 28 (1974) 873–882.



ELSEVIER

Journal of Chromatography A, 693 (1995) 205–216

JOURNAL OF
CHROMATOGRAPHY A

Slow change in the electrical potential at glass and silica surfaces due to Na^+ sorption in the hydrated layer

D. Marc Vermeulen, Frederick F. Cantwell*

Department of Chemistry, University of Alberta, Edmonton, Alberta, T6G 2G2, Canada

First received 23 August 1994; revised manuscript received 17 October 1994; accepted 19 October 1994

Abstract

Controlled Pore Glass (CPG) is a high- SiO_2 content, Vycor-type glass which resembles fused silica. In CPG–Oxine the ligand oxine is covalently bound to the CPG surface. The presence of SiO^- groups on the CPG generates a negative electrical potential at the surface (ψ_o) and also in the solution adjacent to the surface (ψ_x), where the immobilized oxine is to be found. The potential ψ_x influences the extent of complexation of Ca^{2+} (from solution) by oxine so that the bound oxine serves as a probe of electrical potential near the surface. When the solution pH is raised there is a relatively rapid ionization of SiOH groups to SiO^- . Then, slowly (i.e. tens of minutes), Na^+ from solution diffuses into the hydrated gel layer on CPG. This reduces the negative charge, making ψ_x less negative and, consequently, reduces the extent of complexation of Ca^{2+} by oxine. A linear relationship is predicted and experimentally observed between the logarithm of the sorbed Ca^{2+} concentration (mmol/g) and the potential ψ_x (V). The potential ψ_x is expected to correlate strongly with the zeta potential which controls the rate of electroosmotic flow at silicious surfaces.

1. Introduction

Silicious materials such as glass and fused silica possess a thin (e.g. tens of Å) hydrated layer when they are in contact with aqueous solutions. Depending on the solution pH, there is some ionization of the acidic SiOH groups to form SiO^- groups, both at the surface and in the hydrated layer [1–3]. The presence of these SiO^- groups generates a negative electrical potential at the surface (ψ_o) and also in the solution adjacent to the surface (ψ_x). These potentials influence sorption of solutes at the surface and

they are related to the electrokinetic zeta potential (ζ) which controls electroosmotic flow [4–6].

By measuring both the extent of deprotonation of the SiOH groups and the extent to which cations such as Na^+ are sorbed from solution, the total charge is known. However, the development of a quantitative expression to calculate the electrical potentials from a knowledge of the total charge requires the adoption of a detailed physicochemical model. The validity of the adopted model and of the resulting equations for calculating potentials must then be demonstrated experimentally. This is done by introducing a potential-sensitive “probe” whose behavior is a known function of potential. Then the observed behavior of the probe can be compared

* Corresponding author.

to that expected from the potentials calculated from the assumed model.

The present study is based upon earlier observations of the influence of pH, ionic strength and time on the complexation of Ca^{2+} ion by a ligand, when the ligand is covalently bound to the silicious surface of Controlled Pore Glass (CPG) [4,5]. In Controlled Pore Glass–Oxine (CPG–Oxine) the 5-phenylazo derivative of 8-hydroxyquinoline, which is bound to the surface of CPG [7,8], serves as a potential-sensitive probe since its ability to complex Ca^{2+} has a predictable dependence on the local electrical potential. Because only a very small fraction of the surface silanol groups in CPG–Oxine are derivatized with the oxine ligand, the surface of CPG–Oxine is much like that of CPG. Also, although the bound oxine groups have acid–base character, titration studies have demonstrated that most of the charge on CPG–Oxine is due to anionic silanolate groups from the CPG, and only a very small fraction is due to the ionized oxinate groups from the ligand [1].

The way in which the bound oxine ligand acts as a probe for the local electrical potential near the surface is as follows: the negative charge on the CPG creates a negative electrical potential which, via Boltzmann expressions, influences the activities of mobile cations and anions (e.g. H^+ , Ca^{2+} , Na^+ , OH^- , and ClO_4^-) in the solution immediately adjacent to the surface; that is, in the electrical double layer region [6,9]. These altered local solution activities, in turn, influence the equilibria in this region, wherein the immobilized oxine groups are located. In particular, the local pH (pH) in the vicinity of the oxine group is lower than the pH in bulk solution. This pH is what influences the degree of ionization of the immobilized oxine, $\bar{\alpha}_{\text{ox}}$. Also the local ionic activity of Ca^{2+} , \bar{a}_{Ca} , is higher than a_{Ca} in bulk solution. The local $\bar{\alpha}_{\text{ox}}$ and \bar{a}_{Ca} influence the extent to which Ca^{2+} is complexed by immobilized oxine. Using bound oxine as a probe, it has been found that most of the equilibrium properties related to the complexation of Ca^{2+} ion by the immobilized oxine ligand could be explained by a simple version of the “ionizable surface

group, site-binding model” [1,4]. This type of model is used widely in surface and colloid chemistry [6,9].

More recently, studies were undertaken to explain an anomalous aspect of the kinetics of Ca^{2+} sorption by CPG–Oxine [5]. The anomalous behavior was an “overshoot” of equilibrium during the loading of Ca^{2+} onto small columns of CPG–Oxine which had previously been washed with acid and water. The Ca^{2+} -loading curve, which is a plot of moles of Ca^{2+} sorbed versus time, rose to a maximum value in about 2 min and then decreased over the course of about 2 h to a final equilibrium plateau value. The following interpretation of this phenomenon was suggested [5]. The slow desorption of Ca^{2+} from its overshoot sorption value to its equilibrium value is caused by the sorption of Na^+ . The casual relationship between these two is not a stoichiometric one, such as ion exchange, but rather results from the effect that Na^+ -uptake into the hydrated layer has on the potential in the electrical double-layer region. Furthermore, it was suggested that the reason why the sorption of Na^+ is a slow process is because it involves diffusion of Na^+ into this “porous gel” hydrated layer, within which the diffusion coefficient of Na^+ is very small.

In the present paper a physicochemical model is developed to quantitatively explain the kinetic aspects of the cause-effect relationship between slow Na^+ sorption and electrical potential. The validity of this model is tested on CPG using covalently bound oxine as a probe of electrical potential. Since CPG is a high-silica content glass [10], it is likely that a similar slow sorption of alkali metal cations will occur on fused silica and other related materials that are of chromatographic and electrophoretic importance; and that this slow sorption will also be accompanied by a slow change in potential. Because CPG is porous, it possesses a high surface area–mass ratio, which permits accurate measurement of the amounts of sorbed species. In addition to the rate studies, as part of the work, the equilibrium sorption isotherm of Na^+ in the hydrated layer is characterized.

2. Experimental

2.1. Reagents and chemicals

All solutions were prepared with nanopure water (Barnstead) and all chemicals were reagent grade or purer. Preparation of the $\text{Ca}(\text{NO}_3)_2$ stock solution from CaCO_3 , of the NaClO_4 stock solution in water and of the 0.15 M (i.e. 1%) HNO_3 eluent were as previously described [5].

For use in the sorption rate studies of Ca^{2+} on CPG–Oxine and CPG and in the sorption rate study of Na^+ on CPG–Oxine, the single solution contained $2.00 \cdot 10^{-5}$ M Ca^{2+} , 0.0100 M 4-(2-hydroxyethyl)-1-piperazineethanesulphonic acid (HEPES) buffer and 0.0200 M NaClO_4 . It was prepared from stock solutions, adjusting its pH to 7.0₀ with ammonia water. This solution had an ionic strength of 0.0224 M.

For use in the equilibrium Na^+ -sorption study, a series of solutions was prepared which contained $2.00 \cdot 10^{-5}$ M Ca^{2+} with various concentrations of NaClO_4 between 0.00100 and 0.140 M. These solutions contained no HEPES buffer but, rather, were adjusted to pH 7.0₀ using NaOH and HNO_3 . Since no buffer was used, the pH was checked frequently in both the solution in the reservoir bottle and in the effluent from the CPG–Oxine column.

Batch 850605085 of CPG–Oxine and batch 860313081 of underivatized CPG (Pierce Chemical) were used in this work [1,4,5].

2.2. Apparatus

The column equilibration apparatus has been described [5]. The “column” was a small (ca. 4.5 mm × 2.1 mm I.D.) bed of either CPG–Oxine (5.4 mg) or CPG (4.7 mg) that was present in the central hole of the Kel-F slider of a modified injection valve. It was thermostatted at $25 \pm 1^\circ\text{C}$. All other apparatus, such as pH meter, peristaltic pump, Model 4000 spectrometer (Perkin Elmer) for atomic absorption of Ca^{2+} , and Model AA-10 spectrometer (Varian) for flame

atomic emission of Na^+ were as before [5]. The acid eluate from the column was led directly into the flame of the spectrometer via a PTFE capillary tube so that the atomic absorption signal for Ca^{2+} and the atomic emission signal for Na^+ were in the form of a peak, the area of which was measured with a digital integrator.

2.3. Ca^{2+} sorption rate study

The sorption rate of Ca^{2+} was measured on both CPG–Oxine and CPG. Briefly, the solution containing $2.00 \cdot 10^{-5}$ M Ca^{2+} , 0.0100 M NH_4^+ HEPES buffer (pH 7.00) and 0.0200 M NaClO_4 was pumped through the bed of either CPG–Oxine or CPG for various periods of time between about 2 and 250 min (the loading time), after which 0.15 M HNO_3 was used to elute Ca^{2+} from the column into the atomic absorption spectrometer (the elution step). Although all of the Ca^{2+} eluted from the column in less than the 1-min integration time, the elution step was continued for a total of 4 min. After calibrating the spectrometer by injecting various concentrations of Ca^{2+} standard solution, the areas of the eluted Ca^{2+} peaks were used to calculate the amount of Ca^{2+} sorbed by the column during the loading time. In this type of experiment the amount of Ca^{2+} in the column hold-up volume (17 μl) must be subtracted from the amount eluted in order to determine the amount sorbed [11,12]. In the Ca^{2+} sorption rate study on CPG–Oxine the hold-up volume correction was less than 2% of the equilibrium amount of sorbed Ca^{2+} . In the study on CPG the hold-up volume correction varied from a low of 11% at the 2-min point to a high of 20% at the 240-min point.

After the acid elution step the column was washed with water and was then ready for loading of the next sample.

2.4. Na^+ sorption rate study

The procedure for measuring the rate of Na^+ sorption on CPG–Oxine is similar to the Ca^{2+} sorption rate procedure except that a washing

step is interposed between the loading and elution steps. Immediately following the loading step the column was washed for 30 s with sodium-free 0.0200 M NH_4^+ HEPES buffer (pH 7.00) in order to wash out all of the Na^+ -containing interstitial and pore solution. Following the HEPES washing step the column was eluted for 4.00 min with 0.15 M HNO_3 in order to remove all of the strongly sorbed Na^+ and transfer it to the atomic emission spectrometer. Although area integration was performed for the full 4 min, nearly all of the Na^+ eluted within 90 s.

2.5. Na^+ sorption equilibrium study

This new set of experiments was performed on the CPG–Oxine column. A solution containing $2.00 \cdot 10^{-5}$ M of Ca^{2+} and various concentrations of NaClO_4 at pH 7.0₀ was pumped through the column for a sufficiently long time that sorption equilibrium was achieved. Both 2- and 4-h loading times were employed in order to verify that equilibrium was reached. Immediately following this loading step the column was washed with 0.00100 M NH_4^+ HEPES (pH 7.00, Na^+ -free) for 30 s. Then it was eluted for 4.00 min into the atomic emission spectrometer with 0.15 M HNO_3 .

In order to compensate for possible drift in instrument sensitivity and solution composition over the long periods of time involved in the loading studies, Na^+ calibrations were performed both before and after each experimental run. A series of Na^+ standards was injected using valve V2 (Fig. 2 in Ref. [5]), both before and after each experimental point, and averages for the standards were used in the calculations.

3. Results and discussion

Three aspects of the behavior of CPG–Oxine arising from the ionization of silanol groups on the surface and in the hydrated gel layer are quantified. First, the equilibrium sorption of Na^+ by CPG–Oxine is characterized. Second, a quantitative electrical double-layer model is de-

veloped in which the complexation of Ca^{2+} by immobilized oxinate ligand is related to sorption of Na^+ in the hydrated layer via the electrical potential ψ_x . Finally, the desorption rate of Ca^{2+} from CPG–Oxine is quantified as a function of the potential ψ_x in order to validate the model.

3.1. Equilibrium sorption of Na^+

In this study, the CPG–Oxine column was equilibrated with pH = 7.0₀ solutions containing various concentrations of Na^+ , as the ClO_4^- salt, in the range $[\text{Na}^+] = 0.00100$ to 0.140 M. The solutions also contained $2.00 \cdot 10^{-5}$ M of Ca^{2+} , but the small amounts of Ca^{2+} both in solution and sorbed on CPG–Oxine can be ignored in this study of Na^+ sorption. Establishment of equilibrium was verified by finding the same results when the experiments were performed for both a 2- and a 4-h loading time. The concentration of Na^+ sorbed at equilibrium, $\bar{N}_{\text{Na},\text{equil}}$ (mmol/g) is plotted versus $[\text{Na}^+]$ in Fig. 1, where it is seen that the amount of sorbed Na^+ increases toward a limiting value. This plot is a sorption isotherm for Na^+ . The data are presented in Table 1. The sorption isotherm,

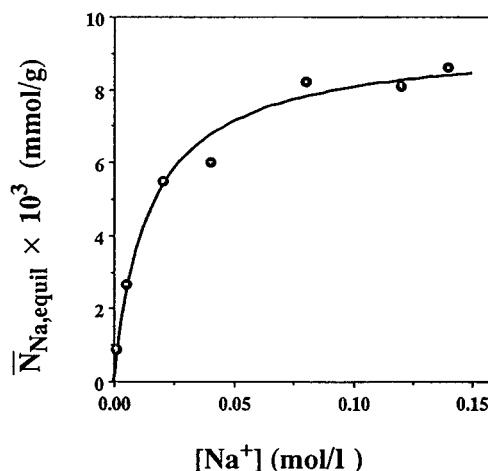


Fig. 1. Sorption isotherm of Na^+ on CPG–Oxine from pH 7.0₀ bulk solution. The points are experimental data. The line is predicted from Eq. 1 using $K = 74$ l/mol, $(\text{SiO}^-)_0 = 9.61 \cdot 10^{-3}$ mmol/g and γ_{Na} from Table 1, as discussed in the text.

Table 1
Parameters relating to the sorption of Na^+ on CPG–Oxine at pH 7.0₀ at various bulk solution concentrations of Na^+

$[\text{Na}^+]$ (mol/l)	γ_{Na}	$\bar{N}_{\text{Na,equil}}$ (mmol/g)
$1.00 \cdot 10^{-3}$	0.965	$0.87 \cdot 10^{-3}$
$5.00 \cdot 10^{-3}$	0.924	$2.67 \cdot 10^{-3}$
$20.0 \cdot 10^{-3}$	0.855	$5.5 \cdot 10^{-3}$
$40.0 \cdot 10^{-3}$	0.803	$6.0 \cdot 10^{-3}$
$80.0 \cdot 10^{-3}$	0.734	$8.2 \cdot 10^{-3}$
$120 \cdot 10^{-3}$	0.684	$8.1 \cdot 10^{-3}$
$140 \cdot 10^{-3}$	0.664	$8.6 \cdot 10^{-3}$

perhaps fortuitously, can be described by the Langmuir equation:

$$\bar{N}_{\text{Na,equil}} = \frac{[\text{Na}^+] \cdot \gamma_{\text{Na}} \cdot K \cdot (\text{SiO}^-)_0}{1 + [\text{Na}^+] \cdot \gamma_{\text{Na}} \cdot K} \quad (1)$$

The activity coefficient γ_{Na} was calculated from the Davies equation with the constant 0.3 in the second term [13]. Values of γ_{Na} are included in Table 1. Both K and $(\text{SiO}^-)_0$ are constants. Eq. 1 was fit to the data points in Table 1 by nonlinear least squares curve fitting. The correlation coefficient is 0.991 and the constants K and $(\text{SiO}^-)_0$ have values of (74 ± 15) l/mol and $(9.61 \pm 0.48) \cdot 10^{-3}$ mmol/g, respectively. The line in Fig. 1 is predicted from Eq. 1.

The parameter $(\text{SiO}^-)_0$ is the concentration of charged SiO^- groups in the hydrated layer at pH 7.0₀ in the absence of sorbed Na^+ . Titration studies have shown that at equilibrium at pH 7.00 there are 0.027 mmol of protons lost per gram from this batch of CPG–Oxine [1]. This quantity, which will be called Q_{max} , is independent of $[\text{Na}^+]$ in solution; at least within the range $[\text{Na}^+] = 0.01$ to 0.2 M [4]. Since the amount of Na^+ sorbed increases with $[\text{Na}^+]$, this means that the degree of dissociation of SiOH groups in the hydrated layer at fixed solution pH is independent of the amount of Na^+ sorbed by the hydrated glass layer. The fact that $(\text{SiO}^-)_0 < Q_{\text{max}}$ is important because it reveals information about the properties of the hydrated layer. These properties are represented diagrammatically in Fig. 2, which is discussed

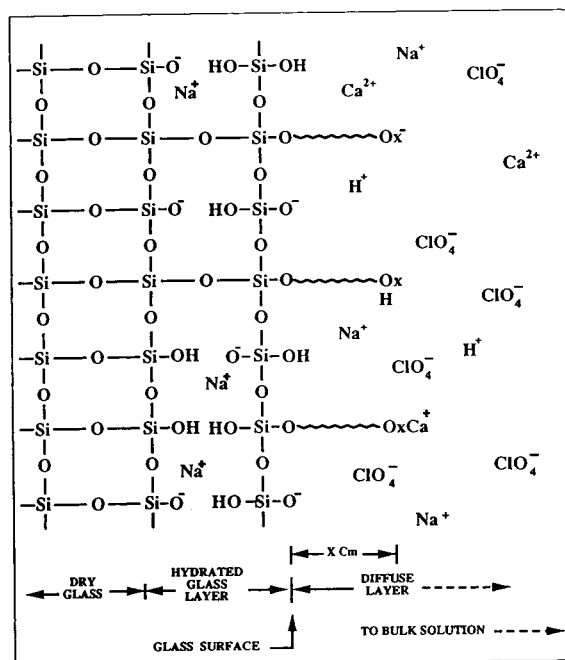


Fig. 2. Diagrammatic representation of the region near the glass-solution interface lining the pores in CPG–Oxine. Average pore diameter is 500 Å, so the pore liquid, to the right of the glass surface, contains both the diffuse part of the electrical “double-layer” and bulk solution. The hydrated layer, to the left of the glass surface, is probably more than one O–Si–O interatomic distance in depth. For ease of representation, bond lengths are inconsistent with one another and not to scale.

below. The specific surface area of CPG–Oxine, lining the pore walls, is $A_{\text{sp}} = 7.0 \cdot 10^5$ cm²/g [7]. The silanol groups on this surface, correspond to between 0.4 and 0.9 mmol of silanol per gram of CPG–Oxine [14–17]. In addition, silanol groups are also present *within* the hydrated layer, which extends from the glass surface toward the underlying dry layer.

At equilibrium, at a bulk solution pH of 7.0₀ some of the silanols on the surface have ionized to SiO^- and some of the silanols within the hydrated layer have likewise ionized, the total amount of SiO^- being Q_{max} (i.e. 0.027 mmol/g). In addition, Na^+ has been sorbed. However, only Na^+ within the hydrated layer is considered to be sorbed. That is, Na^+ is sorbed and contri-

butes to $(\overline{\text{SiONa}})$ only when it has passed through the surface and entered into the hydrated layer, in which it “neutralizes” an equivalent number of SiO^- groups. The term “sorption” as used for Na^+ here does not imply “site-binding” of Na^+ .

In contrast, SiO^- groups at the surface lie in a plane that is well separated from the plane of closest approach of Na^+ ions in solution in the diffuse part of the electrical double layer. It is in the diffuse layer that is to be found the remainder of the “surface excess” of Na^+ , equal in number to the remaining “unneutralized” SiO^- groups in the hydrated layer and at the surface. Since the diffuse layer is in the pore liquid these Na^+ ions would not be detected in this experiment because the pore liquid is washed out with NH_4^+ solution prior to the acid-elution step. Thus, the results of the previous titration experiments combined with the results of the present Na^+ -sorption experiment show that, at pH 7.0, about one-third (i.e. 0.0096/0.027) of the ionized silanol groups lie within the hydrated layer and about two-thirds are to be found at the glass surface. These SiO^- groups at the glass surface represent about 3% of the number of SiOH groups at the glass surface [14–17]. (Since only a small fraction of the surface silanols have been derivatized with 5-phenylazo-8-hydroxyquinoline groups [1], derivatized silanols have been omitted from the discussion.)

It should be noted that the sorption of Na^+ into the hydrated layer arises because H^+ ions have left that region, leaving behind excess negative charge. This phenomenon is therefore an “ion-exchange” process. However, complete 1:1 stoichiometric exchange of Na^+ for H^+ in the hydrated layer is not required; and evidently is not achieved at $[\text{Na}^+]$ below 0.15 M Na^+ , as seen in Fig. 1. The reason why stoichiometric ion exchange is not required is because the hydrated layer is so thin (i.e. tens of Å, Ref. [5]) that local electroneutrality may be violated within it. This is simply another way of saying that part of the equilibrium “surface excess” of negative SiO^- groups lies within the hydrated layer, in addition to the part which lies in the surface plane. (Naturally, local electroneutrality is also violated

within the diffuse part of the double layer in the adjacent solution, which contains a “surface excess” of positive charge that is exactly equal to the sum of the excesses of negative charge in both the hydrated layer and the surface plane.)

3.2. Double-layer sorption model for Ca^{2+}

It has been shown that Ca^{2+} is sorbed on CPG–Oxine from a NaClO_4 solution by two different processes [4]. One sorption process is complexation of Ca^{2+} by the immobilized oxinate ligand, the extent of which depends on the electrical potential, as discussed above. This process is specific “site-binding” of Ca^{2+} . The other sorption process probably is related to cation exchange of Ca^{2+} for Na^+ in the diffuse part of the electrical double layer. (There is no evidence to suggest that Ca^{2+} enters the hydrated layer.) The former of these two processes, complexation, is generally much more important than the latter.

The oxinate moiety of the bound 5-phenylazo-8-hydroxyquinoline, which is the anionic bidentate ligand that complexes Ca^{2+} , is located in the solution in the diffuse part of the electrical double layer at a distance of X cm from the glass surface. It is the electrical potential ψ_x (V), at location X which influences the Ca^{2+} complexation by oxinate. The bound oxine thus acts as a probe of the potential at the location X cm from the surface.

According to the “ionizable surface group, site-binding model” [5], the millimoles of Ca^{2+} complexed per gram of CPG–Oxine, \bar{N}_{Ca} , is related to ψ_x by the expression:

$$\bar{N}_{\text{Ca}} = [\text{Ca}^{2+}] \cdot \gamma_{\text{Ca}} \cdot \bar{\alpha}_{\text{ox}} \cdot \bar{\nu}_{\text{oxine}} \cdot \bar{\beta}_1 \cdot \exp\left(-\frac{2F\psi_x}{RT}\right) \quad (2)$$

in which R is the ideal gas constant [8.314 J/(molK)]; F is the Faraday constant (96 487 C/equiv); T is absolute temperature; $[\text{Ca}^{2+}]$ is the bulk solution concentration (M); γ_{Ca} is the bulk solution ionic activity coefficient of Ca^{2+} ; $\bar{\alpha}_{\text{ox}}$ is the fractional ionization of immobilized oxine as oxinate; $\bar{\nu}_{\text{oxine}}$ is the complexation capacity of

CPG–Oxine which is $(3.6 \pm 0.5) \cdot 10^{-6}$ mmol/g [1]; and $\bar{\beta}_1$ is the formation constant of the 1:1 complex between Ca^{2+} and immobilized oxinate (i.e. $5 \cdot 10^3$ l/mol, Ref. [4]), with all concentrations taken at location X in the diffuse layer. The values of $\bar{\nu}_{\text{oxine}}$ and $\bar{\beta}_1$ are constants.

The value of $\bar{\alpha}_{\text{ox}}$ depends on the value of ψ_x . When ψ_x becomes less negative it causes the local pH at position X to increase which causes $\bar{\alpha}_{\text{ox}}$ to increase. The relationship is derived as follows: $\bar{\alpha}_{\text{ox}}$ is defined in terms of both the activity of H^+ in the bulk solution, $a_{\text{H}} = 1.0 \cdot 10^{-7} M$, and the acid dissociation quotient for the phenolic hydroxyl group on the immobilized oxine, \bar{K}'_{a2} [1,4]:

$$\bar{\alpha}_{\text{ox}} = \frac{\bar{K}'_{\text{a2}}}{a_{\text{H}} + \bar{K}'_{\text{a2}}} \quad (3)$$

The acidity quotient \bar{K}'_{a2} is related to the acidity constant (\bar{K}_{a2}), given in terms of the activity of H^+ , by the following expression [1]:

$$\bar{K}'_{\text{a2}} = \bar{K}_{\text{a2}} \cdot \exp\left(+\frac{F\psi_x}{RT}\right) \quad (4)$$

Combining Eqs. 3 and 4 and taking into account the fact that at pH=7, $a_{\text{H}} \ll \bar{K}'_{\text{a2}}$ gives the following expression:

$$\bar{\alpha}_{\text{ox}} \approx \bar{K}_{\text{a2}} \cdot a_{\text{H}}^{-1} \cdot \exp\left(+\frac{F\psi_x}{RT}\right) \quad (5)$$

Substituting for $\bar{\alpha}_{\text{ox}}$ from Eq. 5 into Eq. 2, rearranging and taking the natural logarithm of both sides yields the expression:

$$\ln\left(\frac{\bar{N}_{\text{Ca}}}{\gamma_{\text{Ca}}}\right) = \ln\left([\text{Ca}^{2+}] \cdot \bar{\nu}_{\text{oxine}} \cdot \bar{\beta}_1 \cdot \bar{K}_{\text{a2}} \cdot a_{\text{H}}^{-1}\right) - \frac{F \cdot \psi_x}{RT} \quad (6)$$

From Eq. 6 it is predicted that a plot of $\ln(\bar{N}_{\text{Ca}}/\gamma_{\text{Ca}})$ versus ψ_x should be linear with slope of $-F/RT$ (i.e. -38.9).

The potential at distance x , ψ_x , can be calculated from the potential at the surface, ψ_0 , using the following series of expressions [18,19]:

$$\psi_x = \frac{2RT}{ZF} \cdot \ln \frac{1 + \gamma_{\text{GC}} \cdot \exp(-\kappa X)}{1 - \gamma_{\text{GC}} \cdot \exp(-\kappa X)} \quad (7)$$

where

$$\gamma_{\text{GC}} = \frac{\exp\left(\frac{ZF\psi_0}{2RT}\right) - 1}{\exp\left(\frac{ZF\psi_0}{2RT}\right) + 1} \quad (8)$$

and

$$\kappa = \left(\frac{2000Z^2F^2}{\epsilon_0 DRT}\right)^{1/2} \cdot c^{1/2} \quad (9)$$

In these expressions Z has the value one (with no sign), ϵ_0 is the permittivity of a vacuum ($1.12 \cdot 10^{-12}$ C/V·cm), D is the dimensionless dielectric constant of water divided by 4π (i.e. $78.3/4\pi$), and c is the ionic strength of the bulk solution (M). Since Ca^{2+} is present at trace-level concentrations, its contribution, both in the complexed state and as an electrolyte component in solution, can be neglected. For this reason, the Gouy–Chapman treatment for uni-univalent electrolytes, with $Z = 1$, is appropriate.

The question then becomes how to calculate the surface potential, ψ_0 . Previously, the relatively simple “surface ionization model” was used [1,4,5], in which it was assumed that the ionized silanolate groups are present only at the two-dimensional glass surface located at the interface between the hydrated layer and the solution [1,2,4–6,9]. This simple model is inconsistent with the “porous gel” assumption which has been invoked to explain the excessively slow sorption of Na^+ by CPG [5] and which has been described above. In a porous gel [6,20,21], ionization of silanol groups occurs throughout the hydrated layer which has a thickness in the range of tens of Å units [22]. The simple “surface ionization” model, which was previously used, can be treated mathematically by the relatively simple Gouy–Chapman theory of the electrical double layer in order to obtain ψ_0 , while in contrast, the porous gel model involves a double-diffuse double layer, for which the theoretical calculation of ψ_0 is more complex [6,20,21]. Although the evidence favors the view that a porous gel model should be used to calculate ψ_0 , it is not possible to do so with the information that is available on the properties of CPG–Oxine. Therefore, as an approximation,

the system will be treated using the simpler “surface ionization model”. That is, although some of the anionic silanolate groups are distributed throughout the hydrated porous gel layer, across a distance in the range of tens of Angstroms, for purposes of calculating their contribution to ψ_o all of the silanolate groups will be treated as though they reside at the surface of the hydrated layer. The Gouy–Chapman theory will be employed. A result of this approximation is that the calculated values of the surface potential, ψ_o , and of the potential at the location of oxine, ψ_x , will be somewhat higher than their true values.

According to the Gouy–Chapman theory, the potential at the surface is given by the expression:

$$\sinh\left(\frac{ZF\psi_o}{2RT}\right) = (8.53 \cdot 10^4)c^{-1/2}\sigma_o \quad (10)$$

where σ_o is the charge density (C/cm^2) due to silanolate groups [19,23,24]. The charge density is related to the excess concentration of negatively charged groups on the glass, Q_t (mmol/g), as follows:

$$\sigma_o = \frac{Z_- F Q_t}{1000 A_{sp}} \quad (11)$$

Here Z_- has the value -1 . The quantity Q_t is equal to the concentration of ionic silanolate groups (i.e. concentration of protons that have left both from within and from the surface of the hydrated layer) *minus* the concentration of Na^+ ions that have entered into the hydrated layer.

3.3. Sorption/desorption rate of Ca^{2+}

Shown in Fig. 2 is a diagrammatic representation of the interfacial region during the time that the slow sorption of Na^+ is taking place. Initially, the CPG–Oxine was washed with dilute acid followed by water. Then the pH and the ionic strength were raised by contacting it with a sample solution containing fixed concentrations of buffer, $NaClO_4$ and Ca^{2+} . As discussed above, some fractions of the silanol groups in the porous gel layer and at the surface ionize to form silanolate and hydrogen ions. The dissociated

hydrogen ions diffuse out of the gel layer at a relatively rapid rate. The “surface excess” of negative SiO^- is the sum of SiO^- at the surface and within the hydrated layer. Gradients of negative electrical potential become established both in the porous gel layer and in the diffuse layer in the adjacent pore liquid.

During this short period of time when dissociated H^+ is rapidly diffusing out of the gel layer and out of the pore liquid into the solution surrounding the CPG–Oxine particle, Ca^{2+} is diffusing to the location X and complexing with the oxinate ligand in order to satisfy the increasingly negative value of ψ_x in Eq. 2. This series of processes leading to the sorption of increasing amounts of Ca^{2+} is completed in about 1 to 2 min, as seen from the rising part of the curve in Fig. 3A in Ref. [5]. Because the diffusion time of H^+ in the gel layer and of both H^+ and Ca^{2+} in the pore solution are all comparable to one another, data obtained at $t \leq 1$ to 2 min do not reveal their rates of diffusion, other than to show that they are all relatively fast.

Now, at a rate much slower than that at which H^+ ions diffused out, Na^+ ions diffuse into the gel layer until equilibrium is established. This is seen in Fig. 6B of Ref. [5]. That is, the establishment of Na^+ sorption equilibrium within the hydrated layer is a slow process. If $\bar{N}_{Na,t}$ (mmol/g) is the concentration of Na^+ sorbed at time t , then the concentration of ionic silanolate groups, Q_t , at time t is:

$$Q_t = Q_{max} - \bar{N}_{Na,t} \quad (12)$$

where Q_{max} has the value of 0.0270 mmol/g. After only 2 min of loading, the H^+ produced by the ionization of $SiOH$ groups has diffused out of the hydrated layer, but very little Na^+ has diffused in. That is, for $t = 2$ min, $\bar{N}_{Na,t} \approx 0$ and $Q_t \approx Q_{max}$. With time, Q_t continues to decrease as more Na^+ diffuses in, and this decrease in Q_t decreases σ_o which, in turn, makes ψ_o and ψ_x less negative and consequently decreases \bar{N}_{Ca} . This is seen from the Ca^{2+} rate curves in Fig. 3B and in Fig. 6A, both in Ref. [5]. After a sufficiently long time $\bar{N}_{Na,t}$ has increased to its constant equilibrium value $\bar{N}_{Na,equl}$ and as a consequence

\bar{N}_{Ca} has decreased (i.e. desorbed) to its equilibrium value. Kinetically, it is assumed that the rates of formation and dissociation of the 1:1 Ca^{2+} -oxinate complex are much faster than the rate of Na^+ sorption into the hydrated layer.

Data for the rates of Na^+ sorption and Ca^{2+} sorption/desorption are taken from Ref. [5]. Based on the above discussion, the time 2.0 min from the start of the experiment is taken to be $t=0$ min in both the Na^+ - and Ca^{2+} - rate experiments. The first column in Table 2 presents the times at which Na^+ sorption was measured experimentally on CPG–Oxine and the second column presents the experimentally measured amounts of Na^+ sorbed at those times.

In the third column are shown the amounts of Ca^{2+} sorbed on CPG–Oxine at the same times. Since Ca^{2+} sorption was measured experimentally at times not identical to those in the first column of Table 2, the amounts of Ca^{2+} sorbed that are shown in the third column were calculated from the least-squares curve fit to the data in Ref. [5]. The first order equation (starting $t=0$ at 2 min) which describes the Ca^{2+} desorption rate on CPG–Oxine is:

$$\bar{N}_{Ca}(\text{CPG-Oxine}) = (5.94 \pm 0.07) \cdot 10^{-4} - 2.275 \cdot 10^{-4} \{1 - \exp[(-0.0273 \pm 0.0011) \cdot t]\} \quad (13)$$

The correlation coefficient is $r = 0.994$. Uncertainties are standard deviations.

In order to identify the amount of Ca^{2+} that is sorbed onto CPG–Oxine by processes other than complexation with immobilized oxinate, Ca^{2+} sorption by CPG (with no oxine) was also measured (Fig. 3C in Ref. [5]). The amount of Ca^{2+} sorbed on CPG is about 10% of the amount sorbed on CPG–Oxine and, taking 2 min to be zero time, its amount, $\bar{N}_{Ca}(\text{CPG})$, is given as a function of time by the equation:

$$\bar{N}_{Ca}(\text{CPG}) = (5.71 \pm 0.05) \cdot 10^{-5} - (1.15 \pm 0.04) \cdot 10^{-7} \cdot t \quad (14)$$

which has a correlation coefficient of $r = 0.997$. Values of $\bar{N}_{Ca}(\text{CPG})$ are presented in the fourth column of Table 2. Because such a small fraction of the silanol groups on the surface of CPG–Oxine is derivatized with oxine, it can be assumed that at any time t the amount of Ca^{2+} sorbed on CPG–Oxine by processes other than complexation with oxinate is equal to $\bar{N}_{Ca}(\text{CPG})$. Thus, the value of \bar{N}_{Ca} , corresponding to Ca^{2+} sorbed on CPG–Oxine only by complexation with oxinate, is given by the expression:

$$\bar{N}_{Ca} = \bar{N}_{Ca}(\text{CPG-Oxine}) - \bar{N}_{Ca}(\text{CPG}) \quad (15)$$

Table 2

Parameters relating to the sorption of Ca^{2+} and Na^+ from a solution containing $2.00 \cdot 10^{-5}$ mol/l Ca^{2+} and 0.0200 mol/l Na^+ at pH 7.00 and ionic strength 0.0224 M employing $X = 5.7 \cdot 10^{-8}$ cm and $\gamma_{Ca} = 0.549$

t^a (min)	$\bar{N}_{Na,t}^b$ (mmol/g)	$\bar{N}_{Ca}(\text{CPG-Oxine})^c$ (mmol/g)	$\bar{N}_{Ca}(\text{CPG})^d$ (mmol/g)	\bar{N}_{Ca} (mmol/g)	Q_t (mmol/g)	σ_o (C/cm ²)	ψ_o (V)	ψ_x (V)	$\ln(\bar{N}_{Ca}/\gamma_{Ca})$
0	0	$5.94 \cdot 10^{-4}$	$5.71 \cdot 10^{-5}$	$5.37 \cdot 10^{-4}$	0.0270	$-3.72 \cdot 10^{-6}$	-0.0768	-0.0536	-6.93
3	$0.926 \cdot 10^{-3}$	$5.77 \cdot 10^{-4}$	$5.68 \cdot 10^{-5}$	$5.19 \cdot 10^{-4}$	0.0261	$-3.59 \cdot 10^{-6}$	-0.0752	-0.0526	-6.96
14	$1.67 \cdot 10^{-3}$	$5.22 \cdot 10^{-4}$	$5.55 \cdot 10^{-5}$	$4.66 \cdot 10^{-4}$	0.0253	$-3.49 \cdot 10^{-6}$	-0.0739	-0.0518	-7.07
28	$3.74 \cdot 10^{-3}$	$4.72 \cdot 10^{-4}$	$5.39 \cdot 10^{-5}$	$4.19 \cdot 10^{-4}$	0.0233	$-3.20 \cdot 10^{-6}$	-0.0700	-0.0495	-7.18
62	$7.89 \cdot 10^{-3}$	$4.08 \cdot 10^{-4}$	$5.00 \cdot 10^{-5}$	$3.58 \cdot 10^{-4}$	0.0191	$-2.63 \cdot 10^{-6}$	-0.0614	-0.0441	-7.33
116	$8.81 \cdot 10^{-3}$	$3.76 \cdot 10^{-4}$	$4.38 \cdot 10^{-5}$	$3.32 \cdot 10^{-4}$	0.0182	$-2.51 \cdot 10^{-6}$	-0.0593	-0.0427	-7.41
179	$9.30 \cdot 10^{-3}$	$3.68 \cdot 10^{-4}$	$3.65 \cdot 10^{-5}$	$3.32 \cdot 10^{-4}$	0.0177	$-2.44 \cdot 10^{-6}$	-0.0582	-0.0420	-7.41
244	$9.44 \cdot 10^{-3}$	$3.67 \cdot 10^{-4}$	$2.90 \cdot 10^{-5}$	$3.38 \cdot 10^{-4}$	0.0176	$-2.42 \cdot 10^{-6}$	-0.0578	-0.0417	-7.39

^a Real time for Na^+ sorption minus 2 min.

^b Experimental data points for Na^+ sorption on CPG–Oxine at times t .

^c From Eq. 13, describing experimental Ca^{2+} sorption rate on CPG–Oxine.

^d From Eq. 14, describing experimental Ca^{2+} sorption rate on CPG.

Values of \bar{N}_{Ca} are presented in the fifth column.

In the sixth, seventh and eighth columns of Table 2 are presented the values of Q_t , σ_o and the surface potential ψ_o which were calculated from Eqs. 12, 11 and 10, respectively. In the last column are shown values of the function $\ln(\bar{N}_{Ca}/\gamma_{Ca})$. The activity coefficient γ_{Ca} is 0.549 [4], which is constant because the ionic strength of the bulk solution is constant.

Eq. 6 describes the relationship between the amount of Ca^{2+} sorbed via complexation by oxinate on CPG–Oxine and the potential ψ_x . The other parameters in Eq. 6, $[Ca^{2+}]$, γ_{Ca} , \bar{v}_{oxine} , $\bar{\beta}_1$ and \bar{K}_{a2} , are constants which would appear in the intercept of the plot of $\ln(\bar{N}_{Ca}/\gamma_{Ca})$ versus ψ_x . The difficulty in making such a plot is the fact that the value of X , which is required in Eq. 7 to calculate ψ_x , is not known. However, it can be obtained by trial and error. A value is assumed for X and is used in Eq. 7 to calculate ψ_x as a function of time. A plot is made of $\ln(\bar{N}_{Ca}/\gamma_{Ca})$ vs. ψ_x . The procedure is repeated for various assumed values of X . The correct value of X is the one which leads to a straight line plot with a slope of -38.9 (i.e. $-F/RT$). For the present system, X is found to be $(5.7 \pm 1.1) \cdot 10^{-8}$ cm (i.e. 5.7 \AA). The corresponding values of ψ_x from Eq. 7 are presented in column 9 of

Table 2 and the plot of $\ln(\bar{N}_{Ca}/\gamma_{Ca})$ vs. ψ_x is shown in Fig. 3. It is linear with a correlation coefficient $r=0.98$, a slope of -38.9 ± 2.9 and an intercept of -9.06 ± 0.14 . The uncertainty in X is estimated from the uncertainty in the slope.

An experimental value of about 6 \AA for X is quite reasonable since the spacer-arm which attaches the oxinate ligand to the glass surface, when fully extended, would place the oxinate about 18 \AA away from the surface [1,25]. Thus, an observed value of $X \approx 6 \text{ \AA}$ suggests that at pH 7 and $c \approx 0.02$ the spacer-arm is folded back on itself, as has previously been suggested [1].

4. Conclusions

Using the immobilized ligand oxine it has been demonstrated that, above the pH of zero charge of the CPG, the surface potential ψ_o and the potential at any location X in the diffuse layer undergo a slow decrease in magnitude of their negative value with time and eventually reach equilibrium values. This slow drift in ψ_o and ψ_x results from the slow sorption of Na^+ , presumably as a result of diffusion of Na^+ into the hydrated gel layer.

The potentials ψ_o and ψ_x both correlate strongly with the electrokinetic ζ -potential at the plane of shear. There is considerable interest in the ζ -potential at the surface of fused silica as it relates to electroosmotic flow in the capillaries that are used for capillary electrophoresis. For example, in a recent study of electroosmosis, the results were interpreted in terms of the formation of a complex between alkali metal ions (e.g. Li^+ and Na^+) and SiO^- groups at the surface of the fused silica [26]. The bound alkali metal was assumed to occupy the Inner Helmholtz Plane rather than to enter a hydrated layer. However, it was mentioned that "to ensure equilibrium was reached between the silica and solution phases, the phosphate buffer... was loaded into the capillary at least 6 h before the measurements were carried out." [26]. In addition, it is often observed that long periods of "conditioning" are required for electroosmotic behavior to stabilize

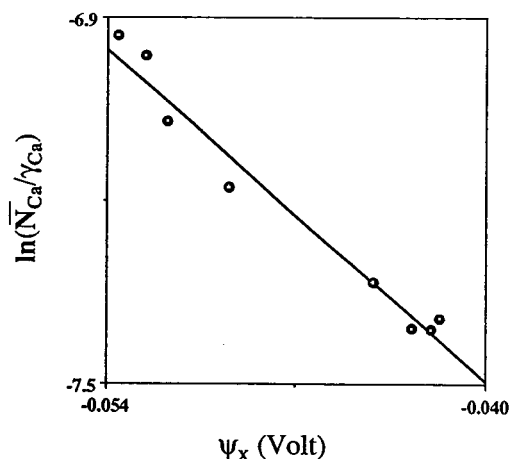


Fig. 3. Plot of $\ln(\bar{N}_{Ca}/\gamma_{Ca})$ vs. ψ_x to test the linear dependence predicted by Eq. 6. Points are data from columns 9 and 10 in Table 2. Oxinate is located at $X = 5.7 \cdot 10^{-8}$ cm. The line is a linear least-squares fit having a slope of -38.9 .

when electrolytes are first put into fused-silica capillaries. Since CPG is a Vycor-type glass that is composed of $\geq 95\%$ SiO_2 , it might be expected that there would be some strong similarities between CPG and fused silica. In fact, a hydrated gel layer is known to form on fused silica [6,22]. Thus, it is likely that slow diffusion of ions such as Na^+ would occur into the hydrated layer on fused silica to produce a slow drift of ζ toward an equilibrium value after, for instance, an electrolyte of higher pH has been introduced into the capillary. This interpretation of the slow “conditioning” of fused silica seems more likely than adsorption of such ions into an Inner Helmholtz Plane, located at the boundary between the silica capillary-surface and the solution, because the latter should not be a particularly slow process.

Finally, it may be noted that when the surface potential, ψ_o is ≤ 0.025 V the so-called Debye–Hückel (D-H) approximation can be made. With this approximation the hyperbolic sine-term on the left-hand side of Eq. 10 simplifies to $(ZF\psi_o/2RT)$, so that Eq. 10 becomes [18]:

$$\psi_o \approx \frac{(8.53 \cdot 10^4)2RT}{ZF} \cdot \sigma_o \cdot c^{-1/2} \quad (16)$$

Also as a result of the D-H approximation, Eq. 7 simplifies to the form [1,4,18]:

$$\psi_x \approx \psi_o \cdot \exp(-3.29 \cdot 10^7 c^{1/2} X) \quad (17)$$

Combining Eqs. 11, 16 and 17 shows that when $\psi_o \leq 0.025$ V, at 25°C , ψ_x can be expressed as:

$$\psi_x \approx -\frac{4.38 \cdot 10^3 Fc^{-1/2}}{1000A_{sp}} Q_t \cdot \exp(-3.29 \cdot 10^7 c^{1/2} X) \quad (18)$$

That is, ψ_x becomes directly proportional to Q_t , the sum of charge on the surface plus hydrated gel layer. Then Eq. 6 can be replaced by an expression of the form:

$$\ln \frac{\bar{N}_{\text{Ca}}}{\gamma_{\text{Ca}}} = A + B \cdot Q_t \quad (19)$$

where A and B are constants.

5. Acknowledgements

This work was supported by the Natural Sciences and Engineering Research Council of Canada and by the University of Alberta.

6. References

- [1] A.K. Kolstad, P.Y.T. Chow and F.F. Cantwell, *Anal. Chem.*, 60 (1988) 1565.
- [2] A. Davidowicz, W. Janusz, J. Szeypa and A. Waksmundski, *J. Colloid Interface Sci.*, 115 (1987) 555.
- [3] I. Altug and M.L. Hair, *J. Phys. Chem.*, 71 (1967) 4620.
- [4] P.Y.T. Chow and F.F. Cantwell, *Anal. Chem.*, 60 (1988) 1569.
- [5] D.M. Vermeulen and F.F. Cantwell, *Anal. Chem.*, 65 (1993) 1360.
- [6] R.J. Hunter, *Zeta Potential in Colloid Science: Principles and Applications*, Academic Press, New York, 1981, Ch. 7.
- [7] *Product Bulletin*, Pierce Chemical, Rockford, IL, 1986.
- [8] I.F. Suguwara, H.H. Weetall and G.D. Schucker, *Anal. Chem.*, 46 (1974) 489.
- [9] R.O. James and G.A. Parks, in E. Matijevic (Editor), *Surface and Colloid Science*, Vol. 12, Plenum Press, New York, 1982, Ch. 2.
- [10] N. Bansal and R. Doremus, *Handbook of Glass Properties*, Academic Press, New York, 1986, Ch. 2.
- [11] G. Persaud and F.F. Cantwell, *Can. J. Chem.*, 70 (1992) 926.
- [12] G. Persaud and F.F. Cantwell, *Anal. Chem.*, 64 (1992) 89.
- [13] C.W. Davies, *Ion Association*, Butterworths, Toronto, 1962, Ch. 3.
- [14] D. Cukman, J. Jadnacek-Biscan, Z. Vekslj and W. Haller, *J. Colloid Interface Sci.*, 115 (1987) 357.
- [15] R. Schnabel and P. Langer, *J. Chromatogr.*, 544 (1991) 137.
- [16] F. Janowski and W. Heyer, *Poröse Gläser*, VEB Deutscher Verlag für Grundstoffindustrie, Leipzig, 1981, Ch. 4.
- [17] S.M. Ahmed and A.B. van Cleave, *Can. J. Chem. Eng.*, 43 (1965) 23.
- [18] D.J. Shaw, *Introduction to Colloid and Surface Chemistry*, Butterworths, Toronto, 3rd ed., 1980, Ch. 7.
- [19] D.C. Grahame, *Chem. Rev.*, 41 (1947) 441.
- [20] J.W. Perram, R.J. Hunter and H.J.L. Wright, *Chem. Phys. Lett.*, 23 (1973) 265.
- [21] J.W. Perram, J.R. Hunter and H.J.L. Wright, *Aust. J. Chem.*, 27 (1974) 461.
- [22] W. Smit, C.L.M. Holten, H.M. Stein, J.J.M. DeGoeij and H.M.J. Theelen, *J. Colloid Interface Sci.*, 67 (1978) 397.

- [23] T.W. Healey and L.R. White, *Adv. Colloid Interface Sci.*, 9 (1978) 303.
- [24] F.F. Cantwell and S.H. Puon, *Anal. Chem.*, 51 (1979) 623.
- [25] M.A. Marshall and H.A. Mottola, *Anal. Chem.*, 55 (1983) 2089.
- [26] T.-L. Huang, P. Tsai, C.T. Wu and C.S. Lee, *Anal. Chem.*, 65 (1993) 2887.

A simple method for the determination of capacity factor on solid-phase extraction cartridges. I

András Gelencsér^a, Gyula Kiss^a, Zoltán Krivácsy^b, Zita Varga-Puchony^b,
József Hlavay^{a,*}

^aDepartment of Analytical Chemistry, University of Veszprém, P.O. Box 158, H-8201 Veszprém, Hungary

^bResearch Group of Analytical Chemistry, Hungarian Academy of Sciences, P.O. Box 158, H-8201 Veszprém, Hungary

First received 30 August 1994; revised manuscript received 9 November 1994

Abstract

In this paper a simple experimental method for the rapid determination of capacity factors of phenolic compounds on off-line solid-phase extraction cartridges is described. A model solution of the analytes is brought into equilibrium with the SPE cartridge by recycling in a closed loop. The capacity factors are calculated from the adsorbed amounts which can be determined by a chromatographic method. The method is shown to give comparable results with those of the breakthrough experiments. The simplicity of the experimental arrangement as well as the low cost and unattended operation offer a viable alternative to the conventional methods of the determination of capacity factors on SPE cartridges. Practical limitations of the proposed method are also considered.

1. Introduction

Sample preparation plays a vital role in the analysis of water samples. As modern analytical instruments are now powerful and highly sensitive, sample preparation has become the “bottleneck” of water analysis in several respects. It is generally the most laborious, time-consuming and least reliable part of the whole analytical procedure. Solid-phase extraction (SPE) has recently come into the focus of interest and offers a viable alternative to the conventional sample preparation methods. Yet many aspects of the reliability and reproducibility of this technique are awaiting to be clarified. Only a

thorough understanding of the critical parameters governing sorption–desorption can secure its efficient and reliable operation.

Although in water analysis there are many steps involved in a complete SPE procedure, one step, sorption from water, is of primary importance. Chromatographically this step of the solid-phase extraction procedure is frontal chromatography. If an aqueous solution of an analyte of c_0 concentration is pumped through a conditioned SPE cartridge and the effluent is monitored online, the curve recorded is known as frontal chromatogram or breakthrough curve as shown in Fig. 1.

From the breakthrough curve the retention volume of the analyte (V_R) can be determined as indicated in Fig. 1. The breakthrough volume (V_B) is usually defined as

* Corresponding author.

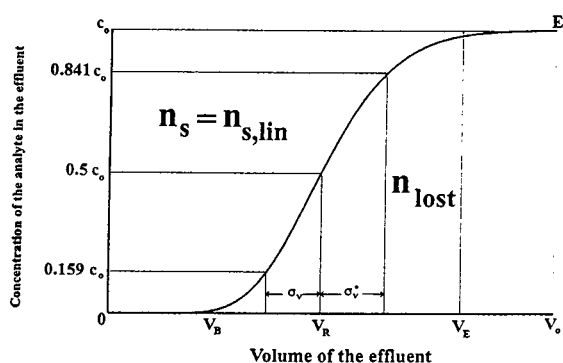


Fig. 1. A frontal chromatogram, the fundamental chromatographic parameters and graphical representation of the SPE preconcentration step.

$$V_B = V_R - 2 \cdot \sigma_V \quad (1)$$

where σ_V is the standard deviation of the derivative curve which can be determined graphically from the breakthrough curve as shown in Fig. 1. σ_V is in direct relation to the efficiency of the SPE column, i.e. the number of theoretical plates (N). Purnell [1] has shown that N can be calculated from the breakthrough curve using the equation

$$N = \frac{V_R \cdot (V_R - \sigma_V)}{\sigma_V^2} \quad (2)$$

Analogously, the equilibrium volume (V_E) can be defined as

$$V_E = V_R + 2 \cdot \sigma_V^* \quad (3)$$

where σ_V^* can be determined graphically from the breakthrough curve as shown in Fig. 1. Its value is usually different from that of σ_V because of the asymmetry of the breakthrough curves on SPE columns. The retention volume (V_R) can be expressed analytically by the fundamental equation of chromatography

$$V_R = V_M \cdot (1 + k) \quad (4)$$

where V_M is the hold-up volume of the SPE cartridge and k is the capacity factor of the solute. In solid-phase extraction there is a fundamental parameter, recovery (r) which can be directly related to the frontal chromatogram. By definition, the recovery of an analyte is the

amount of the analyte recovered after the SPE procedure, expressed in percentage of the total amount of the analyte originally present in the sample. The knowledge of this parameter allows the concentration of the analyte in the sample to be calculated from the concentration determined in the sample extract. In the case shown in Fig. 1 the total amount of the analyte originally present in the sample is the product of the analyte concentration and sample volume, $c_0 \cdot V_0$, graphically represented by the rectangle $0-V_0-E-c_0$ in Fig. 1. The amount lost (n_{lost}) due to breakthrough is graphically represented by the area under the breakthrough curve in Fig. 1. Consequently, the amount taken up by the SPE column (n_s) equals to the difference between the total amount and the amount lost, graphically corresponding to the area above the breakthrough curve within the rectangle of the total amount. In this special case it equals to the linear capacity of the column ($n_{s,lin}$) which can be expressed by the equation [2]

$$n_{s,lin} = V_M \cdot k \cdot c_0 \quad (5)$$

As can be seen from Eq. (5) $n_{s,lin}$ is dependent on both the capacity factor and the concentration of the analyte. The linear capacity, however, cannot be increased ad infinitum by increasing the concentration of the analyte because the concept of linear capacity applies only under the conditions of linear ideal chromatography [1], as the total capacity of a solid-phase extraction cartridge is limited by the amount of the stationary phase in the column. As against linear capacity, the total capacity is an ill-defined property of the column which is only referred to in broad qualitative terms. Deviations from linear adsorption isotherms can be observed if the linear capacity approaches the total capacity of the column. Nevertheless, for most environmental samples it is rather unlikely that in practical situations the total capacity of the sorbent is approached.

Provided that the extraction step governs primarily the recovery of an analyte with losses in other steps of the SPE procedure being negligible, the recovery (r) of the analyte can be expressed as

$$r = \frac{n_s}{c_0 \cdot V_0} \cdot 100\% \quad (6)$$

Based on the frontal chromatogram, two alternative strategies of solid-phase extraction can be distinguished. The first—probably the more popular—method is to achieve quantitative recoveries (within experimental error) by optimizing the volume and composition of the sample solution. In this case the amount of the analyte determined from the sample extract equals to the amount originally present in the sample. Thus the relatively large uncertainty accompanying the determination of recoveries will not contribute to the overall uncertainty of the whole SPE procedure. This mode of operation, however, is restricted only to volumes smaller than the breakthrough volume (V_B) of the least retained compound in the sample. As a result, the linear capacity of other, more strongly retained analytes remain far from being exploited. This mode can be the matter of choice if samples with high level of matrix interference have to be analyzed.

The other strategy of SPE operation, especially for less retained compounds, is to equilibrate the entire column with the sample solution by applying volumes safely in excess of their equilibrium volumes (V_E), as shown in Fig. 1. In this mode the recovery of the analyte will not be quantitative but the linear capacity of the column for the analyte will be fully exploited. Having determined the recoveries in separate recovery tests using spiked model solutions of the same volume, the concentrations of the analytes can be calculated.

In this “equilibrium” mode of solid-phase extraction the linear capacity of the column is exploited and the maximum degree of preconcentration is attained. Whichever mode is preferred, the knowledge of equilibrium (V_E) or breakthrough (V_B) volumes of each analyte is invaluable in method development for solid-phase extraction.

The most straightforward method for obtaining these parameters is to record the breakthrough curves experimentally [3]. This method is, however, quite laborious, time-consuming

and costly. Because of the low efficiency of the SPE cartridges, the breakthrough curves of analytes have to be recorded separately, requiring solutions of pure analytes and a number of SPE cartridges. With this method mutual interferences are difficult to characterize. Further difficulties may arise from the fact that the SPE cartridges are not designed to be operated on-line with a pump and a detector. Moreover, if the composition of the sample solution is changed, which is not unusual in the course of SPE method development, a new series of experiments will have to be carried out.

Prediction of retention or breakthrough values is much less laborious than the conventional experimental method. According to Eq. (4), these predictions are usually simplified to the estimation of capacity factors (k) of the analytes. To predict k values under the conditions of the preconcentration step, various relationships have been studied, based on the correlation between capacity factors and aqueous molar solubilities or octanol–water coefficients [4–6]. The major drawback of these methods is that these physico-chemical data are only available for pure water. In SPE practice, however, organic modifiers or inorganic salts are often added to the sample solution in order to increase the retention of the analytes. These compositions, unfortunately, cannot be characterized by predictions based on physico-chemical data.

Another approach to the prediction of capacity factors is to correlate chromatographic retention data on an analytical column with the same stationary phase at different isocratic organic–water mobile phase compositions [7,8]. As the relationship between the logarithm of the capacity factor and the volume fraction of the organic modifier (Φ) was found to be linear for phenolic compounds, the capacity factors of these solutes in pure water were determined by measuring their capacity factors at two mobile phase compositions and extrapolating to $\Phi = 0$. The extrapolated values were within 15% of the values determined from experimentally recorded breakthrough curves [8]. For other compounds the method proved to be less successful. The method was, however, applied to on-line trace

enrichment on short precolumns filled with particles of the same diameter as the analytical column. As SPE cartridges cannot be used in analytical elution mode due to their very low separation efficiency, extrapolation from retention data obtained on an analytical HPLC column with the same stationary phase can hardly provide an accurate estimate of the capacity factors of the analytes on SPE cartridges.

In this paper a simple experimental method for the rapid determination of capacity factors of phenolic compounds on off-line solid-phase extraction cartridges is described. The method is capable of providing experimental capacity factors at any sample composition. Theoretical approach is made to reveal the limitations of the method in terms of accuracy and precision. The results obtained are compared with those of independent breakthrough measurements.

2. Theory

The method is based on the equilibration of the solutes between the SPE cartridge and the model solution. The scheme of the equilibration process is depicted in Fig. 2. Exactly known volume of aqueous sample solution of known concentration of analytes is pumped through an SPE cartridge and the solution leaving the cartridge is recycled to the stirred solution. The process is finished when steady-state conditions are attained, i.e. the analytes are equilibrated between the stationary phase of the cartridge and the solution. Then the adsorbed amount of each analyte is determined by a chromatographic method. Alternatively, the concentrations of analytes can be determined directly in the solution by HPLC provided that the concentrations

are sufficiently high to facilitate direct determination.

In equilibrium, the capacity factor of an analyte on an SPE cartridge can be calculated as follows:

V_0 volume of aqueous solution is spiked with n_0 moles of an analyte and equilibrated with the stationary phase. If n_s moles of the analyte is adsorbed in the stationary phase of the cartridge and n_m moles is present in the mobile phase of the column hold-up volume V_M , the capacity factor of the analyte can be written as

$$k = \frac{n_s}{n_m} \quad (7)$$

If the concentration of the analyte in the mobile phase is denoted by c_m , then the overall material balance can be formulated as

$$n_0 = n_s + c_m \cdot (V_0 + V_M) \quad (8)$$

which, after rearrangement, yields

$$c_m = \frac{n_0 - n_s}{V_0 + V_M} \quad (9)$$

n_m can be expressed as the product of the mobile phase concentration and the column hold-up volume

$$n_m = c_m \cdot V_M \quad (10)$$

By substituting Eq. (9) into Eq. (10) we obtain

$$n_m = V_M \cdot \frac{n_0 - n_s}{V_0 + V_M} \quad (11)$$

and finally, substituting Eq. (11) into the expression for the capacity factor (7) we have

$$k = \frac{n_s \cdot (V_0 + V_M)}{V_M \cdot (n_0 - n_s)} \quad (12)$$

This expression for the capacity factor contains only known or measurable quantities: V_0 , n_0 , V_M are initially known and n_s is determined by a chromatographic method after elution of the cartridge.

Alternatively, if c_m can be determined directly from the sample solution, the following equation can be derived

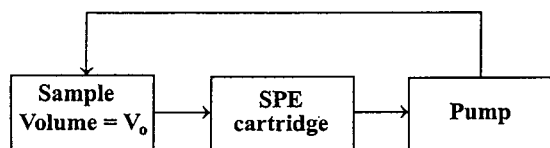


Fig. 2. Scheme of the equilibration process.

$$k = \frac{n_0 - c_m \cdot (V_0 + V_M)}{c_m \cdot V_M} \quad (13)$$

The method is purely an equilibration process and the ultimate goal of this technique is not to achieve separation in the conventional sense but to establish equilibrium of the solutes between the stationary phase of the cartridge and the bulk of the sample solution.

In order to ensure that conditions of linear ideal chromatography hold, the concentrations of the analytes have to be carefully chosen. The individual concentrations have to be sufficiently high to facilitate reliable analytical quantification but the total amount of analytes must remain far inferior to the total capacity of the cartridge.

The time—or preferably the volume pumped through the cartridge—required for attaining steady-state conditions in the system is of primary importance. Its knowledge is necessary to decide whether the calculations are valid, i.e. equilibrium conditions hold. The course of the equilibration process is modelled by Purnell's discontinuous model based on the theoretical plate concept [1]. The input parameters of the model are the initial volume of the sample solution (V_0), the void volume of the cartridge (V_M), the number of theoretical plates of the cartridge (N , determined from experimental breakthrough curves) and the value of the capacity factor (k). The model calculates the concentration of the analyte in the stirred flask (c_1) as a function of the volume pumped through the cartridge. The concentration is expressed in the percentage of the theoretical concentration of analyte ($c_{1,E}$) in the stirred flask as calculated from the input capacity factor assuming equilibrium conditions. The course of the concentration as a function of the volume of the sample solution pumped through the cartridge is depicted in Fig. 3. As it can be seen from the figure, infinite volume would be required for attaining the theoretical (equilibrium) concentration, but a practical equilibrium volume (V_{PE}) may be obtained when $c_1(V)$ approaches its theoretical value within a relative error of 2% (see Fig. 3). If V_{PE} is plotted as a function of the capacity factor, the curve shown in Fig. 4 is

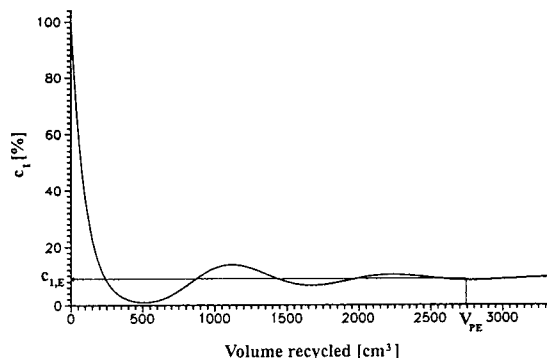


Fig. 3. Modelled course of the concentration of the bulk solution as a function of the volume pumped through the cartridge at a capacity factor of 1250. Sample volume is 100 ml.

obtained. It is obvious from this figure that the application of this technique to compounds with high capacity factors on the cartridge can be impractical due to the excessive volume required to reach equilibrium. The large volume pumped through the cartridge corresponds to prolonged time of the experiment which may result in undesirable loss of analytes due to degradation or other deleterious processes.

The determination of higher capacity factors has another serious limitation. By rearranging Eq. (12) we have

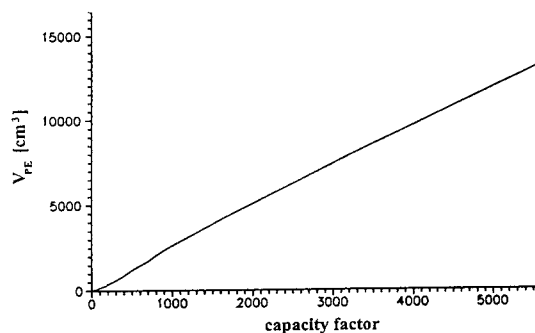


Fig. 4. The calculated volume required to reach equilibrium within a relative error of 2% as a function of capacity factor at a sample volume of 100 ml.

$$n_s \cdot (V_0 + V_M + k \cdot V_M) = k \cdot n_0 \cdot V_M \quad (14)$$

and the ratio of the adsorbed amount to the total amount can be expressed as

$$\frac{n_s}{n_0} = \frac{k \cdot V_M}{V_0 + V_M + k \cdot V_M} \quad (15)$$

Fig. 5 shows this ratio as a function of capacity factor at two different sample volumes. According to Eq. (15) there is only one experimental parameter which can influence the shape of the curve, the sample volume (V_0). In the region of small k values the smaller sample volume is advantageous as it gives better sensitivity, i.e. higher slope value. In this case, however, the working range is quite limited by the worsening sensitivity at larger k values. With the larger sample volume the sensitivity is initially lower, but the working range is somewhat broader. The selection of the experimental sample volume requires compromise between sensitivity and working range. As the relative error of the determination of the adsorbed amount is rarely less than 2%, for capacity factors in excess of 1500 the method may at best give rough estimates due to the excessively large standard deviations accompanying the determination of k . If, however, c_m can be determined directly from

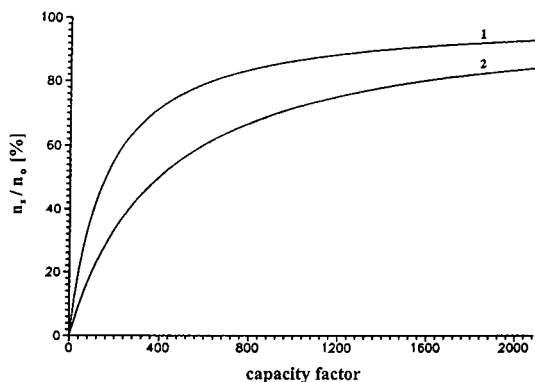


Fig. 5. The ratio of adsorbed amount to the total amount as a function of capacity factor, as calculated from Eq. (15). Lines: (1) $V_0 = 100$ ml; (2) $V_0 = 250$ ml.

the sample solution with the same precision, this limitation is normally not imposed.

3. Experimental

3.1. Conditions

Reagents

Phenol (99.0%), 4-methylphenol (99.4%), 4-chlorophenol (99.0%), 3,4-dimethylphenol (98.0%), 2,4-dichlorophenol (99.0%) and 2,4,6-trichlorophenol (97.0%) were obtained from Supelco (Switzerland). Methanol (HPLC grade) was purchased from ROMIL (UK), hydrochloric acid from Reanal (Hungary). All reagents were used as received without further purification.

The cartridge used was Waters SEP-PAK C18 Plus, 360 mg sorbent weight, 0.7 ml nominal hold-up volume, purchased from Waters Millipore Division, USA. All cartridges were activated with 3 ml of methanol then conditioned with 3 ml of 10^{-3} M hydrochloric acid.

Instrumentation

Breakthrough curves were acquired with a Jasco PU-980 HPLC pump and a Perkin-Elmer LC-55 UV detector. All measurements were performed at 220 nm. Data acquisition was made by Waters Maxima 820 chromatographic software.

GC-MS analysis was carried out with a TRIO-1000 instrument of FISONs (UK). The column was SPB-1 fused silica, 30 m, 0.32 mm I.D., 0.25 μ m film thickness, purchased from Supelco. The chromatographic conditions were: injector temperature 280°C, interface temperature 285°C. The temperature program was 55°C for 1 min, 4.0°C/min to 170°C and 15°C/min to 280°C. 1 μ l was injected in splitless mode, the split valve was opened 30 s after the injection. The MS was operated in selected-ion recording mode in EI. The ion source temperature was 180°C. The following ions were monitored in the retention windows: 94, 107, 122, 128, 162 and 196 amu for phenol, 4-methylphenol, 3,4-dimethylphenol, 4-chlorophenol, 2,4-dichlorophenol and 2,4,6-trichlorophenol, respectively.

Procedures

A stock solution of phenols was prepared in methanol in a 10-ml calibrated flask. The concentrations of the individual compounds in methanol were: 1.34, 1.03, 0.99, 0.96, 0.97 and 0.89 mg/ml for phenol, 4-methylphenol, 3,4-dimethylphenol, 4-chlorophenol, 2,4-dichlorophenol and 2,4,6-trichlorophenol, respectively. This solution was used for all experiments except the recording of the breakthrough curves where the stock solutions of the individual compounds in methanol were used at concentrations of approximately 1 mg/ml.

For the acquisition of each breakthrough curve a solution of the individual compound was prepared in 10^{-3} M hydrochloric acid at a concentration of approximately 1 μ g/ml. The cartridge was fixed in a brass threaded casing. A flow rate of 1.5 ml/min was set and the tubing was filled with the sample solution up to the cartridge inlet. Then the pump was started and measurements begun.

For the equilibration experiments 10^{-3} M of hydrochloric acid was spiked with 10 μ l of stock solution and thoroughly homogenized in a calibrated flask of 100.0 ml. This sample solution was filled in a 120 ml Teflon flask on top of a magnetic stirrer. The cartridge was connected to the tubing of the proportioning pump then immersed into the sample solution. The outlet end of the proportioning pump was connected with Teflon tubing to the flask containing the sample solution thus forming a closed loop. The flow rate was measured before the start and after the end of the experiment. The system was left running for 16 hours and the volume passing the cartridge was determined as a product of the average flow rate and the duration of the experiment.

The cartridge was dried with nitrogen at a flow rate of approximately 100 ml/min for 15 min then eluted with 3 times 0.5 ml methanol. The eluate was collected in a 2-ml calibrated sample vial and filled to the mark with methanol. The extract was then homogenized and injected into the GC-MS.

Four calibration solutions were prepared in methanol with 10 μ l of stock solution in 2-, 5-,

10- and 25-ml calibrated vials and flasks. Each solution was injected three times and the calibration curve was recorded. The regression coefficients of all curves were above 0.998.

The hold-up volume of the cartridges was determined by measuring the weight difference of the dry and conditioned cartridges. Five replicate measurements were made and the cartridge void volume was determined as the average of the five measurements, and was found to be 0.653 ± 0.023 ml.

4. Results and discussion

Breakthrough curves were obtained for all compounds and retention volumes (V_R) as well as σ_V values were determined graphically from the curves. Breakthrough volumes (V_B), number of theoretical plates (N) and capacity factors (k) were calculated according to Eqs. (1), (2) and (4), respectively. These parameters are listed in Table 1.

For the model calculation of the practical equilibrium volume (V_{PE}), the average number of theoretical plates (15) was considered. Its value for the most strongly retained compound, 2,4,6-trichlorophenol, was determined from Fig. 4 and was found to be 2500 ml. To make assurance double sure, a 16-hour equilibrium period was chosen for the experiments with an average flow rate of 3.3 ml/min, corresponding to a volume of 3200 ml. Three parallel equilibration experiments were carried out with a sample volume of 100.0 ml. The cartridges were then eluted and extracts were analyzed by GC-MS. Each extract was injected in triplicate. The average of the adsorbed amounts, in percentage of the spiked amounts and their relative standard deviations, the calculated capacity factors and their 95% confidence intervals together with the capacity factors determined in the breakthrough experiments are summarized in Table 2.

The results of the equilibration experiments are fairly close to the values determined from breakthrough curves implying that the prerequisites for calculations were met. A somewhat larger difference can be observed for 2,4,6-tri-

Table 1
The basic chromatographic parameters of the compounds obtained in breakthrough experiments

Compound	V_R (ml)	σ_v (ml)	V_B (ml)	N	k
Phenol	15.2	3.8	7.6	12	22.3
4-Methylphenol	48.9	10.8	27.3	16	73.9
4-Chlorophenol	62.9	13.5	35.9	17	95.3
3,4-Dimethylphenol	132	29.0	74	16	201
2,4-Dichlorophenol	259	53.4	152	18	395
2,4,6-Trichlorophenol	720	174	372	13	1100

chlorophenol, a compound with relatively large capacity factor. The equilibration experiment seems to underestimate its value by 20%. This finding, however, is in accordance with the theoretical considerations, i.e. at such a large capacity factor any small inaccuracy of the determination of the adsorbed amount will introduce considerable bias into the calculated value of the capacity factor. In spite of the fact that the R.S.D.% values of the adsorbed amounts of analytes are considerably smaller for the more strongly retained solutes, the same parameters of their calculated capacity factors are larger as a result of the lower sensitivity in the region of large capacity factors.

For practical purposes, the precision attainable by the proposed method even for the 2,4,6-trichlorophenol is satisfactory. On the other hand, the values obtained from breakthrough experiments may also be subject to small variations, but their statistical evaluation is quite tedious. Nevertheless the good agreement be-

tween the results of the two independent experiments suggests that the equilibration method can provide reliable estimates of capacity factors of phenolic compounds on solid-phase extraction cartridges. There is an implication that the method —*mutatis mutandis*— can be used for other types of compounds as well. The simplicity of the experimental arrangement as well as the low cost and unattended operation may offer a viable alternative to the conventional methods of the determination of capacity factors on off-line SPE cartridges.

Acknowledgements

The authors are grateful to Lajos Gáspár and Péter Ágh for their indispensable technical assistance. The financial support from OTKA A 167 for purchasing the GC–MS and from OTKA 2561 for financing the project is also gratefully acknowledged.

Table 2

The average adsorbed amounts of analytes in percentage of the total amounts and their relative standard deviations obtained in equilibration measurements, the capacity factors with their 95% confidence intervals calculated from the adsorbed amounts and the capacity factors determined in breakthrough experiments.

Compound	n_s (R.S.D.%)	$k_{\text{equilibration}}$	$k_{\text{breakthrough}}$
Phenol	12.4 (5.6)	21.8 ± 1.7	22.3
4-Methylphenol	30.9 (6.1)	69.0 ± 7.5	73.9
4-Chlorophenol	38.0 (2.6)	94.5 ± 4.9	95.3
3,4-Dimethylphenol	52.7 (4.4)	172 ± 21	201
2,4-Dichlorophenol	74.3 (2.2)	450 ± 50	395
2,4,6-Trichlorophenol	85.2 (1.5)	894 ± 124	1100

References

- [1] H. Purnell, *Gas Chromatography*, Wiley, New York, 1962.
- [2] I. Liska, J. Krupcik and P.A. Leclercq, *J. High Res. Chromatogr.*, 12 (1989) 577.
- [3] R.E. Shoup and G.S. Mayer, *Anal. Chem.*, 54 (1982) 1164.
- [4] M.E. Thurman, R.L. Malcolm and G.R. Aiken, *Anal. Chem.*, 50 (1978) 775.
- [5] G.M. Josefson, J.B. Johnson and R. Trubey, *Anal. Chem.*, 56 (1984) 764.
- [6] S. Bitteur and R. Rosset, *J. Chromatogr.*, 394 (1987) 279.
- [7] P.J. Schoenmakers and H.A.H. Billiet, *J. Chromatogr.*, 205 (1981) 13.
- [8] C.E. Werkhoven-Goewie, U.A.Th. Brinkman and R.W. Frei, *Anal. Chem.* 53 (1981) 2072.



ELSEVIER

Journal of Chromatography A, 693 (1995) 227-233

JOURNAL OF
CHROMATOGRAPHY A

The role of capacity factor in method development for solid-phase extraction of phenolic compounds. II

András Gelencsér^a, Gyula Kiss^a, Zoltán Krivácsy^b, Zita Varga-Puchony^b,
József Hlavay^{a,*}

^aDepartment of Analytical Chemistry, University of Veszprém, P.O. Box 158, H-8201 Veszprém, Hungary

^bResearch Group of Analytical Chemistry, Hungarian Academy of Sciences, P.O. Box 158, H-8201 Veszprém, Hungary

First received 30 August 1994; revised manuscript received 9 November 1994

Abstract

Recently, a simple method was developed for the determination of capacity factors of phenolic compounds on solid-phase extraction cartridges [*J. Chromatogr. A*, 693 (1995) 217]. In the present paper the capacity factors determined by this method are used to predict recoveries of phenolic compounds in solid-phase extraction at three different sample volumes. The values are compared with those of recovery tests from both model solutions and spiked surface water samples. Based on calibration data the minimum sample concentrations which can be determined by the SPE procedure are also calculated from the capacity factors.

1. Theory

1.1. Calculation of recoveries from chromatographic data

The capacity factors determined by the equilibration method [1] can be used to predict the recoveries of phenolic compounds in solid-phase extraction at any sample volume. The knowledge of the experimentally determined capacity factors should by no means replace the conventional recovery tests required for SPE method development. It, however, guides through the time-consuming procedure of the selection of the appropriate stationary phase and the optimization of sample composition and volume. The fact that the precision of the method is limited for strongly retained solutes, does

not restrict the applicability of the method since optimization primarily focuses on the least retained substances.

In order to predict recoveries from capacity factors the basic chromatographic parameters have to be calculated. The retention volume (V_R) is obtained from the basic equation of chromatography

$$V_R = V_M \cdot (1 + k) \quad (1)$$

where V_M is the void volume of the cartridge and k is the capacity factor of the solute. σ_v is determined as

$$\sigma_v = \frac{V_M}{N^{1/2}} \cdot (1 + k) \quad (2)$$

where N is the number of theoretical plates of the cartridge.

* Corresponding author.

The breakthrough volume (V_B) is calculated using the equation

$$V_B = V_R - 2 \cdot \sigma_V \quad (3)$$

Based on the considerations given in Part I, for the solutes having a breakthrough volumes (V_B) larger than the sample volume (V_0), quantitative recovery (100%) is expected within experimental error. For the solutes for which the sample volume is in excess of $V_R + 2 \cdot \sigma_V$, the recovery (r) can be calculated as

$$r = \frac{V_M \cdot k}{V_0} \cdot 100\% \quad (4)$$

In case the sample volume falls between V_B and $V_R + 2 \cdot \sigma_V$ of an analyte, the recovery cannot be calculated analytically, though error (erf) functions which are available in tabulated form can be used to estimate recoveries. As an alternative to these calculations, a simple computer model based on the theoretical plate concept was developed. It established the breakthrough curve from the input parameters of the capacity factor, void volume and number of theoretical plates of the cartridge. The amount lost was determined by numerical integration then the recovery was calculated. If the calculated recovery is plotted as a function of sample volume normalized to V_R between V_B and $V_R + 2 \cdot \sigma_V$ for three different values of capacity factor, the curves shown in Fig. 1 are obtained.

It is interesting to note that the curves are approaching a single curve by increasing the capacity factor as the column void volume is becoming negligible compared to the retention volume.

Thus the recoveries can be predicted for any sample volume under the conditions of the experiment. These values, however, may at best be rough estimates of experimental recoveries determined from conventional recovery tests and should not be relied on as true values to be used in the analysis of samples. Ideally, they represent the theoretically attainable recoveries under the given conditions. The knowledge of the predicted recoveries, however, may assist in revealing the major sources of error in an SPE pro-

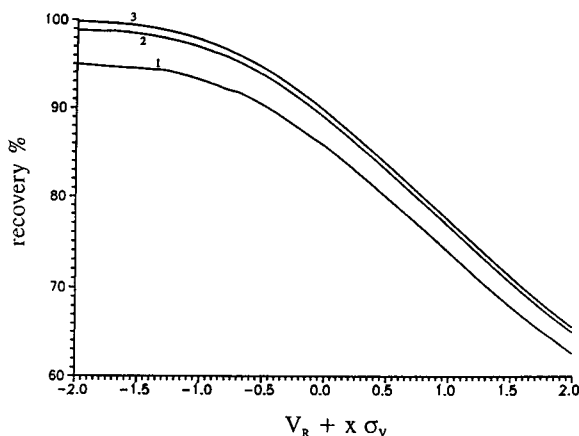


Fig. 1. Recovery as a function of normalized sample volume between $V_R - 2 \cdot \sigma_V$ and $V_R + 2 \cdot \sigma_V$ for capacity factors of 10, 100 and 1000. Lines: (1) $k = 10$; (2) $k = 100$; (3) $k = 1000$.

cedure. If the recovery tests yield recoveries significantly higher than predicted for a compound, either the capacity factor was incorrectly determined or some matrix constituent interferes. Significant negative departures from the predicted values, on the other hand, may indicate competition between the solutes and the matrix interferences or losses in other steps of the SPE procedure.

1.2. Calculation of minimum sample concentrations

From the experimental capacity factors the minimum sample concentrations which can be determined by the SPE method can also be calculated. These concentrations are usually different for each compound as the limits of detection and the attainable enrichment factors are different. In the calculations it was assumed that the sample volume was selected so that the maximum attainable enrichment factor was exploited for each compound, i.e. the sample volume was in excess of $V_R + 2 \cdot \sigma_V$ for each solute.

Recovery (r) is defined as

$$r = \frac{c_f \cdot V_f}{c_0 \cdot V_0} \cdot 100\% \quad (5)$$

where c_f and V_f are the concentration and volume of the final extract, respectively, c_0 is the sample concentration, and V_0 is the sample volume.

By substituting Eq. (4) into Eq. (5) we obtain

$$c_0 = \frac{c_f \cdot V_f}{k \cdot V_M} \quad (6)$$

In an optimized solid-phase extraction procedure V_M and V_f are constant and k is fixed for each compound, therefore c_f is in direct proportion to the sample concentration (c_0). If c_f represents the minimum concentration which can be quantified in the extract by the chromatographic technique (corresponding to a signal-to-noise ratio of 10:1), c_0 stands for the minimum concentration which can—at best—be quantified by the whole SPE procedure. Similarly, if c_f is the minimum detectable concentration in the extract (corresponding to a signal-to-noise ratio of 3:1), c_0 represents the minimum concentration in the sample which can—at best—be detected by the whole SPE procedure.

It should be emphasized, however, that c_0 in either case is a theoretical limit under which the analyte cannot be detected or quantified by the given SPE method whatsoever. Its value can be approached for the least retained compounds but can hardly be realized for the most strongly retained solutes.

2. Experimental

2.1. Conditions

2.2. Reagents

Phenol (99.0%), 4-methylphenol (99.4%), 4-chlorophenol (99.0%), 3,4-dimethylphenol (98.0%), 2,4-dichlorophenol (99.0%) and 2,4,6-trichlorophenol (97.0%) were obtained from Supelco (Switzerland). Methanol (HPLC grade) was purchased from ROMIL (UK), *n*-hexane from Aldrich (Germany), hydrochloric acid from Reanal (Hungary). Turbine oil standard was received from the power plant involved. All

reagents were used as received without further purification.

The cartridges used were Waters SEP-PAK C18 Plus, 360 mg sorbent weight, 0.7 ml nominal hold-up volume, purchased from Waters Millipore Division, USA. All cartridges were activated with 3 ml methanol then conditioned with 3 ml of 10^{-3} M hydrochloric acid.

2.3. Instrumentation

GC-MS analysis was carried out with a TRIO-1000 instrument of FISON (UK). The column was SPB-1 fused silica, 30 m, 0.32 mm I.D., 0.25 μ m film thickness, purchased from Supelco. The chromatographic conditions were: injector temperature 280°C, interface temperature 285°C. The temperature program was: 55°C for 1 min, 4.0°C/min to 170°C and 15°C/min to 280°C. 1 μ l was injected in splitless mode, the split valve was opened 30 s after the injection. The MS was operated in selected-ion recording mode in EI. The ion source temperature was 180°C. The following ions were monitored in the retention windows: 94, 107, 122, 128, 162 and 196 amu for phenol, 4-methylphenol, 3,4-dimethylphenol, 4-chlorophenol, 2,4-dichlorophenol and 2,4,6-trichlorophenol, respectively.

For the determination of potential matrix interferences the following GC conditions were set: injector temperature: 315°C interface temperature 315°C. The temperature program applied was: 45°C for 1 min, 15.0°C/min to 200°C, 5.0°C/min to 310°C, 30 min hold. The MS was operated in EI full scan mode, between 20–300 amu, with 0.9 s scan time and 0.1 s interscan time.

2.4. Procedures

A stock solution of phenols was prepared in methanol in a 10-ml calibrated flask. The concentrations of the individual compounds in methanol were: 1.34, 1.03, 0.99, 0.96, 0.97 and 0.89 mg/ml for phenol, 4-methylphenol, 3,4-dimethylphenol, 4-chlorophenol, 2,4-dichlorophenol and 2,4,6-trichlorophenol, respectively.

In the recovery tests, distilled water was

spiked with 10 μ l of stock solution, acidified with 1 M hydrochloric acid to pH = 3.0 then thoroughly homogenized in a calibrated flask of 100, 250 and 500 ml. The sample solution was passed through the cartridge at a flow rate of 3.5 ml/min. The cartridge was dried with nitrogen at a flow rate of approximately 100 ml/min for 15 min then eluted with three times 0.5 ml of methanol. The eluate was collected in a 2-ml calibrated sample vial and filled to the mark with methanol. The extract was then homogenized and injected into the gas chromatograph.

Six calibration solutions were prepared in methanol with 10 μ l of stock solution in 2-, 5-, 10-, 25-, 50- and 100-ml calibrated vials and flasks. Each solution was injected three times and the calibration curves were recorded. The minimum concentrations of the compounds which can be quantified in the extract were determined as the lowest concentrations which can be quantified in the calibration. The regression coefficients of all curves in the established ranges were above 0.996.

The surface water sample used for the spiking experiments was lake water filtered through a glass microfibre filter GF/D-GF/F. The recovery tests described above were repeated using this filtered water.

The determination of matrix interferences was carried out as follows: 100 ml of filtered lake water was passed through a pre-conditioned SPE cartridge. The cartridge was dried with nitrogen at a flow rate of approximately 100 ml/min for

15 min then eluted with 4.5 ml of *n*-hexane. The eluate was collected in a 5.0-ml calibrated flask and filled to the mark with the *n*-hexane. The extract was then homogenized and injected into the gas chromatograph under the conditions specified above.

For calibration 100 mg of turbine oil standard was weighed into a calibrated flask of 100 ml and dissolved in *n*-hexane. 5, 10 and 20 μ l of this stock solution were added to distilled water in calibrated flasks of 100 ml. These solutions were subjected to the procedure of solid-phase extraction as described above.

3. Results and discussion

3.1. Comparison of calculated and experimental recoveries

The experimentally determined recoveries and their 95% confidence intervals together with the predicted recoveries and their 95% confidence intervals for sample volumes of 100, 250 and 500 ml are summarized in Table 1.

As can be seen from the results, in general good agreement can be observed between the predicted and the experimental values. In some cases the differences are not even statistically significant. This is not surprising in the light of the fact that the recovery tests and the determination of capacity factors were carried out under identical conditions with the exception of sample

Table 1
Experimental and calculated recoveries for sample volumes of 100, 250 and 500 ml in the experiments with model solutions

Compound	Sample volume (ml)					
	100		250		500	
	r_{exp} (%)	r_{calc} (%)	r_{exp} (%)	r_{calc} (%)	r_{exp} (%)	r_{calc} (%)
Phenol	12.1 \pm 2.4	14.9 \pm 1.1	8.1 \pm 1.8	6.0 \pm 0.7	2.8 \pm 0.9	3.1 \pm 0.3
4-Methylphenol	47.9 \pm 3.1	45.7 \pm 4.9	18.1 \pm 2.3	18.3 \pm 1.9	8.7 \pm 1.1	9.2 \pm 0.9
4-Chlorophenol	70.4 \pm 3.6	68.5 \pm 3.2	25.1 \pm 2.4	27.3 \pm 1.5	14.0 \pm 1.0	13.6 \pm 0.7
3,4-Dimethylphenol	90.1 \pm 4.0	93.1 \pm 3.1	41.7 \pm 3.2	45.2 \pm 5.1	24.5 \pm 1.8	22.6 \pm 2.7
2,4-Dichlorophenol	97.6 \pm 3.2	100	90.2 \pm 3.7	94.7 \pm 2.5	62.3 \pm 3.1	59.0 \pm 6.5
2,4,6-Trichlorophenol	98.3 \pm 2.7	100	98.5 \pm 2.5	99.8 \pm 0.2	91.6 \pm 2.0	95.3 \pm 1.6

Table 2

Experimental and calculated recoveries for sample volumes of 100, 250 and 500 ml in the experiments with spiked surface water

Compound	Sample volume (ml)					
	100		250		500	
	r_{exp} (%)	r_{calc} (%)	r_{exp} (%)	r_{calc} (%)	r_{exp} (%)	r_{calc} (%)
Phenol	10.2 ± 3.4	14.9 ± 1.1	5.8 ± 1.9	6.0 ± 0.7	2.3 ± 1.3	3.1 ± 0.3
4-Methylphenol	45.5 ± 3.6	45.7 ± 4.9	15.3 ± 2.7	18.3 ± 1.9	6.5 ± 1.6	9.2 ± 0.9
4-Chlorophenol	63.1 ± 3.8	68.5 ± 3.2	20.2 ± 2.4	27.3 ± 1.5	10.3 ± 2.1	13.6 ± 0.7
3,4-Dimethylphenol	86.2 ± 4.7	93.1 ± 3.1	32.0 ± 3.9	45.2 ± 5.1	17.3 ± 2.0	22.6 ± 2.7
2,4-Dichlorophenol	95.1 ± 5.3	100	91.7 ± 4.4	94.7 ± 2.5	51.5 ± 4.5	59.0 ± 6.5
2,4,6-Trichlorophenol	97.1 ± 3.1	100	98.3 ± 3.2	99.8 ± 0.2	88.6 ± 2.9	95.3 ± 1.6

concentrations which varied in the recovery tests.

In order to study the effect of sample matrix on the accuracy of prediction, the recovery tests described above were repeated with spiked surface water. None of the analytes were detected in the blank sample. The experimentally determined recoveries and their 95% confidence intervals together with the predicted recoveries and their 95% confidence intervals —by analogy with Table 1— for each sample volume are summarized in Table 2.

As it can be seen from the data, the experimental values are in nearly all cases lower than the predicted ones implying that the virtual

capacity of the cartridge (the amount of the accessible stationary phase) was reduced. It may be explained by the presence of interfering compounds dissolved in the water which can be more strongly bound to the apolar octadecyl chain than the more polar phenols, decreasing the volume of stationary phase available for the analytes.

In order to determine the possible interfering compounds the total ion chromatogram (TIC) of the filtered lake water sample was acquired which is shown in Fig. 2.

The major compounds identified were homologues of *n*-alkanes and alkylsiloxanes. As the water of the lake, from which the samples were

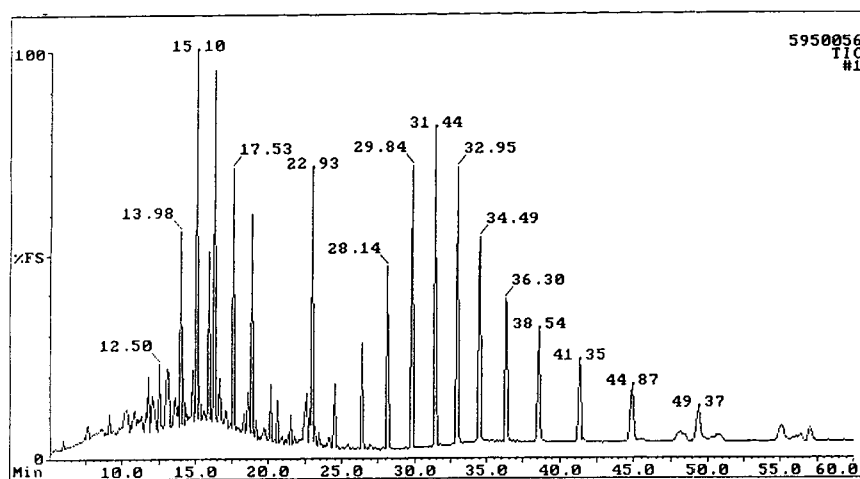


Fig. 2. Total ion chromatogram of the extract of 100 ml lake water.

taken, was suspected to be polluted by oil spillage from a nearby power plant, the experiments were repeated with solutions of the suspected oil standard (see Experimental). The ion chromatograms of 85 amu of the standard and the lake water samples are compared in Fig. 3.

As is obvious from this figure, the major source of pollution was positively identified allowing the estimation of the concentration of the oil in the water without the identification and quantification of the individual compounds. This was accomplished by calibration using the solutions of the oil standard of different concentrations. The calibration and quantification was based on several major peaks in the ion chromatograms. The concentration of the oil in the water sample was found to be $117 \pm 23 \mu\text{g/l}$ (at 95% level of confidence).

It is interesting to note that the amount of oil loaded onto the cartridge even with the sample volume of 500 ml is far inferior to the total capacity of the cartridge, which is reportedly in the ten milligram range [2]. Nevertheless, significant losses of the analytes can be observed in the recovery tests, especially with the larger sample volumes. This may be accounted for by the presence of other compounds, mainly of biological origin, which were not detected in the sample but may also compete with the analytes.

Table 3

Minimum concentrations of phenolic compounds which can be quantified in the final extract ($c_{f,\text{min}}$) and in the sample by the given SPE method ($c_{0,\text{min}}$)

Compound	$c_{f,\text{min}}$ ($\mu\text{g/l}$)	$c_{0,\text{min}}$ ($\mu\text{g/l}$)
Phenol	270	38 ± 3.0
4-Methylphenol	210	9.1 ± 1.0
4-Chlorophenol	380	12 ± 0.6
3,4-Dimethylphenol	200	3.5 ± 0.5
2,4-Dichlorophenol	390	2.6 ± 0.3
2,4,6-Trichlorophenol	360	1.2 ± 0.2

Whatever is the reason for the differences between the experimental and calculated recoveries, it can be concluded that although the estimation of recoveries can be useful in some cases, the analytical practice should not lack the comprehensive study of matrix effect in method development for solid-phase extraction.

3.2. Determination of minimum sample concentration

The minimum concentrations of the compounds which can be quantified from the extract ($c_{f,\text{min}}$) as determined from the calibration are shown in Table 3.

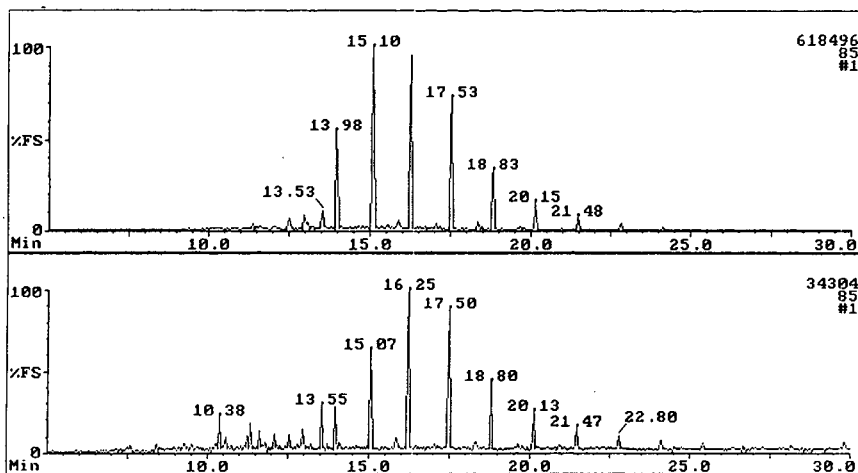


Fig. 3. Ion chromatograms of 85 amu of the extract of 100 ml lake water (top) and the extract of 100 ml oil standard solution of $100 \mu\text{g/l}$ (bottom).

From these concentrations and the experimental capacity factors determined for the compounds the minimum concentrations which can be quantified in the sample ($c_{0,\min}$) by the SPE method were calculated by Eq. (6). These values are also given in Table 3 together with their 95% confidence intervals.

As can be seen from the table, the minimum concentrations of phenolic compounds in the sample which can be quantified by the given SPE method are in the low $\mu\text{g/l}$ range. The worsening sensitivities for the compounds of higher molecular mass are compensated by the higher enrichment factors attainable for these solutes.

The sensitivity of the whole SPE procedure can be enhanced either by the evaporation of the solvent (reducing V_f) or increasing the sensitivity of detection (increasing $c_{i,\min}$).

In summary we can conclude that the knowledge of the capacity factors allows the estimation of the minimum concentrations of phenolic compounds in the sample which can be quantified by the given SPE method. Although the paper referred only to a limited number of phenolic compounds and a single SPE cartridge, the considerations presented can be applied

—mutatis mutandis— for other types of compounds and cartridges as well. The knowledge of the minimum concentrations in the sample which can be quantified by the given SPE method can save a great deal of research effort and may contribute to the procedure of SPE method development. It should not replace, however, the experimental determination of the limit of determination of the SPE method.

Acknowledgement

The financial support from OTKA A 167 for purchasing the GC-MS and from OTKA 2561 for financing the project is gratefully acknowledged.

References

- [1] A. Gelencsér, Gy. Kiss, Z. Krivácsy, Z. Varga-Puchony and J. Hlavay, *J. Chromatogr. A*, 693 (1995) 217.
- [2] M. Zief and R. Kiser, *Solid Phase Extraction for Sample Preparation*, J.T. Baker, 1988.



ELSEVIER

Journal of Chromatography A, 693 (1995) 235–239

JOURNAL OF
CHROMATOGRAPHY A

Silver ion high-performance liquid chromatography of esters of isomeric octadecenoic fatty acids with short-chain monounsaturated alcohols

Boryana Nikolova-Damyanova^{a,1}, William W. Christie^{a,*}, Bengt Herslöf^b

^a*The Scottish Crop Research Institute, Invergowrie, Dundee, Scotland DD2 5DA, UK*

^b*Karlsamns LipidTeknik AB, P.O. Box 6686, S-11384 Stockholm, Sweden*

First received 15 August 1994; revised manuscript received 1 December 1994; accepted 5 December 1994

Abstract

The retention characteristics of a series of positionally isomeric octadecenoic acids, derivatized with allyl, butenyl, pentenyl and hexenyl alcohols, were studied by high-performance liquid chromatography on an ion-exchange column loaded with silver ions. For a given isomer the retention factor, k' , increased with the distance of the double bond in the alcohol moiety from the ester group. The general retention patterns of butenyl, pentenyl and hexenyl esters were similar to those of methyl and phenacyl esters of the same series of isomeric fatty acids. Allyl esters differed in that the effect of double bond position in the fatty acid backbone on retention was weak. The results support the earlier suggestion for simultaneous interaction between one silver ion and one double and one electron-donating atom or group, presumed to be oxygen co-ordinating with silver ions through its free electron pairs.

1. Introduction

In previous papers [1,2], we described the retention characteristics of methyl, phenacyl and phenethyl derivatives of unsaturated fatty acids on high-performance liquid chromatography in either the silver ion (Ag-HPLC) or the combined silver ion and reversed-phase modes. With the former, the results were broadly comparable to those given by silver ion thin-layer chromatography (Ag-TLC) [3,4] in that a distinctive effect of double bond position on retention of isomeric

octadecenoates was established. Appreciable differences in retention of positionally isomeric octadecenoates in dependence of the nature of the derivative were also observed. The part of the molecule which contains the ester moiety is more important than the terminal end for resolution. Based on these results some interesting practical separations were achieved of the phenacyl esters of the three naturally occurring octadecenoate isomers, petroselinic (6–18:1), oleic (9–18:1) and vaccenic (11–18:1), by Ag-TLC as well as HPLC [1,5].

Three possible interactions were proposed for the retention mechanism: (i) the ability of a silver ion to interact with more than one coordination centre [6] —these could be either two

* Corresponding author.

¹ Present address: Institute of Organic Chemistry, Centre of Phytochemistry, Sofia 113, Bulgaria.

double bonds in the fatty acid molecule or one double bond and free electron pairs on an oxygen (or another electron-rich part) of the ester moiety; (ii) different and specific conformations of the fatty acid molecule which expose the double bond(s) in a more favourable way to complex with a silver ion; (iii) participation of the ester moiety in a separate polar interaction with the residual silanol groups on the support material. All three mechanisms are possible and could act simultaneously, although the magnitudes of each may be very different. In order to understand these interactions better we extended the range of derivatives and studied the retention of their esters with monounsaturated short-chain fatty alcohols under the conditions of Ag-HPLC.

2. Experimental

2.1. Materials

Reagents were analytical grade and were purchased from Sigma (Poole, UK). HPLC-grade or analytical-grade solvents (FSA Scientific Apparatus, Loughborough, UK) were used without further purification. The isomeric *cis*-octadecenoates had been prepared earlier [7] by total synthesis. Allyl alcohol, 3-buten-1-ol, 4-penten-1-ol and 5-hexen-1-ol were purchased from Aldrich (Gillingham, UK).

2.2. Derivatization

To produce the various derivatives, the free fatty acids (20 mg) were first converted into the corresponding acid chlorides by reaction with 0.5 ml of oxalyl chloride for 36 h at room temperature. The excess reagent was then evaporated, first under nitrogen and then under vacuum. The residue was dissolved in toluene (1 ml), and 0.25 ml (5 mg of the fatty acid chloride) was immediately reacted with 5 mg of each unsaturated alcohol in toluene (0.5 ml) and pyridine (0.1 ml) at 50°C overnight. The excess solvent and pyridine were removed in a rotary evaporator. Hexane (5 ml) was added to the residue and the

solution was washed with water (2 × 5 ml). Finally, the products were purified by elution through a Florisil column (Pasteur pipette) with hexane–acetone (99:1, v/v). The purity of each derivative was checked by TLC (Alufolio silica gel 60; Merck, Darmstadt, Germany) with a mobile phase of hexane–acetone (100:8, v/v) and detection with iodine vapour.

2.3. High-performance liquid chromatography

A Hitachi L-6200A HPLC pump was used with a Varex Model IIA evaporative light-scattering detector (P.S. Instruments, Sevenoaks, UK). A Nucleosil 5SA column (25 cm × 4.6 mm I.D.) was converted to the silver form as described earlier [8]. The temperature of the column was maintained at 20.0 ± 1.0°C by fitting it into a water jacket through which water was pumped from a temperature control unit. Sample (5 μl) was injected as a solution in dichloroethane. A mixture of dichloroethane–dichloromethane–acetonitrile (50:50:0.25, v/v/v) was used as mobile phase at a flow-rate of 1.5 ml/min. The temperature of the drift tube in the detector was maintained at 80°C. The dead volume of the column was determined by repeated injection of docosane. The mean retention time was 2.847 ± 0.006 min (6 injections). Retention (capacity) factors (k') were determined as a mean of three parallel measurements with relative standard deviations not exceeding 3.2%.

3. Results and discussion

Compared to derivatives studied previously, the esters examined here had a distinctive new feature—a double bond in the alcohol moiety that was a second site for a π -electron interaction with silver ions. Thus, the octadecenoic ester species comprised a variety of combinations of two double bonds at different distances from the ester group and different distances apart, as illustrated for oleic acid in Fig. 1.

It was possible to elute all four derivatives using the same mobile phase of dichloroethane–dichloromethane–acetonitrile (50:50:0.25, v/v/v)

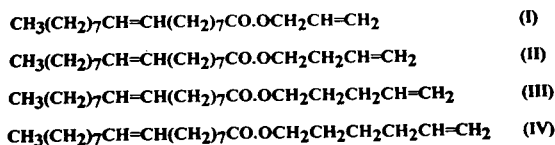


Fig. 1. Esters of oleic acid (9–18:1) with short-chain monoenoic fatty alcohols, allyl (I), butenyl (II), pentenyl (III) and hexenyl (IV).

v). The proportion of acetonitrile in the solvent mixture was higher than that used for the methyl and the phenacyl derivatives (0.01%), and was close to that used earlier to elute the dienoic fatty acids and the unsaturated long-chain fatty acid alcohols (0.35% acetonitrile) [1]. Fig. 2 reveals the distinctive influence of double bond position in the fatty acid backbone on the retention factor. The general pattern for a given ester moiety resembled that obtained for the phenacyl derivatives, e.g. there were maxima for

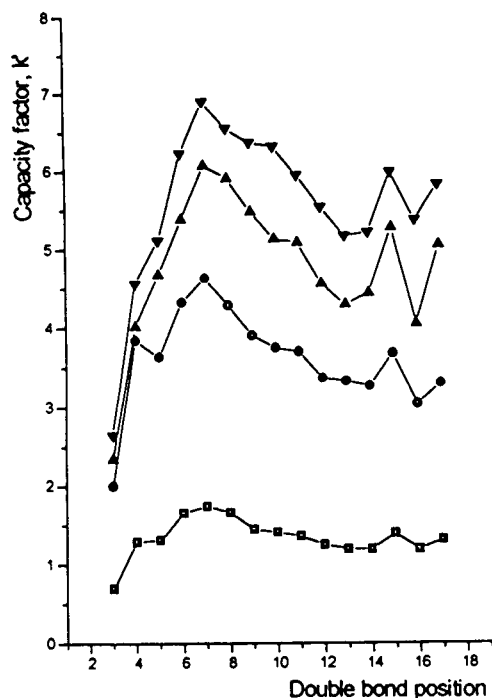


Fig. 2. Retention factors, k' , for silver ion HPLC of allyl (□), butenyl (○), pentenyl (△) and hexenyl (▽) esters of the series of *cis*-octadecenoates at 20°C on a Nucleosil 5SA column with a mobile phase of dichloroethane–dichloromethane–acetonitrile (50:50:0.25, v/v/v).

7- and 15–18:1 isomers. As with all fatty acid derivatives studied so far, a double bond in the acyl chain positioned near the ester group reacted only weakly with the silver ions; hence these derivatives (from 3–18:1 to 5–18:1) had lower k' values. When this bond was located at a distance from the ester group, its complexation ability increased and even the 17–18:1 isomer had a higher k' value than 3–18:1. This may be due to partial delocalization of the π -electrons of the double bond under the influence of the inductive effect of the ester group.

This conclusion is confirmed by the behaviour of the second double bond, positioned in the alcohol moiety, which shows the same effect: the retention factors for a given fatty acid isomer depend on the alcohol, the order being: allyl < butenyl < pentenyl < hexenyl. The same order was observed for the stearic acid esters, where retention is affected only by the double bond of the alcohol, the respective values being 0.0, 0.09 ± 0.01 , 0.26 ± 0.01 , 0.41 ± 0.01 . These values can be considered as the contribution of the alcohol double bond to retention. It is evident that retention factors of ester species are not a simple sum of the fractional values of the two parts of the molecule which can interact with silver ion, thus confirming our earlier observation [1].

Retention tended to increase initially with increasing distance between the two double bonds, the highest k' value established in this work, that of 7–18:1 hexenyl ester ($k' = 6.86$), was about 3 to 7 times lower than those of any of the isomeric octadecadienoates with double bonds separated by more than one methylene group studied previously [1]. This indicates that the existence of a second double bond is not the only factor affecting retention, and presumably the distance between them is also important. Depending on the distance one silver ion could interact either with two double bonds simultaneously or with each double bond separately, or two silver ions could in theory interact with each double bond separately. It seems that there is an optimum distance, and this was found to be the 1,5-diene configuration (as in 1,5-hexadiene [6]).

Allyl esters were held least strongly of all the derivatives examined and showed the smallest differences between the retention factors of the isomers, i.e. the double bond position in the fatty acid backbone has much a weaker effect on retention than usual (Fig. 2). Evidently, the double bond of the alcohol when positioned near the ester group is interacting either very weakly or not at all with silver ions, and this conclusion is confirmed as allyl stearate like methyl stearate has $k' = 0$. In addition, a double bond in the alcohol moiety adjacent to the carboxylic group seems to interfere with the general retention of the molecule, or at least with those factors responsible for the differences in the retention factors of the various fatty acid isomers. In contrast, propyl esters (with the same number of carbon atoms in the alcohol moiety) permit excellent separations of octadecenoate isomers [9]; k' values for propyl esters are greater than those for allyl esters.

Although steric factors may play a part, we believe that the behaviour of allyl ester is a confirmation that the carboxyl moiety has a specific role in the interaction with the silver ions, probably through free electron pairs at the oxygen atom. These may react separately with the silver ion, but could co-ordinate jointly with the double bond in the fatty acid. In the latter case, the distance between the ester moiety and the double bond would be of significance for the interaction and some configurations would be preferable. This may explain the strong retention of phenacyl esters, which have a second carbonyl oxygen attached to the electron-rich phenyl moiety. Evidence that such an interaction is possible has been shown already for unsaturated alcohols [10,11]. It was also observed that mono-unsaturated alcohols were retained very strongly under the conditions of Ag-HPLC, having k' values of the magnitude of those of fatty acids with two separate double bonds, decreasing with the distance of the double bond from the oxygen atom [1].

By participation of the carbonyl oxygen in the interaction with silver ions, it is possible to explain the differences in retention of positional-ly isomeric monoenoic fatty acids and the fact

that the methyl, phenacyl and unsaturated alcohol esters, while providing different absolute retention factors of the isomers, have broadly similar relative patterns with respect to double bond position in the fatty acid. The exception is allyl esters in which the double bond in the alcohol moiety is close to the carbonyl oxygen. Although simple electronic or steric effects are possible in this instance, some kind of mutual interference via a field effect appears more probable. This hinders formation of a favourable structure for the complex, and decreases both the general retention of the isomeric species and the effects of the double bond position in the fatty acid.

4. Conclusions

In general, butenyl, pentenyl and hexenyl esters behaved similarly on Ag-HPLC to methyl and phenacyl esters of the same series of isomeric fatty acids. Allyl esters differed in that the interaction with the silver ions was very weak. This investigation supports an earlier conclusion that a silver ion may interact both with the fatty acid double bond and with other electron-donating parts of the molecule such as the carbonyl oxygen.

Acknowledgements

This research was supported by the Karlshamns Research Board, Sweden, the Scottish Office Agriculture and Fisheries Department and the Bulgarian National Research Foundation.

References

- [1] B. Nikolova-Damyanova, B.G. Herslöf and W.W. Christie, *J. Chromatogr.*, 609 (1992) 133.
- [2] B. Nikolova-Damyanova, W.W. Christie and B.G. Herslöf, *J. Chromatogr. A*, 653 (1993) 15.
- [3] L.J. Morris, D.M. Wharry and E.W. Hammond, *J. Chromatogr.*, 31 (1967) 69.

- [4] F.D. Gunstone, I.A. Ismail and M.S.F. Lie Ken Jie, *Chem. Phys. Lipids*, 1 (1967) 376.
- [5] B. Nikolova-Damyanova, W.W. Christie and B. Herslöf, *J. Planar Chromatogr.*, 7 (1994) 382.
- [6] *Gmelin Handbuch der Anorganischen Chemie, Silver*, Vol. 61, Part B5, Springer, Berlin, 1975, pp. 26–42.
- [7] A. Valicenti, F.J. Pusch and R.T. Holman, *Lipids*, 20 (1985) 234.
- [8] W.W. Christie, *J. High Resolut. Chromatogr. Chromatogr. Commun.* 10 (1987) 148.
- [9] B. Nikolova-Damyanova, unpublished results.
- [10] C.D.M. Beverwijk, G.J.M. van der Kerk, A.J. Leusink and J.G. Moltes, *Organometal. Chem. Rev.*, A5 (1970) 215.
- [11] M. Novak, D.A. Aikens and W.D. Closson, *Inorg. Nucl. Chem. Lett.*, 10 (1974) 1117.



ELSEVIER

Journal of Chromatography A, 693 (1995) 241-249

JOURNAL OF
CHROMATOGRAPHY A

Simple and highly sensitive high-performance liquid chromatographic method for separating enantiomeric diacylglycerols by direct derivatization with a fluorescent chiral agent, (*S*)-(+)-2-*tert.*-butyl-2-methyl-1,3-benzodioxole-4-carboxylic acid

Jeong-Hwan Kim, Yoshihiro Nishida, Hiroshi Ohruai, Hiroshi Meguro*

Department of Applied Biological Chemistry, Faculty of Agriculture, Tohoku University, 1-1 Tsutsumidori-Amamiyamachi, Aoba-ku, Sendai 981, Japan

First received 21 July 1994; revised manuscript received 11 October 1994; accepted 12 October 1994

Abstract

A simple and highly sensitive HPLC method was developed for the determination of the absolute configuration and the optical purity of diacylglycerols. The method involves direct fluorescent labelling of diacylglycerols with (*S*)-TBMB-carbonyl chloride in pyridine and HPLC separation of the derived diastereomeric (*S*)-TBMB-carboxylated diacylglycerol derivatives [(*S*)-TBMB = (*S*)-(+)-2-*tert.*-butyl-2-methyl-1,3-benzodioxole]. Complete separation of the diastereomeric (*S*)-TBMB-carbonyl-diacylglycerol derivatives and thus indirectly of the enantiomers of the parent diacylglycerols and of the *sn*-1,3-regioisomer was achieved using normal-phase silica gel HPLC within 30 min for every saturated single acid ($R_1 = R_2$) diacylglycerol ($C_{12:0}$ - $C_{22:0}$) examined.

1. Introduction

During the last decade, several methods have been proposed for separating chiral diacylglycerols, in which a combination of 3,5-dinitrophenylurethane (3,5-DNPU) derivatization and chiral-phase HPLC was applied by Takagi and co-workers [1-3] and Sempore and Bezard [4]. Alternatively, a combination of chiral urethane derivatization and a normal-phase silica gel column was also employed by Michelsen et al. [5]. Rogalska et al. [6] and Laakso and Christie [7]. However, these methods have limited sen-

sitivities with UV detection and needed relatively long elution times and long columns. Another approach was reported by Kruger et al. [8] to increase the sensitivity by using a fluorescent chiral agent, but chiral separation of diacylglycerols by HPLC was not satisfactory.

In previous papers, we have reported general methods for determining the optical purity and the absolute configuration of diacylglycerols via derivatization into a key compound, 1,2- (or 2,3-) di-*O*-benzoyl-3-*O*-*tert.*-butyldimethylsilyl-*sn*-glycerol, which was determined either by circular dichroism (CD) or chiral column HPLC with UV detection [9,10]. More recently, we have proposed a different approach using a

* Corresponding author.

chiral derivatizing agent, (*S*)-TBMB-carboxylic acid [(*S*)-TBMB = (*S*)-(+) - 2-*tert.*-butyl-2-methyl-1,3-benzodioxole] [11], in order to increase the sensitivity due to the strong fluorescence activity of the reagent [12]. Our previous methods are convenient because they need no authentic sample with a known configuration to determine the absolute configuration and the optical purity of diacylglycerols. However, the derivatizing procedures may be laborious, and acyl moieties of diacylglycerol cannot be characterized, as acylglycerols are deacylated leading to a mono-*O-tert.*-butyldimethylsilyl di-*O*-benzoyl or di-*O*-(*S*)-TBMB-carboxylated derivative. In order to solve these problems, we attempted a direct derivatization of diacylglycerols with (*S*)-TBMB-carboxylic acid and the separation of the diastereoisomers by HPLC with fluorescence detection.

In this paper, we report that all possible isomers of *sn*-1,2-, *sn*-2,3- and *sn*-1,3-diacylglycerols can be completely separated within 30 min and detected in a highly sensitive manner based on the fluorescence of the (*S*)-TBMB reagent. We applied this method to determine the optical purity of sub-microgram levels of diacylglycerols produced by the lipase-catalysed hydrolysis of triacylglycerol.

2. Experimental

2.1. Chemicals

Optically active 1,2-dipalmitoyl-*sn*-glycerol {ca. 100% enantiomeric excess (e.e.) as determined with our previous method [12] by HPLC of the (*S*)-TBMB derivative} and 1,3-dipalmitoyl-*sn*-glycerol were purchased from Sigma (St. Louis, MO, USA) and its racemate, 1,2-dipalmitoyl-*rac*-glycerol, was obtained from Nacalai Tesque (Kyoto, Japan). (*S*)-(+) - 2,2-Dimethyl-1,3-dioxolane-4-methanol and its racemate (solketal) were purchased from Tokyo Kasei (Tokyo, Japan) and used for the synthesis of (*S*)-TBMB derivatives of the saturated single-acid (C_{12:0}-C_{22:0}) diacylglycerols as described below. Lipase AP (Amano PS, EC 3.1.1.3) from

Pseudomonas sp. was purchased from Amano Pharmaceutical (Nagoya, Japan) and PPL (EC 3.1.1.3, type II) from porcine pancreas from Sigma. (*S*)-TBMB-COOH [100% e.e. as determined by ¹H NMR of the (–)-cinchonidine salt] was synthesized according to a previously described method [11].

2.2. (*S*)-TBMB derivatization of diacylglycerols

Diacylglycerols were directly derivatized to the (*S*)-TBMB-carboxylated derivatives according to the scheme in Fig. 1. To a solution of (*S*)-TBMB-COOH (33 mg, 100% e.e., 0.14 mM) in dry benzene (5 ml) was added SOCl₂ (370 mg, 3.11 mM), and the mixture was kept at 60°C. After 10 min, excess SOCl₂ and benzene were removed in vacuo to give (*S*)-TBMB-COCl [12]. A dry pyridine solution (0.5 ml) of 10% of 4-dimethylaminopyridine (DMAP) and (*S*)-TBMB-COCl (24 mg, 0.1 mM) was added to the solution of dipalmitoyl-*rac*-glycerol (17 mg, 0.03 mM) in dry CH₂Cl₂ (5 ml) with stirring at room temperature. After 2 h, the reaction mixture was diluted with CH₂Cl₂ (5 ml) and washed with saturated NaHCO₃ solution (3 × 10 ml) and water (20 ml). The methylene chloride solution was dried over MgSO₄, the latter was removed by filtration and the solvent was evaporated in vacuo at 40°C to afford (*S*)-TBMB-carboxyl-dipalmitoyl-*rac*-glycerol, which was purified by preparative TLC [*n*-hexane–ethyl acetate (10:1, v/v)] (20 mg, yield 85%).

1-(*S*)-TBMB-carboxyl-2,3-dipalmitoyl-*rac*-glycerol: high-resolution electron-impact (EI) MS, found 786.6033, calculated for C₄₈H₈₂O₈,

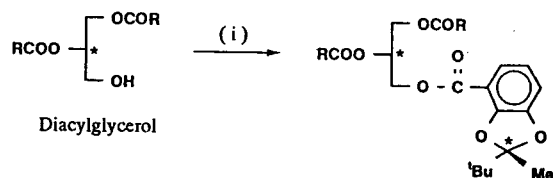


Fig. 1. Scheme for the direct derivatization of diacylglycerols with (*S*)-TBMB-COCl forming diastereomeric derivatives. (i) (*S*)-TBMB-COCl, pyridine, 4-dimethylaminopyridine (DMAP), room temperature.

[M⁺] 786.6005; ¹H NMR (400 MHz, C²HCl₃), δ 0.862–0.896 [12H, m, (dipalmitoyl-Me) × 2], 1.077 and 1.083 [9H × 2, s × 2, (TBMB-*tert.*-Bu) × 2], 1.255 [96H, m, (dipalmitoyl-(CH₂)₁₂-) × 2], 1.513–1.606 [8H, m, (dipalmitoyl-β-CH₂-) × 2], 1.603 and 1.606 [3H × 2, s × 2, (TBMB-Me) × 2], 2.278–2.325 [8H, m, (dipalmitoyl-α-CH₂-) × 2], 4.276–5.392 [10H, m, glycerol (*sn*-1, *sn*-2, *sn*-3) 5H × 2], 6.749–7.327 [6H, m, (TBMB-aromatic 3H) × 2].

(*S*)-TBMB derivatization of 1,2-dipalmitoyl-*sn*-glycerol and optically inactive 1,3-dipalmitoyl-*sn*-glycerol were also conducted in the same manner as described above.

3-(*S*)-TBMB-carbonyl-1,2-dipalmitoyl-*sn*-glycerol: high-resolution EI-MS, found 786.5948, calculated for C₄₈H₈₂O₈, [M⁺] 786.6005; ¹H NMR (400 MHz, C²HCl₃), δ 0.862–0.896 (6H, m, dipalmitoyl-Me), 1.079 (9H, s, TBMB-*tert.*-Bu), 1.250 [48H, m, dipalmitoyl-(CH₂)₁₂-], 1.554 (4H, m, dipalmitoyl-β-CH₂-), 1.603 (3H, s, TBMB-Me), 2.287–2.334 (4H, m, dipalmitoyl-α-CH₂-), 4.263–5.379 [5H, m, glycerol (*sn*-1, *sn*-2, *sn*-3)], 6.756–7.326 (3H, m, TBMB-aromatic).

2-(*S*)-TBMB-carbonyl-1,3-dipalmitoyl-*sn*-glycerol: high-resolution EI-MS, found 786.6027, calculated for C₄₈H₈₂O₈, [M⁺] 786.6005; ¹H NMR (400 MHz, C²HCl₃), δ 0.862–0.897 (6H, m, dipalmitoyl-Me), 1.078 (9H, s, TBMB-*tert.*-Bu), 1.235–1.255 [48H, m, dipalmitoyl-(CH₂)₁₂-], 1.518–1.633 (4H, m, dipalmitoyl-β-CH₂-), 1.595 (3H, s, TBMB-Me), 2.279–2.336 (4H, m, dipalmitoyl-α-CH₂-), 4.275–5.508 [5H, m, glycerol (*sn*-1, *sn*-2, *sn*-3)], 6.749–7.317 (3H, m, TBMB-aromatic).

2.3. Preparation of standard samples of diastereoisomeric (*S*)-TBMB-carbonylated homologous single-acid diacylglycerol derivatives for the HPLC separations

1-(*S*)-TBMB-carbonyl-2,3-diacyl-*rac*-glycerols

(*S*)-TBMB-carbonylated single-acid diacyl-*rac*-glycerols (C_{12:0}–C_{22:0}) were prepared from solketal (*rac*-2,2-dimethyl-1,3-dioxolane-4-methanol) as follows. Solketal (1, 40 mg, 0.3 mM) and

dry pyridine (1 ml) containing 10% of DMAP were added to a solution of (*S*)-TBMB-COCl (24 mg, 0.1 mM) in dry CH₂Cl₂ (5 ml) with stirring at room temperature. After 6 h, the reaction mixture was diluted with CH₂Cl₂ (10 ml) and washed with saturated NaHCO₃ solution (3 × 10 ml) and water (20 ml). The methylene chloride solution was dried over MgSO₄, the latter was removed by filtration and the solvent was evaporated in vacuo at 40°C to afford 1-(*S*)-TBMB-carbonyl-2,3-O-isopropylidene-*rac*-glycerol (2). This mixture of diastereomers was purified by column chromatography on silica gel [*n*-hexane–ethyl acetate (20:1, v/v)] (31 mg, yield 89%).

1-(*S*)-TBMB-carbonyl-2,3-O-isopropylidene-*rac*-glycerol (2): high-resolution EI-MS, found 350.1682, calculated for C₁₉H₂₆O₆, [M⁺] 350.1728; ¹H NMR (400 MHz, C²HCl₃), δ 1.085 and 1.086 [9H × 2, s × 2, (TBMB-*tert.*-Bu) × 2], 1.382 and 1.441 [6H × 2, s × 2, (isopropylidene-2Me) × 2], 1.599 [6H, s, (TBMB-Me) × 2], 3.897–4.454 [10H, m, glycerol (*sn*-1, *sn*-2, *sn*-3) 5H × 2], 6.753–7.357 [6H, m, (TBMB-aromatic 3H) × 2].

A solution of 2 in 75% acetic acid solution (5 ml) was stirred for 4 h at room temperature. The solvent was evaporated in vacuo at 50°C with toluene (10 ml) to give crude 1-(*S*)-TBMB-carbonyl-*rac*-glycerol derivative (3, ca. 100% yield). Compound 3 (mixture of diastereomers) was diacylated with the corresponding acyl anhydride or acyl halide in the following manner using lauroyl chloride as a typical procedure.

Commercially available lauroyl chloride (290 mg, 1.32 mM) and dry pyridine (1 ml) containing 10% of DMAP were added to a methylene chloride solution (5 ml) of 3 (18 mg, 0.06 mM) with stirring at room temperature. After stirring overnight, the reaction mixture was worked up in the same manner as described above for the preparation of 2 to give a diastereomeric mixture of 1-(*S*)-TBMB-carbonyl-2,3-dilauroyl-*rac*-glycerol (4), which was purified by preparative TLC [*n*-hexane–ethyl acetate (20:1, v/v)] (31 mg, yield 77%).

1-(*S*)-TBMB-carbonyl-*rac*-glycerol (3): high-resolution EI-MS, found 310.1451, calculated for

$C_{16}H_{22}O_6$, $[M^+]$ 310.1415); 1H NMR (400 MHz, C^2HCl_3), δ 1.089 and 1.091 [9H \times 2, s \times 2, (TBMB-*tert.*-Bu) \times 2], 1.616 and 1.619 [3H \times 2, s \times 2, (TBMB-Me) \times 2], 3.710–4.541 [10H, m, glycerol (*sn*-1, *sn*-2, *sn*-3) 5H \times 2], 6.786–7.375 [6H, m, (TBMB-aromatic 3H) \times 2].

1-(*S*)-TBMB-carbonyl-2,3-dilauroyl-*rac*-glycerol (**4**): high-resolution EI-MS, found 674.4764, calculated for $C_{40}H_{66}O_8$, $[M^+]$ 674.4754); 1H NMR (400 MHz, C^2HCl_3), δ 0.861–0.895 [12H, m, (dilauroyl-Me) \times 2], 1.079 and 1.084 [9H \times 2, s \times 2, (TBMB-*tert.*-Bu) \times 2], 1.251–1.262 [64H, m, (dilauroyl- $(CH_2)_8$ -) \times 2], 1.568–1.666 [8H, m, (dilauroyl- β - CH_2 -) \times 2], 1.604 and 1.607 [3H \times 2, s \times 2, (TBMB-Me) \times 2], 2.288–2.335 [8H, m, (dilauroyl- α - CH_2 -) \times 2], 4.264–5.405 [10H, m, glycerol (*sn*-1, *sn*-2, *sn*-3) 5H \times 2], 6.756–7.327 [6H, m, (TBMB-aromatic 3H) \times 2].

3-(*S*)-TBM-carbonyl-1,2-diacyl-*sn*-glycerols

3-(*S*)-TBMB-carbonyl-1,2-diacyl-*sn*-glycerols ($C_{12:0}$ – $C_{22:0}$) were prepared from optically active (*S*)-(+)-2,2-dimethyl-1,3-dioxolane-4-methanol in a similar manner to that described for the preparation of the racemates.

3-(*S*)-TBMB-carbonyl-1,2-O-isopropylidene-*sn*-glycerol (**2a**): high resolution EI-MS, found 350.1698, calculated for $C_{19}H_{26}O_6$, $[M^+]$ 350.1728); 1H NMR (400 MHz, C^2HCl_3), δ 1.086 (9H, s, TBMB-*tert.*-Bu), 1.384 and 1.441 (3H \times 2, s \times 2, isopropylidene-2Me), 1.600 (3H, s, TBMB-Me), 3.936–4.469 [5H, m, glycerol (*sn*-1, *sn*-2, *sn*-3)], 6.745–7.365 (3H, m, TBMB-aromatic).

3-(*S*)-TBMB-carbonyl-*sn*-glycerol (**3a**): high-resolution EI-MS, found 310.1387, calculated for $C_{16}H_{22}O_6$, $[M^+]$ 310.1415); 1H NMR (400 MHz, C^2HCl_3), δ 1.088 (9H, s, TBMB-*tert.*-Bu), 1.617 (3H, s, TBMB-Me), 3.769–4.534 [5H, m, glycerol (*sn*-1, *sn*-2, *sn*-3)], 6.783–7.369 (3H, m, TBMB-aromatic).

3-(*S*)-TBMB-carbonyl-1,2-dilauroyl-*sn*-glycerol (**4a**): high-resolution EI-MS, found 674.4783, calculated for $C_{40}H_{66}O_8$, $[M^+]$ 674.4754); 1H NMR (400 MHz, C^2HCl_3), δ 0.861–0.895 (6H, m, dilauroyl-Me), 1.079 (9H,

s, TBMB-*tert.*-Bu), 1.252 [32H, m, dilauroyl- $(CH_2)_8$ -], 1.568–1.666 (4H, m, dilauroyl- β - CH_2 -), 1.604 (3H, s, TBMB-Me), 2.289–2.348 (4H, m, dilauroyl- α - CH_2 -), 4.266–5.394 [5H, m, glycerol (*sn*-1, *sn*-2, *sn*-3)], 6.757–7.327 (3H, m, TBMB-aromatic).

The other homologous (*S*)-TBMB-carbonylated single-acid diacylglycerol derivatives ($C_{14:0}$ – $C_{22:0}$) showed 1H NMR data almost identical with those of **4** or **4a**, except for the integration of $-(CH_2)-$ signals (ca. 1.25 ppm). On the basis of the TBMB-Me (ca. 1.6 ppm), TBMB-*tert.*-Bu (ca. 1.0 ppm) and the other 1H NMR signals and EI-MS data, their structures were confirmed.

2.4. HPLC separations

Prior to the HPLC analysis, the crude (*S*)-TBMB derivatives were preliminarily purified by silica gel TLC [*n*-hexane–ethyl acetate (10:1, v/v)]. The TLC bands of the derivatives were cut out from the TLC sheet and extracted with the HPLC solvents.

HPLC separations were conducted with a Jasco (Tokyo, Japan) Model 880-PU instrument connected to a Tosoh Model FS-8010 fluorescent detector monitoring at λ_{ex} 310 nm and λ_{em} 370 nm. Separations were performed on a Develosil 60-3 (Nomura Chemical) silica gel column (stainless steel, 25 cm \times 4.6 mm I.D.). The analyses were carried out isocratically using a mixture of HPLC-grade *n*-hexane and *n*-butanol (300:1, w/w; flow-rate 0.6 ml/min) as the mobile phase at ambient temperature. For quantitative determinations, peak areas were calculated with a Model 807-IT integrator (JASCO).

2.5. Applications to the determination of stereochemistry of lipase-catalysed hydrolysis of tripalmitin

Tripalmitin obtained from Sigma was purified by chromatography on silica gel using *n*-hexane–ethyl acetate (20:1, v/v) as the mobile phase. A suspension of tripalmitin (20 mg) in 4 ml of 1 M Tris–HCl buffer (pH 7.5) containing the enzyme Amano AP (25 mg) or PPL (20 mg) was incubated at 40°C with vigorous shaking. After the

reaction had proceeded up to ca. 5–10% (1 h), monitored by silica gel TLC [toluene–ethyl acetate (20:1, v/v)], the enzymatic hydrolysate was extracted with diethyl ether [11]. Then, subsequent direct (*S*)-TBMB derivatization of diacylglycerols was conducted as described above.

3. Results and discussion

3.1. Direct (*S*)-TBMB acylation of diacylglycerols and HPLC separation of derivatives

The (*S*)-TBMB-COOH used is optically pure as determined by ^1H NMR analysis of the (–)-cinchonidine salt [11]. (*S*)-TBMB acylations of diacylglycerols as detailed under Experimental (Fig. 1) were performed with yields of >80%. A methylene chloride solution of (*S*)-TBMB-COCl, easily available from (*S*)-TBMB-COOH, was treated with diacylglycerols under mild conditions in the presence of pyridine containing 10% DMAP at room temperature. After ca. 2 h the reaction mixture was worked up and placed on a silica gel TLC sheet (5 cm \times 5 cm) and

eluted with *n*-hexane–ethyl acetate (10:1, v/v). The TLC spots ($R_f = 0.4$) corresponding to fluorescent (*S*)-TBMB-carbonylated diacylglycerol derivatives, owing to the visible fluorescence of the (*S*)-TBMB group, were cut out from the TLC sheet and extracted with the HPLC solvents (*n*-hexane–*n*-butanol) for direct HPLC injection.

Fig. 2i shows HPLC profiles of dipalmitoylglycerols derivatized with (*S*)-TBMB-COCl. Under normal-phase conditions using a Develosil 60-3 silica column (25 cm \times 4.6 mm I.D.) and *n*-hexane–*n*-butanol (300:1, w/w) as the mobile phase, a complete separation of *sn*-1,2-, *sn*-2,3- and 1,3-dipalmitoylglycerols was achieved within 30 min; the *sn*-1,2-isomer (a) was eluted first, followed by the *sn*-2,3-isomer (b), and then the *sn*-1,3-isomer (c), derived from optically inactive 1,3-dipalmitoyl-*sn*-glycerol.

3.2. Reproducibility and quantification

In order to confirm the reproducibility and the quantification of the proposed method, (*S*)-TBMB derivatization was carried out using dipalmitoylglycerols of known optical purities (0,

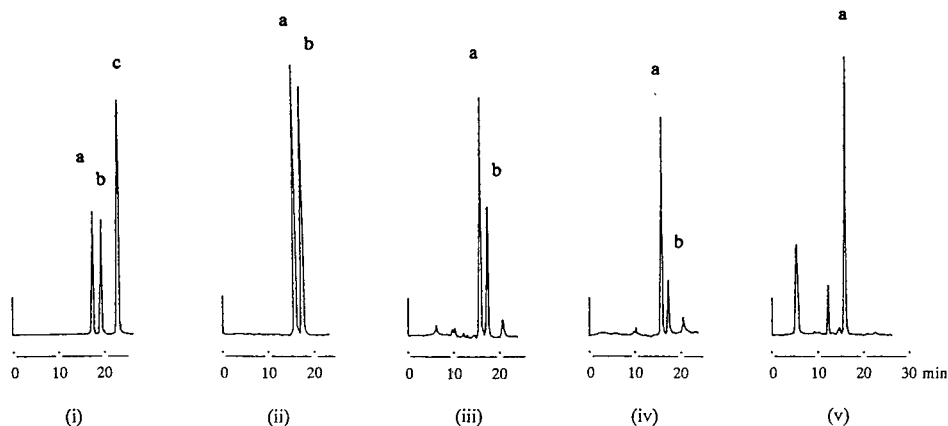


Fig. 2. Typical HPLC separation of isomeric dipalmitoylglycerols labelled with (*S*)-TBMB-COOH and chromatograms of (*S*)-TBMB glycerol derivatives derived from each standard mixture of dipalmitoylglycerols (racemate and *sn*-1,2-) with known ratio (see Table 1). (i) Mixture of 1,3- and 1,2-dipalmitoyl-*rac*-glycerols as their (*S*)-TBMB derivatives (Peaks: a = *sn*-1,2-; b = *sn*-2,3-; c = *sn*-1,3-), (ii) racemate; (iii) 28.5%, (iv) 63.6% and (v) 100% optical purity of dipalmitoylglycerols. HPLC conditions: Develosil 60-3 silica gel column (25 cm \times 4.6 mm I.D.); λ_{ex} 310 nm, λ_{em} 370 nm; eluent, *n*-hexane–*n*-butanol (300:1, w/w); flow-rate, 0.6 ml/min; temperature, 22–24°C.

Table 1
Comparison of optical purities before and after derivatization of standard diacylglycerols

Standard diacylglycerol mixture ^a			After derivatization with (S)-TBMB-COCL ^b		
Before derivatization			After derivatization with (S)-TBMB-COCL ^b		
Dipalmitoyl- <i>rac</i> -glycerol (racemate) (mg)	1,2-Dipalmitoyl- <i>sn</i> -glycerol (<i>sn</i> -1,2) (mg)	Calculated optical purity (% e.e.)	Average of observed optical purity (% e.e.)	<i>n</i>	S.D.
10	0	0	0.3 (<i>sn</i> -1,2)	7	0.72
2.53	1.01	28.5	29.1	2	—
2.89	5.05	63.6	61.2	2	—
0	5	100	98.9–ca. 100	4	0.55

^a Each standard solution was prepared by mixing the racemate and *sn*-1,2-diacylglycerol (ca. 100% e.e.) in the appropriate ratio, and their optical purity was calculated from the ratio of the racemate and *sn*-1,2-diacylglycerol contents [% e.e. before derivatization = $sn-1,2/(racemate + sn-1,2) \times 100$].

^b The HPLC peak areas of (S)-TBMB-diacylglycerol derivatives (*sn*-1,2 and *sn*-2,3) derived from each standard diacylglycerol mixture were used directly to determine the optical purity of the mixture of diacylglycerols without correction [% e.e. after derivatization = $(\text{peak area of } sn-1,2 - \text{peak area of } sn-2,3)/(\text{peak area of } sn-1,2 + \text{peak area of } sn-2,3) \times 100$].

28.5, 63.6 and 100% e.e.) to give the results summarized in Table 1. Fig. 2ii–v show the HPLC traces for (S)-TBMB-glycerol derivatives derived from these standard dipalmitoylglycerols.

As shown in Fig. 2iii and iv, in addition to the peaks of *sn*-1,2- and *sn*-2,3-dipalmitoylglycerols, a small peak of 1,3-dipalmitoylglycerol appeared. This isomer might be generated by acyl migration from *sn*-2 to *sn*-3 or *sn*-1 during the derivatization procedures or the storage of the diacylglycerols, but has no effect on the determination of the optical purities of *sn*-1,2- and *sn*-2,3-diacylglycerols, as all of these three isomers were separated completely. Moreover, excellent agreement was obtained for the optical purities before and after the (S)-TBMB derivatization within the usual limits of variation (S.D. = 0.72, *n* = 7), as summarized in Table 1. Fig. 2ii and v show 100:100 and 100:0 peak area ratios of *sn*-1,2- and *sn*-2,3- isomers in the respective HPLC traces for the racemate and optically pure *sn*-1,2-dipalmitoylglycerol.

These results indicate that the peak areas of (S)-TBMB-diacylglycerols can be used to determine the absolute configuration and the optical purity without a calibration process. Owing

to the strong fluorescence of the (S)-TBMB group, these isomers could be determined in less than picomolar concentrations on the HPLC column; the detection limit of 3-(S)-TBMB-carbonyl-1,2-dipalmitoyl-*sn*-glycerol could be lowered to about 0.3 pmol on-column (signal-to-noise ratio = 3).

3.3. Indirect HPLC separation of enantiomeric single-acid diacylglycerols after derivatization with (S)-TBMB-COOH

Similar indirect enantiomer separations were also achieved for other homologous single-acid diacylglycerols, as shown in Fig. 3. These chromatograms represent the diacyl-*rac*-glycerol derivatives prepared from solketal as detailed under Experimental. In every case, the *sn*-1,2-isomer (a) was eluted faster than the *sn*-2,3-isomer (b), and these two peaks also appeared with equal integration to each other. Identification of the diastereomers (and thus of the parent enantiomers) of each (S)-TBMB derivative was carried out by co-injection of *sn*-1,2-diacyl derivatives synthesized from (S)-(+)-solketal. Another peak (ca. 2% peak area except for ca. 23% in chromatogram i for the dibehenoyl

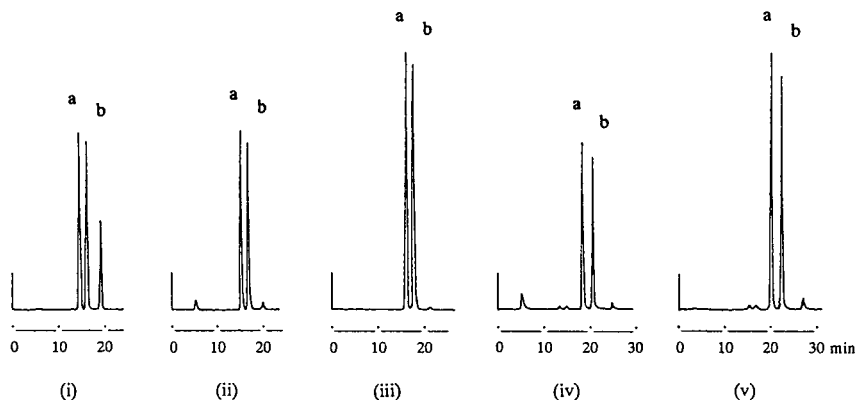


Fig. 3. HPLC separation of each (*S*)-TBMB derivatized homologous saturated single-acid diacyl-*rac*-glycerol ($C_{12:0}$ – $C_{22:0}$) synthesized from solketal. (i) Dibehenoyl-; (ii) diarachidoyl-; (iii) distearoyl-; (iv) dimyristoyl-; (v) dilauroyl-. (Peaks: a = *sn*-1,2- and b = *sn*-2,3- in each chromatogram.) HPLC conditions as in Fig. 2.

derivative) appeared after the *sn*-2,3-isomer (b) in each chromatogram, and this peak is highly likely to be a trace amount of their 1,3-isomer derived from acyl migration during the synthetic procedures in the same manner as for dipalmitoylglycerol, judging from the relative retention volumes, which agreed well with the values expected from that of dipalmitoylglycerol.

The HPLC data summarized in Table 2 clearly

show that all the single-acid diacylglycerols ($C_{12:0}$ – $C_{22:0}$) examined here could be determined by the present method. High separation coefficients ($\alpha = 1.16$) and peak resolutions ($R_s = 2.3$) were obtained for all the isomeric (*S*)-TBMB derivatized diacylglycerols.

Moreover, it is obvious from the retention times that the longer-chain diacylglycerols are eluted faster than the shorter compounds. At-

Table 2

Chromatographic data for homologous single-acid diacylglycerols as their (*S*)-TBMB derivatives

Acyl group	Position	V_r (ml)	k'	α	R_s
Dilauroyl	<i>sn</i> -1,2	8.24	2.71	1.16	3.5
	<i>sn</i> -2,3	9.55	3.14		
Dimyristoyl	<i>sn</i> -1,2	7.35	2.42	1.16	3.3
	<i>sn</i> -2,3	8.53	2.81		
Dipalmitoyl	<i>sn</i> -1,2	6.69	2.20	1.16	3.1
	<i>sn</i> -2,3	7.79	2.57	1.28	5.5
	<i>sn</i> -1,3	9.96	3.28		
Distearoyl	<i>sn</i> -1,2	6.01	1.98	1.16	2.9
	<i>sn</i> -2,3	7.00	2.30		
Diarachidoyl	<i>sn</i> -1,2	5.44	1.79	1.17	2.7
	<i>sn</i> -2,3	6.34	2.09		
Dibehenoyl	<i>sn</i> -1,2	4.81	1.59	1.17	2.3
	<i>sn</i> -2,3	5.62	1.85		

V_r = Retention volume corrected by column void volume (3.04 ml); k' = capacity factor; α = separation coefficient; R_s = peak resolution.

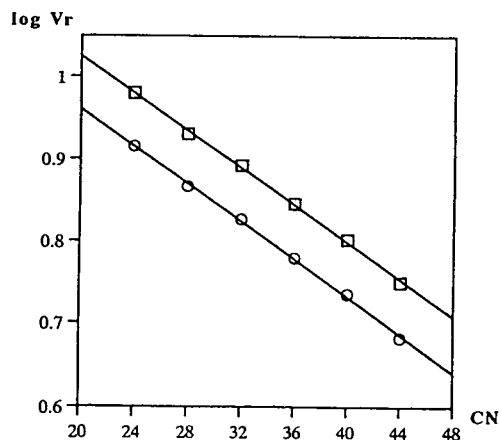


Fig. 4. Relationships of $\log V_r$ (retention volume) versus CN (total number of acyl carbon atoms) for homologous and isomeric diacylglycerols as their (*S*)-TBMB derivatives separated by HPLC on a silica gel column (Develosil 60-3). ○, $\log V_r$ (*sn*-1,2-); □, $\log V_r$ (*sn*-2,3-).

tempts to plot $\log V_r$ (retention volume) versus CN (total number of acyl carbon atoms) revealed a linear relationship, as can be seen in Fig. 4, and a similar relationship using 3,5-DNPU derivatives was reported by Takagi and co-workers [1–3]. The two straight lines for *sn*-1,2- and *sn*-2,3-diacyl derivatives in Fig. 4 are parallel and the relationships could be expressed by following equations: $\log V_r$ (*sn*-1,2-) = $-0.011 CN + 1.191$; $\log V_r$ (*sn*-2,3-) = $-0.011 CN + 1.251$; $E = \log V_r$ (*sn*-2,3-) – $\log V_r$ (*sn*-1,2-) = 0.06 where E is the diastereomer separation factor. The above rules will be useful not only for determining indirectly the enantiomer but also the acyl group composi-

tion of diacylglycerols with the same acyl moieties.

3.4. Applications to the determination of stereochemistry of lipase-catalysed reactions

We applied the present method to re-examine [6,12] the stereoselectivity of the lipase-catalysed hydrolysis of tripalmitin (Table 3). PPL is known to have poor stereoselectivity for triglycerides [6], and our results with the present method also showed low selectivity (less than 10% e.e.) with a weak *sn*-3 preference. On the other hand, Amano-AP showed higher stereoselectivity (43.1% e.e.) with an *sn*-1 preference, which accorded well with our previous results [12]. In order to confirm these results, we tested a lipase-free reaction using optically pure 1,2-dipalmitoyl-*sn*-glycerol in the reaction buffer. Although the 1,3-isomer appeared at levels up to ca. 3%, no *sn*-2,3-isomer by acyl migration appeared for at least 4 h under the present lipase reactions conditions or during (*S*)-TBMB derivatization procedures, which otherwise would affect the quantification by this method.

In conclusion, we have developed a facile and highly sensitive method for determining the optical purity of 1,2- (or 2,3-) diacyl-*sn*-glycerol which involves derivatization with (*S*)-TBMB-carboxylic acid under mild conditions. The diastereomeric derivatives, including the symmetric 1,3-isomer, were completely separated by HPLC on a normal-phase silica column (Develosil 60-3) within 30 min and detected in less than a 1 pM

Table 3

Optical purities of (*S*)-TBMB-dipalmitoylglycerols derived from dipalmitoylglycerols obtained by lipase-catalysed hydrolysis of tripalmitin and reference (lipase-free) with 1,2-dipalmitoyl-*sn*-glycerol (ca. 100% e.e.) in 1.0 M Tris-HCl buffer

Substrate	Lipase reaction (40°C)		Optical purity (% e.e.)		Preference of lipase reaction
	Lipase	Time (h)	Average ($n = 4$)	S.D.	
Reference; 1,2-dipalmitoyl- <i>sn</i> -glycerol	–	1	97.4	0.84	–
	–	2	97.6	0.56	–
	–	4	99.2	0.74	–
Hydrolysis; tripalmitin	PPL	1	8.2	0.51	<i>sn</i> -3
	AP	1	43.1	0.47	<i>sn</i> -1

amount of diacylglycerols, taking advantage of the strong fluorescence of the (*S*)-TBMB group. The study showed also that 3-(*S*)-TBMB-carbonyl-1,2-diacyl-*sn*-glycerol derivatives were always eluted faster than the *sn*-2,3-isomers. This rule is empirically useful for assigning the absolute configurations of chiral diacylglycerols (and for evaluating the optical purity), although the mechanism has still not been clarified sufficiently well to be able to rationalize these phenomena.

Acknowledgement

This work was partially supported by a Grant-in-Aid for Scientific Research from the Ministry of Education, Science and Culture of Japan.

References

- [1] Y. Itabashi and T. Takagi, *J. Chromatogr.*, 402 (1987) 257.
- [2] T. Takagi and T. Suzuki, *J. Chromatogr.*, 519 (1990) 237.
- [3] Y. Itabashi, A. Kukis, L. Marai and T. Takagi, *J. Lipid Res.*, 31 (1990) 1711.
- [4] B.G. Sempore and J.A. Bezard, *J. Chromatogr.*, 557 (1991) 227.
- [5] P. Michelsen, E. Aronsson, G. Odham and B. Åkesson, *J. Chromatogr.*, 350 (1985) 417.
- [6] E. Rogalska, S. Ransac and R. Verger, *J. Biol. Chem.*, 265 (1990) 20271.
- [7] P. Laakso and W.W. Christie, *Lipids*, 25 (1990) 349.
- [8] J. Kruger, H. Rabe, G. Reichmann and B. Rustow, *J. Chromatogr.*, 307 (1984) 387.
- [9] H. Uzawa, T. Noguchi, Y. Nishida, H. Ohrui and H. Meguro, *Biochim. Biophys. Acta*, 1168 (1993) 253.
- [10] H. Uzawa, H. Ohrui, H. Meguro, T. Mase and A. Ichida, *Biochim. Biophys. Acta*, 1169 (1993) 165.
- [11] Y. Nishida, H. Ohrui and H. Meguro, *Tetrahedron Lett.*, 30 (1989) 5277.
- [12] J.H. Kim, H. Uzawa, Y. Nishida, H. Ohrui and H. Meguro, *J. Chromatogr. A*, 677 (1994) 35.



ELSEVIER

Journal of Chromatography A, 693 (1995) 251–261

JOURNAL OF
CHROMATOGRAPHY A

Ionic strength dependence of protein retention on Superose 12 in SEC–IEC mixed mode chromatography

Chun-hua Cai, Vincent A. Romano, Paul L. Dubin*

Department of Chemistry, Indiana University–Purdue University, Indianapolis, IN 46202, USA

First received 16 August 1994; revised manuscript received 21 October 1994

Abstract

Protein retention was studied on Superose 12 in SEC–IEC mixed mode, over a wide range of ionic strength (16.8 mM to 500 mM). A new SEC parameter, K_{int} , which is analogous to the capacity factor k' in IEC was defined. The effect of ionic strength on K_{int} was compared to predictions from two previous models, that of Kopaciewicz et al. [1] and that of Ståhlberg et al. [2]. The ionic strength dependence of K_{int} more closely fits the second model, and the stationary phase surface charge density calculated from the model agrees well with the experimental value.

1. Introduction

Ion-exchange chromatography (IEC) is a valuable tool for the analysis and separation of proteins [3]. IEC is a form of liquid chromatography in which retention is governed by Coulomb forces between the solute and the oppositely charged packing. Experimentally, this retention is described by the capacity factor:

$$k' = \frac{t_r - t_0}{t_0} \quad (1)$$

where t_r is the retention time of the given solute and t_0 is that of an unretained solute.

Several mechanisms have been proposed for protein retention in IEC. These models differ greatly at a fundamental level and also predict different dependencies of t_r and thus k' on the ionic strength (I). Boardman and Partridge [4] (later referred to as BP) proposed a simple mass-

action model which treated the protein as a multivalent ion that displaces a well-defined number of ions on the packing surface corresponding to the “valency” of the protein. Kopaciewicz et al. [1] (later referred to as KRFR) extended this model to include the effect of small ions. Their treatment leads to a linear dependence of $\log k'$ on $\log 1/I$ with a slope related to the number of ions needed to displace the protein from the stationary phase. More recently, Ståhlberg et al. [2] (SJH) proposed a non-stoichiometric model and consequently suggest the term “electrostatic interaction chromatography” for proteins in place of ion-exchange chromatography. The SJH model is based on the assumption that the interaction between a protein and an ion-exchange column can be treated as an electrostatic interaction between two oppositely charged surfaces separated by a salt solution. The magnitude of this interaction is obtained by solving the Poisson–Boltzmann equation for two oppositely charged parallel slabs in

* Corresponding author.

contact with a salt solution. Consequently, SJH predicted a linear relation between $\ln k'$ and $1/\sqrt{I}$ which was supported experimentally. The net charge of the protein may be calculated using the slope and some fundamental physico-chemical constants.

There are several problems associated with the foregoing models. The KRFR model does not take into account the charge density of the column packing. It also provides an unrealistic stoichiometry in that each protein charge must interact with a complementary packing charge. Finally, the role of the salt is only as a “displacer”; therefore, screening effects are ignored. The SJH model considers such screening effects but neglects protein charge heterogeneity (charge patches) inasmuch as the protein charges are considered to be smeared over the surface of a sphere, half of which interacts with the packing surface.

Charge heterogeneity is an important consideration in protein chromatography. Kopaciewicz et al. [1] showed that proteins could be retained even when the protein bears a net charge of the same sign as the column, or even zero charge (at the isoelectric point). For example, β -lactoglobulin can be retained one pH unit below its pI on an anion-exchange column, or one-half pH unit above its pI on a cation-exchange column. Six other proteins also show significant retention at their pI value on both anion- and cation-exchange columns. Lesins and Ruckenstein [5] also found significant retention of positively charged proteins on positively charged anion-exchange columns. These studies reveal the effect of protein “charge patches” on retention in IEC.

How can two theories which give different ionic strength dependence of the capacity factor both be supported by experiment? Experiments such as those in Refs. [1] and [2] tend to be conducted over a relatively small range of ionic strength because the practical range of ionic strengths used in IEC is considered to be between 50 mM and 500 mM [4]. Fig. 1 shows that $\ln 1/I$ and $1/\sqrt{I}$ (the two functions of ionic strength used in Refs. [1] and [2]) are virtually collinear in the range covered by those studies. A clear definition of the relationship between

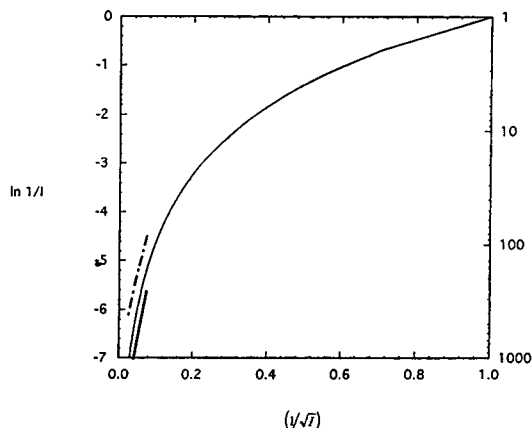


Fig. 1. Hypothetical plot of $\ln(1/I)$ versus $(1/\sqrt{I})$ which are the two functions of ionic strength used by the KRFR and SJH models respectively. The ionic strength ranges used to experimentally test the two models are given by the dashed (KRFR) and solid (SJH) lines drawn outside the curve. Ionic strength is given on the right-hand vertical axis for reference.

capacity factor and ionic strength thus requires data over a wider range of ionic strengths. Such studies can be done on weak ion-exchange resins, one example being the packing used in aqueous size exclusion chromatography (SEC).

In ideal SEC, molecules are separated solely on the basis of size, but in non-ideal SEC, electrostatic or hydrophobic interactions contribute to the solute retention. While hydrophobic interactions in protein SEC are relatively weak at low ionic strength, electrostatic effects may contribute significantly to retention. This allows one to use an SEC column as a weak ion exchanger [6].

The chromatographic partition coefficient in SEC is given by:

$$K_{\text{SEC}} = \frac{(V_e - V_0)}{(V_t - V_0)} \quad (2)$$

where V_e is the retention volume of the solute, V_0 is the interstitial volume of the column, which is obtained as the retention volume of a solute too large to permeate the pores, and V_t is the total volume of the column, which is obtained as the retention volume of a small solute such as D_2O . For ideal SEC, K_{SEC} is purely dependent on the

dimensions of the solute, R , and the dimensions of the column pores, r_p . From a simple geometric model where the solute is treated as a sphere and the column pore is treated as a slab, cylinder, or sphere, this relationship is given by:

$$K = \left(1 - \frac{R}{r_p}\right)^\lambda \quad (3)$$

where $\lambda = 1, 2$, or 3 for slab, cylindrical, or spherical pores respectively [7]. The solute radius, R , generally adopted by protein chemists is the Stokes radius:

$$R_s = \frac{kT}{6\pi\eta D} \quad (4)$$

where R_s is in m, and k is the Boltzmann constant (J/K), T is temperature (K), η is the solvent viscosity (Poise), and D is the diffusion coefficient (m^2/s). A second size parameter more popular among polymer chemists is the viscosity radius [8]:

$$R_\eta = \frac{3[\eta]M^{1/3}}{10\pi N_A} \quad (5)$$

where R_η is in cm, when $[\eta]$ the intrinsic viscosity is in cm^3/g , M the molecular weight is in g/mol, and N_A is Avogadro's number. R_η has been reported to unify the data for globular proteins better than R_s [10]. The relation between K and R is the column calibration curve, which, for cylindrical pores, should appear as a linear plot of $K^{1/2}$ versus R [7]. It should be noted that this last relationship is based on one of many models and is certainly not proven.

In this paper, we study the dependence of

protein retention in SEC on the ionic strength over an extended range of ionic strength. We plot our data according to the KRFR and SJH models for the purpose of comparison of the two conflicting models. A method for normalizing size effects in non-ideal SEC is provided in order to isolate the electrostatic contribution. The effect of column packing charge density is also considered.

2. Experimental

2.1. Materials

Table 1 lists protein characteristics, including source, molecular mass, isoelectric point (pI), Stokes radius (R_s), and viscosity radius (R_η), the last being the solute dimension of preference, for reasons noted above. Amine-core, sodium carboxylate polyamidoamine (PAMAM) dendrimers (lot # ZN-SN-A) were gifts from D. Tomalia at the Michigan Molecular Institute and are described in Table 2. Ficoll fractions, obtained from K. Granath of Kabi Pharmacia, are listed in Table 3. Pullulan samples (Shodex Standard P-82 lot # 20101) from Showa Denko K.K. are described in Table 4. All buffers and salts were reagent grade from Sigma, Fisher or Aldrich.

2.2. Methods

Size-exclusion chromatography

A Superose 12 HR 10/30 (Pharmacia) column (12% cross-linked agarose medium) with a typi-

Table 1
Characteristics of proteins used in this study

Protein ^a	Source	M_r	pI	R_s^b (nm)	R_η^c (nm)
RNase (L-6876)	Bovine pancreas	13 700	9.0	1.8	1.9
Lysozyme (R-5503)	Hen egg white	14 000	11.0	1.9	2.0
Myoglobin (M-0380)	Horse skeletal muscle	18 800	7.3	1.9	2.1
Hemoglobin (H-4632)	Horse	64 650	7.0	3.2	—

^a Sigma lot numbers given in parentheses.

^b Stokes radius, from Ref. [9].

^c Viscosity radius, from Ref. [10].

Table 2
Characteristics of starburst dendrimers

Generation	M_r^a	R_s^b (nm)	R_η^c (nm)
0.5	924	0.95	–
1.5	2173	1.3	–
2.5	4672	1.5	1.5
3.5	9670	2.5	1.9
4.5	19 666	3.1	2.5
5.5	39 657	3.7	3.1
6.5	79 639	4.5	4.0

^a From supplier (MMI).

^b From Ref. [11], in pH 7.0, 0.3 M phosphate buffer, via diffusion coefficient by quasi-elastic light scattering (QELS).

^c From Ref. [12], measured in pH 5.0, 0.38 M phosphate buffer.

cal plate number of 40 000 m^{-1} was used throughout the study. A Rheodyne 0.2 μm filter was used to protect the column. A Milton–Roy miniPump (Riviera Beach, FL, USA) was used with a Rheodyne injector (Cotati, CA, USA) with a 100- μl injection loop. A Gilson UV detector (254 nm) in series with a Millipore–Waters differential refractometer R401 was coupled to a Kipp and Zonen two-channel recorder. The flow rate, typically 0.43 ml/min, was measured by weighing the eluent over a timed period. The buffer pH and ionic strength were confirmed with an Orion pH/millivolt meter 811 and a YSI Conductivity Bridge (Model 31), respectively.

Table 3
Characteristics of ficoll fractions

Fraction	$M \times 10^{-3}^a$	$M_n \times 10^{-3}^a$	M_w/M_n	$[\eta]$ (cm^3/g)	R_s^b (nm)	R_η^c (nm)
T1800, Fr. 9	714	337	2.12	20.0 ^d	17	13.1
T1800, Fr. 12	461	257	1.79	17.5 ^e	13	10.9
T1800, Fr. 15	321	224	1.43	16.2 ^d	11	9.4
T1800, Fr. 20	132	113.7	1.16	12.6 ^d	7.1	6.4
T2580 IVB, Fr. 2	71.8	64.6	1.11	9.9 ^d	–	4.8
T2580 IVB, Fr. 11	21.8	20.3	1.07	7.0 ^e	3.0	2.9

^a From supplier.

^b From Ref. [11], in pH 7.0, 0.3 M phosphate buffer, via diffusion coefficient by quasi-elastic light scattering (QELS).

^c From columns 2 and 5, via Eq. 5.

^d From Ref. [13], measured at 25°C in water.

^e By extrapolation from other data in this column using $[\eta] = 0.35 \times M_r^{0.30}$.

The samples (proteins, pullulans, Ficolls, and dendrimers) were dissolved in the buffer solution by the following procedure: after preliminary mixing with a Vortex Genie (Fisher Scientific), complete dissolution was carried out with a shaker (Thermolyne Speci-mix, Sybron) or a tumbler (Labquake). Samples were filtered (0.45 mm Gelman) prior to injection. K_{SEC} was calculated using Eq. 2 with V_0 determined from pullulan P-1600 ($M_r = 1.66 \cdot 10^6$) and V_t determined from D_2O . Typical values for V_t and V_0 were 20.44 ± 0.04 ml and 7.10 ± 0.08 ml, respectively. Every run was accompanied by at least one measurement with P-1600 and D_2O on the same day.

Superose 12 pH titration

In order to protonate all carboxylate groups on the surface of the gel, about 5 g of Superose 12 column material was acid-washed thoroughly for more than 3 h by tumbling in excess 0.5 M HCl. The excess acid was removed by washing with water at least 30 times until the pH of the top layer became constant (pH = 5.11). The washed gel was dried in an oven over anhydrous $CaSO_4$ at 45°C for more than two days.

362.2 mg of dried gel was suspended in 10.004 g of water (HPLC grade), then degassed by N_2 for 10 min. A layer of N_2 was maintained on the liquid surface throughout the titration process. The gel was titrated using a 0.2 ml microburet

Table 4
Characteristics of pullulan standards

Grade	$M_r \times 10^{-3}$ ^a	M_r/M_n ^a	$[\eta]$ (cm ³ /g)	R_s^b (nm)	R_η^c (nm)
P-1600	1660	1.19	306 ^d	—	43.2
P-400	380	1.12	115.5	17.6	19.1
P-200	186	1.13	70.4	12.8	12.8
P-100	100	1.10	45.9	8.8	9.0
P-50	48	1.09	28.6	6.1	6.0
P-20	23.7	1.07	18.1	4.0	4.1
P-10	12.2	1.06	11.9	3.0	2.9
P-5	5.8	1.07	7.9	2.1	1.9

^a From manufacturer (Showa Denko K.K.), in water at 25°C.

^b From Ref. [11], in pH 7.0, 0.3 M phosphate buffer, via diffusion coefficient by quasi-elastic light scattering (QELS).

^c Calculated from columns 2 and 4 via Eq. 5.

^d By extrapolation from other data in this column using.

(Gilmont) with 0.10 M NaOH from the initial pH value to pH 10. The same amount (by weight) of water was used for blank titrations: an acid blank titrated with 0.103 M HCl (calibrated against 0.10 M NaOH) and a base blank with 0.10 M NaOH. All titrations were carried out using an Orion Research microprocessor pH/millivolt meter (Model #811) with a Beckman combination electrode (Model #39846).

Calculation of Superose 12 surface charge density (σ_s)

A calibration plot of K_{SEC} versus R is given in Fig. 2. The linearity of the plot of $K_{SEC}^{1/2}$ versus R_η supports the cylindrical pore model and allows the calculation of the pore radius (r_p) according to Eq. 3. The second linear region in the plot at large K_{SEC} is attributed to very small pores which will appear non-existent to solute molecules with $R > 2$ nm. The pore radius calculated from an average of the two slopes is 16 nm, which is in good agreement with the value of 14 nm obtained by Potschka [10]. The pore volume, V_p , was calculated using:

$$V_p = V_t - V_0 \quad (6)$$

to give a value of 13.55 ml. The actual column volume, V_c , was calculated using:

$$V_c = \pi r^2 L \quad (7)$$

where L is the length of the column (29.3 cm) and r is the inner radius of the column (0.5 cm) to give a value of 23.6 ml. The mass of Superose 12 per unit volume for a packed column is 0.23 g/ml [14]. Thus the total mass of Superose gel in the column was 23.6 ml \times 0.23 g/ml = 5.4 g. The total pore area, A_p , was obtained from $V_p/A_p = r_p/2$, giving a column pore area of $2V_p/r_p = 1.7 \cdot 10^3$ m². The pore area per gram was thus $1.7 \cdot 10^3$ m²/5.4 g = 310 m²/g. During the titration, 362.2 mg dry gel was used, giving a total pore

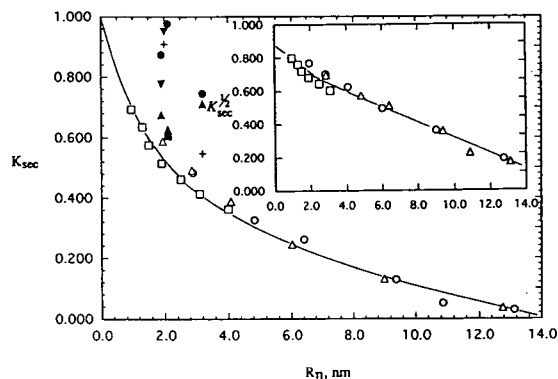


Fig. 2. Dependence of K_{SEC} on protein radius. The insert shows the ideal curve generated from data for pullulan (Δ), Ficoll (\circ), and dendrimers (\square) at pH 4.0 in 400 mM buffer. Proteins were run at pH 5.0 in various ionic strengths: 16 mM (\bullet), 66 mM (\blacktriangle), 84 mM (\blacksquare), 200 mM (\blacktriangledown), and 500 mM ($+$).

area involved in the titration of $0.3622 \text{ g} \times 310 \text{ m}^2/\text{g} = 110 \text{ m}^2$.

Finally, the column surface charge density, σ_s (C/m^2), was calculated by:

$$\sigma_s = \frac{N(V_s - V_b) \cdot N_A \cdot e}{110} \quad (8)$$

where N is the normality (molarity) of the NaOH used in the titration, V_s is the volume of NaOH consumed in the sample titration, V_b is the volume of NaOH consumed in the blank titration, N_A is Avogadro's number, and e is the electronic charge in Coulombs. The $N(V_s - V_b)$ term gives the number of equivalents of carboxyl groups on the surface of the gel.

Computer modeling

Structures for lysozyme (1hel), ribonuclease (7rsa), myoglobin (5mbn), and hemoglobin (2dhh) were imported from the Brookhaven Protein Databank to the Insight II molecular modeling system (Biosym Technologies, San Diego, CA, USA). The structures were set to pH 5.0 using the Set pH option in Biopolymer module which assigns charges to residues based on comparison with their $\text{p}K_a$ values. A DelPhi electrostatics calculation was run and positive potential contours were displayed in order to qualitatively determine the most positive patch on the protein surface. Residues were then colored red, blue, or white according to positive, negative, or neutral formal charges, respectively, and graphic displays were printed out from the Insight II molecular modeling system.

3. Results and discussion

The curve in Fig. 2 shows the dependence of K_{SEC} on solute radius for pullulan, Ficoll, and dendrimers all in $0.4 \text{ M NaH}_2\text{PO}_4\text{-Na}_2\text{HPO}_4$ at pH 4.0. Data for proteins, at pH 5.0 and ionic strength ranging from 16.8 mM to 500 mM are shown by filled symbols. From Fig. 2, the K_{SEC} values for the proteins all deviated from the "ideal calibration curve". The positive deviations reveal electrostatic attraction between charged

proteins and the weakly anionic Superose 12 packing surface.

A parameter analogous to k' in IEC needs to be defined in order to compare SEC data to the KRFR and the SJH models. Initially, ΔK , the vertical deviation between K_{SEC} of the solute and K_i (K_{SEC} of an "ideal" solute of the same size as the solute of interest) was used as this parameter. However, ΔK only measures the difference in the partition coefficients between proteins and "ideal" polymers and it does not isolate the free energy of interaction (ΔG_{int}) involved in the attraction between two charged surfaces. Potschka [15] has used the parameter ΔR , the horizontal displacement from the ideal curve, to describe repulsion in SEC; for attractive interactions, a negative value of ΔR may provide some measure of the magnitude of the non-ideal interaction [16] but has no physical meaning. We define K_{int} , which is analogous to k' , as:

$$K_{\text{int}} = \left(\frac{C_b}{C_f} \right) \quad (9)$$

where C_b is the concentration of bound protein and C_f is the concentration of free protein in the pore. In ideal SEC, C_b is zero and K_{int} is also zero. K_{int} can be measured experimentally by (see Appendix):

$$K_{\text{int}} = \left(\frac{K_{\text{SEC}}}{K_i} \right) - 1 = \left(\frac{\Delta K}{K_i} \right) \quad (10)$$

where K_i is the K_{SEC} of an "ideal" solute of the same size as the solute of interest.

In order to determine an "optimal" pH value where the value of K_{int} changes significantly with ionic strength, a function that corresponds to the Coulombic interaction between the protein and the column packing is required. The two pH-dependent variables involved in the interaction are protein net charge, Z , and column charge density, σ_s . Protein net charge is available from published titration data (for example: lysozyme, [17]) which may be either positive ($\text{pH} < \text{pI}$) or negative ($\text{pH} > \text{pI}$). Fig. 3 shows the dependence of Superose charge density, σ_s , (determined by

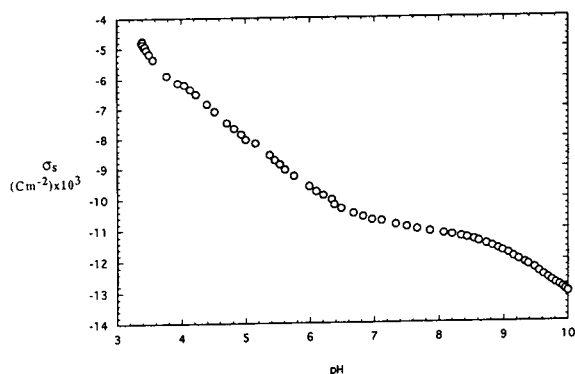


Fig. 3. Superose 12 titration curve in pure water at room temperature.

titration) on pH in pure water. (The addition of salt will shift the curve to higher σ_s but will not affect the trend shown in Fig. 4.) The product of σ_s and Z is plotted versus pH in Fig. 4 for lysozyme. The maximum of the curve in Fig. 4 should correspond to the strongest attraction between protein and packing, which in turn maximizes K_{int} .

Proteins were therefore eluted at pH 5.0 over an extended ionic strength range (16.8 mM to 500 mM) to examine the effect of ionic strength on protein retention. Table 5 lists the values of K_{int} , K_i , and Debye length (κ^{-1}) for the proteins at different ionic strength. All proteins show weaker attraction as ionic strength increases.

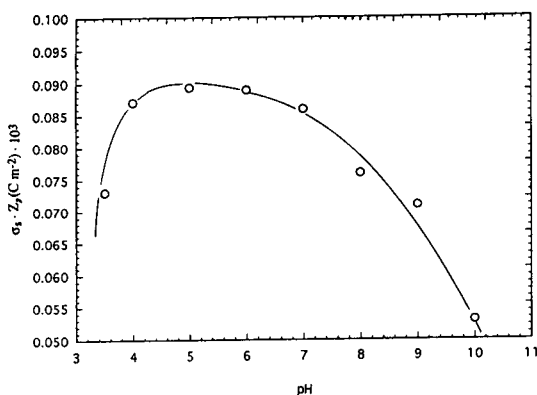


Fig. 4. Column charge density (σ_s) multiplied by lysozyme net charge (Z) versus pH.

Comparison with the KRFR model

The KRFR model predicts a linear dependence of $\ln k'$ with $\ln(1/I)$ and indicates that Z_p , the number of charged sites on a protein that interact with the packing surface, is given by the slope. Fig. 5 shows the relations between $\ln K_{\text{int}}$ and $\ln(1/I)$ for four proteins, all of which appear to display two different slopes with a break point near 100 mM. Table 6 lists the two Z_p values for each protein obtained from the different slopes. Although the trend of the results is reasonable in that there is stronger electrostatic attraction at lower ionic strength, the values are excessively small. In particular, lysozyme was strongly attracted to the column (retention time ~ 2 h at $I = 27$ mM), which is difficult to reconcile with a partial charge of $+0.5$ controlling the interaction. Fig. 6 shows the most positive sides of the four proteins colored black, from which it is apparent that the low values for Z_p are unreasonable. A possible interpretation is that the low charge density of Superose compared to that of the protein does not allow each protein charge to interact with a corresponding column charge.

Comparison with the SJH model

Linear dependence of $\ln k'$ on $1/\sqrt{I}$ over a moderate ionic strength range ($250 \text{ mM} < I < 1000 \text{ mM}$) is predicted by the SJH model. Fig. 7 shows the dependencies of $\ln K_{\text{int}}$ on $1/\sqrt{I}$ for four proteins over an ionic strength range of 16.8 mM to 500 mM. Two proteins, lysozyme and hemoglobin, appear to be in agreement within experimental error with the prediction of the SJH model. However, for the proteins, ribonuclease and myoglobin, linearity is lost at low ionic strength.

According to the SJH model, protein charge can be calculated via the equation:

$$q_{\text{chr}} = \sqrt{\frac{SA_p^\circ}{135}} \quad (11)$$

where S is the slope of the $\ln k'$ versus $1/\sqrt{I}$ plot when I is in M , A_p° is the protein surface area in $\text{\AA}^2/\text{molecule}$ [18], and the constant 135 comes

Table 5
Protein K_{int} results at pH 5.0 (acetic acid buffer)

I (mM)	κ^{-1} (nm)	K_{int}^a			
		Hemoglobin	Myoglobin	RNAse	Lysozyme
6.3	3.78	b	3.00	b	b
12.0	2.74	b	2.46	1.30	b
16.8	2.32	b	0.74	0.48	b
27.3	1.82	b	b	0.33	2.58
42.1	1.46	0.82	0.14	0.18	2.08
66.0	1.17	0.62	0.12	0.15	1.24
84.0	1.04	0.44	0.08	0.14	1.00
200.0	0.67	0.31	0.07	0.12	0.66
400.0	0.47	0.24	0.06	0.10	0.65
500.0	0.42	0.24	0.05	0.09	0.62

^a $K_1 = 0.44$ for hemoglobin, 0.56 for myoglobin, 0.59 for RNAse, and 0.56 for lysozyme.

^b Values of K_{int} not reported primarily due to excessively long retention.

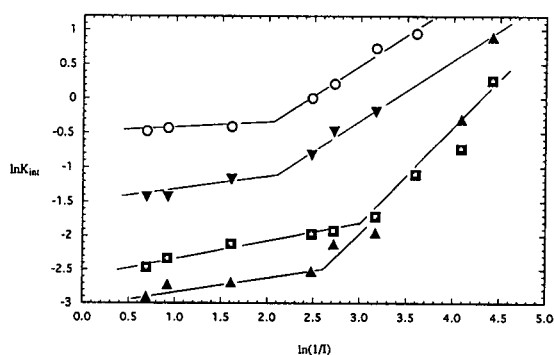


Fig. 5. Comparison with KRFR model: $\ln K_{\text{int}}$ versus $\ln(I/I)$. Proteins were run at pH 5.0 in various ionic strengths as cited in Table 6: lysozyme (\circ), RNAse (\blacksquare), myoglobin (\blacktriangle), and hemoglobin (\blacktriangledown).

Table 6
Protein charge (Z_p) obtained according to the KRFR model, for two ranges of I

Protein	Z_p	
	5–100 mM	200–500 mM
Lysozyme	0.5	0.03
RNAse	0.7	0.14
Myoglobin	0.8	0.17
Hemoglobin	0.4	0.15

from a combination of fundamental constants. Ref. [2] indicates that this equation is only true when the column charge density is greater than the protein charge density. Our case is the opposite: protein charge density is greater than column charge density. Under these conditions, column charge density may be obtained as [2]:

$$\sigma_s = \sqrt{\frac{2 SF(2 RT\epsilon_0\epsilon_r)^{1/2}}{A_p^0}} \quad (12)$$

where σ_s is in C/m^2 when S is the slope of the $\ln k'$ versus $1/\sqrt{I}$ plot with I in mol/m^3 ; F is Faraday's constant given as $96485.31 \text{ C}/\text{mol}$; R , the universal gas constant, is $8.314 \text{ J}/\text{mol}\cdot\text{K}$; T is 298 K ; ϵ_0 , the permittivity of vacuum, is $8.85 \cdot 10^{-12} \text{ C}^2/\text{J}\cdot\text{m}$; and ϵ_r is the dimensionless solvent dielectric (80). The calculated values which range from $7 \cdot 10^{-3}$ to $11 \cdot 10^{-3} \text{ C}/\text{m}^2$ are in excellent agreement with the value of $8 \cdot 10^{-3} \text{ C}/\text{m}^2$ obtained at pH 5.0 from the titration curve (Fig. 3) of Superose 12.

The good agreement between our results and the SJH treatment is interesting in that SJH models the protein as a uniformly surface-charged sphere. This is diametrically opposite to the KRFR approach which emphasizes the charge heterogeneity, and specifies that k' is exclusively controlled by a few charges at one site. The SJH approach is also at variance with

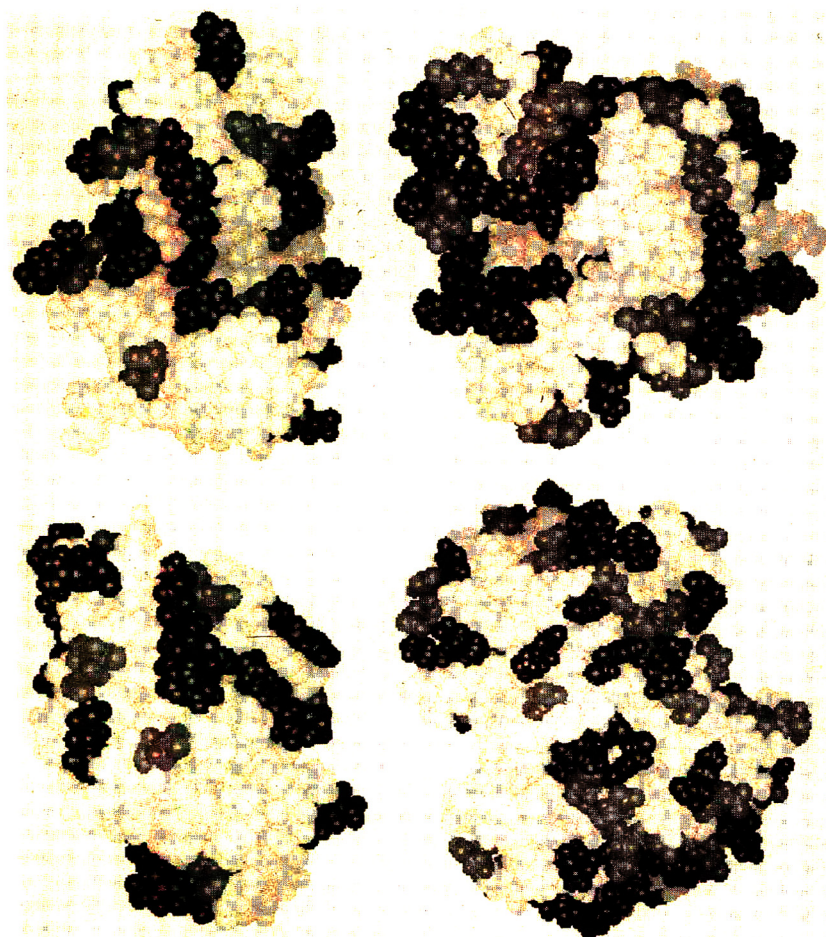


Fig. 6. Computer models of ribonuclease (upper left), myoglobin (upper right), lysozyme (lower left), and hemoglobin (lower right) at pH 5.0. Black, grey, and white indicate positive, negative, and neutral charged residues, respectively. It should be noted that these structures are not drawn to scale.

the observation that proteins are often retained on IEC columns whose charge is of the same sign as the net protein charge. It is possible that the SJH treatment works best on weak ion-exchange resins (such as that used here) to which the protein does not bind in a unique orientation; if all orientations contribute to k' , then the global protein charge may be the dominant factor. On the other hand, the KRFR treatment might be somewhat more realistic in the case of strong IEC columns in low-ionic strength media, where in one particular protein orientation corresponds

to a pronounced energy minimum. In this case, a relatively small number of charged residues could control binding.

4. Conclusion

Experimental data were compared to two semi-empirical expressions for the dependence of protein retention (k') on ionic strength (I). The two corresponding theories differ in both the form of the dependence of k' on I , as well as the

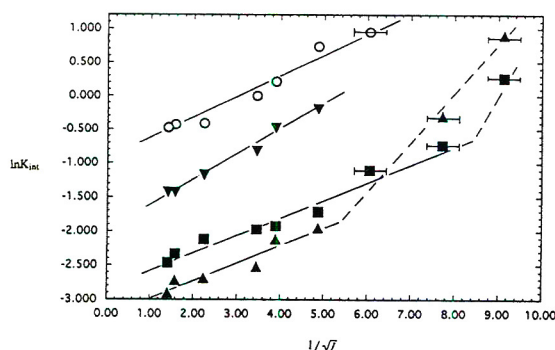


Fig. 7. Comparison with SJH model: $\ln K_{\text{int}}$ versus $(1/\sqrt{I})$. Proteins were run at pH 5.0 in various ionic strengths as cited in Table 6: lysozyme (\circ), RNase (\blacksquare), myoglobin (\blacktriangle), and hemoglobin (\blacktriangledown).

method for calculation of the protein and/or packing charge. The KRFR model does not conform to our results with respect to either the form of the dependence or the calculation of the protein charge. The SJH model agrees with the shape of the dependence of k' on I , and yields therefrom a calculated value for the column packing surface charge density in agreement with the experimental result.

The predictions offered in the context of the SJH theory are presented for two cases: $\sigma_s > \sigma_p$ and $\sigma_s < \sigma_p$ [2]. The validity of the theory was earlier checked against experimental data only for the first case [2], while in the present work the latter case alone was studied. Further experimental work should be carried out over a wider range of σ_s and σ_p , especially at values of σ_s near σ_p , in order to provide a more complete test of the SJH model.

Acknowledgment

This work was supported by NSF grant No. CHE-9021484. We thank Dr. K. Granath for the Ficoll fractions and Dr. Lars Hagel for the Superose column. We also thank Daniel Robertson of the Facility for Computational Molecular and Biomolecular Science at Indiana University–Purdue University for his assistance with the computer modeling.

Appendix

The desired quantity is related to the interaction energy, ΔG_{int} , for the binding (adsorption) of a protein to the column packing. Within a pore of the packing, the concentration of free and bound protein are related by:

$$C_b = C_f e^{-\Delta G_{\text{int}}/RT} \quad (\text{A1})$$

or

$$K_{\text{int}} = \left(\frac{C_b}{C_f} \right). \quad (\text{A2})$$

In ideal SEC, C_b is zero, therefore K_{int} is zero. In non-ideal SEC, the total concentration of protein in the pore is given by:

$$C_p = C_b + C_f. \quad (\text{A3})$$

The observed elution volume is given by:

$$V_{\text{obs}} = V_0 + K_{\text{SEC}} V_p \quad (\text{A4})$$

where K_{SEC} is the relative probability of the protein being inside the pore, given by:

$$K_{\text{SEC}} = \frac{C_p}{C_0} \quad (\text{A5})$$

where C_0 is the concentration of the protein in the mobile phase. For ideal SEC,

$$V_i = V_0 + K_i V_p \quad (\text{A6})$$

where K_i is given by:

$$K_i = \frac{C_p}{C_0}. \quad (\text{A7})$$

Under non-ideal conditions, $K_i = C_f/C_0$. From Eq. A2,

$$\begin{aligned} K_{\text{int}} &= \frac{C_b}{C_f} = \frac{C_b/C_0}{C_f/C_0} = \frac{C_p/C_0}{C_f/C_0} (C_b/C_p) \\ &= \frac{K_{\text{SEC}}}{K_i} \cdot \frac{C_b}{C_p} \end{aligned} \quad (\text{A8})$$

and from Eq. A3,

$$\frac{C_b}{C_p} = \frac{C_b}{C_b + C_f} = \frac{C_b/C_f}{(C_b/C_f) + 1} = \frac{K_{\text{int}}}{K_{\text{int}} + 1} \quad (\text{A9})$$

Now, by substituting A9 into A8, we get:

$$K_{\text{int}} = \frac{K_{\text{SEC}}}{K_i} \left(\frac{K_{\text{int}}}{K_{\text{int}} + 1} \right) \quad (\text{A10})$$

This by rearrangement gives:

$$K_{\text{int}} = \frac{K_{\text{SEC}}}{K_i} - 1 = \frac{\Delta K}{K_i} \quad (\text{A11})$$

References

- [1] W. Kopaciewicz, M.A. Rounds, J. Fausnaugh and F.E. Regnier, *J. Chromatogr.*, 283 (1984) 37.
- [2] J. Ståhlberg, B. Jönsson and Cs. Hörváth, *Anal. Chem.*, 63 (1991) 1867.
- [3] See, for example, K. Gooding and F. Regnier (Editors), *High Performance Liquid Chromatography of Biological Macromolecules: Methods and Applications*, Marcel Dekker, New York, 1988.
- [4] N.K. Boardman and S.M. Partridge, *Biochem. J.*, 59 (1955) 543.
- [5] V. Lesins and E. Ruckenstein, *J. Colloid Interface Sci.*, 132 (1989) 566.
- [6] W. Kopaciewicz and F.E. Regnier, *Nonideal Size-Exclusion Chromatography of Proteins: Effects of pH at Low Ionic Strength*, paper presented at the *International Symposium on HPLC of Proteins and Peptides*, November 16–17, 1981, Washington D.C.
- [7] H. Waldmann-Mayer, *J. Chromatogr.*, 350 (1991) 1.
- [8] P.J. Flory, *Principles of Polymer Chemistry*, Cornell University Press, Ithaca, NY, 1953, p. 606.
- [9] M. le Maire, A. Ghazi, J.V. Moller and L.P. Aggerberk, *Biochem. J.*, 243 (1987) 399.
- [10] M. Potschka, *J. Chromatogr.*, 587 (1991) 276.
- [11] P.L. Dubin, S.L. Edwards, M.S. Mehta, and D. Tomalia, *J. Chromatogr.*, 635 (1993) 51.
- [12] P.L. Dubin, S.L. Edwards, M.S. Mehta, J.I. Kaplan and J. Xia, *Anal. Chem.*, 64 (1992) 2344.
- [13] G. Shah and P. Dubin, unpublished results.
- [14] K. Fjarstedt, Pharmacia Biotech, private communication.
- [15] M. Potschka, *J. Chromatogr.*, 441 (1988) 239.
- [16] S.L. Edwards and P.L. Dubin, *J. Chromatogr.*, 648 (1993) 3.
- [17] C. Tanford, *J. Am. Chem. Soc.*, 76 (1956) 3331.
- [18] J. Ståhlberg, Astra Pharmaceutical, private communication.



ELSEVIER

Journal of Chromatography A, 693 (1995) 263–270

JOURNAL OF
CHROMATOGRAPHY A

High-performance liquid chromatography with chemiluminescence detection of derivatized microcystins

Hideaki Murata^{a,*}, Hiroko Shoji^a, Motoji Oshikata^a, Ken-Ichi Harada^a,
Makoto Suzuki^a, Fumio Kondo^b, Hideko Goto^c

^aFaculty of Pharmacy, Meijo University, Tempaku, Nagoya 468, Japan

^bAichi Prefectural Institute of Public Health, Tsuji-machi, Kita, Nagoya 462, Japan

^cJASCO Corporation, Ishikawa-cho, Hachioji-shi, Tokyo 192, Japan

First received 26 July 1994; revised manuscript received 1 November 1994; accepted 1 November 1994

Abstract

Microcystins, hepatotoxic peptides produced by cyanobacteria, strongly inhibit protein phosphatases 1 and 2A in a manner similar to okadaic acid and possess tumor-promoting activity. Low-dose constant exposure to microcystins is being suspected of incidence of primary liver cancer. We tried to establish a chemical method for individual detection and determination of trace amounts of microcystins in the low femtomole range using peroxyoxalate chemiluminescence (PO-CL) detection. In order to detect microcystins with CL, dansyl-cysteine adducts of microcystins RR, YR and LR (Dns-Cys-RR, -YR and -LR) were prepared. The Dns-Cys adducts of microcystins are based on nucleophilic addition of the thiol group in cysteine to the α,β -unsaturated carbonyl of the N-methyldehydroalanine moiety. A HPLC system with three pumps was constructed, in which one pump is used for delivering the mobile phase, and the other two pumps deliver the imidazole–nitrate buffer and PO-CL reagent, respectively. The optimization of the imidazole–nitrate buffer and PO-CL reagent was investigated. The detection limits for Dns-Cys-RR, -YR and -LR were less than 15 fmol (S/N 10), and the relationship between the peak area and concentration of Dns-Cys-RR, -YR and -LR was linear in the range 15–1670 fmol (Dns-Cys-RR, $r = 0.994$; Dns-Cys-YR, $r = 0.997$; Dns-Cys-LR; $r = 0.999$).

1. Introduction

The occurrence of toxic freshwater blooms of cyanobacteria (blue-green algae) has been reported in many countries. These toxic water blooms have caused deaths of domestic animals and wildlife [1]. Toxins produced by cyanobacteria include hepatotoxins such as microcystins, nodularins and cylindrospermopsin, and neurotoxins such as anatoxin-a, anatoxin-a(s) and

aphantoxins [2]. Much attention has been paid to microcystins because of their biological activities and wide distribution all over the world. They have been produced by *Microcystis*, *Oscillatoria*, *Anabaena* and *Nostoc* [2] and have a common moiety composed of 3-amino-9-methoxy-10-phenyl-2,6,8-trimethyldeca-4,6-dienoic acid (Adda), N-methyldehydroalanine (Mdha), D-alanine, β -linked D-erythro- β -methylaspartic acid, and γ -linked D-glutamic acid and two L-amino acids as variants [1]. Over 50 microcystins have been isolated so far.

* Corresponding author.

Microcystins strongly inhibit protein phosphatases 1 and 2A in a manner similar to okadaic acid and show tumor-promoting activity [3–7]. Although human deaths by cyanobacteria toxicosis have not been reported, low-dose constant exposure of microcystins is suspected of incidence of primary liver cancer (PLC). Yu [8] has reported that there are about 100 000 deaths annually from PLC caused by various factors in China. The higher incidence of PLC in Qidong and Haimen counties near Shanghai does not correlate with PLC-causing agents such as aflatoxin and hepatitis B virus, but people who drank pond and ditch water had a higher risk of PLC than people who drank well water [8]. This may suggest that the incidence of PLC is related to microcystins in the drinking water.

In our preliminary experiments in Japan, microcystins were detected in a eutrophicated lake at concentration of at most $\mu\text{g/l}$ levels. To precisely analyze microcystins in a complex matrix, lower femtomole quantities have to be detected. Although HPLC–UV detection has been widely used for this purpose [9], its detection limit was estimated to be at most at picomole level. There have been several attempts to detect microcystins sensitively using HPLC with fluorescence detection for an oxidation product of microcystins [10], enzyme-linked immunosorbent assay (ELISA) [11,12] and HPLC-linked protein phosphatase bioassay [13,14]. Although these methods are useful for sensitive screening of microcystins, they could not separately determine microcystins. It was reported that protein phosphatases are also inhibited by compounds other than microcystins in cyanobacteria [15].

It is desirable to establish a chemical method for individual detection and determination of trace amounts of microcystins in the low femtomole range. Recently, peroxyoxalate chemiluminescence (PO-CL) detection has been investigated for highly sensitive detection of fluorophores [16,17]. Thus, we tried to apply this detection method to establish a sensitive analysis method for microcystins. However, there is no appropriate fluorophore in the molecules for PO-CL detection. In this paper, we describe a suitable derivatization method for the detection,

optimization of operation conditions including chromatography and an evaluation of the established analysis method with PO-CL detection.

2. Experimental

2.1. Chemicals

Bis[4-nitro-2-(3,6,9-trioxadesyloxycarbonyl)phenyl]oxalate (TDPO), dansyl chloride (Dns-Cl) and hydrogen peroxide (30%) were purchased from Wako (Osaka, Japan), imidazole from Tokyo Chemical Industry (Tokyo, Japan), acetonitrile, phosphoric acid, potassium dihydrogenphosphate from Nacalai Tesque (Kyoto, Japan), and cysteine and Dns-Ala from Sigma (St. Louis, MO, USA). Distilled water was purified with a Barnsted E-pure system (Boston, MA, USA). Microcystins RR and LR were purified from water blooms of Lake Suwa in Japan and microcystin YR from the culture strain *Microcystis aeruginosa* M-228 according to Ref. [18].

2.2. Preparation of Dns-Cys adducts of microcystins

A mixture of microcystin LR (4.5 mg) and cysteine (5.5 mg) in 5% potassium carbonate aqueous solution was stirred for 1 h at room temperature. The reaction mixture was neutralized with 0.2 M hydrochloric acid and applied to an ODS cartridge (Baker, NJ, USA). The cartridge was washed with 10 ml of water and then eluted with 15 ml of methanol–water (90:10) to give 6.2 mg of the reaction product. The reaction product was reacted with 1.5 ml of Dns-Cl acetone solution (10 mg/ml) in 2.0 ml of 0.2 M sodium hydrogencarbonate for 1 h at 40°C. After evaporation of acetone, 10 ml of water were added to the solution, which was then applied to an ODS cartridge. The cartridge was washed with 10 ml of water and then eluted with 15 ml of methanol–water (90:10). The eluate was evaporated to dryness and the reaction product was purified by preparative HPLC to give 1.4 mg of Dns-Cys-LR. Dns-Cys-YR and -RR were simi-

the toxins reacted with cysteine to give the Cys adducts under slightly basic conditions in the first step, and then the adducts were further converted to the Dns-Cys adducts by the usual dansylation reaction in the second step. Finally, three Dns-Cys adducts of microcystins RR, YR and LR were smoothly prepared and used in subsequent studies.

3.2. Parameters for PO-CL detection conditions

PO-CL is known to be one of the most sensitive detection methods in HPLC, and it shows a detection limit in the low femtomole range for many compounds. The proposed mechanism of the PO-CL reaction consists of: (1) the production of a key chemical intermediate such as 1,2-dioxetanedione; (2) the conversion of the chemical energy into electron energy; (3) the emission of the fluorophore. Aryl oxalate and hydrogen peroxide generated PO-CL in the presence of fluorescent compounds. In HPLC using PO-CL detection, imidazole–nitrate buffer has been frequently added to the mobile phase for production efficiency, because it not only adjusts the pH of the mobile phase to around neutral but also serves as a catalyst for the production [21].

Because microcystins and their Dns-Cys adducts are well separated by HPLC using acidic aqueous methanol as a mobile phase such as methanol–0.05 M phosphate buffer (pH 3) or methanol–0.05% TFA in water [9], it was not desirable to use a mobile phase including imidazole–nitrate buffer in our case. We constructed a HPLC system with three pumps, in which pump 1 is used for delivering the mobile phase, and pumps 2 and 3 deliver the imidazole–nitrate buffer and PO-CL reagent, respectively, as shown in Fig. 2 [22]. The mobile phase, acetonitrile–0.05% TFA in water (40:60), was used in the present study, because PO-CL intensity in acetonitrile was significantly higher than that in methanol [23,24] and the mobile phase including acetonitrile resulted in good separation for Dns-Cys-LR, -YR and -RR as shown later.

Acetonitrile–water (50:50) and 100% acetonitrile

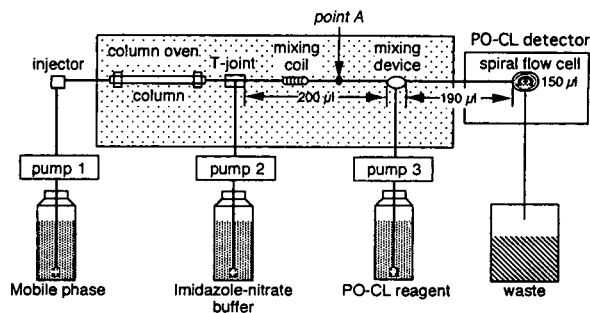


Fig. 2. Schematic diagram of HPLC system for PO-CL detection.

trile were used as the dissolving solvents of the imidazole–nitrate buffer and PO-CL reagent because of smooth mixing with the mobile phase and the stability of PO-CL reagent, respectively [26]. Because the solubility of TDPO in acetonitrile is higher than that of bis(2,4,6-trichlorophenyl)oxalate (TCPO), which has been widely used as an aryl oxalate derivative, and TDPO gives higher PO-CL intensity than that given with TCPO [25], TDPO was selected as the aryl oxalate for the CL reagent. Thus, the optimization of the imidazole–nitrate buffer (pH, concentration of imidazole and flow-rate) and the PO-CL reagent (concentrations of TDPO and hydrogen peroxide, and flow-rate) was mainly investigated for sensitive PO-CL detection.

3.3. Optimization of operating conditions

Firstly, the effect of the pH of the imidazole–nitrate buffer on PO-CL intensity was examined using Dns-Ala as a model compound. Although the maximum PO-CL intensity was observed around pH 7.0 of the imidazole–nitrate buffer, it was essential to adjust the mobile phase at point A (Fig. 2) to pH 6.4 as shown in Fig. 3. The pH at point A was influenced by the concentration of imidazole and the flow-rate of imidazole–nitrate buffer (Table 1). Therefore, we carried out the following experiments for the imidazole–nitrate buffer: (1) imidazole–nitrate buffers (pH 7.0) in acetonitrile–water (50:50) with various concentrations of imidazole were prepared; (2) flow-rates of imidazole–nitrate buffers were de-

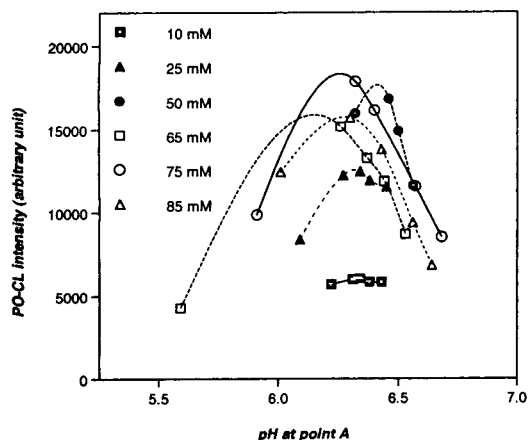


Fig. 3. Effect of imidazole concentration on PO-CL intensity. Mobile phase: acetonitrile–0.05% TFA in water (40:60), 1.0 ml/min; 10–85 mM imidazole–nitrate buffer (pH 7.0) in acetonitrile–water (50:50); flow-rate; see Table 1; PO-CL reagent: 0.25 mM TDPO + 12.5 mM hydrogen peroxide in acetonitrile, 1.5 ml/min. Sample: Dns-Ala 100 pg/ μ l, 2- μ l injection.

terminated to adjust the solution at point A to pH 6.4; (3) PO-CL intensities were measured under the conditions mentioned above (Fig. 3). The PO-CL intensity increased with increasing imida-

zole concentration and reached a maximum at 75 mM. Consequently, a concentration of 75 mM and a flow-rate of 0.2 ml/min for imidazole–nitrate buffer (pH 7.0) were chosen as the optimal conditions.

The effects of TDPO and hydrogen peroxide concentrations on the PO-CL intensity are shown in Fig. 4a and b, respectively. A maximum of the PO-CL intensity was obtained at 0.5 mM TDPO. Although the PO-CL intensity increased with increasing concentration of hydrogen peroxide, it did not change when the concentration exceeded 50 mM. Fig. 4c also shows the relationship between PO-CL intensity and flow-rate of the PO-CL reagent. The PO-CL intensity increased rapidly with increasing flow-rate in the range of 1.0–2.0 ml/min and then remained nearly constant up to 3.0 ml/min, but it decreased rapidly in the range of 3.0–4.0 ml/min. The decrement in the PO-CL intensity at higher flow-rates may be due to a time lag for emission, the volume (190 μ l) between the rotating flow mixing device and the spiral flow cell and the total flow-rate of pumps 1, 2 and 3. It was reported that the time lag of emission is 5 to 10 s in PO-CL detection [26]. When the PO-

Table 1
Relationship between flow-rate and concentration of imidazole–nitrate buffer to adjust to pH 6.4 at point A

Imidazole concentration (mM)		Run				
		1	2	3	4	5
10	ml/min	0.90	1.00	1.10	1.20	1.30
	pH	6.22	6.31	6.34	6.38	6.43
25	ml/min	0.30	0.40	0.45	0.50	0.60
	pH	6.09	6.27	6.34	6.38	6.45
50	ml/min	0.10	0.20	0.25	0.30	0.40
	pH	4.26	6.32	6.46	6.50	6.56
65	ml/min	0.10	0.20	0.25	0.30	0.40
	pH	5.59	6.26	6.37	6.44	6.53
75	ml/min	0.10	0.17	0.20	0.30	0.40
	pH	5.91	6.32	6.40	6.57	6.68
85	ml/min	0.10	0.15	0.20	0.30	0.40
	pH	6.01	6.30	6.43	6.56	6.64

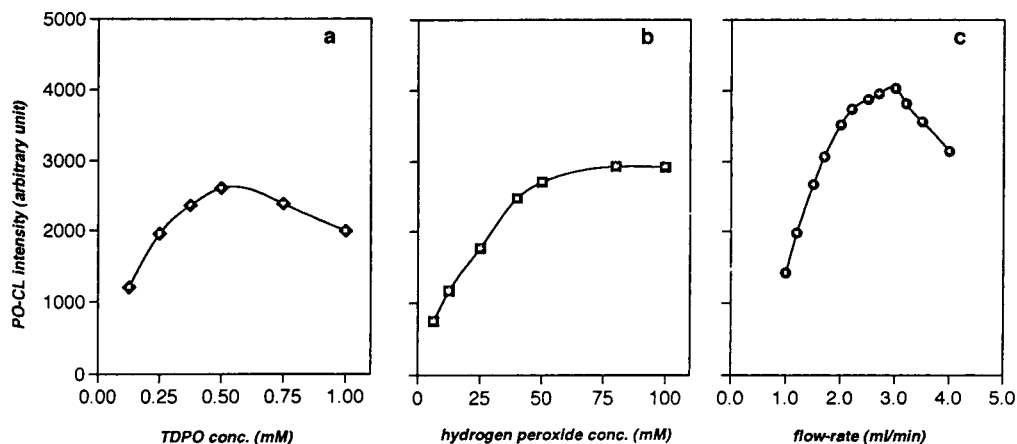


Fig. 4. Effect of (a) TDPO and (b) hydrogen peroxide concentration, and (c) flow-rate of PO-CL reagent on PO-CL intensity. Mobile phase: acetonitrile–0.05% TFA in water (40:60), 1.0 ml/min; 75 mM imidazole–nitrate buffer in acetonitrile–water (50:50) (pH 7.0), 0.2 ml/min; PO-CL reagent: (a) 0.125–1.0 mM TDPO + 100 mM hydrogen peroxide in acetonitrile, 1.5 ml/min, (B) 0.5 mM TDPO + 6.25–100 mM hydrogen peroxide in acetonitrile, 1.5 ml/min, (c) 0.5 mM TDPO + 50 mM hydrogen peroxide in acetonitrile, 1.0–4.0 ml/min. Sample: Dns-Ala 100 pg/ μ l, 2- μ l injection.

CL reagent was delivered at over 3.0 ml/min, a fluorescent compound was mainly emitted out of the spiral flow cell in our apparatus, leading to the conclusion that it is most effective to deliver the PO-CL reagent at 2.0 ml/min. Therefore, 0.5 mM TDPO + 50 mM hydrogen peroxide in acetonitrile (flow-rate 2.0 ml/min) was optimized as the PO-CL reagent. In addition, PO-CL reagent in 100% acetonitrile was found to be stable for 48 h.

3.4. HPLC separation with PO-CL detection

As a result of extensive experiments, the measuring conditions for the Dns-Cys adduct of microcystins were established as follows. Acetonitrile–0.05% TFA in water (40:60) was used as the mobile phase and the flow-rate was set at 1.0 ml/min. The eluent from the column was mixed with 75 mM imidazole–nitrate buffer (pH 7.0) in acetonitrile–water (50:50), whose flow-rate was 0.2 ml/min, and the pH value of the resulting solution was adjusted to 6.4. Then the PO-CL reaction was performed by mixing 0.5 mM TDPO + 50 mM hydrogen peroxide in acetonitrile. The flow-rate of the CL reagent was set at 2.0 ml/min.

The HPLC profile of Dns-Cys-RR, -YR, and -LR with PO-CL detection is shown in Fig. 5, and the three components are clearly separated from one another. The detection limits for Dns-Cys-RR, -YR, and LR were less than 15 fmol (S/N 10), and the relationship between the peak area and the concentration of the microcystin Dns-Cys adducts was linear in the range 15–1670 fmol (Dns-Cys-RR, $r = 0.994$; Dns-Cys-YR, $r = 0.997$; Dns-Cys-LR, $r = 0.999$). Finally, the sen-

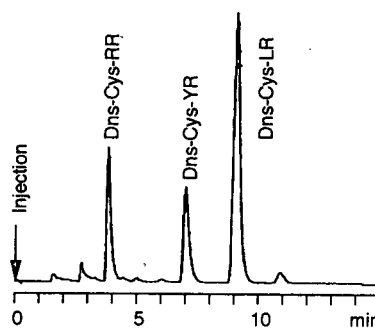


Fig. 5. HPLC separation of Dns-Cys-RR, Dns-Cys-YR and Dns-Cys-LR with PO-CL detection. Mobile phase: acetonitrile–0.05% TFA in water (40:60), 1.0 ml/min; 75 mM imidazole–nitrate buffer in acetonitrile–water (50:50) (pH 7.0), 0.2 ml/min; PO-CL reagent: 0.5 mM TDPO + 50 mM hydrogen peroxide in acetonitrile, 2.0 ml/min.

sitivities of Dns-Cys-LR with UV, FL and CL detection were compared. Although the sensitivity of Dns-Cys-LR with FL was similar to that with UV, the sensitivity with PO-CL was 200 times greater than that with UV and FL detection.

In order to detect microcystins more sensitively, HPLC with PO-CL detection was established. In our system, Dns-Cys adducts of microcystins can be detected in the femtomole range, which was as sensitive as previous methods, such as phosphatase bioassay, ELISA and HPLC–FL for oxydative degradation product of microcystins. While the previous studies could not detect microcystins separately, our method can detect individual microcystins with high sensitivity. Furthermore, the established method also provides the additional advantage that any microcystin can be specifically detected based on nucleophilic addition of a thiol group to the α,β -unsaturated carbonyl of the Mdha moiety followed by dansylation, because the moiety is common with all microcystins isolated.

For an actual analysis of trace amounts of microcystins in a complicated matrix such as lake water, we have to optimize the following three steps: (1) clean-up step for microcystins in environmental samples; (2) derivatization step for CL detection and preparation of an internal standard; (3) analysis step for highly sensitive detection with CL-detection. In the present paper we describe a suitable derivatization for CL detection and its optimization of operation conditions including LC, which corresponds to the third step. Recently, Tsuji et al. [27] reported a clean-up method for analysis of trace amounts of microcystins in lake water, which can be applied to our method. Consequently, we have to establish the second step. The reactivity of the fluorescence derivatization and preparation of an internal standard for the quantitative analysis are being examined.

Acknowledgement

We thank Dr. M.F. Watanabe, Tokyo Metropolitan Research Laboratory of Public Health,

Tokyo, Japan, for providing *M. aeruginosa*, M-228.

4. References

- [1] W.W. Carmichael, in *A Status Report on Planktonic Cyanobacteria (Blue-Green Algae) and their Toxins*, Environmental Monitoring Systems Laboratory, Office of Research and Development, US Environmental Protection Agency, Cincinnati, OH, 1992, p. 15.
- [2] W.W. Carmichael, *J. Appl. Bacteriol.*, 72 (1992) 445.
- [3] S. Yoshizawa, R. Matsushima, M.F. Watanabe, K.-I. Harada, A. Ichihara, W.W. Carmichael and H. Fujiki, *J. Cancer Res. Oncol.*, 116 (1990) 609.
- [4] R. Matsushima, S. Yoshizawa, M.F. Watanabe, K.-I. Harada, M. Furusawa, W.W. Carmichael and H. Fujiki, *Biochem. Biophys. Res. Commun.*, 171 (1990) 867.
- [5] C. MacKintosh, K.A. Beattie, S. Klumpp, P. Cohen and G.A. Codd, *FEBS Lett.*, 264 (1990) 187.
- [6] J.E. Eriksson, D. Toivola, J.A.O. Meriluoto, H. Karaki, Y.-G. Han and D. Hartshorne, *Biochem. Biophys. Res. Commun.*, 173 (1990) 1347.
- [7] R. Nishiwaki-Matsushima, T. Ohta, S. Nishiwaki, M. Saganuma, K. Kohyama, T. Ishikawa, W.W. Carmichael and H. Fujiki, *J. Cancer Res. Clin. Oncol.*, 118 (1992) 420.
- [8] S.-Z. Yu, in Z.-Y. Tang, M.-C. Wu and S.-S. Xia (Editors), *Primary Liver Cancer*, Springer, Berlin, 1989, p. 30.
- [9] K.-I. Harada, K. Matsuura, M. Suzuki, M.F. Watanabe, S. Oishi, A.M. Dahlem, V.R. Beasley and W.W. Carmichael, *J. Chromatogr.*, 448 (1988) 275.
- [10] T. Sano, N. Nohara, F. Shiraishi and K. Kaya, *Int. J. Environ. Anal. Chem.*, 49 (1992) 163.
- [11] F.S. Chu, X. Huang, R.D. Wei and W.W. Carmichael, *Appl. Environ. Microbiol.*, 55 (1989) 1928.
- [12] F.S. Chu, X. Huang and R.D. Wei, *J. Assoc. Off. Anal. Chem.*, 73 (1990) 451.
- [13] C.F.B. Holmes, *Toxicon*, 29 (1991) 469.
- [14] T.W. Lambert, M.P. Boland, C.F.B. Holmes and S.E. Hrudey, *Environ. Sci. Technol.*, 28 (1994) 753.
- [15] A.T.R. Sim and L.-M. Mudge, *Toxicon*, 31 (1993) 1179.
- [16] P.J.M. Kwakman and U.A.Th. Brinkman, *Anal. Chim. Acta*, 266 (1992) 175.
- [17] G.J. de Jong and P.J.M. Kwakman, *J. Chromatogr.*, 492 (1989) 319.
- [18] K.-I. Harada, M. Suzuki, A.M. Dahlem, V.R. Beasley, W.W. Carmichael and K.L. Rinehart, Jr., *Toxicon*, 26 (1988) 433.
- [19] K. Miyaguchi, K. Honda and K. Imai, *J. Chromatogr.*, 316 (1984) 501.
- [20] F. Kondo, Y. Ikai, H. Oka, M. Okumura, N. Ishikawa, K.-I. Harada, K. Matsuura, H. Murata, and M. Suzuki, *Chem. Res. Toxicol.*, 5 (1992) 591.

- [21] H. Neuvonen, *J. Chem. Soc., Perkin Trans. II*, (1990) 669.
- [22] N. Hanaoka, *J. Chromatogr.*, 503 (1990) 155.
- [23] S. Kobayashi and K. Imai, *Anal. Chem.*, 52 (1980) 424.
- [24] R. Weinberger, *J. Chromatogr.*, 314 (1984) 155.
- [25] K. Imai, H. Nawa, M. Tanaka and H. Ogata, *Analyst*, 111 (1986) 209.
- [26] K. Honda, K. Miyaguchi and K. Imai, *Anal. Chim. Acta*, 177 (1985) 103.
- [27] K. Tsuji, S. Naito, F. Kondo, M.F. Watanabe, S. Suzuki, H. Nakazawa, M. Suzuki, T. Shimada and K.-I. Harada, *Toxicon*, 32 (1994) 1251.



ELSEVIER

Journal of Chromatography A, 693 (1995) 271–279

JOURNAL OF
CHROMATOGRAPHY A

Separation of geometrical retinol isomers in food samples by using narrow-bore high-performance liquid chromatography

Elisabeth Brinkmann^a, Lutz Dehne^b, Henny Bijosono Oei^a, Reinhard Tiebach^b,
Werner Baltes^{a,*}

^aInstitut für Lebensmittelchemie der Technischen Universität Berlin, Gustav Meyer-Allee 25, D-13355 Berlin, Germany

^bMax von Pettenkofer-Institut des Bundesgesundheitsamtes, Thielallee 88-92, D-14195 Berlin, Germany

First received 28 February 1994; revised manuscript received 26 October 1994; accepted 26 October 1994

Abstract

By using an analytical column of 100 mm × 2 mm I.D. (narrow-bore) with a 3- μ m stationary phase and a mobile phase consisting of 1-octanol in *n*-hexane as modifier, seven geometrical isomers of retinol were separated. In the unsaponifiable matter of food samples, six retinol isomers were identified. Heat and microwave treatment of foods such as milk and liver induced the formation of *cis*-isomers of retinol.

1. Introduction

HPLC is the most commonly applied method in retinol analysis. In most cases reversed-phase HPLC is used as a rapid method for the determination of total retinol contents in food samples [1–5]. Retention times are short and reproducible. By using reversed-phase material as the stationary phase and mixtures of methanol and water as the mobile phase in HPLC, the geometrical isomers of retinol are not separated completely. The separation of only 13-*cis*- and all-*trans*-retinol has been described [6]. It is presumed that isomers other than 13-*cis*- and all-*trans*-retinol co-elute with one of them. By using reversed-phase HPLC, the different specific extinctions of the isomers cannot be differentiated. *cis*-Isomers mostly absorb UV radiation less intensively than does the all-*trans*-

isomer. Hence the determination of total retinol may lead to underestimation of the retinol content if *cis*-isomers are present [7]. Biological vitamin A activities differ between the isomers. All-*trans*-retinol is defined to possess 100% vitamin A activity. The activities of the *cis*-isomers range from 15% for 11,13-di-*cis*-retinol to 75% for 13-*cis*-retinol [8].

An exact determination and calculation of the vitamin A activity in a food sample is possible only with a knowledge of the isomer distribution.

Several laboratories have reported the HPLC separation of retinol isomers. Some workers only focused on the separation of the main isomers all-*trans*- and 13-*cis*-retinol [9,10]. Others did not achieve a baseline separation of the minor components eluting at very similar retention times to the main isomers [11,12].

Stancher and Zonta separated isomers of retinal, retinol (vitamin A₁) and 3-dehydroretinol (vitamin A₂) in standard solutions [13] and also

* Corresponding author.

in extracts of the unsaponifiable matter of fish samples [14,15]. They applied a normal-phase HPLC column of standard size. As mobile phases they used *n*-hexane with 1-octanol or 2-propanol as modifier.

In food samples other than fish, no data on the exact retinol isomer distribution are available. They do not contain 3-dehydroretinol (vitamin A₂) in detectable concentrations. Hence most attention should be devoted to the separation of retinol (vitamin A₁) isomers. Also, the effect of heat treatment of fermentation on the retinol isomer pattern in food samples has not been studied so far. Therefore, commercially processed foods such as liver sausage or infant food containing liver in preservation vessels were taken for isomer determination. We employed a narrow-bore HPLC column of I.D. 2 mm (in contrast to 5 mm for standard columns) filled with spherical silica gel as stationary phase. The length (100 mm) was also shorter than usual. By using narrow-bore columns it was possible to reduce the flow-rate, which led to a decrease in solvent usage in comparison with the application of standard columns. Good separation results were obtained because of the small particle size (3 μm) while having short retention times.

2. Experimental

2.1. Apparatus

The chromatographic system consisted of a pump (Model 5000; Varian, Palo Alto, CA, USA), a 10-μl loop injector (Rheodyne, Cotati, CA, USA), a photodiode-array detector (Series 991; Waters–Millipore, Milford, MA, USA) with an 8-μl flow cell and a computerized evaluation system (Waters 990 Series PDA, version 6.22 software).

A guard column (7 mm × 2 mm I.D.) was connected to the analytical column (100 mm × 2 mm I.D.) (Knauer, Berlin, Germany), both filled with 3-μm Spherisorb SW silica gel (Phase Separations, Queensferry, Clwyd, UK).

2.2. Reagents and materials

The standards used were all-*trans*-retinol 13-*cis*-retinol and all-*trans*-retinol palmitate (all from Sigma, St. Louis, MO, USA).

The solvents used were absolute ethanol, light petroleum (Merck, Darmstadt, Germany), HPLC-grade *n*-hexane (Merck) and 1-octanol (Sigma). Other chemicals and reagents used were potassium hydroxide pellets, ascorbic acid, Tris [tris(hydroxymethyl)aminomethane] crystalline iodine and Kieselguhr Extrelut (all from Merck), BHT (*tert.*-butylhydroxytoluene) (Fluka, Buchs, Switzerland) and steapsine (crude porcine pancreas lipase) (Sigma). Materials used were glassware of light protective, erg. actinic glassware, disposable cartridges (15 cm length, 2.5 cm diameter) for refilling with Kieselguhr.

2.3. Photolysis

Ethanolic solutions with a concentration of 25 μg/ml 13-*cis*- or all-*trans*-retinol or 100 μg/ml all-*trans*-retinyl palmitate were purged with nitrogen to prevent oxidation and exposed to sunlight for 2 h. The yields of the photolytic process were measured by HPLC with photodiode-array detection.

2.4. Reaction with iodine

According to the method of Brown and Wald [16], 2 ml of a 0.4 mg/ml iodine solution in ethanol were added to 3 ml of a 100 μg/ml ethanolic solution of all-*trans*-retinol palmitate. After adding 60 ml of absolute ethanol, the mixture was stirred for 2 min at room temperature and exposed to daylight. The 11-*cis*-isomer of retinol was obtained in considerable amounts by this reaction.

2.5. Enzymatic influence

A 3-ml volume of a 100 μg/ml ethanolic retinol palmitate solution was added to a reaction mixture consisting of 90 ml of absolute ethanol, 0.5 ml of 1% ethanolic BHT solution,

10 ml Tris buffer (0.1 M Tris, pH 9.0) and a steapsine suspension of 0.1 g in Tris buffer. Enzymatic hydrolysis was carried out with magnetic stirring for 45 min at room temperature. The enzymatic reaction was stopped by adding 5 ml of 60% aqueous KOH.

2.6. Alkaline saponification procedure

Samples

Amounts of 1.0–10.0 g of the homogenized sample were weighed and the solid sample matrix was stirred with 30 ml of water. Volumes of 40 ml of the fluid samples were pipetted into a 250-ml round-bottomed flask. For saponification, 12 ml of 60% aqueous KOH, 80 ml of absolute ethanol, 0.5 ml of 1% ethanolic BHT solution and 0.5 g of ascorbic acid were added. To prevent oxidation, the reaction flask was purged with nitrogen and then connected to a balloon filled with nitrogen. Digestion was carried out for 16 h at room temperature on a magnetic stirrer.

Standards

Approximately 100 mg of retinyl palmitate were weighed exactly into a 100-ml volumetric flask and dissolved in *n*-hexane. The stock solution was diluted 1:100 with ethanol. Volumes of 5–35 ml of this standard solution were saponified according to the method used for the samples.

Extraction

The saponified solution was rinsed into a 250-ml volumetric flask and diluted to volume with water and absolute ethanol to yield a volumetric ratio of water to ethanol of 1:1. An aliquot of 20 ml was pipetted on to a Kieselguhr-filled disposable cartridge of synthetic material. After 20 min elution was carried out with 50 ml of light petroleum. The collected eluate was evaporated using a rotary evaporator. The remaining solvent was removed by purging with nitrogen. The residue was dissolved in volumes of 2–50 ml of isooctane depending on the presumed vitamin A concentration in the sample.

3. Results and discussion

Samples of untreated and photoisomerized standards were injected into the HPLC system and chromatographed employing mobile phases consisting of *n*-hexane and 0.3% or 0.25% of 1-octanol. A decrease in the percentage of 1-octanol led to longer retention times.

Working with a mobile phase containing only small percentages of modifier led to the problem that the stability of the composition became uncertain. The retention times tended to vary by up to 10% during one working day because of evaporation of *n*-hexane. As the corresponding behaviour of all isomers was identical, relative retention times with respect to all-*trans*-retinol were calculated. Table 1 reports relative retention times of all detectable isomers as averages of five determinations (for 11,13-di-*cis*-retinol only two determinations were available).

Fig. 1 shows chromatograms of photoisomerized standard solutions of 13-*cis*- and all-*trans*-retinol. Only of 13-*cis*- and all-*trans*-retinol pure standards were available.

The peak identification of other isomers was achieved by comparison of the spectra obtained in this work with literature data. Stancher and Zonta [13] also applied this type of peak confirmation. Spectra of 13-*cis*-, 9,13-di-*cis*-, 9-*cis*-

Table 1
Relative retention times of *cis*-retinol isomers with respect to all-*trans*-retinol

Isomer	Relative retention time ^a	R.S.D. (%) ^a
11- <i>cis</i> -	0.510	2.4
11,13-Di- <i>cis</i> - ^b	0.568	0.5
13- <i>cis</i> -	0.672	0.7
9,13-Di- <i>cis</i> -	0.740	0.8
9- <i>cis</i> -	0.877	0.6
7- <i>cis</i> -	0.924	0.5
All- <i>trans</i> -	1.000	0.0

Stationary phase, 3- μ m silica gel; column, 100 mm \times 0.2 mm I.D.; mobile phase, 0.3% 1-octanol in *n*-hexane; flow-rate, 0.4 ml/min.

^a *n* = 5.

^b *n* = 2.

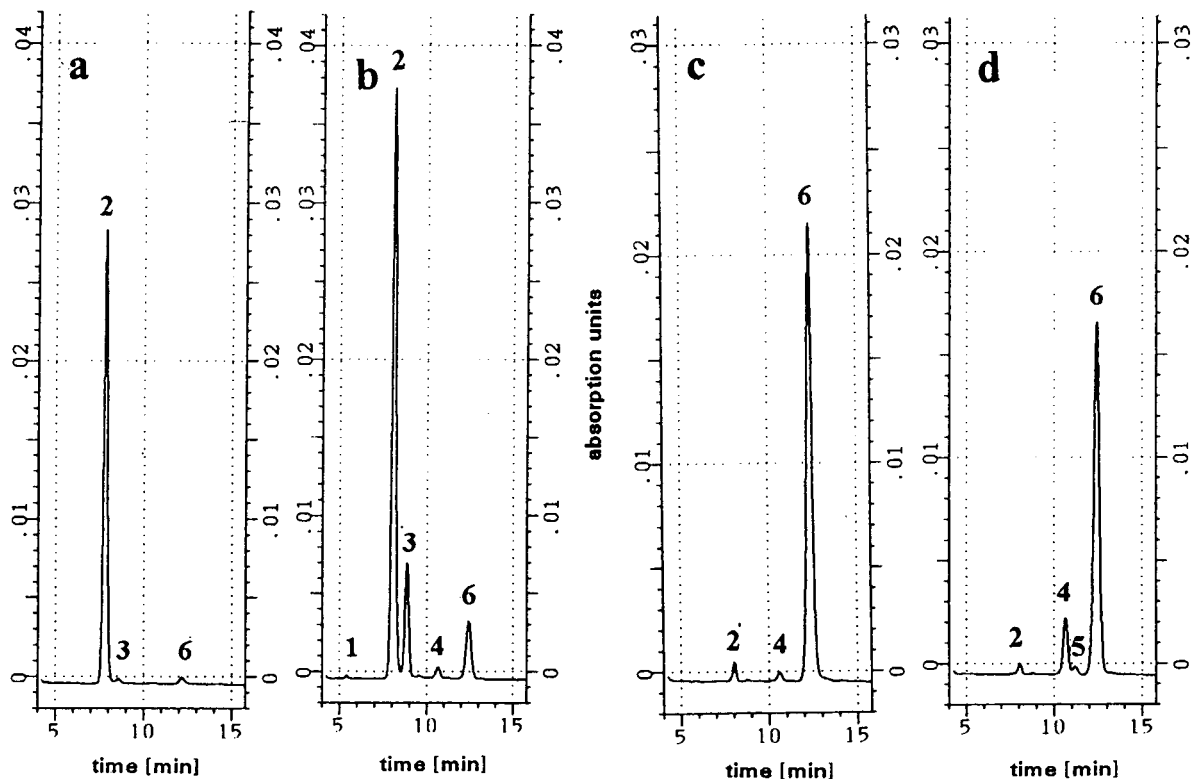


Fig. 1. Chromatograms obtained from untreated solutions of (a) 13-*cis*-retinol and (c) all-*trans*-retinol and (b, d) solutions of both isomers after photoisomerization. Stationary phase, 3- μ m silica gel; column, 100 mm \times 2 mm I.D.; mobile phase, 0.3% 1-octanol in *n*-hexane; flow-rate, 0.4 ml/min; detection wavelength, 325 nm. Peaks: 1 = 11-*cis*-; 2 = 13-*cis*-; 3 = 9,13-di-*cis*-; 4 = 9-*cis*-; 5 = 7-*cis*-; 6 = all-*trans*-retinol.

and all-*trans*-retinol are shown in Fig. 2. Table 2 shows the maximum absorption wavelengths obtained compared with literature data.

The HPLC system applied in this work allowed the separation of seven retinol isomers: 11-*cis*-, 11,13-di-*cis*-, 13-*cis*-, 9,13-di-*cis*-, 9-*cis*-, 7-*cis*- and all-*trans*-retinol (see Fig. 3). Stancher and Zonta [15] achieved the resolution of even more isomers. They worked with a standardized HPLC column and a mobile phase of 3.9% 1-octanol in *n*-hexane. The separation of the 11-*cis*- and 11,13-di-*cis*-isomers was reversed in time compared with our results. The first-eluting peak was confirmed as the signal for 11-*cis*-retinol. According to Brown and Wald [16], on treatment of all-*trans*-retinyl palmitate with iodine, the 11-*cis*-isomer was formed as the main

product. In our investigations, 77% of 11-*cis*-retinol relative to total retinol was found.

The system was calibrated with external standards ranging from 0.8 to 6.0 μ g/ml of total retinol. The concentration of all-*trans*-retinol was determined by measuring a calibration graph at 325 nm, which showed linearity over three orders of magnitude of concentration. The correlation coefficient was 0.9998, the standard deviation of *y*-residuals (s_y) was 47 and the standard deviation of the *x*-value estimated using the regression line (s_{x_0}) was 0.033 (regression line: $y = 1420x - 24$). The detection limit was 0.14 μ g/ml and the determination limit was 0.42 μ g/ml in the solution for analysis (or 1.4 μ g per 100 g and 4.2 mg per 100 g of food sample, respectively). The repeatability of the method was

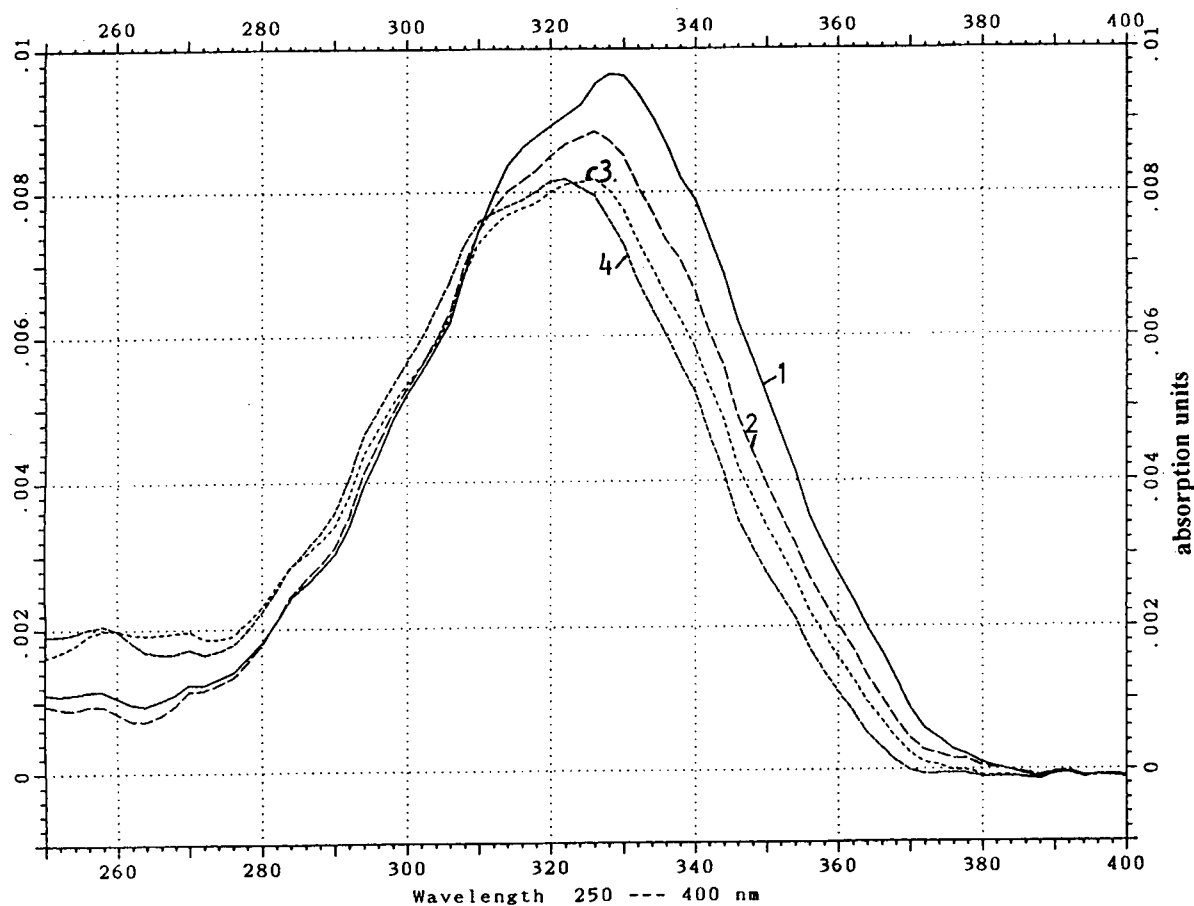


Fig. 2. Spectra of retinol isomers: 1 = 13-*cis*-retinol; 2 = all-*trans*-retinol; 3 = 9,13-di-*cis*-retinol; 4 = 9-*cis*-retinol.

Table 2

Absorption maxima of retinol isomers measured in *n*-hexane containing 0.3% 1-octanol compared with literature data [7,12]

Isomer	Maximum absorption wavelength (nm)		
	This work	Ref. [13]	Ref. [7]
11- <i>cis</i> -	322	322	319
11,13-Di- <i>cis</i> -	314	312	311
13- <i>cis</i> -	328	328	328
9,13-Di- <i>cis</i> -	324	324	324
9- <i>cis</i> -	322	323	323
7- <i>cis</i> -	314	322	No data available
All- <i>trans</i> -	325	326	325

tested by analysing different foods. For example, for beef liver the standard deviation was 0.3 mg per 100 g (2.2%) and for baby food 0.06 mg per 100 g (2.6%). Statistical data were calculated according to Funk et al. [17].

After confirming the signals for the seven isomers mentioned in Tables 1 and 2, the HPLC method was applied to extracts of the unsaponifiable matter of different food samples, such as livers of fattening animals in the raw state and after heating, liver-containing infant food in preservation vessels, liver sausages, different sorts of milk and one sample of sour cream.

As pure standards of most *cis*-isomers were not available, the percentage present in the

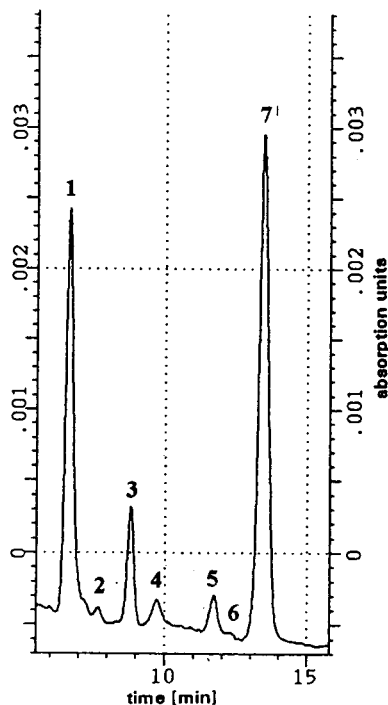


Fig. 3. Chromatogram obtained from an extract of an all-*trans*-retinyl palmitate standard solution after photoisomerization and saponification. Stationary phase, 3- μ m silica gel; column, 100 mm \times 2 mm I.D.; mobile phase, 0.3% 1-octanol in *n*-hexane; flow-rate, 0.4 ml/min; detection wavelength, 325 nm. Peaks: 1 = 11-*cis*-; 2 = 11,13-Di-*cis*-; 3 = 13-*cis*-; 4 = 9,13-di-*cis*-; 5 = 9-*cis*-; 6 = 7-*cis*-; 7 = all-*trans*-retinol.

samples had to be calculated. Two correction constants were applied for calculation: k_1 represents the ratio of the specific extinctions (ϵ) of the *cis*-isomers and all-*trans*-retinol and k_2 represents the ratio of the peak area measured at the maximum absorption wavelength to that at 325 nm. The specific extinction ratio has to be calculated as this value is lower for all *cis*-isomers than for all-*trans*-retinol. Measurement at only one detection wavelength (in our work 325 nm as the maximum absorption wavelength for the main isomer, all-*trans*-retinol, was applied) simplifies the method. To correct for the lower absorption of the *cis*-isomers at this wavelength, which differs from their maximum absorption wavelength (see Table 2), the peak-area ratio was calculated by recording three-dimensional chromatograms (absorption vs. time and wave-

length) for various photoisomerized standard solutions. The evaluation system applied calculated the peak areas at every desired wavelength.

Table 3 shows k_1 and k_2 . The constant k_1 was calculated making use of literature data on the specific extinctions [8]. Relative standard deviations are given for the calculation of k_2 (if sufficient data for calculating these values were available).

For calculation of the percentage of isomers, an equation using k_1 and k_2 was developed:

$$\text{Isomer (\%)} = \frac{A_{\text{isomer, 325 nm}} \cdot k_1 \cdot k_2}{\sum A_{\text{corrected}}}$$

where $A_{\text{isomer, 325 nm}}$ = peak area measured for the isomer peak at 325 nm, k_1 = correction constant representing the ratio of the specific extinctions (ϵ) of the *cis*-isomers and all-*trans*-retinol, k_2 = correction constant representing the ratio of the peak area measured at the maximum absorption wavelength of the *cis*-isomers to that at 325 nm and $\sum A_{\text{corrected}}$ = sum of peak areas that were corrected making use of k_1 and k_2 (denominator of the fraction) for all isomers occurring in the investigated sample.

The concentration of every isomer can be calculated from a knowledge of the all-*trans*-retinol concentration, which was determined with the external standard method.

Table 3
 k_1 (ratio of specific extinctions of all-*trans*-retinol and *cis*-isomers calculated from literature data [7]) and k_2 [ratio of peak areas measured for the isomer signal at its maximum absorbance wavelength to that at 325 nm (measuring wavelength)]

Isomer	k_1	k_2	R.S.D. (%)
11- <i>cis</i> -	1.548	1.054	1.0
11,13-Di- <i>cis</i> -	2.031	1.119	—
13- <i>cis</i> -	1.093	1.013	0.6
9,13-Di- <i>cis</i> -	1.337	—	—
9- <i>cis</i> -	1.248	1.025	0.4
7- <i>cis</i> -	—	—	—
All- <i>trans</i> -	1.000	1.000	—

Conditions as in Table 1.

Table 4
Isomer distributions in liver and liver-containing products (%) and influence of thermal treatment

Food sample	11- <i>cis</i> -	11,13-Di- <i>cis</i> -	13- <i>cis</i> -	9,13-Di- <i>cis</i> -	9- <i>cis</i> -	7- <i>cis</i> -	All- <i>trans</i> -
Beef liver (raw)	n.d. ^a	n.d.	15.3	1.8	5.5	n.d.	77.4
Beef liver (after conventional heating)	n.d.	n.d.	16.1	3.3	8.4	n.d.	72.2
Beef liver (after microwave heating)	n.d.	n.d.	15.7	3.4	8.4	n.d.	72.5
Sheep liver (raw)	tr. ^a	tr.	9.3	1.6	5.5	n.d.	83.6
Pig liver (raw)	tr.	2.1	4.6	0.5	2.7	n.d.	90.1
Infant food (manufacturer 1)	4.7	n.d.	23.3	6.0	9.0	tr.	57.0
Infant food (manufacturer 2)	13.2	n.d.	3.9	tr.	2.7	tr.	80.2
Calf liver sausage	1.2	n.d.	8.7	1.3	3.2	tr.	85.6

^a n.d. = Not detectable; tr = trace.

Tables 4 and 5 report on the isomer distributions of the types of food mentioned above. In all investigated types of liver-containing food, all-*trans*-retinol predominates (see Table 4). 13-*cis*-Retinol also occurred in every sample in detectable amounts. In two infant food samples from different manufacturers the 13-*cis*- and the 11-*cis*-isomers were present in considerable amounts. In one of them 13-*cis*-retinol amounted to 23.3% relative to total retinol. Possibly 11-*cis*-retinol in food may be formed by enzymes that are part of other ingredients. After treatment of a standard solution of all-*trans*-retinol palmitate with steapsine (pancreatic lipase), 6.2% of 11-*cis*-retinol relative to total retinol was found in the hydrolysed and extracted solution.

In raw liver samples of three species of animals, the retinol isomer pattern differed between the species. Only in raw pig liver did 11,13-di-*cis*-retinol occur in detectable amounts. The sample had been frozen for approximately 6 months at

–18°C and had been warmed to room temperature before saponification and clean-up. In sheep liver only a trace of 11,13-di-*cis*-retinol could be demonstrated (see Table 4). Thermal treatment of beef liver with both microwave and conventional heating led to an increase in the percentages of *cis*-isomers, especially of 9,13-di-*cis*- and 9-*cis*-retinol.

In different types of milk that were available on the market, different isomer patterns were found (see Table 5). Untreated pasteurized milk contained 95.1% all-*trans*-retinol relative to total retinol whereas ultra-high temperature (UHT) milk contained more than 10% of *cis*-isomers. The preservation method in pasteurization is carried out at much lower temperature than in UHT treatment. After thermal treatment both with microwave and conventional heating the percentage of *cis*-isomers increased considerably in both kinds of milk. Fig. 4 shows chromatograms of UHT milk samples before and after

Table 5
Retinol isomer distribution in milk and dairy products (%) and influence of thermal treatment

Food sample	11- <i>cis</i> -	11,13-Di- <i>cis</i> -	13- <i>cis</i> -	9,13-Di- <i>cis</i> -	9- <i>cis</i> -	7- <i>cis</i> -	All- <i>trans</i> -
Pasteurized milk (untreated)	n.d. ^a	n.d.	4.9	n.d.	n.d.	n.d.	95.1
Pasteurized milk (after conventional heating)	tr. ^a	tr.	9.8	n.d.	5.4	n.d.	84.4
Pasteurized milk (after microwave heating)	tr.	tr.	6.8	n.d.	6.4	n.d.	86.6
UHT milk (untreated)	tr.	tr.	6.8	n.d.	3.6	n.d.	89.6
UHT milk (after conventional heating)	tr.	tr.	12.3	2.5	5.3	n.d.	79.9
UHT milk (after microwave heating)	tr.	tr.	14.6	3.2	7.5	n.d.	74.7
Pasteurized milk (fermented)	9.8	tr.	9.0	0.8	3.1	tr.	77.3
Sour cream	7.3	tr.	3.7	tr.	2.3	n.d.	86.7

^a n.d. = Not detectable; tr = trace.

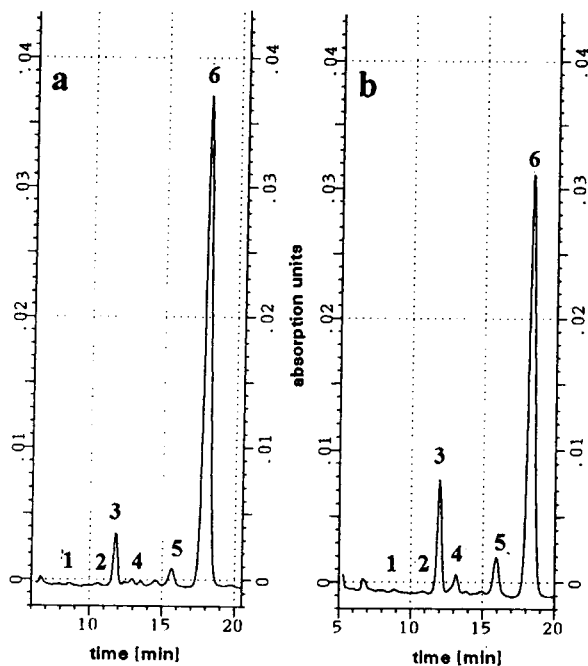


Fig. 4. Chromatograms obtained from extracts of the un-saponifiable matter of (a) untreated and (b) microwave-heated UHT milk. Stationary phase, 3- μ m silica gel; column, 100 mm \times 2 mm I.D.; mobile phase, 0.25% 1-octanol in *n*-hexane; flow-rate, 0.4 ml/min; detection wavelength, 325 nm. Peaks: 1 = 11-*cis*-; 2 = 11,13-di-*cis*-; 3 = 13-*cis*-; 4 = 9,13-di-*cis*-; 5 = 9-*cis*-; 6 = all-*trans*-retinol.

thermal treatment. In unfermented dairy products only traces of 11,13-di-*cis*- and 11-*cis*-retinol were detectable (see Table 5). After leaving a sample of pasteurized milk at room temperature for several days so that it became sour as a result of microbiological fermentation, a considerably

high percentage of 11-*cis*-retinol (9.8% relative to total retinol) was found. In sour cream 7.3% 11-*cis*-retinol relative to total retinol was found.

As all *cis*-isomers possess different vitamin A activities lower than that of all-*trans*-retinol, it is important to know the isomer distribution in food samples. Values of the vitamin A activities of the isomers can be obtained from the literature [8]. 13-*cis*-Retinol possesses 75%, 9,13-di-*cis*-retinol 24%, 9-*cis*-retinol 22%, 11-*cis*-retinol 23% and 11,13-di-*cis*-retinol 15% of the activity of all-*trans*-retinol.

Heating and processing foods result in losses of vitamin A activity by two mechanisms: degradation of retinol and isomerization of all-*trans*-retinol into *cis*-isomers. For liver and milk, investigations were made concerning the losses of total vitamin A and the vitamin A activity calculated by making use of the activity values obtained from literature. Isomer distributions are given in Tables 4 and 5. Vitamin A losses during different heating processes are given in Table 6. Heating of milk led to vitamin A losses between 6.8 and 9.8% whereas the activity losses ranged between 9.5 and 16.0%, as measured by the increase in *cis*-isomers. Also, heating of liver results in vitamin A activity losses higher than the loss of total vitamin A (see Table 6).

4. Conclusions

Applying normal-phase HPLC using narrow-bore columns of 100 mm \times 2 mm I.D., good

Table 6
Losses of total vitamin A and vitamin A activity losses in milk and liver during different heating processes

Food sample ^a	Loss of total vitamin A (%)	Vitamin A activity loss (%)
Pasteurized milk (MW)	6.8	9.5
Pasteurized milk (conv.)	9.3	14.2
UHT milk (MW)	9.8	16.0
UHT milk (conv.)	7.1	11.1
Beef liver (MW)	19.1	22.6
Beef liver (conv.)	32.7	35.6

^a MW = microwave heating, conv. = conventional heating (mass losses after heating processes were considered).

separation results for retinol isomers were achieved. Low percentages of 1-octanol in *n*-hexane as mobile phase allowed the separation of *cis*-retinols and all-*trans*-retinol in photo-isomerized standard solutions and also in extracts of the unsaponifiable matter of diverse food samples.

References

- [1] R.E. Lawn, J.R. Harris and S.F. Johnson, *Sci. Food Agric.*, 34 (1983) 1039.
- [2] S.C. Coverly and R. Macrae, *J. Micronutr. Anal.*, 5 (1989) 15.
- [3] S. Ötles and Y. Hisil, *Nahrung*, 35 (1991) 391.
- [4] E.-S. Tee and C.-L. Lim, *Food Chem.*, 45 (1992) 289.
- [5] A. Bogner, *Z. Lebensm.-Unters.-Forsch.*, 182 (1986) 492.
- [6] E. Brinkmann, *MvP-Hefte*, 1 (1994) 40.
- [7] H. Steuerle, *Z. Lebensm.-Unters.-Forsch.*, 181 (1985) 400.
- [8] O. Isler and G. Brubacher, *Vitamine I*, Georg Thieme, Stuttgart, 1st ed., 1982.
- [9] M.J. Scotter, S.A. Thorpe, S.L. Reynolds, L.A. Wilson and D.J. Lewis, *Food Additives Contam.*, 9 (1992) 237.
- [10] D.C. Egberg, J.C. Heroff and R.H. Potter, *J. Agric. Food Chem.*, 25 (1977) 1127.
- [11] J.N. Thompson and S. Duval, *J. Micronutr. Anal.*, 6 (1989) 147.
- [12] D. Woollard and H. Indyk, *J. Micronutr. Anal.*, 2 (1986) 125.
- [13] B. Stancher and F. Zonta, *J. Chromatogr.*, 287 (1984) 353.
- [14] F. Zonta and B. Stancher, *J. Chromatogr.*, 301 (1984) 65.
- [15] B. Stancher and F. Zonta, *J. Chromatogr.*, 312 (1984) 423.
- [16] P.K. Brown and G. Wald, *J. Biol. Chem.*, 222 (1956) 865.
- [17] W. Funk, V. Dammann, C. Vonderheid and G. Oehlmann, *Statistische Methoden in der Wasseranalytik*, VCH, Weinheim, 1985.

HPLC separation and determination of naphtho[2,3-b]furan-4,9-diones and related compounds in extracts of *Tabebuia avellanedae* (Bignoniaceae)

Jürgen Steinert*, Hosni Khalaf, Manfred Rimpler

Institut für Medizinische Chemie, Medizinische Hochschule Hannover, Konstanty-Gutschow-Strasse 8, 30625 Hannover, Germany

First received 17 February 1994; revised manuscript received 17 October 1994

Abstract

A HPLC method for the separation of some naturally occurring naphtho[2,3-b]furan-4,9-diones and related compounds on a RP column is reported. These compounds were determined in aqueous and various non-aqueous extracts of the inner bark of *Tabebuia avellanedae* (Bignoniaceae). 8-Hydroxy-2-hydroxyethyl-naphtho[2,3-b]furan-4,9-dione, 2-hydroxyethyl-naphtho[2,3-b]furan-4,9-dione and 2,3-dihydro-2-(1-methylethenyl)-naphtho[2,3-b]furan-4,9-dione were predominating in all extracts investigated. Lapachol could not be detected in aqueous extracts known as “lapacho tea”.

1. Introduction

Tabebuia avellanedae (Bignoniaceae) is a tree growing in South America. Preparations from its inner bark are known as “Lapacho”, “Ipe roxo” or “Pau d’arco”. They are used as adjuvants in cancer therapy in South America and the USA [1–3].

For about ten years it has been known that there are some naphtho[2,3-b]furan-4,9-diones with interesting pharmacological properties occurring in the inner bark of *T. avellanedae*. For example, 2-(1-hydroxy-ethyl)-naphtho[2,3-b]furan-4,9-dione is active against leukemia cells in mice [4,5]. This compound can also influence the

immune reaction of human granulocytes and lymphocytes [6].

Lapachol, a constituent of *T. avellanedae* discovered in the last century, has already been tested in clinical studies [7,8]. It is active against the intramuscular Walker carcinosarcoma [9] and shows antiviral [10], antischistosomal [11,12], and anti-inflammatory [13] activities.

So far all publications about the constituents of *T. avellanedae* are dealing with their isolation from stem wood or inner bark by means of various preparative chromatographic techniques (CC, TLC, HPLC) followed by ¹H- or ¹³C-NMR and MS for identification of the pure compounds [4,5,14–16]. It has not been tried to quantify the various quinones in preparations of the inner bark in one analytical run.

So we developed a HPLC method for the separation of some naphtho[2,3-b]furan-4,9-

* Corresponding author.

diones and related compounds and examined aqueous and non-aqueous extracts of the inner bark of *T. avellaneda*.

We prepared aqueous extracts because they are drunk as a tea (“lapacho tea”) and on the other hand non-aqueous extracts, because up to now isolation and identification of the constituents has been done from extracts prepared with organic solvents. Furthermore we wanted to find out which organic solvent gave the highest amount of extractables and which one is best suited for a following HPLC analysis.

Our investigations included nine compounds. The formulas are given in Table 1.

Wagner et al. [15] could identify compounds 1–4 and 7–9 in a CHCl_3 extract of the inner bark

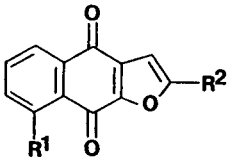
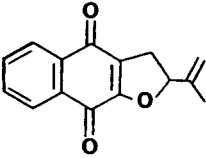
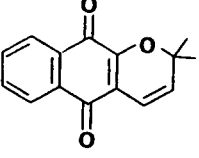
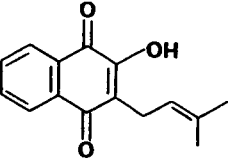
from *T. avellaneda*, 6 is a minor constituent of various Bignoniaceae species and 5 was used as a further standard, although it has not yet been found occurring naturally. Up to the present time a separation of the compounds 1–9 has not yet been described in literature.

2. Experimental

2.1. Apparatus

A Model 2249 liquid chromatograph (LKB Pharmacia, Bromma, Sweden) was used, fitted with a LKB 2141 UV-VIS detector and a Rheodyne injection valve (20 μl loop), connected

Table 1
Structural formulas of the investigated compounds

Compound	Formula	Name
		Naphtho[2,3-b]furan-4,9-diones
		R ¹ R ²
1		H COCH_3
2		H $\text{CH}(\text{OH})\text{CH}_3$
3		OH COCH_3
4		OH $\text{CH}(\text{OH})\text{CH}_3$
5		H CH_2CH_3
6		H $\text{CH}(\text{CH}_3)_2$
7		2,3-Dihydro-2-(1-methyl-ethenyl)-naphtho[2,3-b]furan-4,9-dione
8		Dehydro- α -lapachon
9		Lapachol

with a LKB 2221 integrator with a two-channel module.

2.2. Chromatography

A Spherisorb (Grom, Herrenberg, Germany) ODS-2 column (250 mm × 4 mm I.D.; 5 μm particle size) was used. The mobile phases consisted of water–methanol–acetonitrile mixtures in various ratios. The water was always acidified with phosphoric acid and the flow rate was 1.3 ml/min. The detector was set at 254 nm, and at 280 nm on the second channel.

2.3. Chemicals and materials

Methanol (MeOH), acetonitrile (ACN), water (all purchased from Merck, Darmstadt, Germany), and tetrahydrofuran (THF, from Fluka, Neu-Ulm, Germany) were of HPLC grade. Petroleum ether (50–70°C, PE), diethylether (Et₂O), chloroform (CHCl₃), methylene chloride (CH₂Cl₂), ethyl acetate (EtOAc), acetone and phosphoric acid (H₃PO₄, 85%) were all purchased from Merck and were of analytical grade.

Silica gel 60 (deactivated with 15% (w/w) H₂O), citric acid monohydrate and sodium sulfate were purchased from Merck and of analytical grade.

A buffer solution pH 9 (boric acid–potassium chloride–sodium hydroxide) was purchased from Merck and diluted tenfold prior to use.

Membrane filters (type 0-45/15, 0.45 μm) were purchased from Macherey-Nagel (Dueren, Germany).

Lapachol (**9**) was purchased from Fluka. The other compounds were prepared according to partly modified published procedures: **5**, **1**, and **2** were prepared from 2-hydroxy-1,4-naphthoquinone (2-OH-NQ) and butanal [17–20], **6** from 2-OH-NQ and 3-methyl-butanal [17,18], and **8** from 2-OH-NQ and 3-methyl-2-butenal [21]. 1,5-dihydroxynaphthalene was transformed in three steps into 2,8-dihydroxy-1,4-naphthoquinone [22–26], which in five and six steps, respectively, gave **3** and **4** [17–20]. **7** was obtained from **1** in two steps [27].

Stock standard solutions were prepared by dissolving 5–10 mg of compounds **1–9** in methanol in a 10-ml volumetric flask, except **1** which was dissolved in MeOH–THF (4:1, v/v).

Working standard solutions were obtained by dilution with methanol.

They were used as external standards to determine the content of **1–9** in the *T. avellanadae* inner bark extracts.

2.4. Aqueous extracts

10.0 g of the finely ground inner bark were brought into 500 ml of boiling water or buffer pH 9 (in a 1-l beaker). After covering the beaker with a watch glass the water was kept boiling for 5 min. Then the heater was removed and after 10 min the solution was filtered into a separation funnel. The beaker was washed two times with 25 ml H₂O. After cooling to room temperature the filtrate was acidified with 5 g of citric acid monohydrate and then extracted three times with 100 ml Et₂O. The combined organic layers were washed with 25 ml of H₂O, dried over anhydrous sodium sulfate, filtered, evaporated, and purified (see purification of the extracts).

2.5. Non-aqueous extracts

In each case 10 g of the finely ground inner bark were extracted in a Soxhlet apparatus with 180 ml of PE, Et₂O, CHCl₃, CH₂Cl₂, EtOAc, acetone, ACN or MeOH each for 16 h, and then purified.

2.6. Purification of the extracts

The solvent was evaporated under reduced pressure. The residue was taken up in MeOH–THF (4:1, v/v), filtered into a 10-ml graduated flask and filled up. An aliquot was evaporated to dryness, taken up in 0.5 ml of CH₂Cl₂–MeOH (4:1, v/v), brought on a column (20 cm × 1 cm ID; filled with 5.5 g of silica gel) and eluted with a total of 15 ml CH₂Cl₂–MeOH (9:1, v/v). The first 3 ml were discarded; the remaining effluent was evaporated under reduced pressure. Last residuals of solvent were blown off under a

stream of nitrogen. The residue was taken up in 1.0 ml of MeOH–THF (4:1, v/v) and after membrane filtration used for HPLC.

3. Results and discussion

3.1. Separation of pure compounds

Trials to separate compounds 1–9 with some simple MeOH–H₂O–H₃PO₄ or ACN–H₂O–H₃PO₄ mixtures as eluents on a RP material as stationary phase led to the coelution of some compounds. Compounds 1 and 4 could not be separated with the methanolic eluent, whereas with acetonitrile 7 and 8 coeluted. Separation was successful with a mixture of MeOH–ACN–H₂O–H₃PO₄ (25:35:40:0.1, v/v/v/v) in less than 15 min (Fig. 1). As can be seen from Fig. 1 retention depends on the polarity of the side chain of the furan ring: 2 and 4 are bearing a hydroxyethyl group and elute before 1 and 3 which possess a less polar acetyl group. The compounds with alkyl side chains (5, 6, and 9) have the longest retention times.

The compounds were also separated by means of gradient elution. It is evident from Fig. 1, that the higher quantity of water in the eluent in the beginning of the chromatographic development results in longer retention times of the analytes. This should be helpful for the investigation of plant extracts, so that co-extracted more polar substances elute earlier and do not interfere with the analytes.

The eluents used were acidified with phosphoric acid to repress the dissociation of phenolic OH groups of compounds 3, 4, and 9, which would lead to a tailing of the corresponding peaks.

The detector signal was linear in a wide range of concentration (0.2–50 mg/l), which was proved by injection of standard solutions with various concentrations. The correlation coefficients calculated were greater than 0.999 for all compounds with the exception of 2, which had a correlation coefficient of 0.996.

When investigating plant extracts the identity of peaks should be verified. One possibility is the

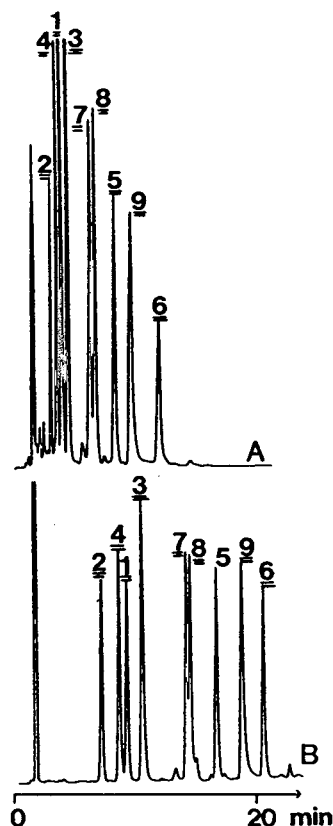


Fig. 1. HPLC separation of 1–9. Flow rate 1.3 ml/min; detection UV at 254 nm; 0.10 AUFS. (A) eluent: MeOH–ACN–H₂O–H₃PO₄ (25:35:40:0.1, v/v/v/v); (B) gradient elution starting with MeOH–ACN–0.1 vol% H₃PO₄ (25:20:55, v/v/v) for 5 min, then in 20 min with linear increase to MeOH–ACN–0.1 vol% H₃PO₄ (25:45:20, v/v/v).

simultaneous detection at two different wavelengths. So the detector was set on 254 nm and 280 nm and the ratios of peak areas were calculated. The ratios of peak areas (280 nm/254 nm) differed over a wide range: from 0.11 (5 and 6), 0.44 (7) to 1.00 (8).

3.2. Choice of extraction solvents and sample clean-up

Extracts were prepared from the air-dried and finely ground inner bark of *T. avellanedae* with various organic solvents because the qualitative

and quantitative composition of extracts from plant material depends on the structure of extractable compounds and on the nature of the solvent used [28]. The selected low-boiling solvents belonged to different chemical groups and included a wide range of polarity: PE, Et₂O, CHCl₃, CH₂Cl₂, EtOAc, acetone, ACN and MeOH.

The extracts obtained varied widely in colour and content. There is a relationship to the polarity of the solvent: with increasing polarity of the solvent, the colour of the extracts changed from slightly yellowish (PE) to almost brown (MeOH) and the amount of extractables increased from 0.76 g/100 g (PE) to 15.27 g/100 g (MeOH).

Before the extracts were subjected to HPLC they had to be cleaned up by column chromatography. TLC investigations of the extracts (on silica gel plates and CH₂Cl₂-MeOH (9:1, v/v) as mobile phase) showed that the analytes wandered near to the solvent front, while the other solutes almost remained on the starting spot. By using this solvent system for column chromatography the effluents of the extracts were clear yellowish solutions, which were ready to use for HPLC. For recovery assay of the analytes, standard mixtures were treated like the samples. The recovery ranged from 67.4 to 98.0%.

In Fig. 2 typical chromatograms of various extracts are shown.

3.3. Results from HPLC investigations of non-aqueous extracts

The quantitative results are graphically shown in Fig. 3.

Clearly the lowest quinone content is in the PE extract and the highest in the MeOH extract. **4** is the main quinone in all extracts: up to 180 mg/kg are extractable (MeOH, CH₂Cl₂). Then there are **7** and **2** with 128 mg/kg and 91 mg/kg, respectively (MeOH extract). **3** is best extractable with acetone (26.4 mg/kg) or EtOAc (22.8 mg/kg) while **1** is especially extractable with ACN (72.7 mg/kg).

Only small amounts of **9** (lapachol) were

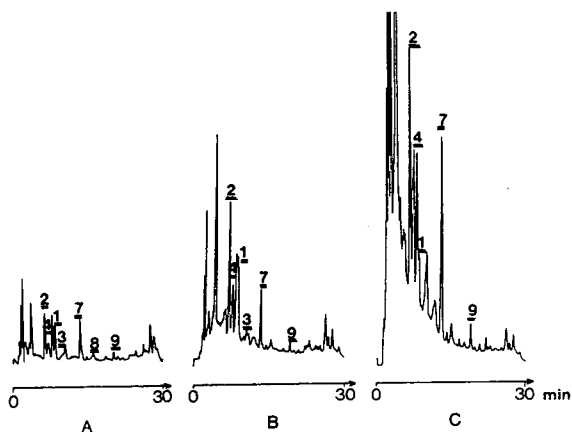


Fig. 2. Chromatograms of various extracts. (A) PE (1.0 g/ml; 0.05 AUFS), (B) Et₂O (0.5 g/ml; 0.05 AUFS) and (C) MeOH (0.2 g/ml; 0.10 AUFS); HPLC conditions as in Fig. 1 with gradient elution.

found in all extracts (less than 10 mg/kg). That means that **9** is a minor constituent of the inner bark whereas it is one of the major constituents

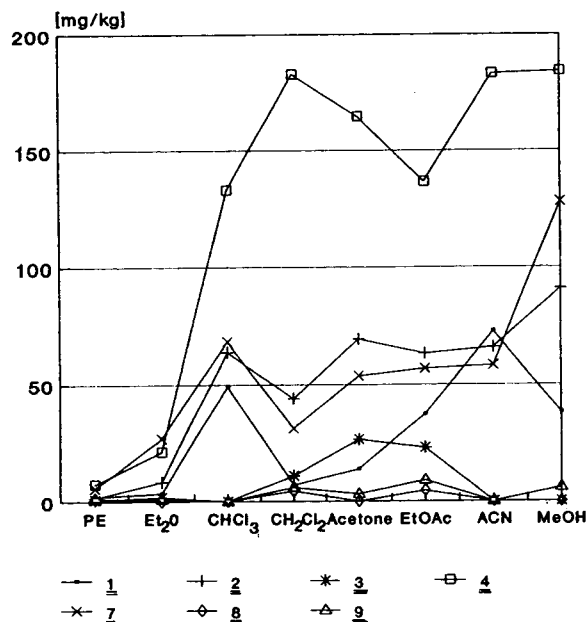


Fig. 3. Quantification of quinonoid constituents from the inner bark of *T. avellanadae* after extraction with different organic solvents; (results in mg/kg air-dried material).

of the heart wood of *T. avellanadae* (for example 2–7% according to [29] or 4% according to [14]).

It was also found that some compounds are not detectable in all extracts. **8**, for example, could only be measured in PE-, CH₂Cl₂- and EtOAc extracts. There are several explanations: first of all some compounds are almost insoluble in the chosen solvents. On the other hand the investigated material was only mechanically ground, so that cell walls largely stay intact. So the cell content is not completely accessible for the following extraction. The cell walls could be corroded with strong acids, which would also cleave the bindings between the quinonoid compounds and carbohydrates or proteins. But this treatment was not chosen because under acidic catalysis changes like isomerizations and cyclizations could occur.

6 and **5** are not detectable in any of the extracts. This is in agreement with literature where **6** has not yet been identified as naturally occurring and **5** has only been known from the wood of another *Tabebuia* species.

Furthermore there are distinct differences in the quinone specimen. That means the ratios of the quinones among themselves vary from solvent to solvent.

When comparing the chromatograms with regard to the appearance of other compounds than the analytes or to overlapping peaks and quantitation, respectively, than PE or Et₂O are the extraction solvents of choice (Fig. 2). On the other hand when extracts with high concentrations of quinones (especially **1**, **2**, **4**, **7**) have to be prepared a very polar solvent should be used (Fig. 2). That means that PE and Et₂O are the best suited extraction solvents for a following analysis whereas for preparative use ACN and MeOH are to be preferred.

All given values correspond to the investigation of one charge of the inner bark of *T. avellanadae*. So the absolute amounts of extractable quinonoid compounds may vary when analysing another charge due to the fact that the content of plant constituents depends on climate, location of the plant, time of harvest, conditions of storage etc.

3.4. Results from HPLC investigations of aqueous extracts

HPLC determination of the quinones in aqueous extracts was possible after re-extraction with an appropriate organic solvent. We compared Et₂O, EtOAc and CH₂Cl₂ as extraction solvents and found that Et₂O was best suited because the compounds had higher partition coefficients between Et₂O and H₂O compared to CH₂Cl₂-H₂O and EtOAc-H₂O. Furthermore re-extraction with EtOAc often led to emulsions.

The quantitative results are graphically shown in Fig. 4.

In aqueous extracts, which correspond to the "lapacho tea", only five of the investigated quinonoid compounds (**1**, **2**, **3**, **4**, and **7**) could be detected. The dominating quinone was **4** (up to 7.1 mg/l), followed by **2** and **7** (1.5 and 1.2 mg/l). The concentrations of **1** and **3** were about 0.4 mg/l each. **9** (lapachol) and **8** (an oxidation product of **9**) were not detectable (limit of detection: 0.04 mg/l).

There is little influence of boiling time (10 min instead of 5 min) and extraction time (30 min instead of 10 min).

Interestingly there is a lower quinone content in a weakly alkaline extract (buffer pH 9). One reason could be chemical changes which decreased the amount of the quinones. The so

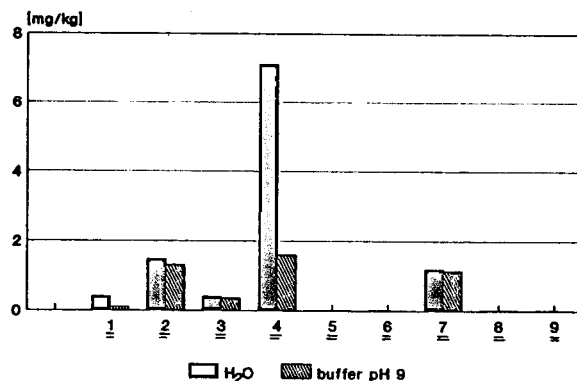


Fig. 4. Quantification of the quinonoid constituents in aqueous extracts (results in mg/l tea; tea preparation: 10 g of material/500 ml H₂O or buffer pH 9).

formed products could not be identified under the conditions chosen. Furthermore the buffer salts could have influenced the extractability of the plant material.

3.5. Conclusions

A method is presented which allows analysis of some quinonoid constituents of the inner bark of *T. avellanedae* or products from it, known as “lapacho”, “pau d’arco”, “ipe roxo” or “taheebo”, by extraction with PE or Et₂O, clean-up, and separation by HPLC.

Lapachol, earlier said to be the active principle of preparations from *T. avellanedae* is only a minor constituent of the inner bark and not detectable in aqueous extracts.

References

- [1] V.E. Tyler, *The new honest herbal*, Philadelphia, PA, 1988, pp. 176–177.
- [2] F.W. Freise, *Bol. Agric. Secr. Agric. (Sao Paulo)*, 34 (1933) 252–496.
- [3] J.L. Hartwell, *Lloydia*, 31 (1968) 71–170.
- [4] D.G.I. Kingston and M.M. Rao, *Planta Med.*, 39 (1980) 230–231.
- [5] M.M. Rao and D.G.I. Kingston, *Planta Med.*, 45 (1982) 600–604.
- [6] B. Kreher, H. Lotter, G.A. Cordell and H. Wagner, *Planta Med.*, 54 (1988) 562–563.
- [7] J.B. Block, A.A. Serpick, P. Wiernik, P.K. Nayak and D. Mollins, *Fed. Proc.*, 29 (1970) 682.
- [8] J.B. Block, A.A. Serpick, W. Miller and P. Wiernik, *Cancer Chemother. Rep. Part 2*, 4 (1974) 27–28.
- [9] K.V. Rao, T.J. McBride and J.J. Oleson, *Proc. Am. Assoc. Cancer Res.*, 8 (1967) 55.
- [10] M.H.D.C. Lagrota, M.D. Wigg, L.O.B. Pereira, M.E.F. Fonseca, N.A. Pereira and J.C. Guimares, *Rev. Microbiol.*, 14 (1983) 21–26.
- [11] B. Gilbert, J.P. DeSouza, M. Fascio, M. Kitagawa, S.S.C. Nascimento, C.C. Fortes and J. Pellegrino, *An. Acad. Bras. Cienc.*, 42 (Supl.) (1970) 397–400.
- [12] A.V. Pinto, M.D.C.R. Pinto and B. Gilbert, *Trans. Roy. Soc. Trop. Med. Hyg.*, 71 (1975) 133–135.
- [13] E.R. de Almeida, A.A. da Silva Filho, E.R. dos Santos and C.A.C. Lopez, *J. Ethnopharmacol.*, 29 (1990) 239–241.
- [14] A.R. Burnett and R.H. Thomson, *J. Chem. Soc. C*, (1967) 2100–2104.
- [15] H. Wagner, B. Kreher and H. Lotter, *Helv. Chim. Acta*, 72 (1989) 659–667.
- [16] M. Girard, D. Kindack, B.A. Dawson, J.C. Ethier and D.V.C. Awang, *J. Nat. Prod.*, 51 (1988) 1023–1024.
- [17] S.C. Hooker, *J. Am. Chem. Soc.*, 58 (1936) 1163–1167.
- [18] V.F. Ferreira, A.V. Pinto, M.C.F.R. Pinto, M.C. da Cruz and A. Clarino, *Synth. Comm.*, 19 (1989) 1061–1069.
- [19] K.H. Dudley and H.W. Miller, *J. Org. Chem.*, 32 (1967) 2341–2344.
- [20] C.C. Lopes, R.S.C. Lopes, A.V. Pinto and P.R.R. Costa, *J. Heterocyclic Chem.*, 21 (1984) 621–622.
- [21] A.V. Pinto, V.F. Ferreira and L.C.M. Coutada, *An. Acad. Bras. Cienc.*, 52 (1980) 477–479.
- [22] C. Grundmann, *Synthesis*, (1977) 644–645.
- [23] N.K. Kapoor, R.B. Gupta and R.N. Khanna, *Tetrahedron Lett.*, 21 (1980) 5083–5084.
- [24] N.K. Kapoor, R.B. Gupta and R.N. Khanna, *Acta Chim. Hung.*, 112 (1983) 163–166.
- [25] R.H. Thomson, *J. Org. Chem.*, 13 (1948) 870–878.
- [26] A.S. Wheeler and B. Naiman, *J. Am. Chem. Soc.*, 44 (1922) 2331–2334.
- [27] A.V. Pinto, M.D.C.R. Pinto, M.A. Aguiar and R.S. Capella, *An. Acad. Bras. Cienc.*, 54 (1982) 115–120.
- [28] D. Fengel and G. Wegener, *Wood: Chemistry, Ultrastructure and Reactions*, W. de Gruyter, Berlin and New York, 1984, pp. 240–267.
- [29] H.A. Hoppe, *Drogenkunde*, Cram, De Gruyter and Co, Hamburg, 1958, p. 889.

HPLC of basic drugs and quaternary ammonium compounds on microparticulate strong cation-exchange materials using methanolic or aqueous methanol eluents containing an ionic modifier

K. Croes¹, P.T. McCarthy², R.J. Flanagan*

Poisons Unit, Guy's and St Thomas' Hospital Trust, Avonley Road, London SE14 5ER, UK

First received 2 August 1994; revised manuscript received 11 November 1994

Abstract

Sulphopropyl (SCX)-modified silica HPLC columns used with methanolic or aqueous methanol eluents of appropriate pH and ionic strength can give good retention and peak shape for quaternary ammonium compounds and basic drugs. In the system studied, eluent pH influenced retention via protonation of basic analytes, the pK_a indicating the pH where retention began to decrease at constant ionic strength. At constant eluent pH retention was inversely proportional to ionic strength for protonated bases and quaternary ammonium compounds. However, this effect was less marked at pH 8.3 as compared to results obtained under acidic conditions. Except for codeine, morphine and lignocaine, the addition of water had no major effects on retention or selectivity at concentrations up to 30% (v/v) at pH 6.7. However, and in contrast to behaviour on unmodified silica, the addition of up to 5% (v/v) water under strongly acidic conditions caused a doubling of retention for most analytes studied.

SCX-modified silica columns can be used in the HPLC of a range of basic drugs, including many compounds which are poorly retained on unmodified silica using methanol-rich eluents. The underlying retention mechanism appears to be ion exchange with the SCX moieties, although ionized surface silanols may also contribute to retention at higher eluent pH values. Applications of SCX columns in the HPLC of basic drugs include the analysis of antimalarials such as chloroquine, desethylchloroquine, hydroxychloroquine and quinine, benzodiazepines such as clonazepam, bronchodilators such as salbutamol and terbutaline, cardioactive drugs such as flecainide and lignocaine, and tricyclic antidepressants such as amitriptyline, dothiepin, and imipramine, and their N-demethyl, hydroxyl and sulphoxide metabolites.

1. Introduction

Chemically modified (bonded phase) silica-aqueous methanol or acetonitrile eluent ('reversed-phase') systems have been widely used in the HPLC of basic drugs. However, in addition to buffer salts, various additives (pairing- or counter-ions, such as alkylsulphonates, alk-

* Corresponding author.

¹ Present address: Gasthuisberg, Onderwijs en Navorsing, Laboratory of Pharmacology, Herestraat 49, 3000 Leuven, Belgium.

² Present address: Coagulation/Vitamin K Research Unit, Haemophilia Centre, 1st Floor, North Wing, St Thomas' Hospital, London SE1 7EW, UK.

ylamines, or quaternary ammonium compounds) are often needed to give efficient performance [1]. Moreover, the effect of altering the eluent water content on retention may not be predictable in terms of interaction with the bonded phase. This is probably because ionic interactions between the (protonated) analyte and (ionized) surface silanols are as strong or stronger than hydrophobic interactions with the stationary phase [2]. Similar considerations apply when using chemically modified silica solid-phase extraction columns [3–5].

In the HPLC of basic drugs similar retention and selectivity (and generally better peak shapes) to those obtained on bonded phase packings can often be obtained on unmodified silica using 'reversed-phase' eluents, i.e. aqueous methanol or acetonitrile eluents of an appropriate pH and ionic strength [6–12]. Ion exchange with surface silanols is thought to be the predominant retention mechanism, eluent pH influencing retention via (i) the ionization of surface silanols and (ii) the protonation of basic analytes. Although the fact that acidic or neutral compounds and indeed some basic drugs are either not retained or very poorly retained excludes interference from such sources, the analysis of compounds in these latter categories is not possible using unmodified silica unless very high eluent water contents are employed. However, if this is attempted very poor efficiencies are attained [13].

When analyzing basic drugs by reversed-phase HPLC, evaporation of solvent extracts and reconstitution in an aqueous medium is often required. The use of nonaqueous ionic eluents was originally investigated with the aim of analyzing solvent extracts directly [14]. It was found that efficient performance could be obtained for many basic drugs on unmodified silica using 100% methanol containing perchloric acid (0.01 or 0.02% v/v, approximately 1 or 2 mmol/l) as eluent. An ammonium perchlorate-modified (10 mmol/l, apparent pH 6.7) 100% methanol eluent balances retention, peak shape and electrochemical oxidation response for many analytes [15,16]. Perchloric acid, ammonium perchlorate, and some sulphates and sulphates are useful ionic modifiers since they have UV

cutoffs below 210 nm, and are adequately soluble and appear to be highly dissociated in methanolic solution [14].

Spherisorb S5W silica (5 μ m average particle size) has been used extensively with nonaqueous ionic eluents, although similar results may be obtained on other silicas [15,17]. Microparticulate sulphopropyl- (SCX) or sulphophenylpropyl-modified silicas also give good retention of many basic drugs with nonaqueous ionic eluents. The use of two such materials, Zorbax 300 SCX (Du Pont) and Spherisorb S5SCX (Phase Separations), has been described [12,17–19]. The aims of the present paper are (i) to present data to aid the use of microparticulate SCX columns in the HPLC of basic drugs and quaternary ammonium compounds, (ii) to compare some results obtained using the sulphopropyl-modified material to those obtained on unmodified silica and on phenylpropyl-modified silica, and (iii) to discuss the mechanism whereby retention of basic drugs is achieved on unmodified silica and on SCX-modified silica.

2. Experimental

2.1. Materials and reagents

Methanol and acetonitrile (HPLC grade) were from Rathburn (Walkerburn, UK), perchloric acid (60% w/v) and sodium hydroxide (both analytical reagent grade) from BDH (Poole, UK), and ammonium perchlorate from Aldrich (Gillingham, UK). Water was deionised (Elgastat Option 3). Pure drugs used as test compounds were obtained from a variety of manufacturers. Drug nomenclature follows that of Reynolds [20]; pK_a values were obtained from this same source.

2.2. High-performance liquid chromatography

A constant-flow reciprocating pump (Shimadzu, Model LC-9A) was used with a syringe-loading injection valve (Rheodyne, Model 7125). Column effluents were monitored by UV absorption (Applied Chromatography Systems, Model 750/11/AZ) or fluorescence

(Applied Biosystems Model 980, glass photomultiplier tube). The columns used were (i) stainless-steel packed with Spherisorb S5SCX (sulphopropyl-modified silica), S5P (phenylpropyl-modified silica), or Spherisorb S5W (unmodified silica) (all from Phase Separations, Deeside, UK), or (ii) PEEK (polyether ether ketone) (Jour No-Met) packed with Spherisorb S5SCX (Hichrom, Reading, UK). Spherisorb S5W is a spherical packing [size of particles: 90% in the range $5 \pm 2 \mu\text{m}$ (area distribution), surface area: $220 \text{ m}^2/\text{g}$, mean pore diameter: 8 nm (range $5.4\text{--}11 \text{ nm}$)]. Spherisorb S5P and S5SCX are prepared from S5W (maximum carbon loadings 3 and 1.2% w/w, respectively). S5SCX has a maximum ion-exchange capacity of $6 \mu\text{mol/g}$ ($6 \mu\text{Equiv/g}$).

The eluents were solutions of perchloric acid or ammonium perchlorate of appropriate pH and ionic strength. Eluent pH values were measured without correction using a standard glass electrode (Jenway 3020) calibrated against aqueous buffers. Experiments designed to study the effects of eluent pH, ionic strength and water content on retention and peak shape of the test compounds (Fig. 1) were performed at ambient temperature (normally 22°C) and at a flow rate of 2.0 ml/min . Effluent pH was measured to ensure column equilibration was complete before each experiment. Analyte retention times were measured using a Hewlett-Packard Model 3392A recording integrator. Retention factors (k , also known as mass distribution ratio, capacity factor, capacity ratio, k') were calculated using the formula $k = (t_R - t_0)/t_0$ where t_R is the retention time of the analyte and t_0 is the retention time of the non-retained peak (taken as the first deviation of the baseline following the injection of $5 \mu\text{l}$ acetone).

3. Results and discussion

3.1. HPLC of basic drugs and quaternary ammonium compounds on Spherisorb S5SCX

Effect of pH on retention at constant ionic strength: methanol eluent

When studying the effect of pH on retention at

constant ionic strength on unmodified silica, Flanagan and Jane [15] used sodium perchlorate (10 mmol/l) to provide the eluent ionic strength. However, this salt has no buffering capacity. The silica column itself provided buffering at acidic-neutral pH values, but it was difficult to obtain stable readings at pH values >7 . To obviate this problem, ammonium perchlorate (50 mmol/l) was used to provide the eluent ionic strength in this study, pH adjustment being by adding either perchloric acid or sodium hydroxide (both 50 mmol/l in methanol). Unfortunately, it was not possible to obtain stable pH values between 1 and 5 using ammonium perchlorate and 8.7 was the highest pH which could be attained.

Given the above constraints, the results obtained using the Spherisorb S5SCX column (Fig. 2) were similar to those obtained using unmodified silica [15] except that (i) retention on the SCX column was much greater for a given eluent ionic strength, and (ii) the effect of changes in pH on retention under strongly acidic conditions were much less marked on SCX than on silica. In addition, methdilazine gave a very poor peak shape under strongly acidic conditions on SCX but not on silica. The reason for this finding is not clear. Other phenothiazines tested, for example chlorpromazine and thioridazine, also gave very poor peak shapes at pH 0 on SCX.

Thus, methdilazine excepted, the retention of all the test compounds increased slightly as the pH increased from 0 to 5 (Fig. 2). This may have been due to ionization of residual silanols on the SCX material rather than increased ionization of the very strongly acidic sulphopropyl moieties. At eluent pH values >5 the N,N-diethylamines amiodarone and lignocaine and the alicyclic N-methylamines codeine and morphine showed marked decreases in retention. Desethylamiodarone and the N,N-dimethylamines ($\text{p}K_a$ values <9.5) also showed decreased retention at pH 7 and above, although this was less marked than with lignocaine and amiodarone. In contrast, the retention of emepromonium and the primary and secondary aliphatic amines studied ($\text{p}K_a$ values generally 9.7 or greater) was maintained up to pH 8. Emepromonium then showed increased retention on going to pH 8.7, possibly reflecting

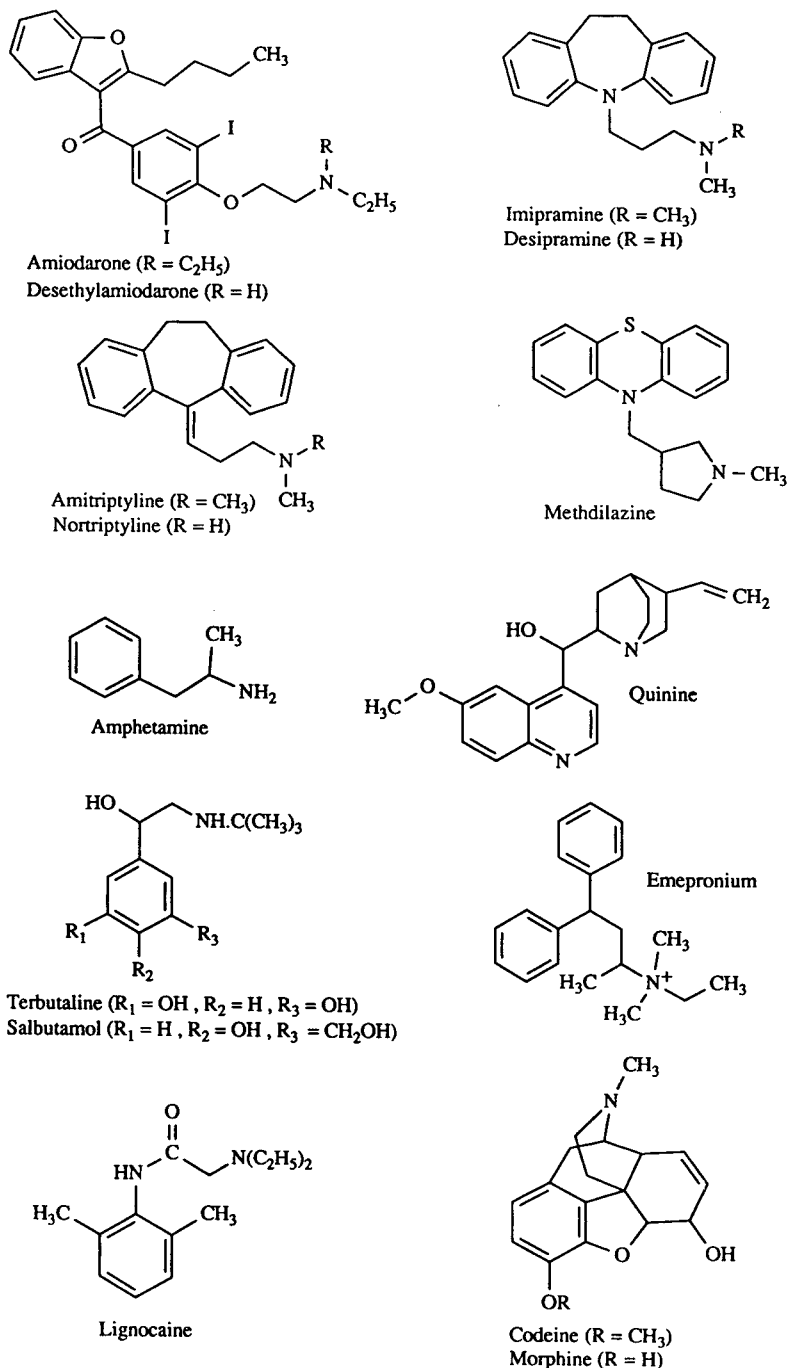


Fig. 1. Test compounds. Amiodarone (pK_a 5.6); desethylamiodarone (DEA, no published pK_a); amitriptyline (pK_a 9.4); nortriptyline (pK_a 9.7); imipramine (pK_a 9.5); desipramine (pK_a 10.2); methdilazine (pK_a 7.5); amphetamine (pK_a 9.9); quinine (pK_a 4.1, (amine) 8.5); terbutaline [pK_a 8.7, (amine) 10.0, 11.0]; salbutamol [pK_a 9.3, (amine) 10.3]; lignocaine (lidocaine, pK_a 7.9); emepronium; codeine (pK_a 8.2); morphine [pK_a (amine) 8.0, 9.9].

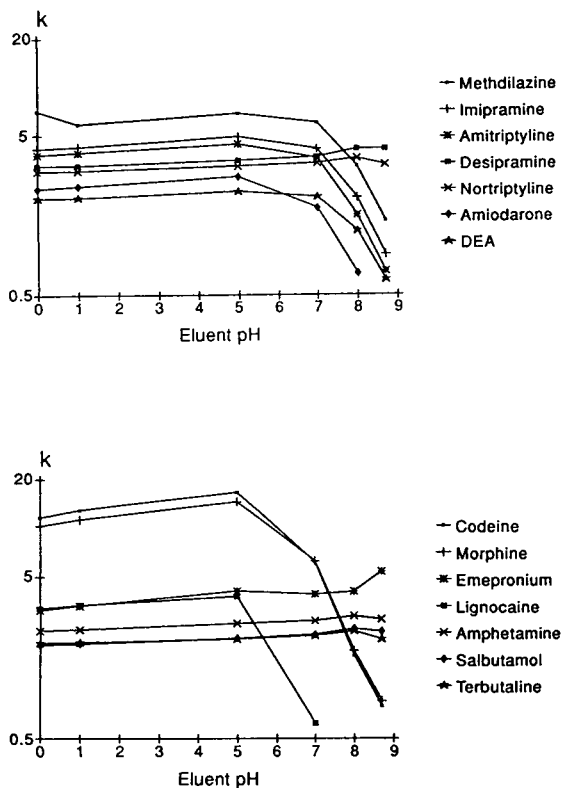


Fig. 2. Effect of eluent pH on the retention (k) of some test compounds at constant ionic strength. Column: 100×4.6 mm I.D. stainless steel packed with Spherisorb S5SCX. Eluent: methanol containing ammonium perchlorate (50 mmol/l) adjusted to the appropriate pH by adding either perchloric acid or sodium hydroxide (both 50 mmol/l in methanol). Flow rate: 2.0 ml/min. Detection: UV, 254 nm. Injections: 20–100 μ l each analyte (10 mg/l) in methanol.

increased ionization of residual surface silanols, but the remaining compounds showed decreased retention. By analogy with the results obtained using unmodified silica [15], the retention of the basic drugs would be expected to continue to decrease at higher eluent pH values although the retention of the quaternary ammonium should be maintained.

Effect of pH on peak shape at constant retention: methanol eluent

The test compounds (amphetamine, nortriptyline, amitriptyline, imipramine, methdilazine, morphine, emepromium and quinine)

and eluents [methanolic perchloric acid (pH < 0) and methanolic ammonium perchlorate (pH 6.7 and pH 8.3)] used were those studied by Flanagan and Jane [15] on unmodified silica. Eluent ionic strengths were adjusted to give similar retention times at each pH to facilitate comparison of peak shapes.

The elution sequence of the test compounds at pH < 0 and at pH 6.7 (Fig. 3) was similar to that obtained on unmodified silica [15]. For example, the sequence amphetamine < nortriptyline < amitriptyline < imipramine < methdilazine was the same on both columns. The efficiency and shape of the amphetamine, nortriptyline, amitriptyline, imipramine and methdilazine peaks were similar at each pH on both columns except that methdilazine gave a badly tailing peak on SCX at pH < 0. The emepromium peak was similar (very slight tail) at each pH (compare Ref. 15, Fig. 5). Quinine, which gave a badly tailing peak on unmodified silica at pH < 0, was not eluted at this pH on the SCX column. At higher pH values quinine gave a good peak shape on silica [15] and on SCX (Fig. 3). Finally, and in marked contrast to the results obtained with unmodified silica, morphine gave a symmetric although relatively broad peak at pH < 0 but broad, tailing peaks at pH 6.7 and at pH 8.3.

Effect of ionic strength on retention at constant pH: methanol eluent

In HPLC, plots of retention against the reciprocal of eluent ionic strength may give information on the retention mechanism. A straight line plot is expected if an ion-exchange mechanism is operating, the intercept on the y axis (infinite ionic strength) indicating the contribution of retention mechanism(s) other than ion exchange to retention [21].

The eluent pH values employed in the present study were again those used by Flanagan and Jane [15] with unmodified silica, i.e. < 0, 6.7 and 8.3. The k values measured on SCX at different eluent ionic strengths are presented in Table 1. Representative data are plotted (k vs. $1/\text{ionic strength}$) in Fig. 4; some data points have been omitted at higher ionic strengths to clarify presentation. Straight line plots with intercepts

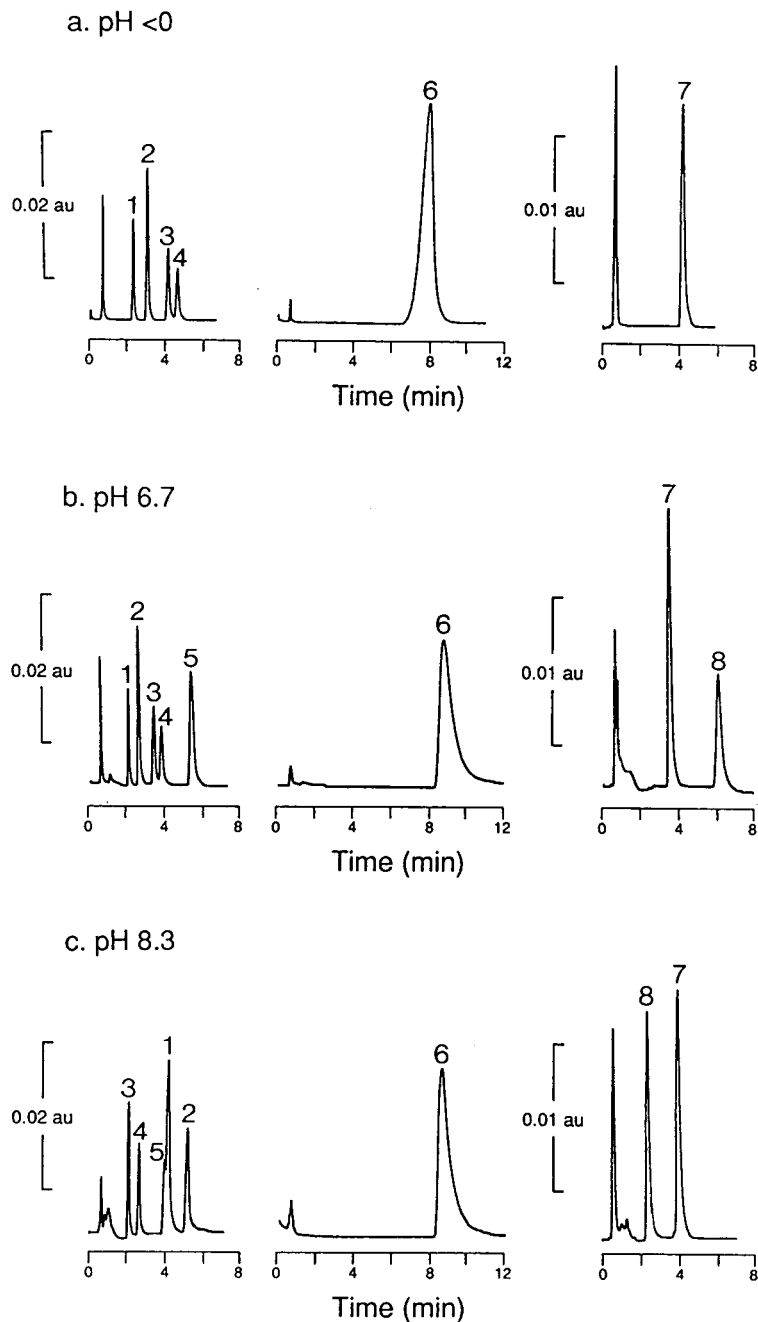


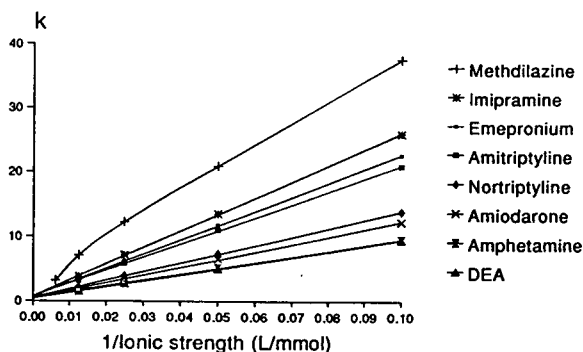
Fig. 3. Chromatography of some test compounds: SCX column. Eluents: (a) pH <0. Methanolic perchloric acid (25 mmol/l). (b) pH 6.7. Methanolic ammonium perchlorate (40 mmol/l). (c) pH 8.3. Methanolic ammonium perchlorate (20 mmol/l) (3 mmol/l morphine; 40 mmol/l emepronium–quinine). See legend to Fig. 2 for other chromatographic conditions. Injections: 10 μ l (100 μ l emepronium, quinine) 10 mg/l each analyte (100 mg/l emepronium, 0.5 g/l amphetamine, 1 g/l morphine). Peaks: 1 = amphetamine, 2 = nortriptyline, 3 = amitriptyline, 4 = imipramine, 5 = methdilazine, 6 = morphine, 7 = emepronium, 8 = quinine.

Table 1
Effect of eluent ionic strength on the retention (*k*) of some test compounds on SCX column

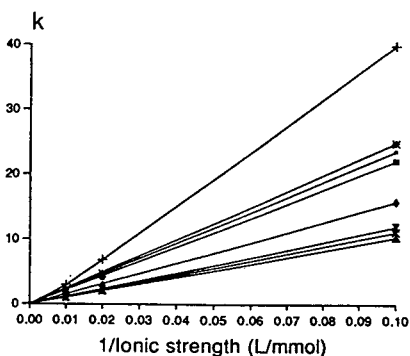
Compound	Ionic strength (mmol/l)								
	10	20	40	50	80	100	160	200	400
<i>Eluent: methanol containing perchloric acid, pH < 0</i>									
Amiodarone	12.2	6.5	3.4		1.8		1.0		
Amitriptyline	20.8	11.1	5.8		3.1		1.6		
Amphetamine	9.5	5.1	2.8		1.6		0.9		
Codeine	58.5	30.7	16.3		8.6		4.3		
Desethylamiodarone	9.4	5.0	2.6		1.4		0.8		
Desipramine	16.8	8.9	4.8		2.6		1.4		
Emepronium	22.6	11.7	6.3		3.3		1.7		
Imipramine	25.9	13.5	7.1		3.8		1.9		
Lignocaine	16.4	8.5	4.6		2.5		1.3		
Methdilazine	37.5	20.8	12.2		7.0		3.2		
Morphine	50.0	26.3	14.0		7.4		3.8		
Nortriptyline	13.8	7.3	3.9		2.2		1.2		
Salbutamol	6.8	3.7	2.1		1.2		0.7		
Terbutaline	6.7	3.6	2.0		1.2		0.7		
<i>Eluent: methanol containing ammonium perchlorate, pH 6.7</i>									
Amiodarone	11.2			2.2		1.0		0.5	0.3
Amitriptyline	22.1			4.1		1.8		0.9	0.5
Amphetamine	12.0			2.3		1.2		0.6	0.4
Codeine	61.2			11.6		5.1		2.8	1.3
Desethylamiodarone	10.4			2.0		0.9		0.5	0.3
Desipramine	17.8			3.9		1.6		0.8	0.4
Emepronium	23.5			4.5		1.8		0.9	0.4
Imipramine	24.8			4.7		2.1		1.0	0.5
Lignocaine	4.6			1.3		0.6		0.4	0.3
Methdilazine	39.8			6.8		3.0		1.4	0.7
Morphine	57.2			11.0		5.0		2.6	1.3
Nortriptyline	15.8			2.9		1.4		0.7	0.4
Salbutamol	8.6			1.8		1.0		0.6	0.3
Terbutaline	9.2			1.9		1.1		0.6	0.4
<i>Eluent: methanol containing ammonium perchlorate, pH 8.3</i>									
Amiodarone	1.2			0.3		0.3		0.2	0.1
Amitriptyline	4.2			1.1		0.7		0.6	0.4
Amphetamine	13.2			2.7		1.3		0.7	0.4
Codeine	3.6			1.2		0.9		0.9	0.7
Desethylamiodarone	3.5			0.9		0.6		0.3	0.2
Desipramine	20.0			3.9		1.9		1.0	0.6
Emepronium	31.3			4.6		2.0		1.0	0.5
Imipramine	5.5			1.4		0.9		0.6	0.5
Lignocaine	0.2			0.1		0.1		0.1	0.1
Methdilazine	9.1			2.2		1.4		1.0	0.6
Morphine	3.9			1.3		1.0		0.9	0.7
Nortriptyline	16.6			3.2		1.7		0.8	0.5
Salbutamol	10.5			2.2		1.2		0.7	0.5
Terbutaline	9.6			2.0		1.1		0.6	0.4

See legends to Figs. 2 and 4 for details of chromatographic conditions.

(a) pH <0



(b) pH 6.7



(c) pH 8.3

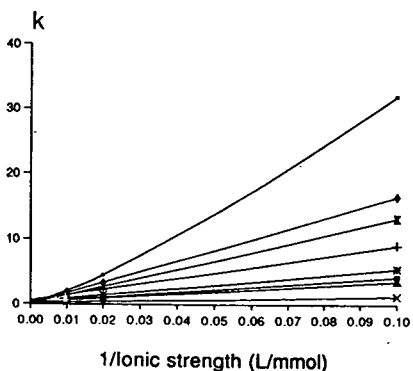


Fig. 4. Effect of eluent ionic strength on the retention (k) of some test compounds. Column: 100×4.6 mm I.D. Spherisorb S5SCX. Eluent: methanol containing (a) perchloric acid, (b) ammonium perchlorate adjusted to pH 6.7 by adding methanolic sodium hydroxide, (c) ammonium perchlorate adjusted to pH 8.3 by adding methanolic sodium hydroxide. See Fig. 2 for other experimental details.

passing close to the origin (intercept of approximately 0.4 in the case of the pH < 0 plots) were obtained at all three pH values except for methdilazine (pH < 0, very poor peak shape, convex curve at higher ionic strengths; pH 6.7, slight concave curve at higher ionic strengths) and emepronium (pH 8.3, concave curve). Codeine and morphine (results not shown) gave straight line plots with small intercepts on the y axis except at pH < 0 (intercepts approximately 1.4).

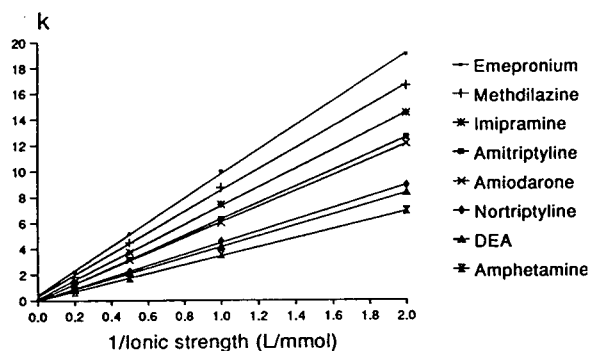
In order to facilitate comparison with the results obtained on unmodified silica (Spherisorb S5W, Ref. 15), analogous plots (k vs. $1/\text{ionic strength}$) are given in Fig. 5. Some data points have again been omitted at higher ionic strengths to clarify presentation. At pH 0 all of the test compounds gave approximately straight line plots and all of the plots passed through the origin except those given by emepronium and methdilazine (intercepts at $k = 0.3$). At pH 6.7 all the plots again approximated to straight lines. Methdilazine gave the biggest intercept on the y axis (0.4) and emepronium one of the smallest (0.1). At pH 8.3, however, all the plots were convex curves, that given by emepronium having the biggest slope and passing closest to the origin. The intercepts given by the other plots ranged up to 0.8 in the case of methdilazine. Codeine and morphine behaved similarly giving intercepts of approximately 0.5 (results not shown).

Effect of eluent water content on retention: constant pH and ionic strength

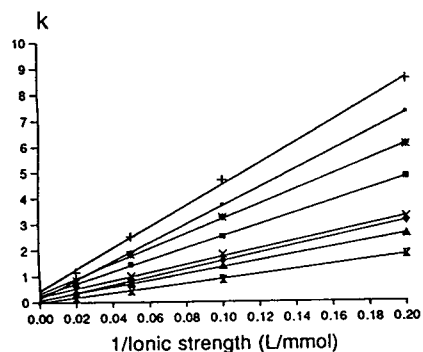
(i) Initial pH < 0

All of the test compounds showed marked increases in retention on raising the eluent water content from 0 to 5% (v/v) on the SCX column under strongly acidic conditions (Fig. 6). The retention of codeine and morphine decreased thereafter up to 50% water. The retention of the remaining compounds stayed relatively constant except that amiodarone and desethylamiodarone showed proportionately greater increases in retention at eluent water contents of 30% (v/v) and above. Flanagan et al. [17] reported only very slight increases in retention up to 1% water

(a) pH 0



(b) pH 6.7



(c) pH 8.3

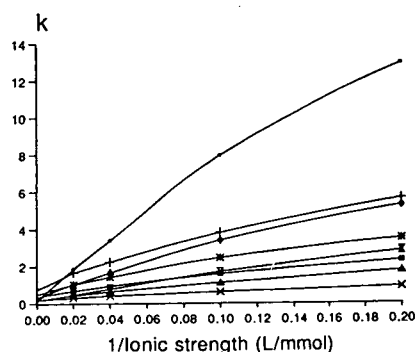


Fig. 5. Effect of eluent ionic strength on the retention (k) of some test compounds. Column: 250×4.9 mm I.D. Spherisorb S5W silica. Eluent: methanol containing perchloric acid or ammonium perchlorate at an appropriate pH and ionic strength. See Flanagan and Jane [15] for other experimental details.

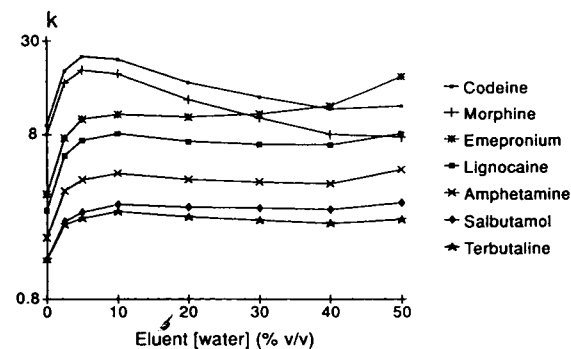
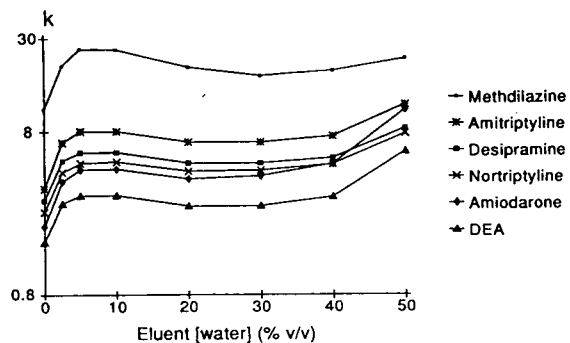


Fig. 6. Effect of eluent water content on the retention (k) of some test compounds: SCX column. Eluent: methanol or methanol-water containing perchloric acid [50 mmol/l (0.5% v/v)]. See legend to Fig. 2 for other chromatographic conditions.

(perchloric acid eluent) when studying strong bases and emepronium on unmodified silica. Subsequently there was little change in retention up to 10% water. The reason for this difference in behaviour between the SCX column and unmodified silica is not clear.

(ii) pH 6.7

In contrast to the results obtained under strongly acidic conditions on the SCX column, the retention of all test compounds generally decreased slightly on going from 0 to 10% water at pH 6.7 and increased thereafter at higher eluent water contents (Fig. 7). Amiodarone and desethylamiodarone again showed proportionately greater increases at eluent water con-

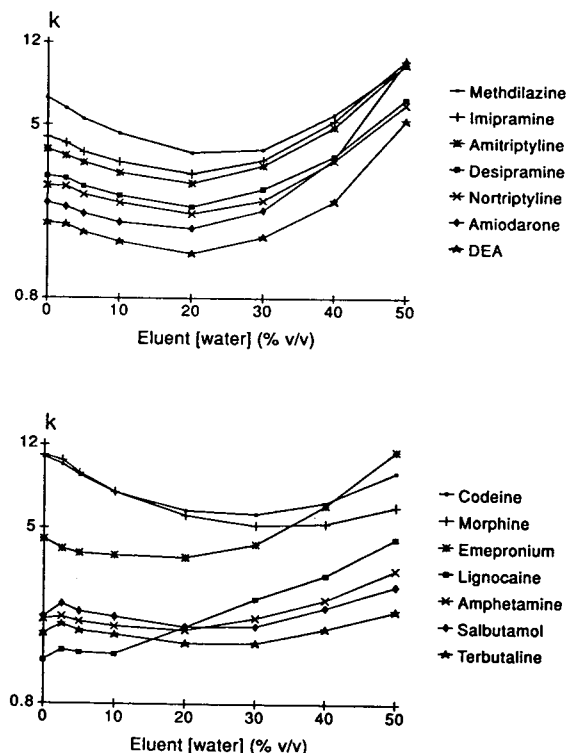


Fig. 7. Effect of eluent water content on the retention (k) of some test compounds: SCX column. Eluent: methanol or methanol–water containing ammonium perchlorate (50 mmol/l) adjusted to pH 6.7 with sodium hydroxide (50 mmol/l). See legend to Fig. 2 for other chromatographic conditions.

tents above 30% (v/v). However, lignocaine showed marked increases in retention with increasing water content from 10% (v/v). The retention of codeine and morphine decreased up to 30% water and thereafter showed relatively small increases up to 50% water. Similar results were obtained on unmodified silica [15], although lignocaine, codeine and morphine were not studied.

The behaviour of amiodarone, desethylamiodarone and lignocaine in the presence of water (Figs. 6 and 7) deserves further comment. In summary, amiodarone and desethylamiodarone showed similar retention characteristics to each other (and to the other compounds studied except at higher eluent water contents) under strongly acidic conditions, at pH 5.4 (results not

presented graphically), and at pH 6.7. Lignocaine, however, behaved similarly to the other compounds studied (codeine/morphine excepted) under strongly acidic conditions and at pH 5.4, but showed marked increases in retention with increasing water content from 10% (v/v) at pH 6.7 (Fig. 7). The reason for these differences in chromatographic behaviour is not clear but could be related to the fact that both amiodarone and lignocaine are *N,N*-diethylamines which have relatively low pK_a values compared to the *N,N*-dimethylamines studied (see Fig. 1).

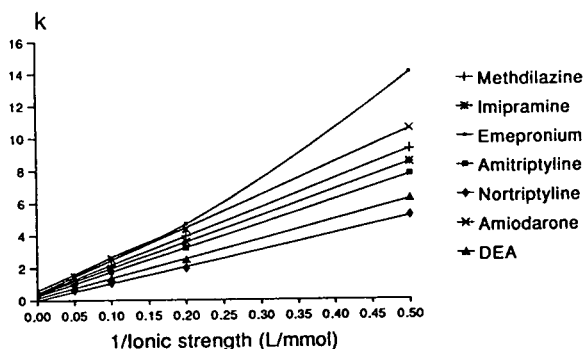
We have not studied systematically the effect of eluent water content on retention at eluent pH values above 6.7. However, addition of water (1.5% v/v) to a methanolic ammonium perchlorate eluent was effective in resolving chloroquine and monodesethylchloroquine at pH 8.0 on an SCX column [19].

Effect of ionic strength on retention at pH 6.7: methanol–water eluent

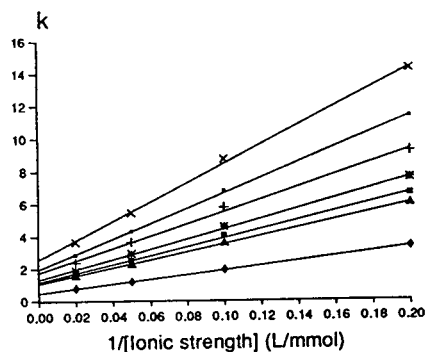
In order to investigate the possible contribution of the propyl moiety of the sulphopropyl-modified silica to retention in the presence of water, the effect of changes in ionic strength on retention using methanol–water (7 + 3), pH 6.7 as eluent was studied. Unmodified silica (S5W) and phenylpropyl-modified silica (S5P) were studied under these same conditions in order to provide comparative data. The results are presented in Fig. 8; some data points have again been omitted at higher ionic strengths in order to clarify presentation. Amphetamine was not studied in detail on the S5W and S5P columns since elution was so rapid on the 100 mm columns used that k values could not be measured accurately at higher ionic strengths. On the SCX column amphetamine co-eluted with amiodarone at all the ionic strengths studied.

The results obtained on the SCX column were similar to those obtained in the absence of water (Fig. 4) save that methdilazine gave a linear plot. All the plots had an intercept on the y axis of approximately 0.4. Other compounds studied on SCX behaved similarly except that the codeine and morphine plots had intercepts on the y axis

(a) Spherisorb S5W



(b) Spherisorb S5P



(c) Spherisorb S5SCX

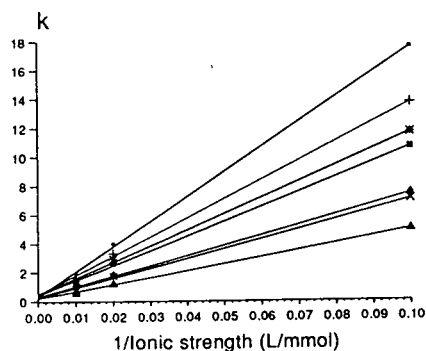


Fig. 8. Effect of eluent ionic strength on the retention (k) of some test compounds at pH 6.7 in the presence of water. Columns: 100×4.6 mm I.D. stainless steel packed with (a) Spherisorb S5W silica, (b) Spherisorb S5P phenylpropyl-modified silica, and (c) Spherisorb S5SCX sulphopropyl-modified silica. Eluent: methanol–water (70:30) containing ammonium perchlorate adjusted to pH 6.7 with sodium hydroxide (50 mmol/l) in methanol–water (70:30). See legend to Fig. 2 for other chromatographic conditions.

of 0.7 (results not shown). The results obtained on unmodified silica were also very similar to those obtained using methanol alone (Fig. 5) except that the plot given by emepronium, which was linear in the absence of water, was a concave curve. Codeine and morphine behaved similarly to the other basic drugs studied and gave linear plots (intercepts on the y axis of 0.7 and 0.9, respectively; results not shown).

Spherisorb S5P gave interesting results in that, although all the plots were linear, none passed through the origin, intercepts on the y axis of between 0.4 (nortriptyline) and 2.4 (amiodarone) being obtained. The codeine and morphine plots were also linear and had intercepts on the y axis of 1.6 and 1.2, respectively (results not shown). Further points of interest were (i) that amiodarone was strongly retained in comparison to results on unmodified silica and SCX, and (ii) that the ionic strength needed in order to promote elution at a given retention time lay in general between that needed on unmodified silica (lowest) and on SCX (highest). Presumably this is because a trifunctional silylating reagent was used in preparing the S5P material and this served to add additional silanols (ion-exchange sites) as well as the phenylpropyl moiety (S5SCX is prepared using a monofunctional silylating reagent [information from Phase Separations]). However, the presence of water is also important since under nonaqueous conditions at pH 6.7 retention of nortriptyline, amitriptyline, imipramine and methdilazine on S5P was only half that on S5W at a given ionic strength, selectivity being unaffected [12].

3.2. Use of Spherisorb S5SCX in the HPLC of basic drugs

Lignocaine (Fig. 1) is poorly retained on unmodified silica columns under acidic or neutral conditions [14,16]. However, the use of an SCX-modified silica column gives good retention and forms the basis of a reliable assay [18]. Salbutamol and terbutaline (Fig. 1) are also relatively poorly retained on unmodified silica and an SCX-modified column used with methanol–acetonitrile–water (40:40:20) containing per-

chloric acid (20 mmol/l) has proved valuable in the analysis of these compounds in plasma extracts. Addition of water to the eluent under strongly acidic conditions served to enhance retention and improve the separation attained (compare Fig. 6), whilst acetonitrile was added to the eluent to reduce the column back-pressure [22].

The measurement of the antiarrhythmic flecainide is sometimes requested in the presence of the lipophilic β -adrenoceptor blocker propranolol. Although these compounds can be analyzed independently using an unmodified silica column [17], they are difficult to separate. However, this analysis is easy using an SCX column under strongly acidic conditions (Fig. 9). As with the salbutamol–terbutaline assay discussed above, water and acetonitrile were added to the eluent to improve the separation and lower the back-pressure, respectively. An SCX-modified column has also been used in the assay of chloroquine, desethylchloroquine, hydroxy-

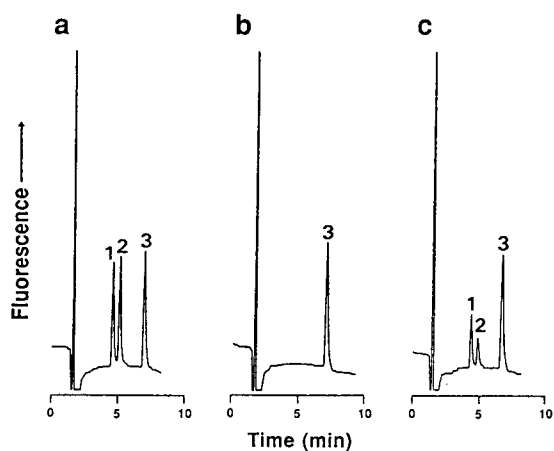


Fig. 9. Analysis of flecainide in the presence of propranolol in plasma–serum. Column: 150×4.6 mm I.D. Spherisorb S5SCX. Eluent: Methanol–acetonitrile–water (2:2:1) containing perchloric acid (25 mmol/l). Flow rate: 2.0 ml/min. Detection: Fluorescence: excitation 215 nm, no emission filter. Injection: $100 \mu\text{l}$ sample extracts. Chromatograms: (a) Standard solution prepared in newborn calf serum containing flecainide (0.50 mg/l) and propranolol (0.10 mg/l). (b) Drug-free human plasma. (c) Plasma from a patient treated with flecainide and propranolol (plasma concentrations 0.26 and 0.03 mg/l, respectively). Peaks: 1 = flecainide, 2 = propranolol, 3 = benzimidazole (internal standard).

chloroquine and quinine in plasma [19]. Here a methanolic ammonium perchlorate (66 mmol/l, pH 8.0) eluent was used. This gave good peak shapes for all the compounds of interest but the addition of water (1.2% v/v) was required in order to separate chloroquine and desethylchloroquine effectively (Fig. 10). Further increases in the eluent water content had little effect on the separation.

A consistent but unexplained finding is the very poor peak shape given by phenothiazines such as methdilazine and chlorpromazine under strongly acidic conditions on the SCX column. Clearly a higher eluent pH is needed to assay such compounds satisfactorily on SCX (see Fig. 3), although the corollary is that interference from phenothiazines themselves in assays carried under strongly acidic conditions will be minimal. Strong acid conditions are sometimes mandatory if an ion-exchange mechanism is to be exploited, as in the analysis of very weak bases such as benzodiazepines. The separation of some benzodiazepines and of dothiepin and some metabolites is illustrated in Fig. 11. In conjunction with appropriate sample preparation procedures, this system can be used to assay (i) benzodiazepines such as clonazepam, and (ii) tricyclic antidepressants such as amitriptyline, dothiepin, or imipramine and their N-demethyl, hydroxyl and sulphoxide metabolites.

3.3. General discussion

The factors influencing the retention of basic drugs and quaternary ammonium compounds on unmodified silica and on SCX-modified silica using 100% methanol or aqueous methanol eluents containing an ionic modifier clearly have many similarities. It is appropriate therefore to review previous work on the HPLC of basic drugs on unmodified silica prior to discussing general aspects of the use of SCX-modified packings.

HPLC of basic drugs on unmodified silica

Silica column–nonaqueous ionic eluent systems are useful in the HPLC of basic drugs in biological extracts since only protonated bases

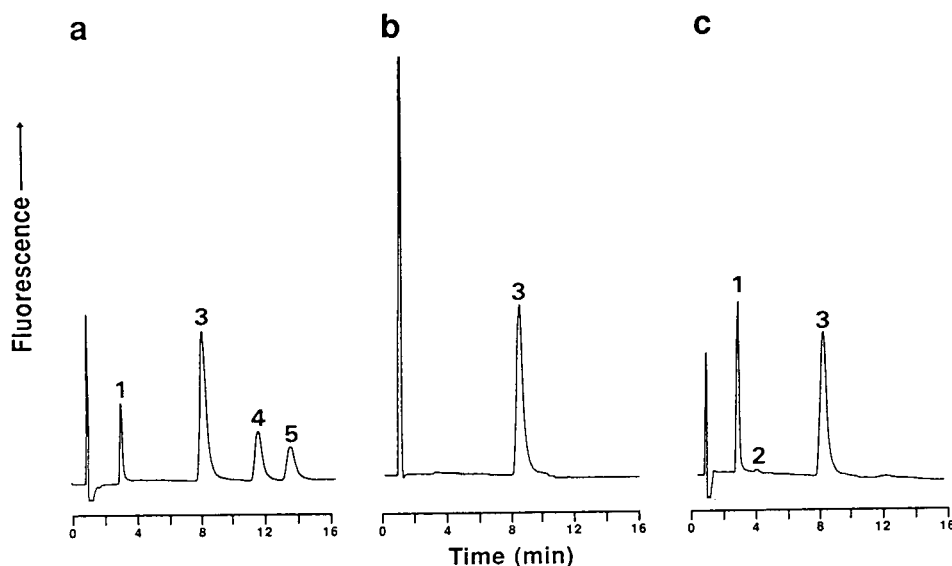


Fig. 10. Analysis of chloroquine and quinine in plasma or serum [19]. Column: 150×5 mm I.D. Spherisorb S5SCX. Eluent: Methanol–water (98.5:1.5) containing ammonium perchlorate (80 mmol/l), adjusted to pH 8.0 with 50 mmol/l methanolic sodium hydroxide (final eluent ammonium perchlorate concentration 66 mmol/l). Flow rate: 1.5 ml/min. Detection: Fluorescence: excitation 215 nm, no emission filter. Injection: $100 \mu\text{l}$ sample extracts. Chromatograms: (a) Standard solution prepared in newborn calf serum containing chloroquine (0.50 mg/l), monodesethylchloroquine (0.25 mg/l) and quinine (1.00 mg/l). (b) Drug-free human plasma. (c) Plasma from a patient treated with quinine (plasma concentration 2.2 mg/l). Peaks: 1 = quinine, 2 = hydroquinine, 3 = hydroxychloroquine (internal standard), 4 = monodesethylchloroquine, 5 = chloroquine.

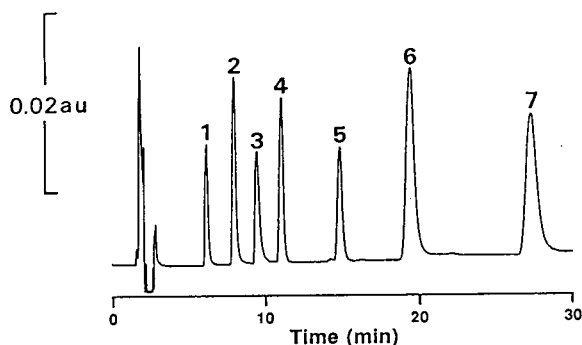


Fig. 11. Analysis of some benzodiazepines, tricyclic antidepressants and metabolites. Column: 250×4.6 mm I.D. PEEK packed with Spherisorb S5SCX. Eluent: methanol–water–perchloric acid (60%) (97.5:1.75:0.75). Flow rate: 1.0 ml/min. Detection: UV, 220 nm. Injection: $30 \mu\text{l}$ methanolic solution containing (1) clonazepam, (2) nordiazepam (both 0.7 mg/l), (3) diazepam, (4) nordothiepin, (5) dothiepin, (6) nordothiepin sulphoxide (all 2.1 mg/l), and (7) dothiepin sulphoxide (4.3 mg/l).

and quaternary ammonium compounds are retained. In addition, N-dealkylated, phenolic, and other metabolites such as sulphoxides are often resolved from the parent compound [14,23]. However, one experimental finding which has not been explained is that the peak shape of some analytes, most notably alkaloids such as morphine, quinine, and strychnine, is influenced by eluent pH, higher pH values usually giving better peaks.

The retention of protonated bases and of quaternary ammonium compounds on unmodified silica using methanol or aqueous methanol eluents is thought to be mediated largely by cation exchange with surface silanols [7,15]. Eluent pH is thus a major influence on retention, ionization of surface silanols increasing at higher eluent pH values and thus giving increased retention for quaternary ammonium compounds and protonated bases. Reduced protonation of basic drugs at higher eluent pH values reduces retention, however, analyte pK_a

values indicating the eluent pH of maximum retention at constant ionic strength.

Ionic strength is also a major influence on retention, although the effect of ionic strength becomes less pronounced as the degree of protonation of basic analytes falls (see Fig. 5). Eluent water content had little effect on retention or selectivity for the fully protonated bases and the quaternary ammonium compound studied at concentrations up to 10% (v/v) at pH < 0 and up to 40% at pH 6.7 [15,17]. The use of more than 50% water enhanced retention markedly for most analytes at pH 6.7. However, except for amiodarone and desethylamiodarone, selectivity remained largely unaltered [7,15].

Smith, Gill and colleagues [24–28] have also used unmodified silica in the HPLC of a range of basic drugs with a methanol–water (9:1) eluent (pH in the range 9.2–10.1) based on that used by Jane [6] and have reported some variation in the retention of particular analytes. However, at alkaline pH values small alterations in eluent pH will alter the ionization of surface silanols and will also alter protonation of basic analytes. Changes in ionic strength may also alter selectivity at constant pH (Fig. 5). A complicating factor here is that ammonium hydroxide and ammonium salts of organic acids such as acetate used as modifiers in such systems may not be completely dissociated in methanol-rich media. Eluent water content and possible pH-induced breakdown of the silica matrix are further potential variables.

Much of the variation observed initially by Smith et al. was attributed to differences in the ammonium hydroxide solution used to prepare the buffer [25]. In subsequent work a non-volatile buffer was used but here certain compounds, notably dipipanone, pipazethate and prolintane (all of which contain an alicyclic tertiary amine moiety and are relatively weak bases; pK_a dipipanone, for example, 8.5), showed a consistent decrease in retention relative to protriptyline with increasing time since manufacture of the silica packing. These changes were attributed to increased hydroxylation of the silica surface arising from conversion of surface siloxanes to silanols [28]. Whilst this might be expected to

give increased retention if ion exchange is the predominant retention mechanism, it may be that ion exchange is relatively unimportant for the compounds showing greatest variation since they are all relatively weak bases and thus will be present at pH 10.1 largely if not entirely in the unprotonated form. Even using methanolic ammonium perchlorate at pH 8.3 the plots of k vs. $1/\text{ionic strength}$ for basic drugs on silica were markedly different in slope to the plot given by the quaternary ammonium compound studied (Fig. 5).

Cox and Stout [21] have reported on a study of the retention mechanism of “a set of nitrogenous bases” on various silicas “over the entire range of concentration of organic solvent”. Unfortunately, the only basic drug studied (morphine) is atypical as regards the HPLC of basic drugs on unmodified silica [14,15] and indeed on SCX-modified silica (this study), the quaternary ammonium compound studied (thiamine) is actually a thiazolium compound, whilst no methanol concentrations higher than 75% (v/v) were employed. A further complication is that sodium orthophosphate adjusted to an appropriate pH with orthophosphoric acid was used to provide the eluent ionic strength. This compound may not be fully dissociated at higher eluent methanol concentrations thus providing a possible explanation for their observation that apparent eluent pH increased with added methanol concentration from 4.6 (0% methanol) to 6.4 (75% methanol). Cox and Stout [21] interpreted this as showing that ionization of surface silanols would be increased at higher eluent methanol contents thereby explaining the increased retention of morphine and thiamine caused by simply adding methanol. In contrast, added water has no effect on apparent pH at eluent water contents from 0 to 60% (v/v) if ammonium perchlorate is used to provide the eluent ionic strength at pH 6.7 [15].

Retention mechanism(s) other than ion exchange with surface silanols must operate on unmodified silica using methanol or acetonitrile–water eluents at high eluent water contents (60% v/v or more). Adamovics [13], for example, has reported the analysis of acidic antibiotics on unmodified silica, whilst Flanagan [12] has shown

that a series of chlorophenoxy herbicides including 2,4-dichlorophenoxyacetic acid (pK_a 2.6) can be retained and have the same elution sequence on unmodified silica as on a number of bonded-phase materials at pH 3.5. Absolute retention could be increased by increasing the eluent water content, although efficiency decreased markedly with increasing retention. It is possible that hydrogen bonding with protonated silica silanols contributes to retention in such circumstances.

Use of SCX-modified silica

SCX-modified silica packings used with nonaqueous ionic eluents give good retention and peak shape for many basic drugs (Fig. 3). Ionization of the sulphopropyl moiety appears little influenced by eluent pH and residual silanols on the SCX material appeared to have little effect on the retention of the basic drugs studied (Fig. 2). As on unmodified silica, the retention of basic analytes decreases at higher eluent pH values, the pK_a indicating the eluent pH where retention begins to decrease at constant ionic strength. This property can be used to adjust selectivity for certain compounds. When using published pK_a values in this way, however, it must be remembered (i) that such measurements are performed in aqueous solution, and (ii) that there is always the possibility of error in published data. The published pK_a values for amiodarone (5.6) and methdilazine (7.5), for example, do seem rather low when compared to those for the structurally similar compounds lignocaine (7.9) and thioridazine (9.5).

At constant pH, retention on SCX columns is inversely proportional to ionic strength for fully protonated analytes and quaternary ammonium compounds (Table 1, Fig. 4). At pH 8.3 this effect is less marked for some of the weaker bases studied. Except for lignocaine, codeine and morphine, the addition of water had no major effect on retention or selectivity on SCX at concentrations below 30% (v/v) at pH 6.7 (Fig. 7). However, in contrast to behaviour with unmodified silica, the addition of up to 5% (v/v) water under strongly acidic conditions caused a doubling of retention for most analytes studied

(Fig. 6). The reason for this is unclear. There was little further effect on going to 40% water.

Our approach to the HPLC of basic drugs on either unmodified or SCX-modified silica is to use acidic or neutral conditions if possible since the effect of changes in eluent pH and ionic strength (and even water content) are in general relatively predictable. The only reason for using high pH eluents in the HPLC of basic drugs on unmodified silica is in those instances when compounds (morphine, for example) give bad peak shapes at acid or neutral eluent pH values, as discussed above. If screening for a wide range of basic drugs is to be performed then Binder et al. [9] have shown that unmodified silica can be used with acetonitrile–aqueous potassium dihydrogen orthophosphate (6 mmol/l) containing tetramethylammonium hydroxide (5 mmol/l) and dimethyloctylamine (2 mmol/l), pH 6.50 (33:67) as eluent. Alternatively, if electrochemical oxidation detection is to be employed then the eluent described by Jane et al. [16] (10 mmol/l ammonium perchlorate in 100% methanol, pH 6.7) has the advantage of giving a relatively low background current at applied potentials up to +1.2 V vs. Ag/AgCl.

Practical advantages of nonaqueous ionic eluent systems are that methanol is much less viscous than water–methanol or water–acetonitrile mixtures and thus column back-pressures are low. Eluent degassing is not normally needed. In addition, use of methanol as the eluent solvent minimises the risks of silica dissolution. A further advantage of ionic eluent systems is that relatively large volume solvent extracts can be injected directly in a “non-eluting” (zero ionic strength) solvent with no loss of efficiency [14].

One problem with silica column–nonaqueous ionic eluent systems used under strongly acidic conditions (methanol–perchloric acid eluent) is that the ionic strength required to promote elution at a given retention time decreases with prolonged use of the column [14]. This could be due to, for example, dehydration of adjacent silanols to form a siloxane moiety or to irreversible binding of exogenous molecules at cation exchange sites. Although we have not studied

systematically the stability of SCX-modified columns used under strongly acidic conditions for the analysis of basic drugs, our experience is that such systems are probably more stable than those employing unmodified silica. This could be because the contribution of surface silanols to retention is relatively unimportant on the SCX materials and thus any tendency of adjacent silanols to lose water to form siloxane bridges, etc. will also be unimportant. Certainly hydrolysis of the sulphopropyl moieties under strongly acidic conditions does not seem to be important in routine use. A factor here may be the high organic content of the eluents used: the high methanol content of the methanol–water (9:1) pH 9.2–10.1 eluent used by Jane [6] and followers with unmodified silica is presumed to be an important factor in the stability of these systems.

A major consideration in HPLC is the hazard posed by the eluent. With SCX materials the hazard presented by use of relatively high perchlorate concentrations in methanolic or methanol–acetonitrile-rich media has to be balanced against the practical benefit obtained. The use of ammonium perchlorate at the concentrations discussed does not seem to cause excessive corrosion of stainless HPLC components. However, the perchloric acid-modified eluent used in the analysis of tricyclic antidepressants (Fig. 11), for example, is very corrosive and for this reason PEEK columns and fittings have been preferred. It should prove possible to use sulphuric acid, ammonium sulphate or even organic sulphonates such as camphorsulphonic acid as the ionic modifier [14] in order to obviate the requirements for perchlorates. Secondly, synthesis of SCX-modified materials with lower phase loadings should facilitate the use of eluents of lower ionic strength.

Observations on the mechanism of retention: ionic eluent systems

Although the underlying mechanism whereby separations are achieved either on unmodified silica or on SCX-modified silica packings using ionic eluent systems under acidic or neutral conditions appears to be ion exchange, the reason why separations are achieved remains

obscure. The key analyte functionality is clearly the protonated basic group or quaternary ammonium moiety. The loss of an N-alkyl group from a tertiary or secondary amine (amitriptyline–nortriptyline, for example) is enough to give rise to a good separation under appropriate eluent conditions. If both analytes are fully protonated then the stronger base (nortriptyline, pK_a 9.7) is eluted before (has less affinity for the stationary phase than) amitriptyline (pK_a 9.4).

This apparent anomaly could be due to steric effects, the lack of one N-methyl group on nortriptyline as compared to amitriptyline permitting easier access of counter-ions (solvated H^+ or NH_4^+) to ionized silanols or SCX moieties and thus more rapid elution. Alternatively, the lack of the N-methyl group on nortriptyline could permit greater solvation of the analyte and thus reduce the affinity of the solvated complex for the stationary phase. At higher eluent pH values the net charge carried by amitriptyline, and thus ionic interaction with the stationary phase, is reduced hence permitting more rapid elution for a given ionic strength. In the case of the stronger base nortriptyline this process presumably begins at a higher eluent pH thus providing a possible explanation for the fact that nortriptyline elutes after (has greater affinity for the stationary phase) than amitriptyline at higher pH values.

Recently Law [11] has published a 'strategic' approach to the analysis of basic drugs by HPLC. However, the suggested 'tau' values (attempts to relate separation of parent compounds and metabolites to molecular structure) are only valid for the eluent used [methanol–aqueous ammonium acetate, pH 9.1 (9:1)] and are clearly subject to change with eluent pH, and also with ionic strength at alkaline pH (Figs. 4 and 5), and may be influenced by other factors such as eluent water content. Moreover, as noted above, Smith, Gill and colleagues [24–28] have reported variation in the k values obtained on such systems, especially with weaker bases.

In unmodified and SCX-modified silica HPLC systems eluent water may act to either (i) alter the affinity of the (solvated) analyte for the stationary phase or (ii) alter the affinity of the

(solvated) counter-ion for the stationary phase. Water could also influence the accessibility of the cation-exchange sites, as appears to happen on SCX under strongly acidic conditions (Fig. 6). Given that all the analytes studied (protonated or unprotonated) are very soluble in methanol it is unlikely that the solubility in the eluent contributes to retention except possibly when adding relatively large amounts of water (40% v/v or more). However, at higher concentrations water might act to hinder access of the counter-ion (increased solvation shell?) to the ionized silanol-SCX moiety thus giving increased analyte retention.

4. Conclusions

Microparticulate SCX-modified silica used with methanolic or aqueous methanol eluents containing an ionic modifier can be employed in the analysis of quaternary ammonium compounds and basic drugs, including compounds which are poorly retained on unmodified silica. The effects of changes in eluent pH and ionic strength on retention and selectivity are relatively predictable. The addition of water has little overall effect on retention or selectivity at concentrations up to 30% (v/v) at pH 6.7 except for certain compounds, notably lignocaine. However, addition of up to 5% (v/v) water under strongly acidic conditions caused a doubling of retention for most of the analytes studied. No SCX materials other than Spherisorb S5SCX have been evaluated systematically. However, use of materials with a lower SCX loading should permit lower eluent ionic strengths to be used. Past experience suggests that Zorbax 300 SCX (sulphophenylpropyl-modified silica) might be suitable.

Acknowledgements

We thank Mr B. King and Dr P. Myers (Phase Separations, Deeside) for the gift of the Spherisorb S5SCX and some of the other HPLC columns used, Dr R. Whelpton (Queen Mary

and Westfield College, London) and Mr S. Binder (Bio-Rad Laboratories, Hercules, CA, USA) for helpful criticism, and the British Council for financial assistance (KC).

References

- [1] R. Gill, S.P. Alexander and A.C. Moffat, *J. Chromatogr.*, 247 (1982) 39.
- [2] D.C. Leach, M.A. Stadalius, J.S. Berus and L.R. Snyder, *LC·GC Internat.*, 1 (1988) 22.
- [3] B. Law, S. Weir and N.A. Ward, *J. Pharmaceut. Biomed. Anal.*, 10 (1992) 167.
- [4] B. Law and S. Weir, *J. Pharmaceut. Biomed. Anal.*, 10 (1992a) 181.
- [5] B. Law and S. Weir, *J. Pharmaceut. Biomed. Anal.*, 10 (1992b) 487.
- [6] I. Jane, *J. Chromatogr.*, 111 (1975) 227.
- [7] B.A. Bidlingmeyer, J.K. Del Rios and J. Korpi, *Anal. Chem.*, 54 (1982) 442.
- [8] H. Lingeman and W.J.M. Underberg, *Trends Anal. Chem.*, 7 (1988) 346.
- [9] S.R. Binder, M. Regalia, M. Biaggi-McEachern and M. Mazhar, *J. Chromatogr.*, 473 (1989) 325.
- [10] B. Law, *Trends Anal. Chem.*, 9 (1990) 31.
- [11] B. Law, in E. Reid and I.D. Wilson (Editors), *Bioanalytical approaches for drugs, including antiasthmatics and metabolites*, Royal Society of Chemistry, Cambridge, 1992, p. 57.
- [12] R.J. Flanagan, in R.B. Holman, A.J. Cross and M.H. Joseph (Editors), *High Performance Liquid Chromatography in Neuroscience Research*, Wiley, Chichester, 1993, p. 321.
- [13] J.A. Adamovics, *J. Pharmaceut. Biomed. Anal.*, 5 (1987) 267.
- [14] R.J. Flanagan, G.C.A. Storey, R.K. Bhamra and I. Jane, *J. Chromatogr.*, 247 (1982) 15.
- [15] R.J. Flanagan and I. Jane, *J. Chromatogr.*, 323 (1985) 173.
- [16] I. Jane, A. McKinnon and R.J. Flanagan, *J. Chromatogr.*, 323 (1985) 191.
- [17] R.J. Flanagan, R.K. Bhamra, S. Walker, S.C. Monkman and D.W. Holt, *J. Liquid Chromatogr.*, 11 (1988) 1015.
- [18] S.C. Monkman, S. Rosevear, R. Armstrong, R.J. Flanagan and D.W. Holt, *Biomed. Chromatogr.*, 3 (1989) 88.
- [19] K. Croes, P.T. McCarthy and R.J. Flanagan, *J. Anal. Toxicol.*, 18 (1994) 255.
- [20] J.E.F. Reynolds (Editor), *Martindale, The Extra Pharmacopoeia*, Edition 30, Pharmaceutical Press, London, 1993.
- [21] G.B. Cox and R.W. Stout, *J. Chromatogr.*, 384 (1987) 315–336.

- [22] P.T. McCarthy, S. Atwal, A.P. Sykes and J.G. Ayres, *Biomed. Chromatogr.*, 7 (1993) 25.
- [23] J.R. Cashman and Z-C. Yang, *J. Chromatogr.*, 532 (1990) 405.
- [24] R.M. Smith, T.G. Hurdley, J.P. Westlake, R. Gill and M.D. Osselton, *J. Chromatogr.*, 455 (1988) 77.
- [25] R. Gill, M.D. Osselton and R.M. Smith, *J. Pharm. Biomed. Anal.*, 7 (1989) 447.
- [26] R.M. Smith and J.O. Ravour, *J. Chromatogr.*, 464 (1989) 117.
- [27] R.M. Smith, J.P. Westlake, R. Gill and M.D. Osselton, *J. Chromatogr.*, 514 (1990) 97.
- [28] R.M. Smith, J.P. Westlake, R. Gill and M.D. Osselton, *J. Chromatogr.*, 592 (1992) 85.



ELSEVIER

Journal of Chromatography A, 693 (1995) 307–314

JOURNAL OF
CHROMATOGRAPHY A

Cation-exchange high-performance liquid chromatographic assay of piperazine in some pharmaceutical formulations

Henry S.I. Tan*, Jianling Xu¹, Yaohan Zheng¹

College of Pharmacy, University of Cincinnati Medical Center, 3223 Eden Avenue, P.O. Box 670004, Cincinnati, OH 45267-0004, USA

First received 21 July 1993; revised manuscript received 24 October 1994; accepted 24 October 1994

Abstract

An assay method for the quality control of piperazine in some formulations was developed utilizing cation-exchange high-performance liquid chromatography. A sample solution, containing 1-phenylpropanolamine-HCl as internal standard, was chromatographed on a 250 × 4.6 mm I.D. Ultrasil CX column with an aqueous mobile phase containing 0.07 M KH₂PO₄ (pH 3.0)–triethylamine (100:0.01), and differential refractive index detection. Piperazine and 1-phenylpropanolamine-HCl eluted at about 4.9 and 6.4 min, respectively, with a resolution of 2.1. Piperazine/internal standard peak area ratio was linear over 4–477 μg of piperazine dihydrochloride monohydrate injected ($r = 0.9994$). The limit of quantitation was 5.3 μg of piperazine dihydrochloride monohydrate injected. Recovery studies covering a range of ± 33% of label amount of piperazine in commercial formulations gave an overall recovery (\pm S.D., $n = 6$) of $100.2 \pm 0.8\%$ from spiked tablet placebos, and $100.3 \pm 1.0\%$ from spiked syrup placebos. The method was tested to be rugged based on Youden and Steiner's experimental design. The assay results of commercial formulations were higher than those obtained by the USP method. Stability tests indicated that degradation products of piperazine, formed upon hydrogen peroxide treatment, did not interfere with the piperazine peak, whereas piperazine dihydrochloride aqueous solutions were fairly stable in acid, base, and exposure to short-wavelength UV light.

1. Introduction

Piperazine (diethylenediamine), a heterocyclic nitrogenous compound, is an anthelmintic agent. It has been used in the treatment of severe infections due to *A. lumbricoides* and *E. vermicularis* [1]. The commercial formulations are available in the form of tablets, granules, syrups and incorporated into feeds. These

formulations usually contain piperazine as either the dihydrochloride, sulfate, or citrate.

Analysts have utilized many methods for the assay of piperazine and its salts. These methods include gravimetric [2–5], colorimetric [6–9], titrimetric [4,10], spectrophotometric [11], polarographic [12] and gas chromatographic methods [13–17].

The official assay methods listed in both USP XXII [18] and British Pharmacopoeia 1988 [19] for piperazine base and piperazine citrate are based on non-aqueous titration with acetous perchloric acid titrant. The non-aqueous titration

* Corresponding author.

¹ Present address: Ben Venue Labs, Cleveland, OH, USA.

is currently also being proposed as the assay method for piperazine dihydrochloride [20]. Although the non-aqueous titration method gave fairly good results, the use of acetous perchloric acid is not desirable as perchloric acid is a hazardous material. Furthermore, glacial acetic acid is a liquid that fills the room with a pungent odor (even when working in the hood) and produces burns on the skin upon contact. The official assay methods for the dosage forms of piperazine salts (tablets, syrups) are gravimetric in which trinitrophenol (picric acid) is used as precipitating reagent. These methods are time consuming and somehow dangerous, because picrates may explode during the drying of piperazine picrate at 105°C to constant mass. In addition, the method calls for washing the piperazine picrate with absolute ethanol. This step is the source for losses as the picrate redissolves in absolute ethanol that contains traces of moisture. This paper describes a direct and simple HPLC assay method for both piperazine and piperazine dihydrochloride in bulk material and some commercial formulations.

2. Experimental

2.1. Apparatus

The following apparatus were used: a Beckman Model 330 isocratic liquid chromatograph with a Model 110A single-piston reciprocating pump (Beckman Instruments, Fullerton, CA, USA); an Altex Model 210 high-pressure sample injection valve with a 20- μ l sample loop; a Model R-401 refractive index detector (Waters Chromatography, Milford, MA, USA), and a Varian 4270 electronic integrator (Varian Instruments, Walnut creek, CA, USA); Chromato-Vue CC-20 (Ultraviolet Products, San Gabriel, USA).

2.2. Reagents and materials

The following reagents were used: anhydrous piperazine (crystalline), piperazine dihydro-

chloride monohydrate, piperazine citrate tetrahydrate, 1-phenylpropanolamine hydrochloride, picric acid (Sigma, St. Louis, MO, USA); triethylamine, potassium monobasic phosphate (Fisher Scientific, Fair Lawn, NJ, USA); simulated tablet placebo (containing: corn starch, lactose, mannitol, magnesium stearate, calcium phosphate, methyl cellulose, povidone, talcum, FD&C Blue No. 1 lake); simulated syrup placebo (containing tartrazine, methylparaben, sorbitol, water), deionized water (Millipore, Bedford, MA, USA). All were used as received. Other chemicals used were analytical grade.

2.3. HPLC conditions

A 250 \times 4.6 mm I.D. 10 μ m Ultrasil CX (Beckman Instruments) cation-exchange column was used at ambient temperature with an isocratic aqueous mobile phase containing 0.07 M KH_2PO_4 (pH 3.0) buffer–triethylamine (100:0.01) at a flow-rate of 1.0 ml/min. The differential refractometer (24°C) was set at attenuation of 16 \times and its reference cell was filled with mobile phase. The electronic integrator was set at an attenuation of 4 and a chart speed of 0.5 cm/min. The mobile phase was filtered through a 0.45- μ m nylon-66 membrane filter and degassed prior to use.

2.4. Internal standard solution

About 1.770 g of 1-phenylpropanolamine–HCl was accurately weighed and transferred into a 50-ml volumetric flask, dissolved and diluted to volume with 0.07 M KH_2PO_4 buffer (pH 3.0).

2.5. Standard solution preparation

About 55 mg of piperazine dihydrochloride monohydrate (equivalent to about 27 mg of anhydrous piperazine base) was accurately weighed and transferred into a 10-ml volumetric flask. Exactly, 1.0 ml of internal standard solution was added, and the solution was diluted to volume with 0.07 M KH_2PO_4 buffer (pH 3.0).

2.6. Sample solution preparation

Tablets

Twenty tablets were weighed accurately and finely pulverized in a mortar. An aliquot, equivalent to 55 mg piperazine dihydrochloride monohydrate, was weighed accurately and transferred into a 10-ml volumetric flask. After addition of 1.0 ml of internal standard solution, the mixture was diluted to volume with 0.07 M KH_2PO_4 buffer (pH 3.0), sonicated for 15 s, and filtered. After discarding the first 5 ml, the filtrate was collected and chromatographed.

Syrups

The specific gravity of the syrup was determined following the compendial procedure [21]. An amount of syrup, containing the equivalent of about 275 mg of piperazine dihydrochloride monohydrate (equivalent to about 134 mg of anhydrous piperazine base), was weighed accurately into a 50-ml volumetric flask. After addition of 5.0 ml of the internal standard solution, the mixture was diluted to volume with 0.07 M KH_2PO_4 buffer (pH 3.0) buffer and chromatographed. Following chromatography, the amount of piperazine dihydrochloride monohydrate found in mg/g was multiplied with the specific gravity to convert it to mg/ml.

2.7. Chromatographic procedure

Exactly 20 μl of the sample solution and the standard solution were injected separately by means of the sample loop and chromatographed under the operating conditions described above. Quantitation was based on comparing the piperazine/internal standard peak area ratio of the sample to that of the standard.

2.8. Stability tests

About 800 mg of piperazine dihydrochloride were transferred into a 10-ml volumetric flask, dissolved, and diluted to volume with water. Three 0.5-ml aliquots of the solutions were each pipetted into separate 10-ml test tubes. After addition of 1 ml of one of the testing reagent

described below, the tubes were tightly closed with PTFE-lined screw caps. The three tubes were heated at 80°C for 15, 30 and 45 min, respectively. At the end of each heating period, the tubes were immersed in an ice bath to cool the contents. The contents were extracted first with diethyl ether and then with chloroform. The remaining aqueous phase was adjusted to pH 14 with 8 M sodium hydroxide for test solutions treated with acid (1 M for solutions treated with hydrogen peroxide) or to pH 1 with 1 M hydrochloric acid for test solution with base, and again extracted with ether and chloroform as described above. Both extracts were evaporated to dryness under a gentle stream of nitrogen gas. The residues were reconstituted with 1.0 ml KH_2PO_4 buffer (pH 3.0), and chromatographed. The resulting chromatograms were evaluated by comparison with those obtained from control.

The following test reagents were used: *acid*: concentrated sulfuric acid; *base*: 1 M sodium hydroxide; *hydrogen peroxide*: 33.3% hydrogen peroxide; *control*: a 0.5-ml aliquot of the stock solution was first made alkaline with 1 M NaOH to pH 14, and extracted with ether and chloroform as above. The remaining aqueous phase was then acidified with 1 M hydrochloric acid to pH 1, and extracted also with ether and chloroform. Both extracts were subjected to the same treatment as the extracts with the test reagents.

In addition, three 0.5-ml aliquots, each in 10-ml tubes with PTFE-lined screw caps were exposed to short-wavelength UV light (254 nm) for 15, 30 and 45 min, respectively. Following acidification to pH 1 with 1 M hydrochloric acid, the solution was extracted with ether and chloroform as above. The aqueous phase was basified with 1 M sodium hydroxide to pH 14 and extracted also with ether and chloroform. The organic extracts were treated in a similar manner as described above.

2.9. Ruggedness test

The mobile phase factors: pH, potassium dihydrogenphosphate concentration, triethylamine content and flow-rate, along with column

temperature, water source and integrator attenuation were selected as the seven variables for Youden and Steiner's [22] ruggedness test. Each variable was studied at two levels, indicated by upper case and lower case letter in Table 1, to bracket the standard condition of the variable described under HPLC conditions. Two different batches of spiked tablet placebos were prepared, giving 1.42 and 2.84 mg/ml of solutions before chromatography, which were assayed following Youden and Steiner's experimental design shown in Table 1. The two levels of each variable studied are shown in Table 2.

2.10. Limit of quantitation

Exactly 1.0, 2.0 and 3.0 ml of a 1 mg/ml solution of piperazine dihydrochloride monohydrate solution were pipetted into three separate 10-ml volumetric flasks, each containing 65 mg of tablet placebos. After 1 ml of a 7 mg/ml solution of internal standard solution was added to each flask, the contents of each flask were diluted to volume with 0.07 M KH_2PO_4 buffer (pH 3.0), sonicated for 15 s, and filtered, discarding the first 5 ml of filtrate. Each filtrate was chromatographed seven times under the HPLC conditions described above and the peak area ratios calculated. The standard deviation of each set was calculated and plotted against the corresponding

concentration level expressed in terms of amount of piperazine dihydrochloride monohydrate injected. The *y*-intercept of the regression line was calculated and multiplied by 10.

3. Results and discussion

Initial attempts to chromatograph piperazine with aqueous potassium diphosphate mobile phase (pH 3.0) resulted in broad tailing peaks. Addition of triethylamine to the mobile phase greatly reduced the tailing as triethylamine masked the polar silanol sites on the column particles. However, the amount of triethylamine in the mobile phase is critical; high concentrations of triethylamine resulted in poor resolution of piperazine from both solvent peak and internal standard peak.

Under the proposed experimental conditions piperazine and 1-phenylpropanolamine eluted as fairly symmetrical peaks with a tailing factor (\pm S.D., $n = 20$) at 5% height of 1.38 ± 0.18 and 1.80 ± 0.01 , respectively, and were well separated from each other with a resolution of 2.06 ± 0.11 . The average retention times (\pm S.D., $n = 20$), determined over a period of one month with five separately prepared mobile phases, were 4.93 ± 0.05 min for piperazine and 6.41 ± 0.04 min for 1-phenylpropanolamine with height equivalent to a theoretical plate (HETP) values

Table 1
Experimental design for Youden and Steiner's ruggedness test

Variable	Experiment No.							
	1	2	3	4	5	6	7	8
KH_2PO_4 Concentration ^a	A	A	A	A	a	a	a	a
pH	B	B	b	b	B	B	b	b
Triethylamine ratio	C	c	C	c	C	c	C	c
Flow-rate	D	D	d	d	d	d	D	D
Column temperature	E	e	E	e	e	E	e	E
Water source	F	f	F	F	F	f	f	F
Integrator attenuation	G	g	g	G	g	G	G	g
Observed results	s	t	u	v	w	x	y	z

^a Upper case letter denotes high and lower case letter denotes low level of variable.

Table 2
Results of ruggedness test

Variables	Levels	Piperazine recovery (%)	
		1.42 mg/ml	2.84 mg/ml
KH ₂ PO ₄ Concentration	0.075 M (A)	100.5	101.3
	0.065 M (a)	100.3	100.9
pH	3.10 (B)	99.5	100.0
	2.90 (b)	100.6	101.2
Triethylamine ratio	0.011 (C)	101.1	100.7
	0.009 (c)	100.3	99.9
Flow-rate	1.2 ml/min (D)	100.4	100.7
	0.8 ml/min (d)	100.4	100.3
Column temperature	26°C (E)	100.7	100.7
	22°C (e)	100.1	100.4
Water source	Milli-Q (F)	99.8	100.2
	Distilled (f)	101.2	100.5
Integrator attenuation	8 × (G)	100.5	99.8
	16 × (g)	100.3	101.2

(\pm S.D., $n = 20$) of 0.39 ± 0.07 mm and 0.36 ± 0.04 mm, respectively. Results showed that the piperazine peak appeared with the same retention time regardless whether it was injected as the free base, dihydrochloride, sulfate or citrate salt because of the low pH of the mobile phase. Piperazine with pK_{a1} of 9.83 and pK_{a2} of 5.56 (23.5°C) exists predominantly as the doubly protonated form at the mobile phase pH of 3.0 regardless of the initial salt form.

The relationship between piperazine/internal standard peak area ratio and the amount of piperazine injected was established. Linearity was obtained between 4 and 477 μ g of piperazine dihydrochloride monohydrate injected ($r = 0.9994$). A typical regression equation for the standard curve was $A = 0.039C - 0.001$, where A = peak area ratio of piperazine/internal standard and C = amount of piperazine dihydrochloride monohydrate injected (μ g). A similar linearity range was obtained upon injecting piperazine dihydrochloride or piperazine citrate.

In all recovery studies the dihydrochloride salt was used for the preparation of the standard solution since it was obtained with a higher degree of purity and it is easier to handle than the free base which is hygroscopic. Where appropriate, the equivalent amount of the piperazine dihydrochloride monohydrate of the salts was calculated for recovery study computations. The latter makes it possible for assaying the syrup because the commercial syrup contains piperazine sulfate. Attempts to obtain a pure sample of piperazine sulfate were unsuccessful. However, as is the case with the dihydrochloride and citrate salts, upon chromatographing piperazine sulfate, the piperazine peak appeared at the same location on the liquid chromatogram. The recovery studies were designed to investigate the recoveries of piperazine dihydrochloride by the proposed method from both spiked simulated tablet and syrup placebos. The placebos were prepared based on all possible excipients given for piperazine formulations [23] to cover as many different formulations

from different manufacturers. One batch of piperazine tablets was blue-colored. Qualitative analysis indicated that the coloring agent is FD&C No. 1. The studies covered a range from -33% to $+33\%$ of the label amount of piperazine or equivalent piperazine salts in commercial products. The chromatograms from these samples were similar to those of standard solutions. The tablet placebo gave a small extra peak before the piperazine peak at about 4 min, but did not interfere with it. No extraneous peaks were given by the syrup placebo between 1 and 10 min after injection. The overall percent recoveries (\pm S.D., $n = 6$) were $100.2 \pm 0.8\%$ for the spiked tablet placebo and $100.3 \pm 1.0\%$ for the syrup placebo spiked with piperazine dihydrochloride.

A ruggedness test was performed on the proposed method based on Youden and Steiner's experimental design [22] to determine if a small variation of an operating variable can be tolerated (Table 1). For example, to determine the effect of the KH_2PO_4 concentration on the assay result, the result averages of runs 1–4 were compared to those of runs 5–8. In other words, $(s + t + u + v)/4$ is compared to $(w + x + y + z)/4$ (Table 1). The experimental design shows that the other six factors appear twice at the high level and twice at the lower level in each set. Consequently, their effects on the results in each set are identical. Any difference in the results between the two sets must be due to the effect of KH_2PO_4 . Results of this ruggedness test are shown in Table 2. In the case of the column temperature, the 26°C was achieved by using a column heating mantle. The standard deviations in percent recovery for both sample sizes are small indicating that this method is rugged within minor fluctuations of the seven operating variables.

The limit of quantitation was determined by the extrapolation method [24]. The y-intercept of the plot of standard deviation vs. the corresponding concentration represents the standard deviation of the analytical blank S.D.₀. Multiplying S.D.₀ by 10 provides an estimate for the limit of quantitation in terms of peak area [25]. Further comparison of this value with the peak

area of a standard solution gives the limit of quantitation in terms of concentration. As measured the limit of quantitation was $5.3 \mu\text{g}$ of piperazine dihydrochloride monohydrate injected under the described experimental conditions.

The precision was determined by injecting the same sample seven times. The experiments were repeated three more times at 5-day intervals, using freshly prepared samples each time, and measuring the peak area ratios each time. The percent relative standard deviations were 1.75, 1.40, 1.63 and 1.13%, respectively.

The method was applied to the assay of commercial tablets and syrups. Fig. 1A shows a typical liquid chromatogram from commercial tablets. As with spiked tablet placebos, the

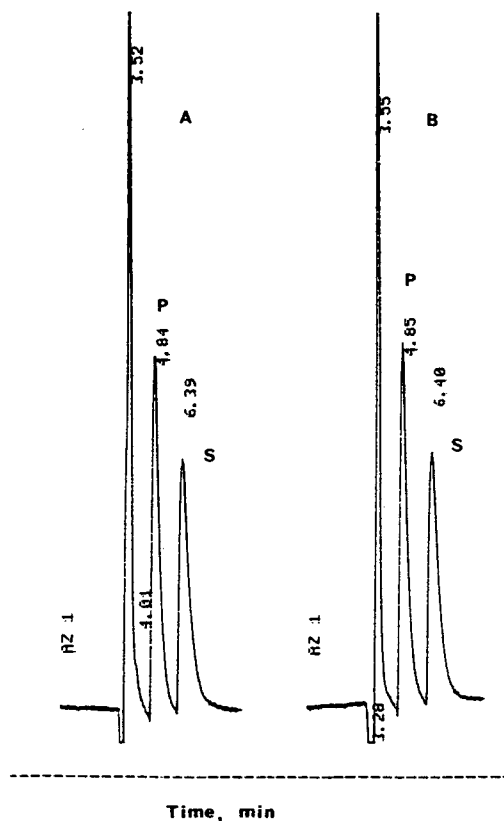


Fig. 1. Typical liquid chromatogram of an aqueous extract of a commercial tablet (A) and of a diluted solution of a commercial syrup (B). P = Piperazine; S = internal standard.

liquid chromatogram also showed an extra peak eluting before the piperazine peak at about 4 min. However, this extra peak co-elutes with the solvent peak and did not interfere with the piperazine peak. Fig. 1B is a liquid chromatogram from a commercial syrup. The assay results are shown in Table 3 which also includes the results obtained by the USP method for comparison. The results indicate that, in general, the compendial results gave consistently low results and may very well lead to a negative systematic bias. The compendial method is a gravimetric assay of piperazine after precipitating it as the picrate salt. The low results were presumably due to incomplete precipitation and/or losses during the washing of the precipitate with “absolute” ethanol. In spite of the discrepancies between the proposed and the compendial methods, a correlation ($r = 0.999$) is obtained between the two methods. The regression equation for the correlation line is $USP = 0.989 \cdot LC - 0.389$ ($USP = USP$ method; $LC = HPLC$ method).

Semi-quantitative stability tests results showed that aqueous piperazine dihydrochloride solutions were relatively stable when subjected to acid or base at 80°C for 45 min because, within experimental errors, the area of the piperazine peak in the liquid chromatogram was similar in size as that of control. Subjecting the solution to

short-wavelength UV light (254 nm) for 45 min did not change the size of the piperazine peak in the liquid chromatogram either. As expected, the compound was not stable toward hydrogen peroxide. The liquid chromatograms after the hydrogen peroxide treatment gave an additional peak, presumably of the mono- and/or dinitroso derivatives (Fig. 2). Fig. 2A is the liquid chromatogram of the acidic extract showing the extraneous peak X at about 5.4 min. Fig. 2B is the liquid chromatogram of the subsequent basic extraction to which internal standard was added. No effort was undertaken to identify the extraneous peaks. The oxidation products eluted at different retention times which means that the oxidized products can be detected by the proposed assay method, and they did not interfere

Table 3
Assay results of commercial formulations by the proposed and USP methods

Label claim (mg/tablet or ml)	Label claim (%) ^a	
	HPLC	USP
<i>Tablet</i>		
50	99.0	92.4
50	98.4	92.2
250	98.1	93.6
250	97.9	95.1
<i>Syrup</i>		
340	99.8	96.5
340	101.2	101.2

^a Average of duplicate results.

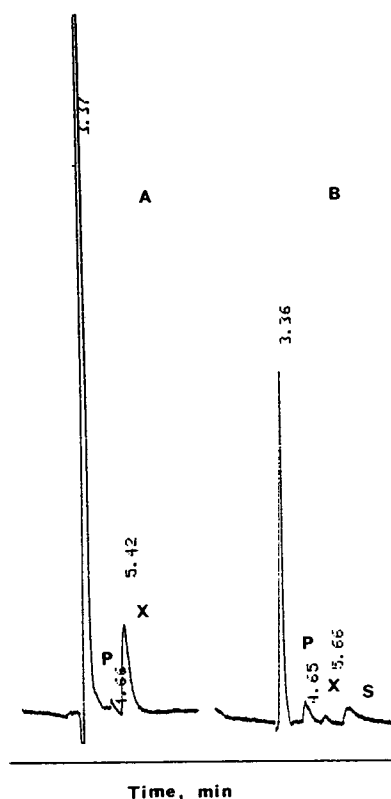


Fig. 2. Liquid chromatogram of piperazine after H_2O_2 treatment at 80°C for 30 min. (A) Acidic extract; (B) subsequent basic extract spiked with internal standard (S). P = Piperazine; X = extraneous peak.

with the piperazine peak. Samples in strong acid, in strong base, and in strong hydrogen peroxide required extensive dilution before injecting on the column. The low amounts of piperazine used in the studies will become so diluted that degradation compounds may not be detected, if the diluted solutions were directly injected onto the column. Consequently, the samples were simply extracted under acidic as well as basic conditions as described. Since the control needed to be extracted also, the samples which were subjected to UV radiation, were also extracted.

The above results indicate that the method is simple and provides quantitative, reproducible results for the assay of piperazine in commercial formulations for quality control purposes. The method is rugged for the seven variables tested. For the dosage forms, the proposed method is safer and requires a much shorter assay time than the USP gravimetric method.

References

- [1] *Drug Information for the Health Care Professional*, Vol. I, USP DI 14th ed., United States Pharmacopeial Convention, Rockville, MD, 1994, p. 2960.
- [2] R.E. Pankratz, *J. Pharm. Sci.*, 50 (1961) 175.
- [3] I. Ganescu and A. Popescu, *Anal. Abstr.*, 21 (1971) 309.
- [4] S. Ramotowski and M. Szczesniak, *Anal. Abstr.*, 19 (1970) 675.
- [5] T. Kekesi and Z. Toth, *Anal. Abstr.*, 9 (1962) 350.
- [6] S. Hanna and A. Tang, *J. Pharm. Sci.*, 62 (1973) 2024.
- [7] Y.M. Dessouky, *Analyst*, 99 (1974) 482.
- [8] V.D. Gupta, *Am. J. Hosp. Pharm.*, 33 (1976) 283.
- [9] T.R. Baggi, S.N. Mahajan and G.R. Rao, *J. Assoc. Off. Anal. Chem.*, 57 (1974) 1144.
- [10] R.B. Maybury, J.P. Barrette and R. Payfer, *J. Assoc. Off. Anal. Chem.*, 46 (1963) 1060.
- [11] L. Mohn, *J. Assoc. Off. Anal. Chem.*, 48 (1965) 590.
- [12] J.D. Mclean and O.L. Daniels, *J. Assoc. Off. Anal. Chem.*, 54 (1971) 555.
- [13] G. Skarping, L. Renman and C. Sango, *J. Chromatogr.*, 346 (1985) 191.
- [14] N.O. Ahnfelt, P. Hgryvig and K.E. Karlsson, *Chromatographia*, 16 (1982) 60.
- [15] F.T. Delbeke and M. Debackere, *J. Chromatogr.*, 273 (1983) 141.
- [16] G. Audunsson and L. Mathiasson, *J. Chromatogr.*, 315 (1984) 299.
- [17] S. Olajos and D. Sztaniszlav, *J. Chromatogr.*, 378 (1986) 155.
- [18] *The United States Pharmacopeia*, United States Pharmacopeial Convention, Rockville, MD, 22nd revision, 1990.
- [19] *British Pharmacopoeia, 1988 Version*, Her Majesty's Stationery Office, London, 1988.
- [20] US Pharmacopeial Convention, *Pharmacopeial Forum*, 18 (1992) 3042.
- [21] *The United States Pharmacopeia*, United States Pharmacopeial Convention, Rockville, MD, 22nd revision, 1990, p. 1609.
- [22] W.J. Youden and E.H. Steiner, *Statistical Manual of the AOAC*, Association of Official Analytical Chemists, Arlington, VA, 1975, p. 33.
- [23] *Physician's Desk Reference*, Med. Econ. Data Production, Montvale, NJ, 48th ed., 1994.
- [24] J.A. Glaser and D.L. Foerst, *Environ. Sci. Tech.*, 15 (1981) 1426.
- [25] *The United States Pharmacopeia*, United States Pharmacopeial Convention, Rockville, MD, 22nd revision, 1990, p. 1711.



ELSEVIER

Journal of Chromatography A, 693 (1995) 315–323

JOURNAL OF
CHROMATOGRAPHY A

Elimination of adsorption effects of polarity parameters determined by inverse gas chromatography

A. Voelkel*, J. Janas

Poznań University of Technology, Institute of Chemical Technology and Engineering, Pl. M. Skłodowskiej-Curie 2,
60-965 Poznań, Poland

First received 19 July 1994; revised manuscript received 18 October 1994; accepted 18 October 1994

Abstract

A procedure for the elimination of adsorption contributions to retention parameters is presented and discussed. It is shown that the corrected retention volume may be used in the calculation of polarity parameters from their basic equations. The influence of the elimination procedure on corrected polarity parameters is presented and discussed.

1. Introduction

Gas chromatography is not only the most widespread analytical method used for determination of components of complex volatile mixtures, but may also be applied as a method for the physico-chemical characterization of different systems. Inverse gas chromatography (IGC) in particular has become a reliable, fast and accurate method for the investigation of polymers, synthetic fibers, surfactant mixtures and organic and inorganic fillers. In this technique the examined material, e.g., molten surfactant, is placed in a chromatographic column and its properties are studied by injecting test solutes on to the column. The retention times and/or peak elution profiles of carefully selected standard solutes are used to estimate the interactions between the solute and stationary phase. On the basis of the column contents one may divide

inverse gas chromatography into inverse gas-liquid and inverse gas-solid chromatography.

Surface-active agents of different types have been examined as stationary phases in GLC experiments [1–10] and characterized in terms of their polarity. Poole and Poole [11] defined this as the capacity of a solvent for various intermolecular interactions. They indicated also that particular attention must be paid to the influence of interfacial adsorption, at both the gas-support and gas-liquid interfaces. There are at least three ways in which a test solute might interact with a column packing: (i) partitioning between the gas and liquid phases, (ii) adsorption at the gas-liquid interface and (iii) adsorption at the liquid-solid interface.

The well known Berezkin equation [12,13] represents the relationship between the net retention volume (V_N) and different increments of the retention mechanism:

$$V_N = K_L V_L + K_{GL} S_{GL} + K_{LS} S_{LS} \quad (1)$$

* Corresponding author.

where K_L is the partition coefficient, V_L is the volume of the liquid phase and K_{GL} and K_{LS} are the adsorption coefficients at the gas–liquid and liquid–solid interfaces, respectively.

Poole and Poole [11] used K_L estimated from Eq. 1 to calculate the polarity and selectivity parameters of stationary phases. However, in doing so, they had to redefine the well known Kováts equation for the retention index. Other polarity parameters used in the characterization of surfactants [1–10] were defined in terms describing only the partitioning process of the analyte between the stationary phase and the carrier gas.

Physico-chemical (also polarity) parameters may only be properly determined if the influence of adsorption processes at the interfaces are eliminated or minimized. Adsorption effects are usually minimized by the application of a non-active support, careful chemical deactivation of the support surface and/or the use of a high liquid loading. However, the methods of adsorption elimination are not completely satisfactory. Poole and Poole [11] showed that even at a high stationary liquid phase loading both adsorption processes are significant contributors to the retention mechanism. Therefore, we decided to evaluate a procedure of data reduction which permits the isolation of the increment of retention volume corresponding only to the partition mechanism, i.e., bulk retention. We therefore eliminated retention volume contributions corresponding to adsorption at both the gas–liquid and liquid–solid interfaces. Hence the corrected retention volume may be used directly to calculate polarity parameters from appropriate equations. The influence of the retention volume corrections on the values of the polarity parameters is also discussed.

2. Experimental

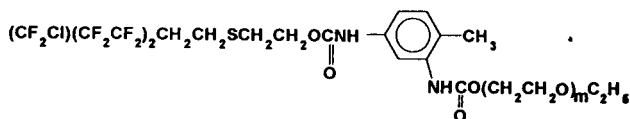
2.1. Materials

Two groups of fluorinated oxyethylene derivatives were used as liquid stationary phases in IGC experiments. The synthesis and surface

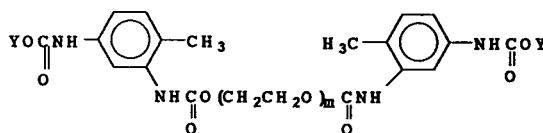
Table 1
Molecular masses of investigated liquid phases in group I

No.	Compound	Molecular mass (g mol)
1	R _{n1} M340	936.5
2	R _{n1} M456	1052.5
3	R _{n1} M666	1262.5
4	R _{n1} M1005	1601.5
5	R _{n1} M1500	2096.5
6	R _{n1} M2250	2846.5
7	R _{n1} M2000	3115.0

properties of these surfactants have been described earlier [10]. The general formulae of these compounds are as follows:



and



where $\text{Y} = \text{CF}_3\text{CF}(\text{CF}_2\text{Cl})(\text{CF}_2\text{CF}_2)\text{CH}_2\text{CH}_2\text{SCH}_2\text{CH}_2$. Their molecular masses are presented in Tables 1 and 2, where R_{n1}M340 and R_{n2}M1500 denote structures having one or two CF_2CF_2 groups in the hydrophobic part of the surfactant molecule and the molecular masses of the oligooxyethylene chain are 340 and 1500, respectively.

Table 2
Molecular masses of investigated liquid phases in group II

No.	Compound	Molecular mass (g mol)
8	R _{n2} M456	1192.36
9	R _{n2} M666	1402.36
10	R _{n2} M1005	1741.36
11	R _{n2} M1500	2236.36
12	R _{n2} M2250	2986.36
13	R _{n2} M2000	3198.72

2.2. IGC experiments

The conditions for the IGC experiments were as follows: column, 1 m × 3 mm I.D.; column temperature, 70, 90, and 110°C; column loading, 5, 10 and 25% (w/w) supported on 80–120-mesh Celite; carrier gas, helium at a flow-rate of 40 ml min⁻¹; detector, flame ionization, gas chromatograph, Chrom 5 (Kovo, Czech Republic). The volatile test compounds employed were non-polar *n*-alkanes with chain lengths from C₅ to C₁₀, the aromatic hydrocarbons benzene, toluene, xylene and ethylbenzene, polar *n*-alkanols from C₁ to C₄, 2-butanone, 2-pentanone, nitropropane and pyridine. Each solute was injected five times and retention times were averaged. These mean retention times were used in further calculations of net retention volumes. All experiments were carried out for three different liquid phase loadings.

2.3. Calculations

Elimination of adsorption effects

Berezkin and co-workers [12–14] have shown that the net retention volume (V_N) is the sum of the partial retention volumes corresponding to the absorption of chromatographed test solutes in the liquid phase [$V_{N(i)}$] and its adsorption at all interfaces [$V_{N(sj)}$], respectively:

$$V_N = \sum_{i=1}^m V_{N(i)} + \sum_{j=1}^n V_{N(sj)} \quad (2)$$

or

$$V_N = \sum_{i=1}^m \overline{K_{L(i)}} V_{L(i)} + \sum_{j=1}^n \overline{K_{S(j)}} S_{S(j)} \quad (3)$$

Of critical importance is the selection of the component of the net retention volume corresponding to the dissolution in the liquid phase, i.e.

$$V_N^s = K_L V_L \quad (4)$$

Therefore, Eq. 1 can be rearranged into the linear relationship

$$\frac{V_N}{V_L} = \Phi \left(\frac{1}{V_L} \right) \quad (5)$$

in which the slope equals the partition coefficient, $K_L \cdot K_L$ values may be then used in Eq. 4 to calculate V_N^s . The selected increment of the net retention volume corresponding only to absorption process or free of adsorption effects may be used to calculate polarity parameters from appropriate equations.

The retention times of a series of *n*-alkanes were used to calculate the retention time corresponding to the void volume of the column [15].

Polarity parameters

The following polarity parameters were used for characterization of examined stationary phases:

(i) The retention index I of selected test solutes was calculated from the Kováts equation, expressing ΔI as the difference in retention indices of a given solute measured on the experimental liquid phase (I_p) and a reference phase, e.g., squalane (I_{np}):

$$\Delta I = I_p - I_{np} \quad (6)$$

Commercial stationary phases are often characterized by the sum of retention index differences of the first five McReynolds' [16] solutes, i.e., benzene, 1-butanol, 2-pentanone, 1-nitropropane and pyridine, $\sum_{i=1}^5 \Delta I_i$.

(ii) The polarity index, PI [17],

$$PI = 100 \log(C - 4.7) + 60 \quad (7)$$

where C is the number of carbon atoms in a hypothetical *n*-alkane having the same retention time as the alcohol test solute (methanol or ethanol).

(iii) The coefficient ρ [18] is the relative retention of a polar test substance (methanol, ethanol) and a standard non-polar substance (*n*-hexane):

$$\rho = \frac{t'_{R(\text{EtOH})}}{t'_{R(\text{n-hexane})}} \quad (8)$$

(iv) Criterion A [19]:

$$A = \frac{t'_{R(n+1)} - t'_{R(n)}}{t'_{R(n)} - t'_{R(n-1)}} \quad (9)$$

where $t'_{R(n+1)}$, $t'_{R(n)}$ and $t'_{R(n-1)}$ denote the adjusted retention times of n -alkanes having $n + 1$, n and $n - 1$ carbon atoms, respectively.

(v) Partial molar excess Gibbs energy of solution per methylene group [20], defined as

$$\Delta G^E(\text{CH}_2) = \frac{1}{k} \cdot RT \ln \left[\frac{V_{gn} \times p_{i(n)}^0}{V_{g(n+k)} \times p_{i(n+k)}^0} \right] \quad (10)$$

where V_{gn} and $V_{g(n+k)}$ are specific retention volumes and $p_{i(n)}^0$ and $p_{i(n+k)}^0$ are saturated vapour pressures of two homologues having n and $n + k$ methylene groups in their molecules, respectively.

(vi) The partial molal Gibbs free energy of solution for a methylene group, $\Delta G_s^m(\text{CH}_2)$ [21], was calculated from the following equations:

$$\ln V_g = -\frac{\Delta H_s^m}{RT} + \left[\frac{\Delta S_s^m}{R} - \ln \left(\frac{1000}{273.15R} \right) \right] \quad (11)$$

$$\Delta G_s^m = \Delta H_s^m - T\Delta S_s^m \quad (12)$$

and the linear relationship between $\Delta G_s^m(\text{CH}_2)$ for the series of n -alkanes and number of carbon atoms in their molecules.

Calculation steps

The calculations of uncorrected and corrected polarity parameters were carried out according to the following scheme:

(i) five measurements were made for each test solute;

(ii) retention times were averaged and the mean value was used in the following steps;

(iii) the net retention volume was calculated for each solute;

(iv) polarity parameters were calculated from uncorrelated net retention volumes of test solutes;

(v) Eq. 5 was used and K_L values were calculated at significance level $\alpha = 0.05$;

(vi) corrected net retention volumes V_N^s were calculated from Eq. 4;

(vii) corrected polarity parameters were calcu-

lated from V_{Ni}^s values ($i = \text{appropriate test solute}$).

3. Results and discussion

3.1. Adsorption contribution to the retention volume

The magnitude of the influence of the adsorption effect depends on the type of support, the polarity of the liquid phase and the polarity of the injected solute. To minimize this effect, a high loading of liquid phase and chemical deactivation of the support surface were used. However, as has been demonstrated [11], even in such a case the adsorption effect is not completely eliminated. This was the reason for evaluating the procedure for the isolation of the increment of retention volume corresponding only to the mechanism of partitioning of the solute between the gas and liquid phases.

As an example, K_L values for two stationary phases determined for a number of test solutes are presented in Tables 3 and 4. The K_L values were calculated from linear regression at the significance level $\alpha = 0.05$; the correlation coefficient was always higher than 0.96. Poole and co-workers [11,22] have shown that strong linearity described by Eq. 5 exists. We have assumed a universal character of their statement, which is confirmed by our results. Therefore, we limited the number of liquid phase loadings used to three. Graphical representations of Eq. 5 for two selected stationary phases and several test solutes are shown in Fig. 1. The partition coefficient K_L decreases with increase in the temperature of the experiment and increases with an increase in the molecular mass of a given test solute. According to the suggestions of Kersten et al. [22], fluorine-containing compounds may be classified as stationary phases of relatively limited selectivity (such as OV-17, OV-105, OV-225 and QF-1). The proportion of adsorption interactions for these compounds is small [23]. As expected, an increase in the content of liquid phase in the column filling decreases the propor-

Table 3
Values of the partition coefficient K_L for test solutes on $R_{n1}M340$

Test compound	Temperature (K)		
	343	363	383
Pentane	8.8	6.4	4.8
Hexane	17.6	12.4	8.1
Heptane	37.0	22.4	15.3
Octane	78.7	43.6	25.9
Nonane	165.9	83.8	47.0
Decane	348.4	162.0	83.7
Benzene	115.7	62.8	36.5
Methanol	79.7	42.6	22.7
Ethanol	110.1	55.8	29.9
1-Propanol	231.6	107.9	54.7
1-Butanol	491.5	219.5	105.9
2-Butanone	128.6	70.9	41.5
2-Pentanone	235.7	123.5	67.8
Nitropropane	685.2	317.9	159.3
Pyridine	778.7	356.5	179.1
Toluene	236.6	127.1	71.4
Xylene	504.7	187.7	128.5
Ethylbenzene	445.2	222.2	119.4

Table 4
Values of the partition coefficient K_L for test solutes on $R_{n2}M1005$

Test compound	Temperature (K)		
	343	363	383
Pentane	9.4	7.2	5.7
Hexane	17.8	12.2	9.2
Heptane	34.2	21.5	14.9
Octane	71.6	40.9	25.1
Nonane	146.9	76.7	44.2
Decane	300.9	145.0	75.5
Benzene	138.2	74.3	40.7
Methanol	93.5	53.4	30.2
Ethanol	119.5	60.1	33.3
1-Propanol	239.9	115.9	58.1
1-Butanol	516.1	232.0	108.5
2-Butanone	122.2	67.3	39.0
2-Pentanone	215.2	113.2	60.8
Nitropropane	809.0	369.8	178.6
Pyridine	716.6	341.5	169.5
Toluene	283.6	145.6	79.3
Xylene	558.5	271.5	138.0
Ethylbenzene	517.4	251.0	126.8

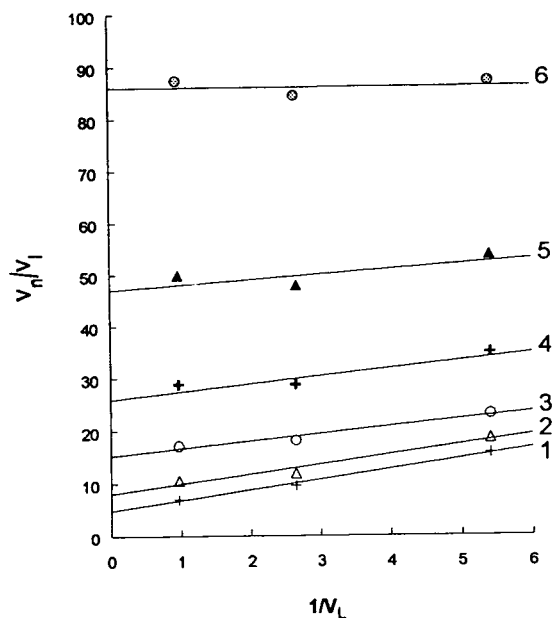


Fig. 1. Relationship $V_n/V_1 = \Phi(1/V_1)$ for $R_{n1}M340$ at 383 K for n -alkanes: 1 = n -pentane; 2 = n -hexane; 3 = n -heptane; 4 = n -octane; 5 = n -nonane; 6 = n -decane.

tion of adsorption effects in the retention parameter (Tables 5 and 6).

The greatest influence of adsorption effects is observed on the retention of non-polar aliphatic hydrocarbons and decreases with increase in their molecular masses. Similarly, the adsorption effect decreases with increase in molecular mass in the n -alkanol series. The adsorption contribution to the retention of polar test solutes having high molecular mass is insignificant or not observed at all. An increase in liquid phase loading significantly decreases the adsorption contribution to retention in the case of n -alkanes (Tables 5 and 6). The symbols A and R used in Tables 5 and 6 denote the adsorption and bulk retention (partition) increment to the retention volume, respectively. Therefore, $100 [A/(A + R)]$ (%) express adsorption contribution to retention. The influence of the adsorption effect is higher for two of the stationary phases, $R_{n1}M2000$ and $R_{n2}M2000$ (Table 6), owing to the screening of the oligooxyethylene chain by two large hydrophobic groups.

Table 5

Influence of liquid phase loading on the adsorption contribution $\{100[A/(A+R)]\%$ for $R_{n1}M340$ (at 383 K) (A and R are the adsorption and bulk retention increments to the net retention volume, respectively)

Test compounds	Liquid phase loading (%)		
	5	10	25
Pentane	69.5	50.2	31.5
Hexane	56.5	32.4	23.6
Heptane	33.7	15.8	13.4
Octane	25.8	6.0	10.2
Nonane	12.6	10.4	6.3
Decane	4.1	0.0	7.3
Benzene	27.3	10.9	8.7
Methanol	42.8	20.9	15.5
Ethanol	32.1	13.8	10.6
1-Propanol	12.3	2.0	4.6
1-Butanol	0.0	0.0	0.5
2-Butanone	22.5	8.8	5.2
2-Pentanone	5.6	0.0	3.9
Nitropropane	0.0	0.0	0.9
Pyridine	0.0	0.0	0.0
Toluene	5.1	0.0	2.9
Xylene	0.0	0.0	2.9
Ethylbenzene	0.0	0.0	1.9

No clear relationship (e.g. linear) was found between the adsorption contribution to the retention mechanism and the structure of the compounds examined (Fig. 2). However, in group I the highest adsorption contribution was observed for homologues having a short oligooxyethylene chain. This contribution decreases with increase in the number of ethylene oxide (EO) units up to 20–22. Further increase in the oligooxyethylene chain length causes an increase in the adsorption contribution to the retention volume of *n*-octane. The corresponding relationship for oxyethylates in group II is irregular. However, the adsorption contribution to the retention of *n*-octane on liquid phases from this group is often lower than the corresponding value for group I.

3.2. Influence of elimination of the adsorption effect on polarity parameters

The procedure for eliminating the adsorption effect was also applied in the determination

Table 6

Influence of liquid phase loading on the adsorption contribution $\{100[A/(A+R)]\%$ for $R_{n2}M2000$ (at 383 K) (A and R are the adsorption and bulk retention increments to the net retention volume, respectively)

Test compounds	Liquid phase loading (%)		
	5	10	25
Pentane	91.57	85.06	65.77
Hexane	80.22	68.48	40.82
Heptane	67.87	52.88	26.66
Octane	56.81	40.48	19.06
Nonane	45.47	29.15	13.66
Decane	39.81	24.91	10.95
Benzene	28.69	14.92	8.02
Methanol	34.91	21.01	9.20
Ethanol	28.14	16.03	6.98
1-Propanol	21.18	11.74	4.84
1-Butanol	17.04	9.33	3.70
2-Butanone	31.78	19.01	7.92
2-Pentanone	25.28	14.34	6.01
Nitropropane	12.55	7.53	2.10
Pyridine	14.84	9.08	2.60
Toluene	21.51	12.85	4.38
Xylene	17.23	10.27	3.14
Ethylbenzene	0.0	0.0	0.0

process of polarity parameters, i.e., the corrected net retention volumes calculated from Eqs. 6–13. The influence of the liquid phase

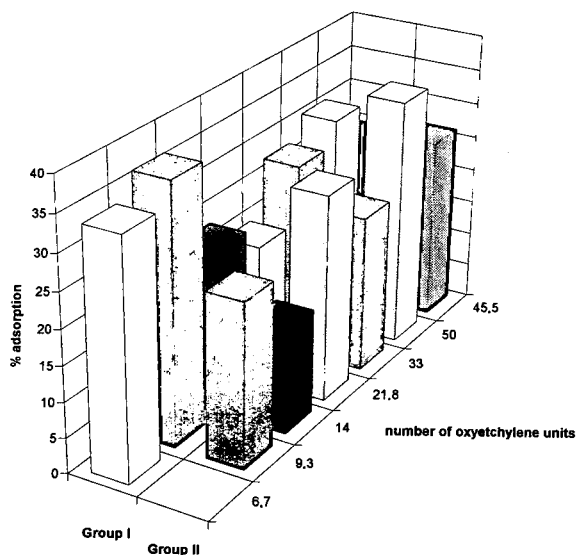


Fig. 2. Adsorption contribution to *n*-octane retention for liquid phases used at 383 K (25% liquid phase loading).

loading on the retention index of several test solutes before and after this correction is presented in Fig. 3a and b, respectively. The application of the correction procedure significantly decreases the variations in retention index with liquid phase loading.

Similarly, this procedure also decreases the variations in the polarity index (Fig. 4). A narrow scatter of results is observed when both methanol and ethanol are used as test solutes. As an example, PI^{EtOH} for $R_{n_2}M2000$ at 365 K varies from 119.1 to 127.5 index units before correction, whereas after the application of the elimination procedure it changes from 126.9 to 127.9 index units (Table 7). Similar changes were found for the coefficient ρ . Values of both of these polarity parameters increase after the

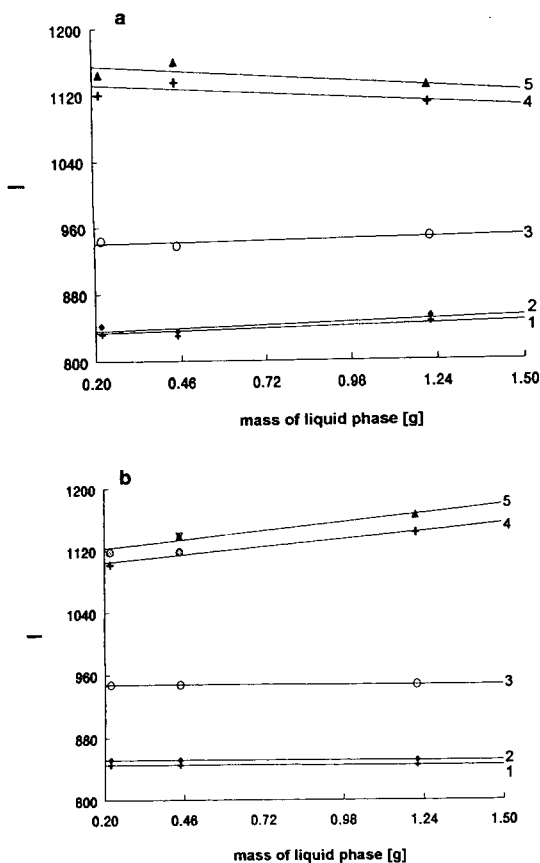


Fig. 3. Dependence of the retention index I on the liquid phase loading, (a) before and (b) after correction due to adsorption contribution for (1) benzene, (2) ethanol, (3) 2-pentanone, (4) nitropropane and pyridine.

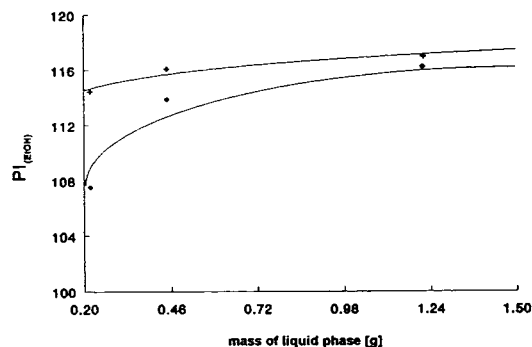


Fig. 4. Relationship between polarity index PI^{EtOH} and mass of the liquid phase ($R_{n_1}M340$ at 343 K), (\blacklozenge) before and ($+$) after correction.

elimination of the adsorption contribution from retention volume of test solutes.

The most significant results were found for criterion A . The correction of the retention data for adsorption effects leads to criterion A being independent of the liquid phase loading (Table 8). Criterion A was calculated with the use of n -alkane retention data. Before correction, the net retention volumes were significantly influenced by adsorption effects, which led to different values being found for three liquid phase loadings. The use of corrected net retention volumes V_N^s gave the same criterion A values in each instance.

Thermodynamic parameters of solution were also used to characterize fluorinated oligooxyethylene derivatives. The values for the partial molar excess Gibbs function of solution per methylene group, $\Delta G^E(CH_2)$, and partial molal Gibbs function of solution, $\Delta G_s^m(CH_2)$, depend significantly on the liquid phase loading. The contribution of adsorption effects to the numerical values of these parameters is lowered after the use of the correction procedure (Figs. 5 and 6).

4. Conclusions

In the proposed method for the elimination of adsorption effects, a computational method is used to account for the bulk retention (partition) increment in retention data and the adsorption

Table 7

Values of polarity index, PI^{EtOH} , at 343 K for 5, 10 and 25% (w/w) liquid phase loadings before and after correction for adsorption contribution

Compound	Polarity index, PI_{EtOH}					
	Before correction			After correction		
	5%	10%	25%	5%	10%	25%
$R_{n1}M340$	107.5	113.9	115.9	114.6	116.1	116.9
$R_{n1}M456$	112.3	118.9	119.8	119.3	120.5	121.1
$R_{n1}M666$	113.0	117.2	119.3	118.5	119.7	120.2
$R_{n1}M1005$	117.7	118.3	120.1	120.7	121.0	122.0
$R_{n1}M1500$	115.6	120.2	122.2	121.8	122.8	122.7
$R_{n1}M2250$	116.4	121.3	124.1	124.2	124.8	124.9
$R_{n1}M2000$	124.6	128.1	129.4	130.4	130.1	129.8
$R_{n2}M456$	107.6	112.7	116.6	115.0	116.7	118.0
$R_{n2}M666$	107.4	113.8	117.8	114.8	118.3	119.5
$R_{n2}M1005$	111.9	116.3	119.7	118.3	119.3	120.0
$R_{n2}M1500$	113.0	118.4	120.9	120.0	121.3	121.8
$R_{n2}M2250$	116.5	120.4	122.4	121.2	122.3	123.0
$R_{n2}M2000$	124.0	127.3	128.9	129.9	129.8	129.2

effects at gas–liquid phase and liquid phase–solid support interfaces are eliminated. This leads to the precise determination of physico-chemical parameters. Corrected retention data

may be used to calculate polarity parameters from appropriate equations. The use of a high liquid phase loading was not always effective. In the authors' opinion, the proposed procedure

Table 8

Values of Criterion A at 343 K for 5, 10 and 25% (w/w) liquid phase loadings before and after correction for adsorption contribution

Compound	Criterion A			
	Before correction			After correction ^a
	5%	10%	25%	
$R_{n1}M340$	2.114	2.105	2.136	2.132
$R_{n1}M456$	2.017	2.069	2.106	2.127
$R_{n1}M666$	1.986	2.034	2.124	2.150
$R_{n1}M1005$	2.417	2.127	2.094	2.053
$R_{n1}M1500$	2.051	2.027	2.098	2.091
$R_{n1}M2250$	2.009	2.020	2.069	2.079
$R_{n1}M2000$	2.018	1.987	2.007	1.995
$R_{n2}M456$	1.976	2.061	2.117	2.176
$R_{n2}M666$	2.291	2.108	2.167	2.110
$R_{n2}M1005$	2.102	2.103	2.065	2.073
$R_{n2}M1500$	2.111	2.038	2.069	2.049
$R_{n2}M2250$	1.966	2.043	2.072	2.108
$R_{n2}M2000$	2.127	2.006	2.006	1.954

^a For all liquid phase loadings.

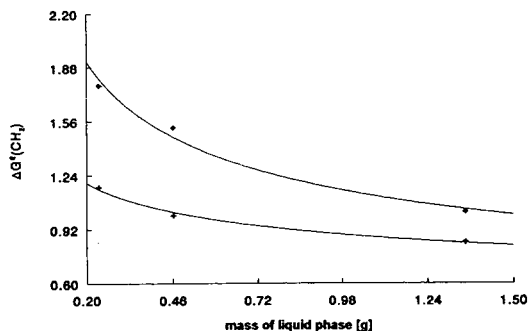


Fig. 5. Relationship between partial molar excess Gibbs function per methylene group, $\Delta G^E(\text{CH}_2)$ (kJ mol^{-1}), for n -alkanes and mass of the liquid phase (R_{n1} M340 at 343 K), (\blacklozenge) before and ($+$) after correction.

provides the most favourable solution of the problem. The discussed polarity parameters calculated with the use of corrected retention volumes V_N^s do not depend on the liquid phase loading, or the dependence is much lower than before correction.

The applicability of the proposed procedure for the elimination of adsorption effects was demonstrated in the calculation of polarity parameters. However, the corrected retention volume may be used in calculating any physico-chemical parameter defined in terms of the partition retention mechanism.

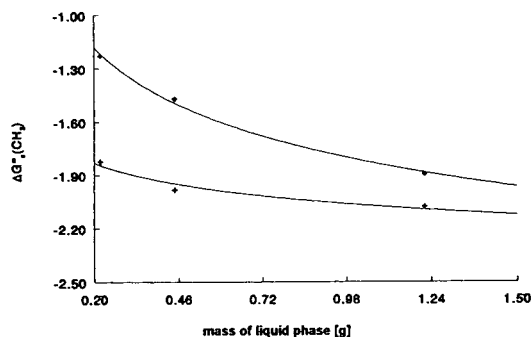


Fig. 6. Relationship between partial molal Gibbs function of solution per methylene group, $\Delta G_s^m(\text{CH}_2)$ (kJ mol^{-1}), and mass of the liquid phase (R_{n1} M340 at 343 K), (\blacklozenge) before and ($+$) after correction.

Acknowledgement

This work was supported by grant PTU DS 32/220/94, which is gratefully acknowledged.

References

- [1] J. Szymanowski, A. Voelkel, J. Beger and H. Merkwitz, *J. Chromatogr.*, 330 (1985) 61.
- [2] A. Voelkel, J. Szymanowski, J. Beger and K. Ebert, *J. Chromatogr.*, 398 (1987) 31.
- [3] A. Voelkel, *Chromatographia*, 23 (1987) 195.
- [4] A. Voelkel, *J. Chromatogr.*, 435 (1988) 29.
- [5] A. Voelkel, *Chromatographia*, 25 (1988) 95.
- [6] A. Voelkel, J. Szymanowski, J. Beger and H. Ruestig, *J. Chromatogr.*, 442 (1988) 219.
- [7] A. Voelkel, *J. Chromatogr.*, 450 (1988) 291.
- [8] J. Szymanowski, *CRC Crit. Rev. Anal. Chem.*, 21 (1988) 407.
- [9] A. Voelkel, J. Szymanowski and W. Hreczuch, *J. Am. Oil Chem. Soc.*, 70 (1993) 711.
- [10] A. Voelkel, J. Szymanowski, E. Meissner and J. Myszkowski, *J. Fluorine Chem.*, 64 (1993) 177.
- [11] C.F. Poole and S.K. Poole, *Chem. Rev.*, 89 (1989) 377.
- [12] V.G. Berezkin, *Gazo- i Zhidko-Tverdogaznaya Khromatografiya*, Khimiya, Moscow, 1986.
- [13] V.G. Berezkin, *J. Chromatogr.*, 159 (1978) 359.
- [14] M. Burova, M.H. Lunski and V.G. Berezkin, *Zh. Fiz. Khim.*, 49 (1975) 446.
- [15] A. Grobler and G. Balizs, *J. Chromatogr. Sci.*, 12 (1974) 57.
- [16] W.O. McReynolds, *J. Chromatogr. Sci.*, 8 (1970) 685.
- [17] V.R. Huebner, *Anal. Chem.*, 181 (1961) 351.
- [18] P. Becher and R.L. Birkmeier, *J. Am. Oil Chem. Soc.*, 41 (1964) 169.
- [19] J. Sevcik and M.S.H. Lowentap, *J. Chromatogr.*, 217 (1981) 139.
- [20] M. Roth and J. Novak, *J. Chromatogr.*, 134 (1982) 337.
- [21] T.M. Risby and P.C. Jurs, *J. Chromatogr.*, 99 (1974) 173.
- [22] B.R. Kersten, C.F. Poole and K.G. Furton, *J. Chromatogr.*, 411 (1987) 43.
- [23] A. Voelkel, *Zesz. Nauk. Politech. Poznańskj, Ser. Rozprawy*, No. 214 (1989).



ELSEVIER

Journal of Chromatography A, 693 (1995) 325-338

JOURNAL OF
CHROMATOGRAPHY A

Polycyclic aromatic sulfur heterocycles

IV. Determination of polycyclic aromatic compounds in a shale oil with the atomic emission detector[☆]

Jan T. Andersson*, Bernhard Schmid

Department of Analytical and Environmental Chemistry, University of Ulm, D-89069 Ulm, Germany

First received 16 August 1994; revised manuscript received 7 November 1994; accepted 10 November 1994

Abstract

A method for the determination of alkylated benzothiophenes and dibenzothiophenes, naphthothiophenes and several other aromatic compounds in a shale oil as an example for a very complex matrix is presented. Fluorinated aromatics were used as internal standards. The isolated aromatic fraction of the shale oil was separated according to the number of aromatic rings. Oxidation of the two-ring compounds led to benzothiophene sulfones which were further separated by liquid chromatography according to the number of side-chain carbon atoms. The three-ring compounds were separated into a sulfur aromatics-free and a sulfur aromatics-containing fraction using palladium chloride/silica gel. The GC stationary phases necessary for the quantification of all compounds of interest are discussed. Quantitative data obtained with an atomic emission detector are given for 22 compounds in the shale oil. Conventional quantification, without the elaborate separations described here, would overestimate the phenanthrene content of the shale oil by ca. 15% and that of dibenzothiophene by nearly 50%.

1. Introduction

One of the main forms of organic sulfur in fossil fuels and many of their industrial conversion products are the thiophenes. A large part of this sulfur is bound in polycyclic aromatic sulfur heterocycles (PASHs) which in oils mainly consist of alkylated benzothiophenes (BTs) and

dibenzothiophenes (DBTs) [1]. Lately an increasing interest in PASHs can be noticed for several reasons, e.g. their potential mutagenic/carcinogenic properties [2], the difficulty of desulfurizing them for the production of low-sulfur fuels [3], their photoreactions in the aqueous phase after oil spills [4], their microbial metabolism [5,6] and their potential as possible indicators for the maturity of crude oils and their source rocks [7,8].

The analysis of PASHs exhibits several problems. For example, there is no known generally satisfactory method of separating them from the polycyclic aromatic hydrocarbons (PAHs) [9]. Additionally, sulfur-selective detection in gas

* Corresponding author. Present address: University of Münster, Wilhelm-Klemm-Strasse 8, D-48149 Münster, Germany.

[☆] In part presented at the 18th International Symposium on Chromatography, Amsterdam, September 1990. Taken in part from the Ph.D. Thesis of B.S., University of Ulm, 1991.

chromatography (GC) was until recently essentially limited to flame photometric detection which shows severe drawbacks, particularly for quantifications. The advent of two new detection methods in the last years, sulfur chemiluminescence [10] and atomic emission detection (AED) [11,12] may change the situation, however. A remaining problem will always be the large number of isomers of alkylated PASHs [9] which necessitates complex work-up schemes.

In the present work we tried to find a way to realize the quantification of the C₁-substituted benzothiophenes and of all the four parent three-ring PASHs (DBT and the three naphthothiophene isomers). The alkylated derivatives are expected to provide information on e.g. the maturity and history of the oil, whereas a reliable determination of the naphthothiophenes is interesting not only in its own right but—as will be shown below—is *necessary* for an accurate quantification of DBT and phenanthrene. In the past, the coelution of naphtho[1,2-*b*]thiophene with DBT and that of naphtho[2,1-*b*]thiophene with phenanthrene on the common GC stationary phases has been ignored, by necessity therefore leading to false quantitative data for all those compounds when the coeluting compounds are present and, for the latter, a universal GC detector is used.

In this work we will demonstrate (a) that the selection of the proper GC stationary phase will permit the separation of the four C₁₂H₈S isomers (dibenzothiophene and the three naphthothiophenes) which is not possible on the columns most frequently used; (b) how a judiciously optimized work-up procedure will make it possible, for the first time, to quantitate all the six methylbenzothiophenes in a complex sample; (c) how the use of fluorinated internal standards can give reliable corrections for losses in the different work-up steps; and (d) how the selective and molar response of the atomic emission detector can be used to great advantage for the quantification of PASHs.

We have chosen a shale oil as sample because of its very complex aromatic pattern which is expected to readily expose the weaknesses of any analytical scheme.

2. Experimental

2.1. Chemicals and standards

All solvents used for the preparation of test or analyte solutions as well as those used for chromatographic purposes were of analytical-reagent grade. The 3-chloroperbenzoic acid was about 55% (Fluka, Germany). The same is true for the palladium chloride, used for preparation of the PdCl₂/silica material (60%, Fluka). PAH reference compounds were commercially available (Aldrich, Germany). PASH reference compounds, with the exception of benzothiophene and dibenzothiophene (Aldrich), were synthesized in our own laboratory or obtained from Astec (Münster, Germany). The following fluorinated PAH and PASH compounds were prepared using synthetic methods: 2-fluoronaphthalene, 3-fluorophenanthrene, 5-fluorobenzothiophene and 2-fluorodibenzothiophene. Additionally, octafluoronaphthalene (Fluka) was used as internal standard. An Austrian shale oil distillate (b.p. < 400°C) from Pertisau/Tirol was chosen as test matrix for the suitability of the work-up scheme.

2.2. Sample work-up

Column chromatography

Isolation of the aromatic fraction was achieved on 10 g aluminum oxide (ICN Alumina B-Super I) in an open glass column of about 1 cm diameter and 25 cm length. Prior to use, the aluminium oxide was stored at 160°C for at least 24 h. The aromatic fraction was eluted with 50 ml benzene after removal of the aliphatics with 25 ml hexane. Separation of three-ring sulfur heterocycles from other three-ring sample constituents was performed on 2 g PdCl₂/silica in a 10 × 0.5 cm glass column. To destroy the soluble palladium complexes of the PASHs, a small amount of aminopropyl silica was added at the end of each column [13]. PAHs were eluted with 70 ml hexane, followed by 60 ml trichloromethane for the PASHs. The PdCl₂/silica was prepared by stirring silica gel (230–400 mesh) in water together with 5% (w/w) of the PdCl₂

powder. After 10 min stirring, the water was removed at 80°C, the remaining material was sieved (100- μ m sieve) and stored at 200°C until use.

The two-ring PASHs were separated from the two-ring PAHs after oxidation with a few mg of 3-chloroperbenzoic acid (stirring the analyte solution in 10 ml dichloromethane with the peroxy-acid at room temperature for 1 h) by chromatography on 5 g aluminium oxide (same type as above) with 40 ml benzene for the elution of the PAHs, followed by 50 ml benzene–methanol (5:1) for the sulfones.

2.3. HPLC separations

All HPLC separations were performed on an HPLC Pump 64 (Knauer, Berlin, Germany), combined with either an Altex UV detector with fixed wavelength at 254 nm, or a Gynkotheke SP6 variable-wavelength UV detector. The latter was necessary for detection of the PASH sulfones at 230 nm. The separation of two- and three-ring compounds from the aromatic fraction was done by means of normal-phase HPLC on aminopropyl silica gel. We used a semipreparative 25 cm \times 2 cm column, containing Nucleosil 100-5 NH₂ material purchased from CS Chromatographie Service, Germany. Hexane (10 ml/min) was used as mobile phase. The separation of PASH sulfones according to the number of side-chain carbon atoms was achieved on a Sepralyte diphenyl column, 12 cm \times 0.8 cm (Analytichem/ICT) with methanol–water (1:1) as eluent (2 ml/min). After each work-up step, the sample volume was reduced to about 100 μ l under a gentle stream of nitrogen at room temperature. Reversed-phase HPLC fractions were extracted into dichloromethane, after dilution with water, before the volume was reduced and the fraction analyzed by GC.

2.4. GC separations

Instrumentation

A GC–AED system was mainly used for the GC investigations. It consisted of a gas chromatograph HP 5890 with automatic sampler

HP 7673A, combined with an HP 5921A atomic emission detector. The gas chromatograph was equipped with a splitless/split injection port. The system was controlled by the HP 5895A work station, using the HP 35920A software package.

Helium 4.6 was used as carrier and plasma gas, after further purification with an HP1-220 helium purifier from VICI Valco Instruments. Other auxiliary gases (hydrogen and oxygen) were used as required by the manufacturer depending on the element detected. Gas selection and detector tuning was computer controlled whereas the plasma gas flow-rate, essential for optimal sensitivity and peak shape in the sulfur trace, was set manually to about 60 ml/min [12].

Columns

The following fused-silica capillary columns were used.

Column 1: SB-Biphenyl-30, Lee Scientific, 25 m \times 0.32 mm, 0.25 μ m film.

Column 2: SP 2331 (100% cyanopropyl), Supelco, 60 m \times 0.32 mm, 0.2 μ m film.

Column 3: DB5, J & W Scientific, 30 m \times 0.25 mm, 0.25 μ m film.

Helium flow-rates were set to about 30 cm/s, samples were injected in the splitless/split mode with a purge delay time of 30 s. Chromatographic conditions are specified in the figures.

Evaluation

Quantitative data were calculated using several internal standards. Due to the linear and molar elemental response of AED [12], neither a correction factor for the different compounds of interest nor a calibration graph was necessary for evaluation. Analyte concentrations were simply calculated by the area ratios of analyte and internal standard (in the elemental traces) multiplied by the amount of internal standard related to C or S.

2.5. Peak numbering

Sulfur-containing compounds were numbered according to their elution order on SB-30-Bi-

phenyl (see Table 1). The PAH numbering is taken from Ref. [14].

3. Results and discussion

3.1. GC separations

First the GC properties of the compounds under study were investigated with reference compounds. Severe coelution is known to occur for many PASHs on the non-polar phases normally used for the separation of aromatics [9]. A biphenyl phase has been shown to provide a useful separation of the important C_1 -DBTs [15] but it does not allow the complete separation of the four-ring parent compounds. On screening several columns we discovered that the very polar cyanopropyl phase is capable of separating the four three-ring PASHs. The retention data on this and on the biphenyl phase are reported in Table 1 which thus complements and extends the data already reported for the C_1 - and C_2 -BTs on three other phases [9]. The retention indices in Table 1 are reported in two forms, depending on whether sulfur selective detection is used or not. The I_C scale is based on benzene, naphthalene, phenanthrene, chrysene and picene as the basis [16,17] and is used for universal detectors and the carbon-selective mode of AED. The I_S scale [9] is used for sulfur-selective detectors and is based on thiophene, BT, DBT and benzo[*b*]naphtho[2,1-*d*]thiophene as reference points.

The retention data listed in Table 1 show that on the non-polar (but polarizable) biphenyl phase the elution is quite similar to that on e.g. DB-5. The same coelutions are observed for C_1 -BTs (3- with 4- and 5- with 6-methylbenzothiophene) as on DB-5, resulting in four peaks for the six isomers. The C_2 -BTs also show considerable coelution problems. A better resolution is obtained for the methyl dibenzothiophenes which are resolved to an analytically useful degree, although no complete baseline separation is reached for 2- and 3-methyl dibenzothiophene. Coelution of dibenzothiophene with naphtho[1,2-*b*]thiophene and of anthracene

with naphtho[2,1-*b*]thiophene causes problems for the quantification of both PAH and PASH parent ring systems on this phase.

The cyanopropyl column has a fairly low upper thermal limit of 250°C and therefore does not allow the detection of four-ring aromatics during the temperature program. Consequently, retention indices over 300 cannot be calculated properly. Therefore, in Table 1, indices exceeding this value are given in parenthesis to indicate this deviation from theory and hence should be used with some caution; they are included here mainly in order to show the relative order of elution of the analytes on this phase.

This polar stationary phase discriminates better between PAHs and PASHs than the non-polar phases traditionally used. The introduction of a sulfur atom into the aromatic system of a terminal ring leads to a stronger retention on the cyanopropyl phase compared to other phases. On the biphenyl phase, BT elutes 2.3 index units after naphthalene and thieno[2,3-*b*]thiophene 2.5 units after BT. On the cyanopropyl phase, those differences increase to 7.6 and 7.0 units, respectively (Table 2). For the four three-ring PASHs (dibenzothiophene and the three naphthothiophenes), a similar albeit somewhat less pronounced effect is obtained. Thus their I_C indices change from 295.35, 295.68, 300.94 and 306.29 on biphenyl to 295.45, 297.22, 305.65 and 310.63 on cyanopropyl. Significantly, dibenzothiophene, with an internal thiophenic ring, displays the same index on both phases but the naphthothiophenes, which possess a terminal thiophenic ring, are more strongly retained. As a result, on the cyanopropyl phase, the four three-ring PASHs can be separated from each other and from other interferences and therefore, for the first time, can be quantified individually. In very complex samples however, problems may occur due to the strong retention of the naphthothiophenes and a possible interference from C_1 -dibenzothiophenes and/or C_1 -naphtho[1,2-*b*]thiophenes might be noticed.

The data in Table 1 make it obvious that the polar phase separates the analytes not only according to boiling points but that electronic effects also play a role. The degree of methyl-

Table 1
Retention indices of two- and three-ring sulfur heterocycles on three different stationary phases

No.	Compound	SB-30-Biphenyl		SP-2331		DB-5 I_C
		I_C	I_S	I_C	I_S	
1	Benzothiophene	202.29	200.00	207.59	200.00	201.88
2	Thieno[2,3- <i>b</i>]thiophene	204.83	202.67	214.05	207.33	202.73
3	Thieno[3,2- <i>b</i>]thiophene	205.81	203.78	215.68	209.19	203.92
4	7-Methylbenzothiophene	217.19	216.00	212.98	206.12	
5	2-Methylbenzothiophene	218.46	217.38	213.78	207.03	219.34
6	5-Methylbenzothiophene	220.71	219.79	217.50	211.25	
7	6-Methylbenzothiophene	220.75	219.83	217.50	211.25	
8	3-Methylbenzothiophene	221.86	221.03	219.09	213.06	
9	4-Methylbenzothiophene	222.07	221.25	219.48	213.51	
10	7-Ethylbenzothiophene	230.92	230.79			
11	2-Ethylbenzothiophene	233.06	233.09			
12	2,7-Dimethylbenzothiophene	233.25	233.27	219.32	213.32	
14	6-Ethylbenzothiophene	234.84	235.01			
15	5-Ethylbenzothiophene	234.87	235.04			
16	5,7-Dimethylbenzothiophene	235.72	235.92	224.71	217.34	
17	2,6-Dimethylbenzothiophene	236.13	236.37	223.85	218.46	
18	2,5-Dimethylbenzothiophene	236.36	236.61			
19	3,7-Dimethylbenzothiophene	236.45	236.70	224.29	218.96	
21	2,4-Dimethylbenzothiophene	237.41	237.73	226.68	221.68	
22	4,7-Dimethylbenzothiophene	237.53	237.87	224.71	219.44	
23	3,5-Dimethylbenzothiophene	239.71	240.21	229.76	225.18	
24	3,6-Dimethylbenzothiophene	239.89	240.45	230.04	225.50	
25	4,6-Dimethylbenzothiophene	240.17	240.71	229.40	224.78	
26	2,3-Dimethylbenzothiophene	240.43	240.99	228.87	224.16	
28	6,7-Dimethylbenzothiophene	241.28	241.89	231.02	226.60	
29	5,6-Dimethylbenzothiophene	244.77	245.65	236.36	232.67	
30	4,5-Dimethylbenzothiophene	245.96	246.93	238.01	234.55	
31	3,4-Dimethylbenzothiophene	248.90	250.15	241.50	238.55	
36	Benzo[<i>b</i>]thieno[2,3- <i>d</i>]thiophene	293.21	297.70	295.40	299.73	293.28
39	Dibenzothiophene	295.35	300.00	295.45	300.00	295.35
40	Naphtho[1,2- <i>b</i>]thiophene	295.68	300.40	297.22	(301.88)	295.01
41	Benzo[<i>b</i>]thieno[3,2- <i>d</i>]thiophene	296.02	300.81	(300.43)	(305.22)	295.51
42	[1,2- <i>b</i> ;3,4- <i>b'</i>]Dithienobenzene	297.22	302.27	(304.05)	(308.65)	301.35
43	Naphtho[2,1- <i>b</i>]thiophene	300.94	306.65	(305.65)	(310.16)	300.00
44	[1,2- <i>b</i> ;4,3- <i>b'</i>]Dithienobenzene	303.16	312.22	(312.82)	(316.94)	301.35
45	Naphtho[2,3- <i>b</i>]thiophene	306.29	312.36	(310.63)	(314.86)	303.78
46	4-Methyldibenzothiophene	309.24	315.52	(297.87)	(302.56)	
47	2-Methyldibenzothiophene	213.13	318.60	(303.66)	(308.28)	316.25
48	3-Methyldibenzothiophene	312.94	319.46	(304.46)	(309.03)	
49	1-Methyldibenzothiophene	317.00	323.80	(307.30)	(311.72)	
50	4-Ethyldibenzothiophene	321.09	328.34			
51	4,6-Dimethyldibenzothiophene	323.34	330.74			
52	2-Ethyldibenzothiophene	324.26	331.72			
53	3,6-Dimethyldibenzothiophene	326.79	334.42			
55	2,8-Dimethyldibenzothiophene	326.43	336.16	(313.25)	(317.34)	
56	3,8-Dimethyldibenzothiophene	329.33	337.12	(314.24)	(318.28)	
57	3,4-Dimethyldibenzothiophene	333.12	341.16	(316.24)	(320.17)	
58	1,9-Dimethyldibenzothiophene	334.22	342.33			
59	2,3-Dimethyldibenzothiophene	335.80	344.01	(322.45)	(326.03)	

(Continued on p. 330)

Table 1 (continued)

No.	Compound	SB-30-Biphenyl		SP-2331		DB-5 I_C
		I_C	I_S	I_C	I_S	
62	Phenanthro[4,5- <i>bcd</i>]thiophene	350.38	359.56			
63	Benzo[<i>b</i>]indeno[1,2- <i>d</i>]thiophene	364.33	374.42			
65	Benzo[<i>b</i>]phenanthro[4,5- <i>bcd</i>]thiophene	373.26	383.93			
66	Benzo[<i>b</i>]naphtho[2,1- <i>d</i>]thiophene	388.35	400.00			
67	Benzo[<i>b</i>]naphtho[2,3- <i>d</i>]thiophene	395.53	(407.67)			
68	Phenanthro[3,4- <i>b</i>]thiophene	396.96	(409.18)			
69	Phenanthro[2,1- <i>b</i>]thiophene	(402.05)	(414.61)			

tion seems to be less important than for the non-polar phase. Thus the earliest-eluting dimethyl-BT elutes faster than the last-eluting monomethyl-BT; in contrast, on the biphenyl phase, a difference of no less than 11 retention index units exists between the same two compounds. As on other phases, the six C_1 -BTs show four peaks so that this phase cannot be used for the analysis of the C_1 -BTs; however, the four C_1 -DBTs are resolved.

3.2. Work-up and separation of PAHs and PASHs

For complex samples such as crude oils, the aromatic fraction is preferentially isolated through adsorption chromatography on alumina or mixtures of alumina and silica gel. The aliphatic compounds are eluted in a first fraction typically with hexane as eluent, and in a second fraction the polycyclic aromatic compounds (PACs) are obtained with a more polar eluent, e.g. toluene. Despite the high selectivity of AED

for sulfur over carbon the large number of alkylated PASHs generally present in such oils makes this aromatic fraction too complex for direct quantification of many compounds.

Traditionally two principally different schemes are used for the further separation of PAHs and PASHs. Oxidation of the sulfur functionality to a sulfone, followed by adsorption chromatographic separation of the polar sulfones from the non-polar unreacted PAHs, is one possibility. Favored oxidant is *meta*-chloroperbenzoic acid (MCPBA), whereas hydrogen peroxide was recently reported as being completely unsuitable [9]. A major drawback of the oxidation approach is the fact that with the exception of BTs and some of its alkyl derivatives, PASHs containing terminal thiophene rings are largely lost, probably through oxidation of other molecular features. Thus the naphthothiophenes cannot be analyzed after oxidation with MCPBA.

The second separation process involves liquid chromatography on palladium chloride deposited on silica gel [18]. In this work we used a small

Table 2
Influence of an aromatic sulfur atom on the retention behavior of some PACs

Column	I_C naphthalene	Increment	I_C benzothiophene	Increment	I_C thieno[2,3- <i>b</i>]- thiophene	Increment	I_C thieno[3,2- <i>b</i>]- thiophene
DB-5	200.00	1.88	201.88	0.85	202.73	1.19	203.92
SB-30- Biphenyl	200.00	2.29	202.29	2.54	204.83	0.98	205.81
SP-2331	200.00	7.59	207.59	6.46	214.05	1.63	215.68

amount of aminopropyl silica to destroy the soluble complexes between palladium and the sulfur aromatics [13]. Problematic is the fact that PASHs with terminal thiophenic rings seem to elute much faster than those with an internal ring, thus being collected in the PAH fraction [13]. The naphthothiophenes can only be collected with the dibenzothiophenes if the cut between PAHs and PASHs is done very accurately; PAHs with more than three rings must not be present since they are somewhat more strongly retained and could elute with the sulfur heterocycles.

In order to make possible the quantification of a large number of PASHs, we decided on the following somewhat elaborate work-up procedure which is a combination of the two principles just discussed and which enabled us to use the mild $\text{PdCl}_2/\text{silica}$ separation also for the naphthothiophenes.

As a first step, the aromatic fraction of the shale oil was separated on an aminopropyl HPLC phase resulting in a two-ring and a three-ring fraction. In the following step the second (three-ring) fraction was subjected to a separation on $\text{PdCl}_2/\text{silica}$. The first one (two-ring fraction) was oxidized with MCPBA (we were unable to get satisfactory results with the suggested replacement for MCPBA, the magnesium salt of monoperoxyperphthalic acid [19]) and the resulting two-ring PASH sulfones (PASHO_2) were separated from the unchanged PAHs on silica. An overview of the complete work-up scheme is presented in Fig. 1.

3.3. Fluoroaromatics as internal standards

Since all sample manipulations are associated with losses of analytes, internal standards (ISs) are preferentially added to the sample before work-up. In PAC work, essentially with mass spectrometric methods, deuterated aromatics have long been used for this purpose [20–22]. We have recently shown [23,24] that fluorinated PACs offer several advantages and thus they were tested here for their suitability for the analysis of PASHs.

Selected as ISs for the two-ring PAHs were

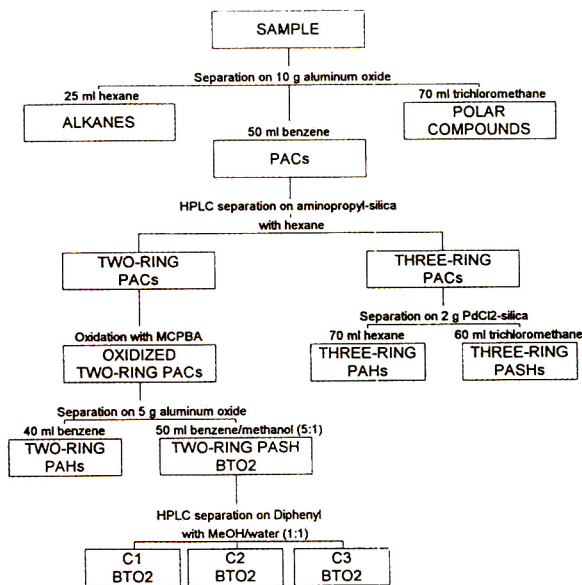


Fig. 1. Flow chart for the separation of two- and three-ring PACs from complex matrices.

2-fluoronaphthalene and octafluoronaphthalene; for the three-ring PAHs, 3-fluorophenanthrene was chosen. The benzothiophenes were quantified using 5-fluorobenzothiophene whereas 2-fluorodibenzothiophene was found to be suitable for the three-ring PASHs. Those fluoro derivatives were chosen because they are well separated from other sample constituents which typically occur in complex oil samples and because they show suitable elution characteristics in the several separation steps of the sample work-up (Fig. 2).

In order to establish the viability of the proposed separation scheme and the use of the internal standards mentioned, a test solution was made up of four benzothiophenes, six three-ring PASHs and six PAHs together with a fluorinated derivative of each of the four parent compounds studied here (BT, DBT, naphthalene, phenanthrene). The test solution was taken through all the steps described above and quantified following each of them. The relative amounts of recovered analytes present after each work-up step, based on a comparison with the fluorinated ISs, are summarized in Fig. 2. It is obvious that

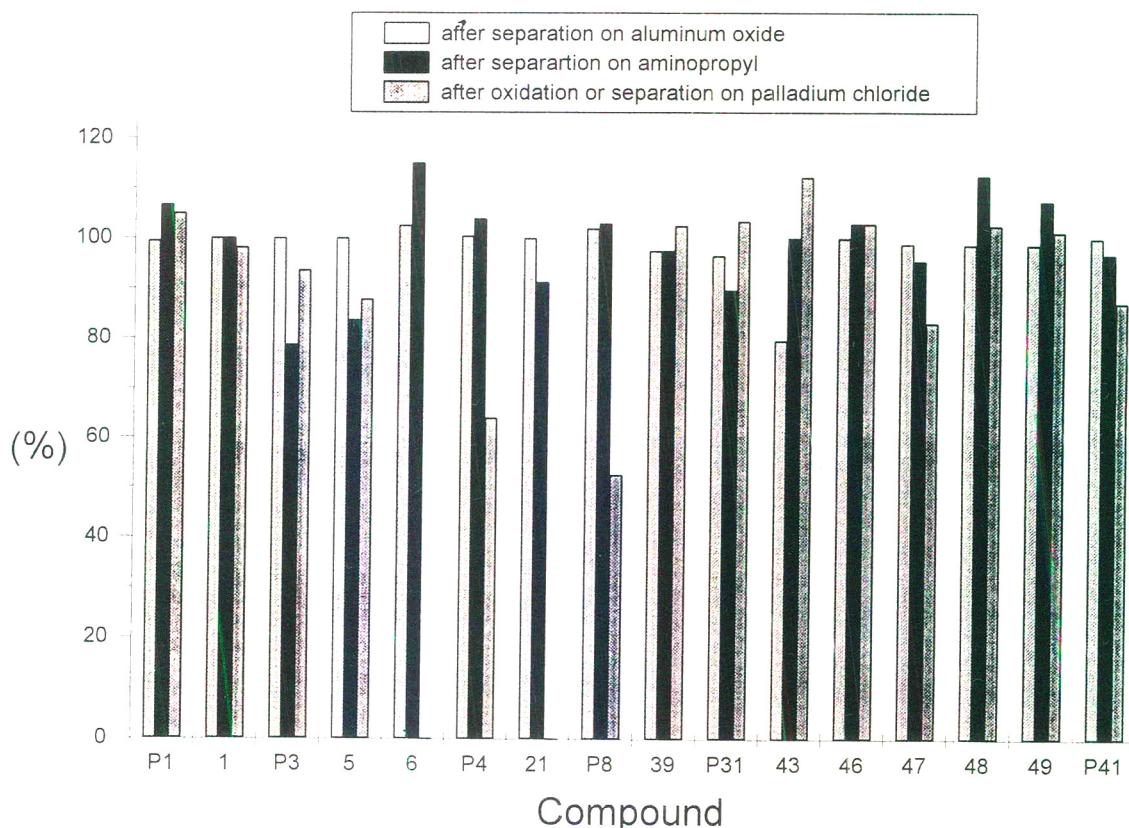


Fig. 2. Recovery of the PACs in the test mixture after each of the several clean-up steps; starting amount = 100%. Compounds: P1 = naphthalene; P3 = 2-methylnaphthalene; P4 = 1-methylnaphthalene; P8 = 2,3-dimethylnaphthalene; P31 = phenanthrene; P41 = 1-methylphenanthrene; 1 = benzothiophene; 5 = 2-methylbenzothiophene; 6 = 5-methylbenzothiophene; 21 = 2,4-dimethylbenzothiophene; 39 = dibenzothiophene; 43 = naphtho[2,1-*b*]thiophene; 46 = 4-methyldibenzothiophene; 47 = 2-methyldibenzothiophene; 48 = 3-methyldibenzothiophene; 49 = 1-methyldibenzothiophene.

most analytes show excellent quantitative data even after several work-up steps and, for the BTs, a chemical reaction.

As demonstrated by the data in Fig. 2, the chromatographic steps on alumina and aminopropyl silica lead to no serious selective losses of any of the compounds. The separation of the PASHs from the PAHs is more problematic. Although the oxidation with MCPBA does not seem to change the pattern of the BTs, considerable losses are recorded for some PAHs, notably 1-methyl- (P4) and 2,3-dimethylnaphthalene (P8). This is in line with the susceptibility of these compounds to oxidation with hydrogen peroxide [9] and stresses that the oxidation of

interfering PASHs in order to remove them for an interference-free determination of PAHs, a fairly common practice, should be avoided. Several large new peaks were detected in the carbon-selective trace as products of PAH oxidation; they were not further characterized (Fig 3).

The losses after chromatography on PdCl₂/silica are less severe. Only 2-methyl-DBT deviates slightly from the other compounds, the cause probably being the very strong retention of this compound on PdCl₂/silica [13], which necessitates a large volume of solvent to wash it quantitatively out of the column. The strong retention of 2-methyl-DBT is further increased by the thermal pretreatment of the PdCl₂/silica

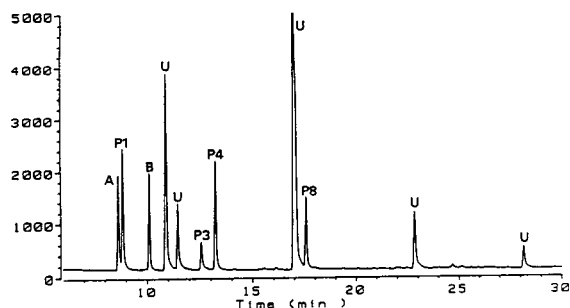


Fig. 3. GC-AED chromatogram of the two-ring PAH fraction obtained from the test mixture after oxidation with 3-chloroperbenzoic acid and LC separation on aluminum oxide, on the SB-30-Biphenyl column. $T_{\text{oven}} = 80^{\circ}\text{C}$ (2 min), then $4^{\circ}\text{C}/\text{min}$ to 280°C . Carbon-selective mode. Peaks: A = 2-fluoronaphthalene; B = octafluoronaphthalene; U = unknown oxidation product; other peaks as in Fig. 2.

(see Experimental), which is necessary for the complete elution of the naphthothiophenes in the PASH fraction. The marginally higher recoveries for several three-ring analytes may be due to the fact that the internal standard used (2-F-DBT) is somewhat more volatile than the analytes and therefore shows slightly higher losses on reduction of the volume of the solution (under a gentle stream of nitrogen) after the last separation.

This initial experiment thus shows that it should be possible to quantify PASHs after several work-up steps, using fluorinated ISs, with very good (relative) recovery, independent of the method used for separating PAHs and PASHs.

3.4. Analysis of shale oil

The distillate of an Austrian shale oil boiling below 400°C was used for the following investigation. The aromatics were isolated through column chromatography on alumina after addition of the same fluorinated IS as were used above. The carbon and sulfur selective traces were recorded using GC-AED (Fig. 4). It is obvious that the complexity of the sample is so high that despite the use of sulfur-selective detection, only BT, 2- and 7-MeBT can be quantified without further work-up.

The HPLC fractionation on aminopropyl led

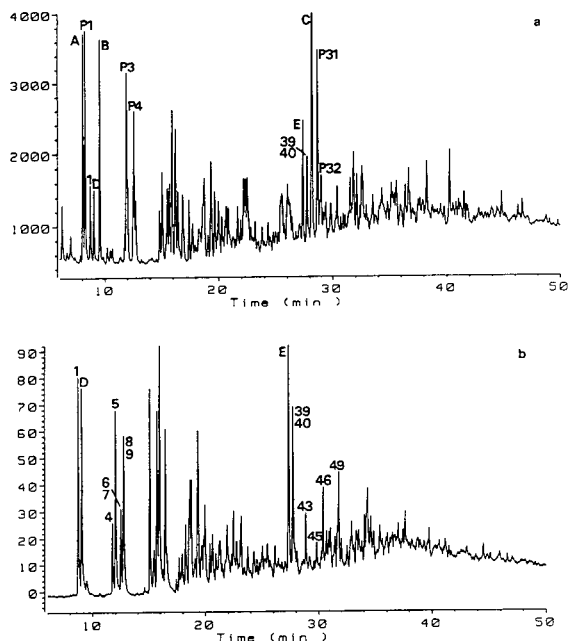


Fig. 4. GC-AED chromatogram of the aromatic fraction obtained from the Austrian shale oil after LC separation on aluminum oxide, on the SB-30-Biphenyl column. $T_{\text{oven}} = 80^{\circ}\text{C}$ (2 min), then $4^{\circ}\text{C}/\text{min}$ to 280°C (15 min). (a) Carbon-selective mode, (b) sulfur-selective mode. Peaks: A = 2-fluoronaphthalene; B = octafluoronaphthalene; C = 3-fluorophenanthrene; D = 5-fluorobenzothiophene; E = 2-fluorodibenzothiophene; P1 = naphthalene; P3 = 2-methylnaphthalene; P4 = 1-methylnaphthalene; P31 = phenanthrene; P32 = anthracene; 1 = benzothiophene; 4 = 7-methylbenzothiophene; 5 = 2-methylbenzothiophene; 6 = 5-methylbenzothiophene; 7 = 6-methylbenzothiophene; 8 = 3-methylbenzothiophene; 9 = 4-methylbenzothiophene; 39 = dibenzothiophene; 40 = naphtho[1,2-*b*]thiophene; 43 = naphtho[2,1-*b*]thiophene; 45 = naphtho[2,3-*b*]thiophene; 46 = 4-methyldibenzothiophene; 49 = 1-methyldibenzothiophene.

to a two-ring and a three-ring fraction. The corresponding gas chromatograms are depicted in Fig. 5.

Even with this fractionation no further two-ring compounds could be reliably quantified. Note the overlap of MeBTs with methylnaphthalenes in the carbon-selective trace which makes a determination of the latter impossible under those conditions. In the three-ring chromatograms (Fig. 5c and d), possibly phenanthrene (C) could be quantified without interfer-

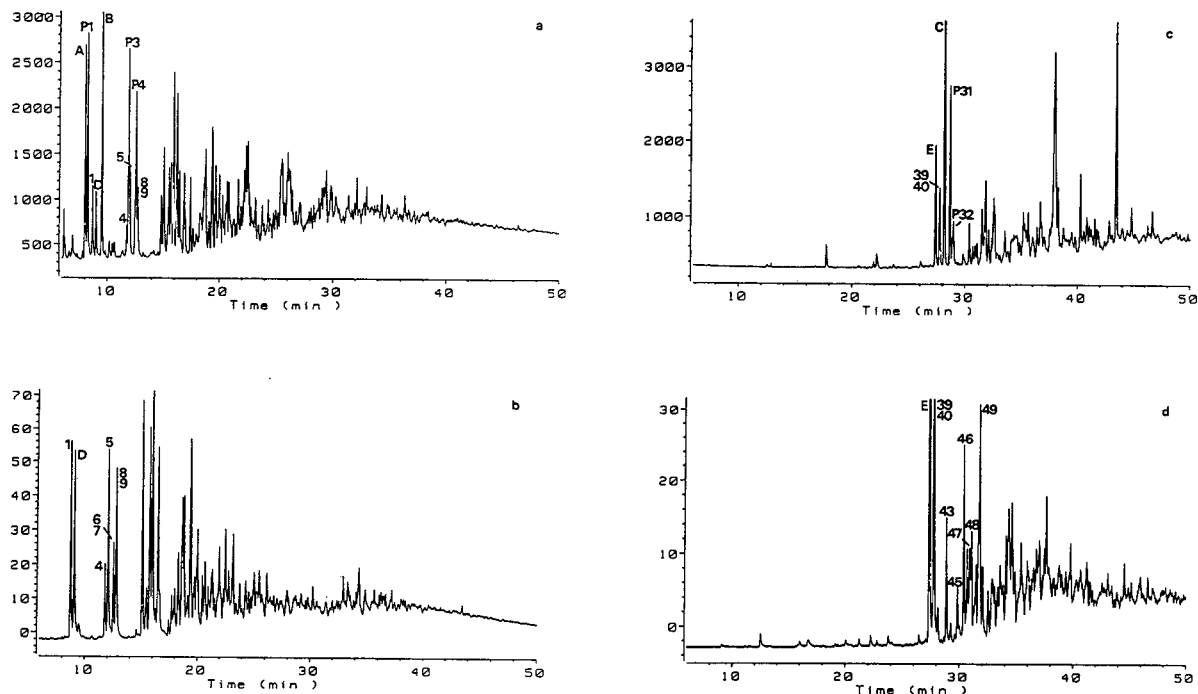


Fig. 5. GC-AED chromatograms of the two-ring PAC and three-ring PAC fraction obtained from the aromatic fraction of an Austrian shale oil after HPLC separation on an aminopropyl column, on the SB-30-Biphenyl column. $T_{\text{oven}} = 80^{\circ}\text{C}$ (2 min), the $4^{\circ}\text{C}/\text{min}$ to 280°C (15 min). (a) Two-ring fraction in the carbon-selective mode, (b) two-ring fraction in the sulfur-selective mode, (c) three-ring fraction in the carbon-selective mode, (d) three-ring fraction in the sulfur-selective mode. Peaks: 47 = 2-methyldibenzothiophene; 48 = 3-methyldibenzothiophene; other peaks as in Fig. 4.

ences. Other parent compounds, for example DBT, naphtho[2,1-*b*]thiophene and anthracene, cannot be determined due to the coelution problems noted above. Likewise the alkylated derivatives are too numerous to be sufficiently resolved, in the carbon- as well as the sulfur-selective trace. Consequently further separations become necessary.

3.5. Two-ring PASHs

The oxidation of the two-ring fraction with MCPBA was performed in the usual way but instead of the traditional liquid-liquid separation of the spent reagent and the products, which is followed by an open column separation of oxidized and non-oxidized compounds, we developed a more convenient and faster procedure combining these two steps into one using chromatog-

raphy of the crude product solution (see Experimental). Although sulfones of PASHs can advantageously be analyzed by GC [9], the oxidized fraction obtained here cannot be used directly. The numerous sulfones do not elute according to the number of carbon atoms in the side chains as do the parent aromatics, thus resulting in serious coelution problems (Fig. 6a). One example among many may be the sulfones of 5-methyl-BT and 2,4-dimethyl-BT which co-elute on non-polar phases although the parent compounds are separated by about 17 retention index units. A mass-selective detector will of course solve this problem since the masses for compounds of different degrees of alkylation can be selectively monitored.

If such a detector is not available, a final separation becomes necessary. An LC step was chosen here. On an octadecyl phase an un-

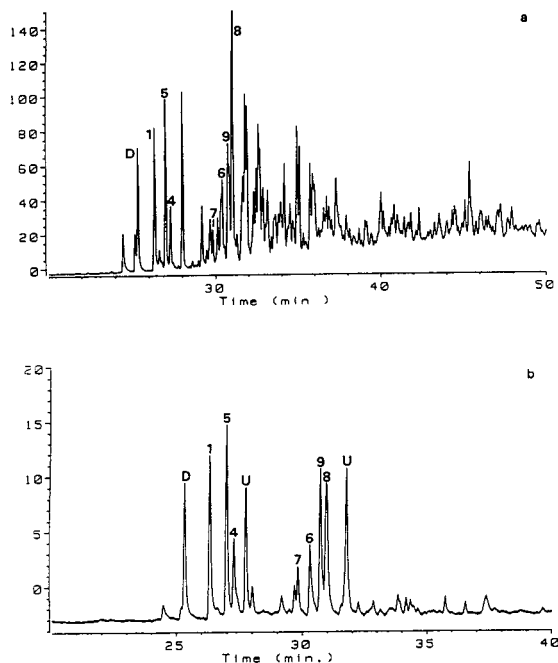


Fig. 6. GC-AED chromatogram of the oxidized PASH fraction obtained from an Austrian shale oil after several separation steps on an SB-30-Biphenyl column (sulfur-selective mode). $T_{oven} = 80^{\circ}\text{C}$ (2 min), then $4^{\circ}\text{C}/\text{min}$ to 280°C . (a) Oxidized two-ring fraction prior to separation on Sepsalyte Diphenyl, (b) first fraction of the Sepsalyte Diphenyl separation (see Fig. 7). Peaks: see Fig. 4 (all compounds as sulfones).

wanted resolution of individual sulfones is obtained, whereas a diphenyl stationary phase provided exactly the desired separation according to the number of side-chain carbon atoms (Fig. 7). The $\text{C}_1\text{-BTO}_2$ eluate, marked in Fig. 7, was collected; the corresponding gas chromatogram is reproduced in Fig. 6b and shows complete resolution of all the $\text{C}_1\text{-BTO}_2$ s although some minor interfering peaks can be seen in the chromatogram. To our knowledge this is the first time that all the six monomethyl-BTs can be quantified simultaneously.

Although it was not done here, it is conceivable to analyze the $\text{C}_2\text{-BT}$, $\text{C}_3\text{-BT}$, $\text{C}_4\text{-BT}$ etc fractions in the same way. A separate internal standard would be needed for each value of x in $\text{C}_x\text{-BT}$. If only the $\text{C}_1\text{-BT}$ ($\text{C}_2\text{-BT}$, etc.) pattern is of interest in a particular sample, there is no

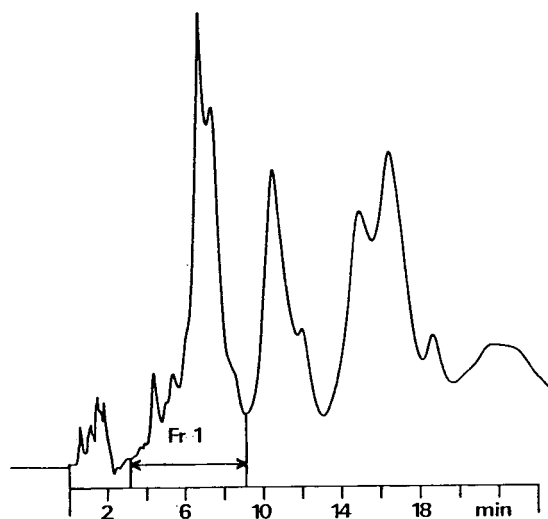


Fig. 7. HPLC chromatogram of the oxidized two-ring PASH fraction obtained from the two-ring fraction of an Austrian shale oil after oxidation with 3-chloroperbenzoic acid, on a Sepsalyte Diphenyl column. Flow-rate: 2 ml/min methanol-water (1:1), detection at 230 nm. Fr 1 = First fraction, containing the monomethylbenzothiophene sulfones.

need to perform the separation according to the number of aromatic rings on aminopropyl silica. The whole aromatic fraction can be reacted with MCPBA and the oxidized products fractionated on diphenylsilica as described here. A quantification of three-ring PACs is, however, only possible after this separation step.

3.6. Three-ring PASHs

Following separation on $\text{PdCl}_2/\text{silica}$ (see Experimental), the resulting PAH and PASH fractions were analyzed on the biphenyl column using GC-AED (Fig. 8). A comparison of the carbon trace in Fig. 8a with that of Fig. 5 demonstrates the complete separation of PAH and PASH. Since the naphthothiophenes have now been successfully separated from the PAHs, phenanthrene, anthracene and some methylphenanthrenes can be quantified reliably (i.e., no coelution with PASHs).

The quantification of the unsubstituted sulfur heterocycles was somewhat more complicated.

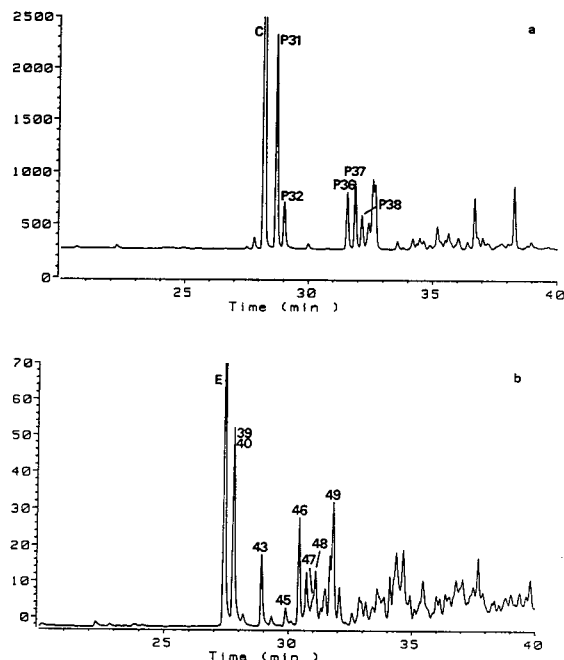


Fig. 8. GC-AED chromatograms of the three-ring PAC fraction obtained from an Austrian shale oil after separation on palladium chloride/silica, on SB-30-Biphenyl. $T_{oven} = 80^{\circ}\text{C}$ (2 min), then $4^{\circ}\text{C}/\text{min}$ to 280°C . (a) Three-ring PAH fraction in the carbon-selective mode, (b) three-ring PASHs in the sulfur-selective mode. Peaks: P36 = 3-methylphenanthrene; P37 = 2-methylphenanthrene; P38 = 2-methylanthracene; other peaks as in Figs. 4 and 5.

Dibenzothiophene and naphtho[1,2-*b*]thiophene were quantified on the cyanopropyl column (Fig. 9), since they coelute on the biphenyl phase. The other two isomers of naphthothiophene were not resolved from alkylated PASHs on cyanopropyl and had thus to be quantified on the biphenyl phase (Fig. 8b). Again, the use of a mass-selective detector in combination with the cyanopropyl column would obviate the use of two different columns for this quantification. In this sample the concentration of the methyl-naphthothiophenes is so high that, due to the coelution, it is impossible to quantify the methyl-dibenzothiophenes with any degree of accuracy. A mass-selective detector would bring no benefit since all these compounds are isomers and show identical mass spectra.

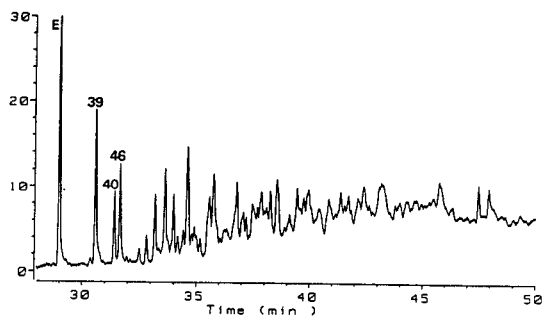


Fig. 9. GC-AED chromatogram of the three-ring PASH fraction obtained from an Austrian shale oil after several separation steps, on a SP 2331 cyanopropyl column in the sulfur-selective mode. $T_{oven} = 90^{\circ}\text{C}$ (3 min), then $10^{\circ}\text{C}/\text{min}$ to 160°C , then $2^{\circ}\text{C}/\text{min}$ to 230°C , then $10^{\circ}\text{C}/\text{min}$ to 250°C (10 min). Peaks as in Fig. 4.

The quantitative data for all compounds determined in this shale oil are collected in Table 3.

Table 3
Quantitative data for some of the aromatic compounds in the Austrian shale oil

Compound	Concentration ($\mu\text{g}/\text{g}$)
Naphthalene	2600
2-Methylnaphthalene	(2003) ^a
1-Methylnaphthalene	(1857) ^a
Phenanthrene	1030
Anthracene	415
3-Methylphenanthrene	363
2-Methylphenanthrene	377
Benzothiophene	768
7-Methylbenzothiophene	405
2-Methylbenzothiophene	974
5-Methylbenzothiophene	341
6-Methylbenzothiophene	197
3-Methylbenzothiophene	515
4-Methylbenzothiophene	662
Dibenzothiophene	445
Naphtho[1,2- <i>b</i>]thiophene	204
Naphtho[2,1- <i>b</i>]thiophene	183
Naphtho[2,3- <i>b</i>]thiophene	65
4-Methyldibenzothiophene	(255) ^a
2-Methyldibenzothiophene	(123) ^a
3-Methyldibenzothiophene	(124) ^a
1-Methyldibenzothiophene	(274) ^a

^a Only semiquantitative values.

4. Conclusions

The shale oil used in this work is extremely rich in alkylated two- and three-ring polycyclic aromatic compounds, making the task of determining individual aromatic sulfur heterocycles a great challenge indeed.

A separation according to the number of aromatic rings was necessary, partly because some highly alkylated benzothiophenes elute with similar retention times as the three-ring compounds on gas chromatographic analysis, and partly because on oxidation with MCPBA, especially the naphthothiophenes are lost and escape quantification.

The oxidation of the two-ring fraction was necessary not for the separation of the benzothiophenes from the naphthalenes, since these compounds could in principle be determined with the sulfur-selective detector but for the excellent GC resolution obtained for the BT sulfones on practically any standard GC phase. It should be stressed again that the non-oxidized BTs coelute to a very much larger extent than the sulfones.

The oxidation also permitted the naphthalenes to be collected as an individual fraction free of interfering sulfur heterocycles. However, several naphthalenes are attacked by MCPBA and show considerable losses. The determination of alkylated naphthalenes in a sample with such high concentrations of C_x-BTs would probably best be done with a mass-selective detector (without oxidation).

The separation on PdCl₂/silica is necessary for the quantification of phenanthrenes and anthracenes; the sulfur heterocycles can in principle be determined using a sulfur-selective detector since there are GC phases available which allow their separation. Here it should be repeated that a universal detector like the flame ionization detector will produce wrong results for phenanthrene (if naphtho[2,1-*b*]thiophene is present) on the so frequently used methyl silicone phases. In the shale oil phenanthrene would be overestimated by ca. 15%. The quantification of dibenzothiophene will likewise be erroneous, here by nearly 50%, because of coelution with

naphtho[1,2-*b*]thiophene unless a phase such as cyanopropyl is used.

Despite a certain complexity, the scheme presented here allows the determination of a relatively large number of PASHs, which have so far not been accessible, and of phenanthrene. The use of fluorinated internal standards was of considerable use, and in future work their role will be expanded since a standard can easily be synthesized for use with each subfraction of interest.

Acknowledgements

Hewlett-Packard, Germany, is thanked for lending us the AED system, and Professor K. Ballschmiter for his kind support.

References

- [1] R.L. Martin and J.A. Grant, *Anal. Chem.*, 37 (1965) 644.
- [2] J. Jacob, *Sulfur Analogues of Polycyclic Aromatic Hydrocarbons (Thiaarenes)*, Cambridge Univ. Press, Cambridge, 1990, p. 70.
- [3] A. Attar and F. Dupuis, *Adv. Chem. Ser.*, 192 (1981) 239.
- [4] J.T. Andersson and S. Bobinger, *Chemosphere*, 24 (1992) 383.
- [5] S. Saftic, P.M. Fedorak and J.T. Andersson, *Environ. Sci. Technol.*, 26 (1992) 1759.
- [6] S. Saftic, P.M. Fedorak and J.T. Andersson, *Environ. Sci. Technol.*, 27 (1993) 2577.
- [7] W.B. Hughes, in J.G. Polacas (Editor), *Petroleum Geochemistry and Source Rock Potential of Carbonate Rocks*, AAPG, Tulsa, 1984, p. 181.
- [8] H. Budzinski, P. Garrigues, J. Connan and J. Belloq, in P. Garrigues and M. Lamotte (Editors), *Polycyclic Aromatic Compounds —Synthesis, Properties, Analytical Measurements, Occurrence, and Biological Effects; PAH XIII*, Gordon & Breach, London, 1993, pp. 611–620.
- [9] J.T. Andersson, *Int. J. Environ. Anal. Chem.*, 48 (1991) 1.
- [10] S.E. Eckert-Tilotta, S.B. Hawthorne and D.J. Miller, *J. Chromatogr.*, 591 (1992) 313.
- [11] B.D. Quimby and J.J. Sullivan, *Anal. Chem.*, 62 (1990) 1027.
- [12] J.T. Andersson and B. Schmid, *Fresenius' J. Anal. Chem.*, 346 (1993) 403.
- [13] J.T. Andersson, *Anal. Chem.*, 59 (1987) 2207.

- [14] M. Nishioka, H.C. Chang and M.L. Lee, *Environ Sci. Technol.*, 20 (1986) 1023.
- [15] M. Nishioka, J.S. Bradshaw and M.L. Lee, *Anal. Chem.*, 57 (1985) 309.
- [16] J.T. Andersson, *J. Chromatogr.*, 354 (1986) 83.
- [17] D.L. Vassilaros, R.C. Kong, D.W. Later and M.L. Lee, *J. Chromatogr.*, 252 (1982) 1.
- [18] M. Nishioka, R.M. Campell, M.L. Lee and R.N. Castle, *Fuel*, 65 (1986) 270.
- [19] G. van Zyl and R.A. Koster, *J. Org. Chem.*, 29 (1964) 3558.
- [20] S.A. Wise, L.R. Hilpert, R.E. Rebbert, L.C. Sander, M.M. Schantz, S.N. Chesler and W.E. May, *Fresenius' Z. Anal. Chem.*, 332 (1988) 573.
- [21] K. Speer, P. Horstmann, T. Kühn and A. Montag, *J. High Resolut. Chromatogr.*, 13 (1990) 104.
- [22] N.D. Bedding, A.E. McIntyre, J.N. Lester and R. Perry, *J. Chromatogr. Sci.*, 26 (1988) 605.
- [23] J.T. Andersson and U. Weis, in P. Garriues and M. Lamotte (Editors), *Polycyclic Aromatic Compounds—Synthesis, Properties, Analytical Measurements, Occurrence, and Biological Effects; PAH XIII*, Gordon & Breach, London, 1993, p. 85.
- [24] J.T. Andersson and U. Weis, *J. Chromatogr. A.*, 659 (1969) 151.

Solid-phase extraction on C₁₈ in the trace determination of selected polychlorinated biphenyls in milk

Y. Picó*, M.J. Redondo, G. Font, J. Mañes

Laboratori de Toxicologia, Facultat de Farmàcia, Universitat de València, Av. Vicent Andres Estelles s/n, 46100 Burjassot, València, Spain

First received 9 June 1994; revised manuscript received 10 October 1994; accepted 10 October 1994

Abstract

The utility of solid-phase extraction with octadecylsilica for determining fifteen polychlorinated biphenyl (PCB) congeners from milk samples was examined. Recoveries higher than 80% and relative standard deviations better than 10% were obtained for PCBs from different kinds of milk (whole, skimmed, 2%, powdered, breast and evaporated). A comparison with other procedures was made. The described method provides better detection limits than those attainable with the liquid–liquid extractions currently used as standard methods, when capillary gas–liquid chromatography is used for the final determination. A study of the separation was also performed using six different fused-silica capillary columns and an electron-capture detector.

1. Introduction

Different solid-phase extraction (SPE) procedures for the determination of polychlorinated biphenyls (PCBs) based on adsorption chromatography using Florisil [1], anhydrous sodium sulphate [2], silica gel [3] or lipophilic gels [4] have been used. The advantage of the reversed-phase mode is that the amount of solid phase and organic solvent used and the analysis time are reduced. Octadecylsilica has been used to isolate PCBs in different matrices, such as water [5], fat [6] and blood and serum [7]. The procedure could be applied to milk samples, but the results obtained in previous studies demonstrate that the method must be optimized to obtain satisfactory recoveries of PCBs from whole milk

[8] and that the fat globules in milk must be disrupted [9].

The main objective of this study was therefore the application of the SPE procedure to the determination of PCBs in milk, previously proposed for the determination organochlorine pesticides [9], and to verify its applicability to different kinds of milk.

2. Experimental

2.1. Chemicals

Fifteen biphenyls, 2-PCB (Ballschmitter No. 1), 2,2'-PCB (No. 4), 2,4-PCB (No. 7), 4,4'-PCB (No. 15), 2,4,4'-PCB (No. 28), 2,4,5-PCB (No. 29), 2,2',5,5'-PCB (No. 52), 3,3',4,4'-PCB (No. 77), 2,2',4,5,5'-PCB (No. 101), 2,3',4,4',5,5'-PCB (No. 118), 2,2',3,4,4',5,5'-

* Corresponding author.

PCB (No. 138), 2,2',4,4',5,5'-PCB (No. 153), 2,2',3,3',4,4',5-PCB (No. 170), 2,2',3,4,4',5,5'-PCB (No. 180) and decachlorobiphenyl (No. 209) were chosen as model compounds. Analytical standards were purchased from Riedel-de Haën with a purity of 99%.

A certified standard of powdered milk (CRM 450) was supplied by the EEC Community Bureau of Reference (BCR).

n-Hexane and methanol were of pesticide grade. Solvents were shown to be free of interfering residues by GC with electron-capture detection following 200-fold concentration.

Potassium hydroxide solution (2 M in ethanol) was purchased from Merck (Darmstadt, Germany). To prepare chromic acid solution, 5 g of chromium(VI) oxide (Merck) were dissolved in 3 ml of water, and 60 ml of glacial acetic acid (Merck) were added.

Preparative octadecylsilica (55–105 μm) was obtained from Water-Millipore (Bedford, MA, USA).

2.2. Capillary gas chromatographic analysis

The gas chromatograph used for PCB isomers was a Konik 3000 equipped with a ^{63}Ni electron-capture detector and the following fused-silica columns: two Supelco BP-5 columns (25 \times 0.22 mm I.D. and 50 m \times 0.22 mm I.D., respectively); a Supelco BP-10 column (50 \times 0.22 mm I.D.); a J & W Scientific DB-17 column (30 \times 0.22 mm I.D.); a Scharlau OV-1701 column (25 \times 0.25 mm I.D.); and a Delta Scientific CP-cyclodextrin-B-2,3,6-M-19 column (30 m \times 0.25 mm I.D.). All of them had a film thickness of 0.25 μm .

The temperature programme for the columns with lengths between 25 and 30 m was 0.8 min at 50°C then increased at 30°C min^{-1} to 140°C, which was held for 2 min, then at 5°C min^{-1} to 280°C, the final temperature being held for 10 min. The temperature programme for the columns with a 50-m length was 0.8 min at 50°C then increased at 30°C min^{-1} to 200°C, which was held for 2 min, then at 2°C min^{-1} to 260°C. The final temperature was held for 8 min.

The injector and detector temperatures were

285 and 300°C, respectively. Helium was used as the carrier gas at a flow-rate of 1 ml min^{-1} . A sample volume of 3 μl was injected in the splitless mode and the splitter was opened after 0.7 min.

2.3. Procedure

Octadecylsilica (1 g) was transferred to a 100 mm \times 9 mm I.D. glass column fitted with a coarse frit (No. 3) and covered with a silanized glass-wool plug. The microcolumn was treated with 10 ml of methanol and 10 ml of distilled water.

In an erlenmeyer flask, 5 ml of milk, 5 ml of water and 10 ml of methanol were mixed by sonication and passed through the microcolumn. A vacuum was applied to obtain a flow-rate about 1–20 ml min^{-1} . The microcolumn was washed twice with 10 ml of distilled water and the washings were discarded. The C_{18} -bonded silica was then dried by passing room air (previously filtered) through the column using a vacuum. The adsorbed residues were then eluted with 10 ml of *n*-hexane. The extract was concentrated at 45°C to 0.5 ml and 3 μl were injected into the gas chromatograph.

For milk powder, 1 g of the powder milk was reconstituted with distilled water (1:9), and for evaporated milk, 2 ml of milk were mixed with 6 ml of distilled water.

Recovery experiments were made preparing contaminated milk at different concentrations, 1 l of milk was transferred into a glass bottle and fortified with a known amount of the analytes by adding 20 μl of the stock solution (prepared in hexane) directly into the milk, the mixture was shaken vigorously for 2 h in an automatic vibrator and left to stand overnight at 4°C. The samples were equilibrated to room temperature before proceeding with the above procedure.

The quantification of the PCBs was made on the basis of individual congeners and not as Aroclors [10].

Alkali and oxidative treatment procedures have fully described elsewhere [11,12], and can be summarized as follows: extract-containing PCBs were mixed with 2 M ethanolic potassium

hydroxide or chromium(VI) oxide in glacial acetic acid at 75–80°C, shaken for a few minutes, washed to eliminate the excess of the reagents and then the organic layers were recovered and re-analysed by GC.

3. Results and discussion

3.1. Chromatographic separation

The selection of PCB congeners to evaluate the analytical method was based on their common presence in milk (Nos. 28, 52, 101, 118, 138, 153 and 180), on their proved toxicity (Nos. 77 and 170) and the fact that they cover all the possible range of the retention times in GC analysis (Nos. 1, 4, 7, 15, 29 and 209) to enclose the retention time interval where the PCBs can appear.

The fifteen PCBs studied are well separated with the six columns, except the pair PCB 15–29, which cannot be separated with the OV-1701 and cyclodextrin columns, which are the most polar columns used. Additional problems arise when a PCB fraction is studied in milk samples because among the 209 possible PCB congeners, around 150 have been found in environmental samples. Although the use of a single capillary column of BP-5, DB-17 or cyclodextrin phase allowed the separation and determination of the PCB congeners studied, a combination of two of them was selected to avoid quantification errors caused by other PCBs congeners not included in this study.

The use of capillary columns is essential for congener-specific analysis, but there is no single column available that can separate all 209 PCB congeners. The literature data reported that using the most common stationary phases, which usually contain 95% dimethyl–5% phenyl polysiloxane (BP-5, DB-5, SE-54), there are co-elution problems with PCBs 110–77, 126–129, 101–84–90, 123–149, 153–105–132, 123–149 and 171–156–202 [10,13]. This problem has also been noted for PCBs 31–28 using a more polar stationary phase containing 50% phenylmethyl

siloxane (DB-17, BP-10) [13]. However, the PCBs can be determined unambiguously in terms of the individual congeners using different polarity capillary columns in combination with electron-capture detection (ECD).

3.2. Solid-phase extraction on C_{18}

The different variables of the solid-phase extraction procedure were checked to establish which values provide the best recoveries. The optimum conditions for the solid-phase extraction on C_{18} in the trace determination of polychlorinated biphenyls in milk are the same as were established in a previous study for the organochlorine pesticides in the same matrix [9]. Organochlorine compounds are usually present in milk samples and can constitute interfering compounds.

Whole milk with a fat content of 3.4% spiked with fifteen PCBs was analysed according to the present procedure.

Data referring to the recovery and the repeatability of the method are given in Table 1. For the fifteen PCB congeners, the recovery was better than 83% and the relative standard deviation was below 11%. The detection limits (signal-to-noise ratio = 3) are also given in Table 1.

Table 2 demonstrates the performance of the SPE when skimmed, 2%, powdered, breast and evaporated samples were spiked with a mixture of PCBs. The recoveries were similar for the different kinds of milk, except for decachlorobiphenyl, the recovery of which varied between 89 and 43% depending on the kind of milk. This may be due to the binding of the high-chlorine-content compounds to proteins [4].

Recovery data for whole milk spiked with fifteen PCBs and analysed according to Suzuki et al. [14] and the sulphuric acid–hexane extraction procedure [15] are similar. Although the recoveries obtained by the three procedures are satisfactory, the detection limits obtained by the solid-phase extraction procedure are better.

The extraction efficiency can be checked by analysing field-treated samples and comparing the data with those obtained by specific methods of known effectiveness. The results obtained

Table 1
Results obtained using SPE on C₁₈

PCB	Detection limit ($\mu\text{g l}^{-1}$) ^a	Concentration ($\mu\text{g l}^{-1}$)	Recovery (%) ^b
1	12.4	500	92 ± 6
		50	91 ± 7
4	9.9	250	94 ± 6
		25	96 ± 10
7	1.3	50	93 ± 5
		5	96 ± 9
15	9.9	250	92 ± 10
		25	97 ± 13
29	0.8	30	91 ± 9
		3	87 ± 8
28	5.0	200	99 ± 11
		20	102 ± 15
52	0.7	50	97 ± 8
		5	101 ± 13
101	0.4	20	96 ± 9
		2	93 ± 9
77	0.6	30	97 ± 8
		3	104 ± 10
118	0.2	8	98 ± 7
		0.8	91 ± 11
153	0.2	9	83 ± 10
		0.9	79 ± 14
138	0.2	8	99 ± 8
		0.8	102 ± 10
180	0.1	8	85 ± 9
		0.8	92 ± 12
170	0.1	10	88 ± 9
		1	80 ± 9
209	0.1	6	83 ± 10
		0.6	75 ± 16

^a Signal-to-noise ratio = 3.

^b Mean ± R.S.D. ($n = 5$).

with the certified standard are given in Table 3 and corroborate the previous results.

The identification and determination of PCBs in milk samples are sometimes difficult because there are a large number of chlorinated compounds with similar chemical and physical prop-

erties, including pesticides (e.g., DDT, hexachlorobenzene, dieldrin, chlordane), polychlorinated dibenzo-*p*-dioxins (PCDDs) and dibenzo furans (PCDFs) [16].

However, the interferences produced by PCDDs and PCDFs are highly hypothetical

Table 2
Results obtained using for different kinds of milk SPE on C₁₈

	PCB Recovery (%) ^a			Detection limit ($\mu\text{g l}^{-1}$)	Powdered milk		Evaporated milk	
	2% milk	Skimmed milk	Breast milk		Recovery (%) ^a	Detection limit ($\mu\text{g kg}^{-1}$)	Recovery (%) ^a	Detection limit ($\mu\text{g l}^{-1}$)
1	90 ± 8	88 ± 10	91 ± 10	13.0–15.0	96 ± 7	120	94 ± 7	42.0
4	89 ± 9	98 ± 7	83 ± 9	9.0–10.0	94 ± 9	99	96 ± 9	33.0
7	87 ± 6	87 ± 8	94 ± 8	1.0–2.0	91 ± 7	20	88 ± 9	4.4
15	89 ± 5	93 ± 9	82 ± 9	8.0–10.0	94 ± 8	99	95 ± 6	34.0
29	93 ± 6	98 ± 8	104 ± 8	0.6–0.8	95 ± 10	7	94 ± 9	2.8
28	94 ± 9	90 ± 8	86 ± 10	5.0–7.0	94 ± 8	50	93 ± 8	17.0
52	90 ± 7	92 ± 8	96 ± 11	0.7–1.0	96 ± 6	7	94 ± 9	2.4
101	89 ± 5	94 ± 7	91 ± 9	0.4–0.6	94 ± 7	4	90 ± 10	1.5
77	92 ± 8	96 ± 10	100 ± 8	0.5–0.7	91 ± 7	6	88 ± 8	2.3
118	86 ± 9	90 ± 8	106 ± 9	0.1–0.4	84 ± 4	2	82 ± 6	1.0
153	82 ± 6	95 ± 8	95 ± 5	0.1–0.2	92 ± 9	2	90 ± 8	1.0
138	83 ± 10	89 ± 10	74 ± 10	0.2–0.4	89 ± 9	2	84 ± 7	1.0
180	87 ± 5	80 ± 8	67 ± 9	0.1–0.6	77 ± 9	1	76 ± 10	0.5
170	85 ± 8	79 ± 9	84 ± 10	0.1–0.3	77 ± 5	1	77 ± 9	0.5
209	70 ± 9	89 ± 10	54 ± 11	0.1–0.3	54 ± 11	1	43 ± 12	0.5

Extraction recoveries and R.S.D.s (at the higher concentrations indicated in Table 1). Detection limits obtained depending on the sample.

^a Mean ± R.S.D. ($n = 5$).

Table 3
Concentrations of PCBs in a certified standard (CRM 450 natural milk powder).

PCB	Concentration ($\mu\text{g kg}^{-1}$) ^a			
	Certified value ^b	C ₁₈	Suzuki et al. [14]	H ₂ SO ₄ - <i>n</i> -hexane [15]
1				
4				
7				
15				
29				
28				
52	1.16 ± 0.17			
101				
77				
118	3.3 ± 0.4	3.2 ± 0.5		
153	19.0 ± 0.7	18.5 ± 1.6	18.1 ± 2.0	19.7 ± 2.3
138		14.8 ± 2.01	14.0 ± 2.5	15.03 ± 1.3
180	11.0 ± 0.7	10.1 ± 1.25	9.2 ± 1.5	8.3 ± 2.2
170	4.8 ± 0.7	4.0 ± 0.6		5.8 ± 1.76
209				

^a Mean ± S.D. ($n = 5$).

^b The standard also certified the value for PCB 156, which was not included in this study.

when ECD is used because the level of these substances found in milk are about 50 times lower than those of PCBs [4] and strong alkali degrades PCDDs and PCDFs [16].

Concentrated sulphuric acid destroys certain pesticides, e.g., dieldrin [11,12,15], and chromic acid eliminates most of the organochlorine pesticides [11,12]. No drastic difference in the PCB composition was observed in the milk samples after the treatments.

In this study, the treatments were applied only to real samples and not spiked samples because the latter were checked before spiking in order to obtain extracts where probably no organochlorine contamination occurred.

3.3. Application

Samples of whole, 2%, skimmed, evaporated, powdered and human milk (two samples of each)

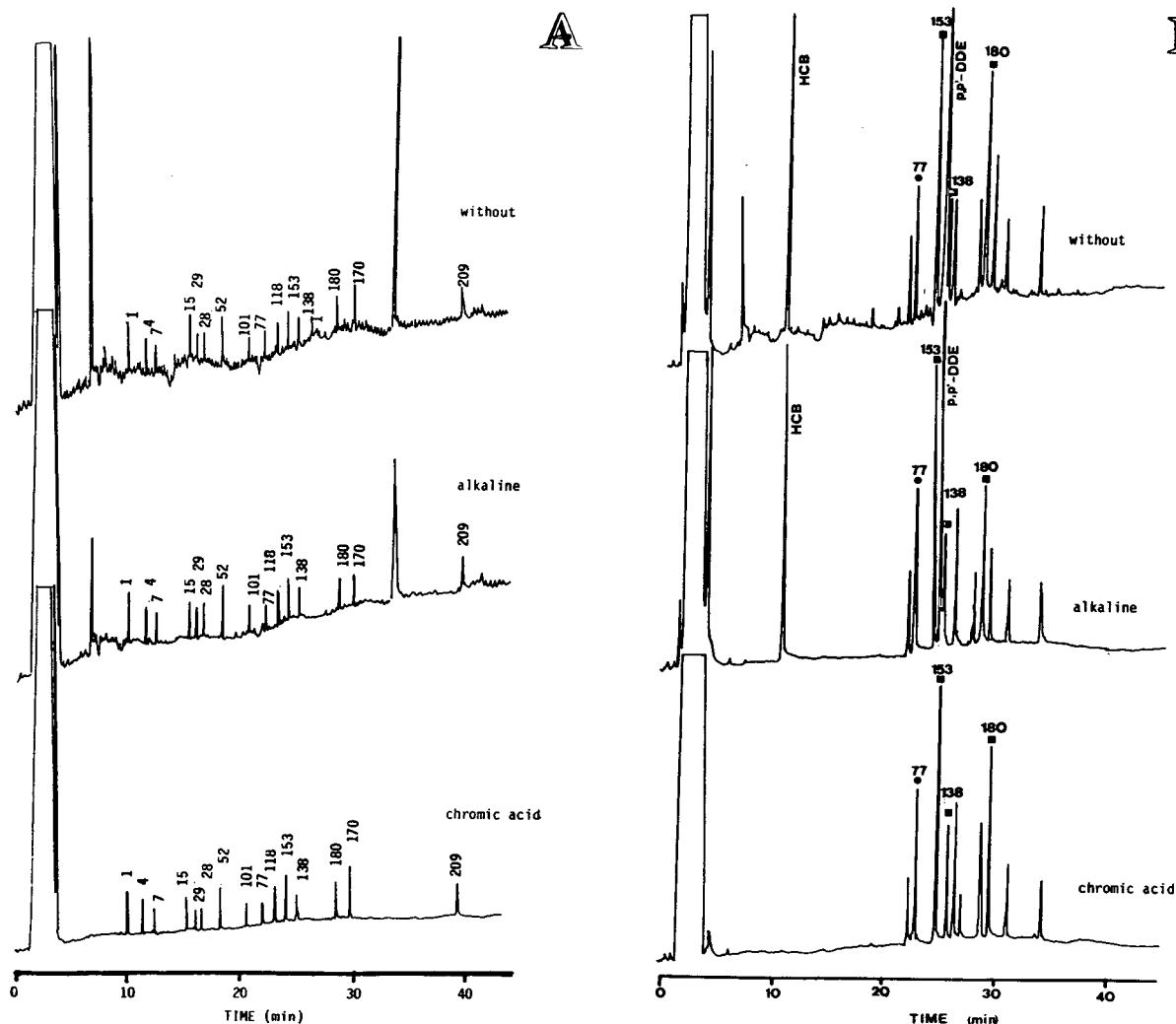


Fig. 1. Chromatograms obtained using a BP-5 column (25 m × 0.25 mm I.D.) for extracts processed according to the proposed procedure without treatment, after ethanolic KOH treatment and after chromic acid treatment of (A) spiked human milk at detection limit levels and (B) human milk sample No. 1 (the levels found are given in Table 4). ○ = possible PCB congener not confirmed with other columns; ◻ = possible PCB congener confirmed with other columns.

Table 4
Content of PCB congeners and organochlorine pesticides found in human milk samples using two extraction methods

Sample No.	Compound	Concentration ($\mu\text{g l}^{-1}$)	
		C ₁₈	H ₂ SO ₄ - <i>n</i> -hexane [15]
1	HCB	5	5
	<i>p,p'</i> -DDE	12	11
	PCB 138	2	3
	PCB 153	8	8
	PCB 180	6	7
2	HCB	10	8
	<i>p,p'</i> -DDE	20	15
	PCB 138	0.3	0.3
	PCB 153	10	9.8
	PCB 180	4	4.5
	PCB 170	0.8	0.7

were analysed by the proposed method and by the sulphuric acid–hexane procedure. Table 4 shows the PCB isomer contents of positive samples determined by two extraction techniques. Only in human milk could some PCBs be detected, always together with HCB and *p,p'*-DDE, the concentrations of which are also given in Table 4. The results demonstrate that the PCB concentrations are in most instances lower than those of organochlorine pesticides, as has been noted by other workers [4]. In the other kinds of milk analysed, some organochlorine pesticides were identified but PCBs were not detected.

The alkali treatment to eliminate organochlorine compounds and the chromic acid treatment to destroy the organochlorine pesticides was applied to all the real samples.

Fig. 1 shows chromatograms of spiked (at the detection limit level) and real human milk samples. In the real sample, the importance of co-elution of the different PCB congeners can be observed.

Using the BP-5 column, PCB 77 was found at twice the concentration of PCB 138. However, the latter is one of the main environmental PCB compounds whereas the former is one of the coplanar congeners typically found at far lower levels [7,10,12]; as an example, Norén et al. [4]

reported the PCB 138-to-PCB 77 concentration ratio in human milk to be approximately 5000:1.

Using the DB-17 or OV-1701 column, no peak appears at the retention time of PCB 77. The erroneous identification with BP-5 could be caused by PCB 110, which co-elutes with PCB 77 in a BP-5 column [10,13] and is typically present in environmental samples.

4. Conclusions

Solid-phase extraction is advantageous compared with liquid–liquid partitioning as no emulsions are formed and the passage of the sample through the column bed replaces repeated extractions and centrifugations. The use of capillary columns of different polarity and an electron-capture detector allows the accurate assessment of the milk levels of the different PCB congeners.

Acknowledgement

The authors thank the CICYT (ALI 88-471) for financial support.

References

- [1] M.P. Seymour, T.M. Jefferies, A.J. Floyd and L.J. Notarianni, *Analyst*, 112 (1987) 427.
- [2] A.D. Viveros, L.A. Albert and D. Namihira, *Rev. Toxicol.*, 6 (1989) 209.
- [3] H. Steinwandter, *Fresenius' J. Anal. Chem.*, 312 (1982) 342.
- [4] K. Norén, A. Lundén, J. Sjövall and A. Bergmann, *Chemosphere*, 20 (1990) 935.
- [5] J.C. Moltó, Y. Picó, J. Mañes and J. Font, *J. Assoc. Off. Anal. Chem.*, 75 (1992) 714.
- [6] A.R. Long, M.M. Soliman and S.A. Barker, *J. Assoc. Off. Anal. Chem.*, 74 (1991) 493.
- [7] K.S. Harlin and G.O. Bordson, *LC·GC*, 9 (1991) 284.
- [8] M.J. Redondo, Y. Picó, J. Server-Carrió, J. Mañes and G. Font, *J. High Resolut. Chromatogr.*, 14 (1991) 597.
- [9] J. Mañes, G. Font and Y. Picó, *J. Chromatogr.*, 642 (1993) 195.
- [10] N. Kannan, G. Petrick, D.E. Schultz-Bull and J.C. Duinker, *J. Chromatogr.*, 642 (1993) 425.

- [11] E. Viana, J.C. Moltó, J. Mañes and G. Font, *J. Chromatogr. A*, 655 (1993) 285.
- [12] E. Viana, J.C. Moltó, J. Mañes and G. Font, *J. Chromatogr. A*, 678 (1994) 109.
- [13] M.T. Galceran, F.J. Santos, D. Barceló and J. Sánchez, *J. Chromatogr. A*, 655 (1993) 275.
- [14] T. Suzuki, K. Ishikawa, N. Sato and K. Sakai, *J. Assoc. Off. Anal. Chem.*, 62 (1979) 681.
- [15] D. Barceló and L. García, *Rev. Agroquim. Tecnol. Aliment.*, 27 (1987) 583.
- [16] J.J. Ryan, R. Lizotte, L.G. Panopio and B.P.Y. Lau, *Chemosphere*, 18 (1989) 49.

Calculation of the composition of sample zones in capillary zone electrophoresis

I. Mathematical model

J.L. Beckers

Eindhoven University of Technology, Laboratory of Instrumental Analysis, P.O. Box 513, 5600 MB Eindhoven, Netherlands

First received 10 August 1994; revised manuscript received 25 October 1994; accepted 25 October 1994

Abstract

A mathematical model was set up for the calculation of all parameters in sample zones in capillary zone electrophoresis. In this model, sample peaks are divided into small segments with varying sample component concentrations and all parameters of a segment can be calculated from the parameters of the preceding segment with a steady-state model, based on the mass balances of the co- and counter ions, the electroneutrality equation and the modified Ohm's law. In this way, non-steady-state electrophoretic processes can be estimated by a repeated application of a steady-state model. Although in this model only the electrodispersive effect is considered and other peak broadening effects, such as diffusion, are neglected, this model is very useful to obtain an insight into the electrophoretic separation procedure and to calculate how parameters change in a sample zone. Calculations with this model show that linear relationships are obtained between the concentration of the sample component and other parameters, such as the pH, concentrations of co- and counter ions, electric field strength and specific resistance in the sample zone, if the sample concentration is not extremely high. With this model electropherograms can be simulated on a spatial basis whereby all possible detector signals can be calculated. The combined effect of a change in pH, resulting in a change in effective mobility for weak acids and bases, and a change in the electric field strength leads to a change in the apparent mobility of the different segments of the sample peaks. For sample ions, both anions and cations, with a mobility higher than that of the co-ions of the background electrolyte a diffuse front side results from the calculations whereas tailing peaks are obtained for sample components with low mobilities.

1. Introduction

In capillary zone electrophoresis (CZE), ionic sample components migrate superimposed on a background electrolyte (BGE). Often it is stated that the influence of the presence of sample components on the composition of the BGE can be neglected if the sample concentrations are at least a factor of 100 lower than that of the BGE [1]. In that case, the composition of the BGE can be considered to be constant through the

whole system. In practice, this is often not true. Component peaks often have a strong tailing or fronting character if the mobilities of the sample components differ from those of the co-ions of the BGE, whereas experimentally determined mobilities, calculated from the migration times of the top of the peaks, differ considerably from values in the literature, indicating a large influence of electrodispersive effects. Of course, these effects can be minimized by choosing a BGE with a co-ion, the mobility of which is

nearly equal to that of the sample component to be determined [1]. Nevertheless it is of interest to study whether arithmetic corrections can be carried out for electrodispersive effects. For this purpose, a mathematical model is needed to calculate all parameters in the sample zones in the electrophoretic process.

For isotachopheresis (ITP), whereby generally a steady-state is reached, steady-state models are often applied [2]. In such steady-state models the number of reduced parameters is generally four [3] and the equations needed for all calculations are the buffer balance, the isotachopheretic condition, the electroneutrality equation and the modified Ohm's law. For zone electrophoretic processes, dynamic models are generally applied, based on the continuity equations for all ionic species. Simulations of the CZE process can be carried out by means of a numerical solution of the basic transport equations [4,5]. Neglecting diffusion and generally applied for fully ionized monovalent electrolytes, Kohlrausch's regulating function can be derived from the continuity equations and solutions for zone electrophoretic processes can be given [6,7]. Such models produce for CZE the typical triangle-shaped peaks indicating that diffusional effects are significantly dominated by electrodispersive effects.

With such models, no information can be obtained about, e.g., the pH in the sample zones. Also, the application of the concept of the "eigenvalues" [8] did not lead to a simple solution for the calculation of the various parameters in the sample zones in CZE. Recently, Beckers [9] applied a steady-state mathematical model to estimate non-steady-state processes in capillary electrophoresis and from calculations with this model the character of system peaks and moving boundaries originating from discontinuities in pH and concentrations of the BGE could be explained. With this model, parameters such as the pH and the concentrations of all ionic species in system peaks could be calculated. Component peaks in CZE can be treated in a similar way. In this paper the calculation of the composition of sample peaks is considered, applying a steady-state model. With this model a computer program is set up for the simulation of electropherograms on a spatial basis.

2. Theoretical

Most mathematical models applied in CZE are based on Kohlrausch's regulating function (KRF), derived from the continuity equations for fully ionized monovalent ionic species and neglecting diffusion effects. Often the KRF is applied in the form

$$\sum_i \frac{c_i}{m_i} = \omega \quad (1)$$

where c_i and m_i represent the ionic concentrations and absolute values of the effective ionic mobilities of all ionic constituents. The numerical value ω of the KRF is locally invariant with time [10]. Sometimes moving boundary zones can be created by the presence of discontinuities in concentrations of the co-ions and/or pH of the BGE. In such cases the ω value of KRF seems not to be locally invariant with time. Beckers [9] estimated these non-steady-state processes in capillary electrophoresis with a steady-state mathematical model. In a similar way, a mathematical model will be set up for the calculation of the parameters in sample zones in capillary zone electrophoresis.

2.1. Mathematical model

The shift in the baseline of the UV signal in electropherograms for a sample peak corresponds with a variation in the concentration of one of more UV-absorbing components present in the sample peak. For the derivation of a mathematical model, this shift is thought to be built up of small segments with increasing concentrations of the sample component. Calculations are started from the BGE zone with an electric field strength E_1 , a pH_1 and a total concentration of the co-ions A of $c_{A,1}$. In the pure BGE solution no sample ions are present and because the composition of the BGE is known all parameters in the BGE can be calculated. For each following segment a total concentration of the sample component $c_{S,2}$ is assumed (see Fig. 1) and the other parameters E_2 , pH_2 and $c_{A,2}$ are calculated with the given mathematical model. In this way, the number of

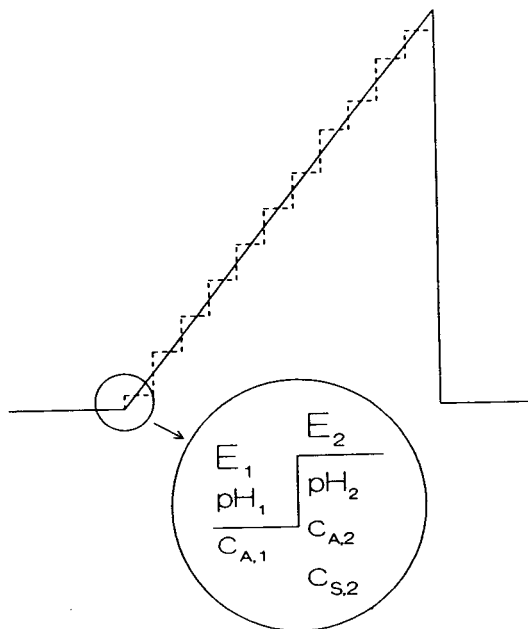


Fig. 1. For the calculation of parameters in sample peaks, the shift in the baseline is considered to be built up of small segments with increasing concentrations of the sample component. Calculations are started from the BGE with an electric field strength E_1 , a pH_1 and a total concentration of the co-ions A of $c_{A,1}$. For each following segment a total concentration of the sample component $c_{S,2}$ is assumed and the other parameters E_2 , pH_2 and $c_{A,2}$ are calculated with the given mathematical model.

unknown parameters in these segments is four, viz. the E_2 , pH_2 , $c_{A,2}$ and the concentration of the counter ions $c_{C,2}$. To calculate these parameters four equations are needed, viz., the mass balance of the co-ions A, the mass balance of the counter ions C, the modified Ohm's law and the electroneutrality equation. Analogously to a mathematical model already given [9], the mass balance of the hydrogen ions was not taken into account. In the calculations the following equations are used (see Refs. [2] and [9] for a complete description of all equations).

The principle of electroneutrality

In accordance with the principle of electroneutrality (EN), the arithmetic sum of all products of the concentration of all forms for all ionic species and the corresponding valences, present in each zone, must be zero [2].

Modified Ohm's law

According to Ohm's law, the product of the electric field strength E and electrical conductivity σ must be constant for all zones. The electrical conductivity, σ , of a zone is the sum of the values $c|mz|F$, where z and F represent the valency of the ionic species and the Faraday constant, respectively.

Mass balance of the co-ions A

The following derivation is given under the assumption that no electroosmotic flow (EOF) is present and that the mobility of the sample ions, S, m_S , is higher than that of the co-ions, m_A . In accordance with Ref. [9], all mass balances are taken over the front side of the adjacent segments. The notation m refers to the absolute values of the effective mobilities of the ionic components. The velocity of the zone boundary between the two segments 1 and 2 is determined by the velocity of the sample component S in zone 2, and this zone boundary moves in a unit of time from point 1 at time $t = 0$ (see Fig. 2A) to point 3 at time $t = 1$, over a distance $E_2 m_{S,2}$. The co-ions A present at point 2 at time $t = 0$ will just

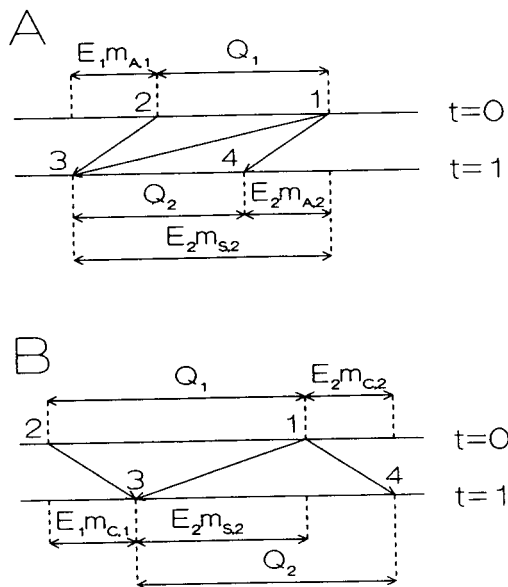


Fig. 2. Migration paths over a zone boundary between the segments 1 and 2 for (A) the co-ions A and (B) the counter ions C. For further explanation, see text.

reach the zone boundary at point 3 at time $t = 1$. The distance between point 2 and 3 is $E_1 m_{A,1}$. Co-ions in zone 2 present at point 1 at time $t = 0$ move over a distance $E_2 m_{A,2}$ to point 4 at time $t = 1$. This means that the co-ions present in zone 1 at a total concentration $c_{A,1}$ at time $t = 0$ between the points 1 and 2 will be present between the points 4 and 3 at a total concentration $c_{A,2}$ at time $t = 1$, i.e. that the amounts of the co-ions Q_1 and Q_2 are equal. Therefore, the mass balance of the co-ions over the zone boundary will be

$$\begin{aligned} c_{A,1}(E_2 m_{S,2} - E_1 m_{A,1}) \\ = c_{A,2}(E_2 m_{S,2} - E_2 m_{A,2}) \end{aligned} \quad (2)$$

or

$$\frac{E_1}{E_2} = \frac{m_{S,2}}{m_{A,1}} - \frac{c_{A,2}(m_{S,2} - m_{A,2})}{c_{A,1}m_{A,1}} \quad (3)$$

Identical equations are obtained if the co-ions have a mobility higher than that of the sample ions and are valid for both negatively and positively charged sample components even in the presence of an EOF.

Mass balance of the counter ions C

The zone boundary moves in a unit of time from point 1 at time $t = 0$ (see Fig. 2B) to point 3 at time $t = 1$ over a distance $E_2 m_{S,2}$. The counter ions C present at point 2 at time $t = 0$ will just reach the zone boundary at point 3 at time $t = 1$. The distance between points 2 and 3 is $E_1 m_{C,1}$. The counter ions present at point 1 at time $t = 0$ will move over a distance $E_2 m_{C,2}$ and will reach point 4 at time $t = 1$. All counter ions C present between point 1 and 2 in zone 1 at a total concentration $c_{C,1}$ will be present in zone 2 between 3 and 4 at a total concentration $c_{C,2}$ at time $t = 1$. The amount of counter ions Q_1 and Q_2 will be equal and the mass balance of the counter ions C will therefore be

$$c_{C,1}(E_2 m_{S,2} + E_1 m_{C,1}) = c_{C,2}(E_2 m_{S,2} + E_2 m_{C,2}) \quad (4)$$

or

$$\frac{E_1}{E_2} = \frac{c_{C,2}(m_{S,2} + m_{C,2})}{c_{C,1}m_{C,1}} - \frac{m_{S,2}}{m_{C,1}} \quad (5)$$

Identical equations are obtained in the presence of an EOF and all equations are identical for negatively and positively charged sample components with the understanding that for negatively charged components the negative ions of the BGE are the co-ions whereas the positive ions of the BGE are the counter ions, and vice versa.

2.2. Procedure of calculation

In order to calculate all parameters in the sample zones in CZE, the set of equations described above has to be solved. Starting from the known parameters of the BGE zone, for all segments of a sample zone with a specific sample component concentration of $c_{S,2}$ the parameters E_2 , pH_2 , $c_{A,2}$ and $c_{C,2}$ have to be calculated from those in the preceding segment. In Fig. 3 the relationships between the calculated ratios E_1/E_2 , according to Eqs. 3 (dashed lines) and 5 (solid lines), and varying concentrations $c_{A,2}$ are given for different assumed pH_2 values for a BGE consisting of (A) 0.01 M imidazole adjusted to pH 5 by adding acetic acid and the sample component potassium at a concentration of 0.0001 M and (B) 0.01 M Tris adjusted to pH 8.0 by adding acetic acid and a sample component chloride at a concentration of 0.0001 M. All mobilities at infinite dilution and pK values of the ionic species used in the calculations are given in Table 1. Because the values of E_1/E_2 according to Eq. 3 are nearly equal for all pH_2 values, they are represented by a single dotted line, whereas the E_1/E_2 values obtained from Eq. 5 vary considerably for different $c_{A,2}$ and pH_2 values. From Fig. 3A and B, it can be concluded that for each $c_{A,2}$ value always a pH_2 value can be found whereby the values of E_1/E_2 calculated with Eqs. 5 and 3 are equal. Application of the EN and Ohm's law results in the correct pH_2 and $c_{A,2}$ values for a given $c_{S,2}$ value.

The calculation of the parameters of segment 2

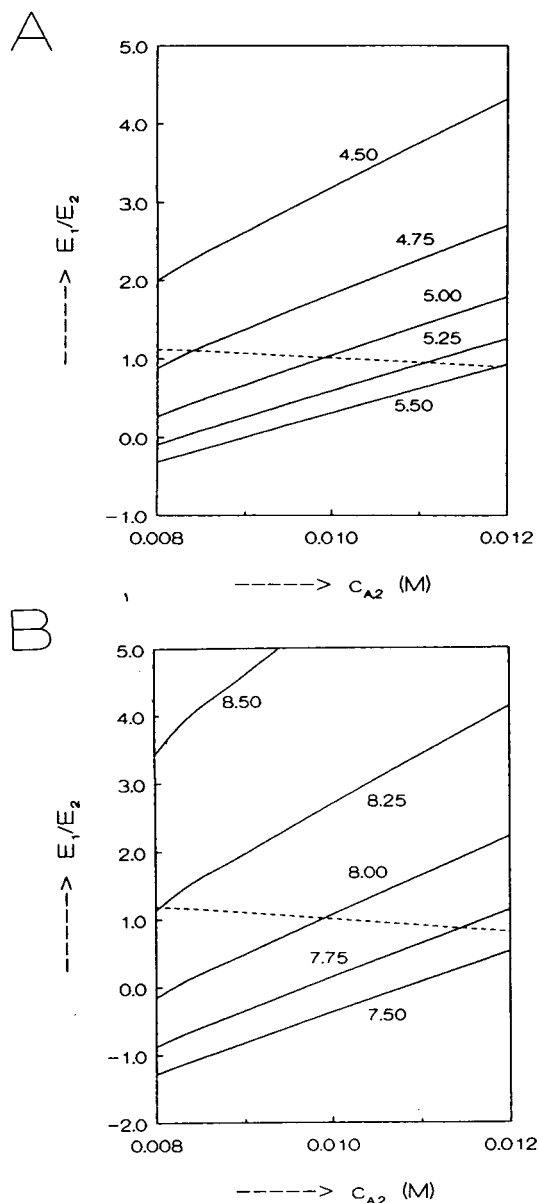


Fig. 3. Calculated relationships between the ratios E_1/E_2 , according to Eqs. 3 (dashed lines) and 5 (solid lines), and varying concentrations $c_{A,2}$ are given for different assumed pH_2 values for a BGE consisting of (A) 0.01 M imidazole adjusted to pH 5 by adding acetic acid and the sample component potassium at a concentration of 0.0001 M and (B) 0.01 M Tris adjusted to pH 8.0 by adding acetic acid and a sample component chloride at a concentration of 0.0001 M. The values of E_1/E_2 according to Eq. 3 are nearly equal for all pH_2 values. The numbers refer to the corresponding pH_2 values. For further information, see text.

Table 1
Ionic mobilities at infinite dilution, m ($\text{m}^2/\text{V}\cdot\text{s}$), and pK values for ionic species used in the calculations

Ionic species ^a	$m \cdot 10^9$	pK
Acetic acid	-42.4	4.76
Benzoic acid	-33.6	4.203
Formic acid	-56.6	3.75
Histidine	29.7	6.03
Hydrochloric acid	-79.1	-2.0
Imidazole	50.4	6.953
Lithium	40.1	14.0
MES	-28.0	6.095
Potassium	76.2	14.0
TBA	25.0	>9.0
Tris	29.5	8.10

^a MES = 2-(N-Morpholino)ethanesulphonic acid; TBA = tetrabutylammonium; Tris = Tris(hydroxymethyl)amino-methane.

starting from these of the BGE is as follows (see Fig. 4). The concentration of the sample component, $c_{S,2}$, is assumed. Then a pH_2 is assumed whereby all pH -dependent parameters, such as the effective mobilities, can be calculated. Further, a $c_{A,2}$ is assumed whereby the total concentration of the counter ions $c_{C,2}$ can be calculated from the EN equation. Iterating between a low and a high value of $c_{A,2}$ the correct value of $c_{A,2}$ can be found whereby the values of E_1/E_2 are equal, applying Eqs. 3 and 5. The correct value for pH_2 can be found by iterating between a high and a low pH_2 until the modified Ohm's law is obeyed. The parameters for each following segment can be calculated with the same procedure starting from the parameters of the preceding segment.

2.3. Significance of the mathematical model

With a computer program, based on the foregoing mathematical model several parameters for sample zones in CZE are calculated. In the calculations corrections are made for activity coefficients and the mobility dependence according to Debye-Huckel-Onsager. In Fig. 5A the relationship is given between the concentration of the sample component c_s and the calculated pH in the sample zone for (1) potassium as

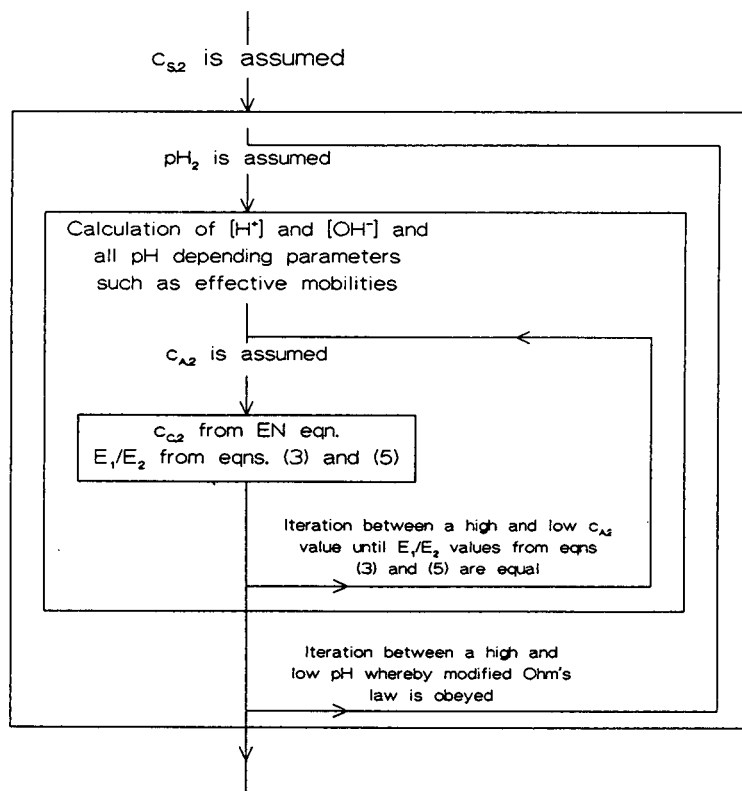


Fig. 4. Calculation procedure for the parameters in sample zones in capillary zone electrophoresis. In the calculation the mass balances of the co- and counter ions, the EN equation and the modified Ohm's law are used.

sample ions and (2) tetrabutylammonium (TBA) ions applying a BGE consisting of 0.01 M lithium ions adjusted to pH 5 by adding acetic acid. From Fig. 5A, it can be concluded that the pH in sample zones changes linearly with increasing concentrations of the sample components, whereby the pH in the zone decreases for sample components with a mobility lower than that of the co-ions in the BGE and increases for higher mobilities. This is in accordance with ITP, where the pH decreases for sample components with lower mobilities in cationic systems. In Fig. 5B, the relationships are given between c_s and (3, 4) the calculated ionic concentrations of the co-ions lithium and (5, 6) counter ions acetate for (3, 5) the sample component potassium and (4, 6) TBA, respectively. As expected from Kohlrausch's law, the ionic concentration of the co-ion lithium decreases for both sample com-

ponents. Because the transfer ratio, representing the number of co-ions replaced by one sample ion [11], is smaller than unity for potassium, because its mobility is higher than that of the co-ions, the decrease in concentration of the co-ions lithium is smaller than for TBA (transfer ratio > 1) at the same c_s . Further, the total ionic strength and the total concentration of the counter components increase in the case of potassium sample ions. Because of these effects, potassium ions would give a peak and TBA a dip on applying the indirect UV mode with UV-absorbing counter ions [12]. In Fig. 5C the ratios of the electric field strengths in sample zone and BGE, E_s/E_{BGE} , are given as a function of the concentrations c_s for (1) potassium and (2) TBA. For sample components with a mobility higher than that of the co-ions the E gradient decreases, whereas it increases for larger c_s values for

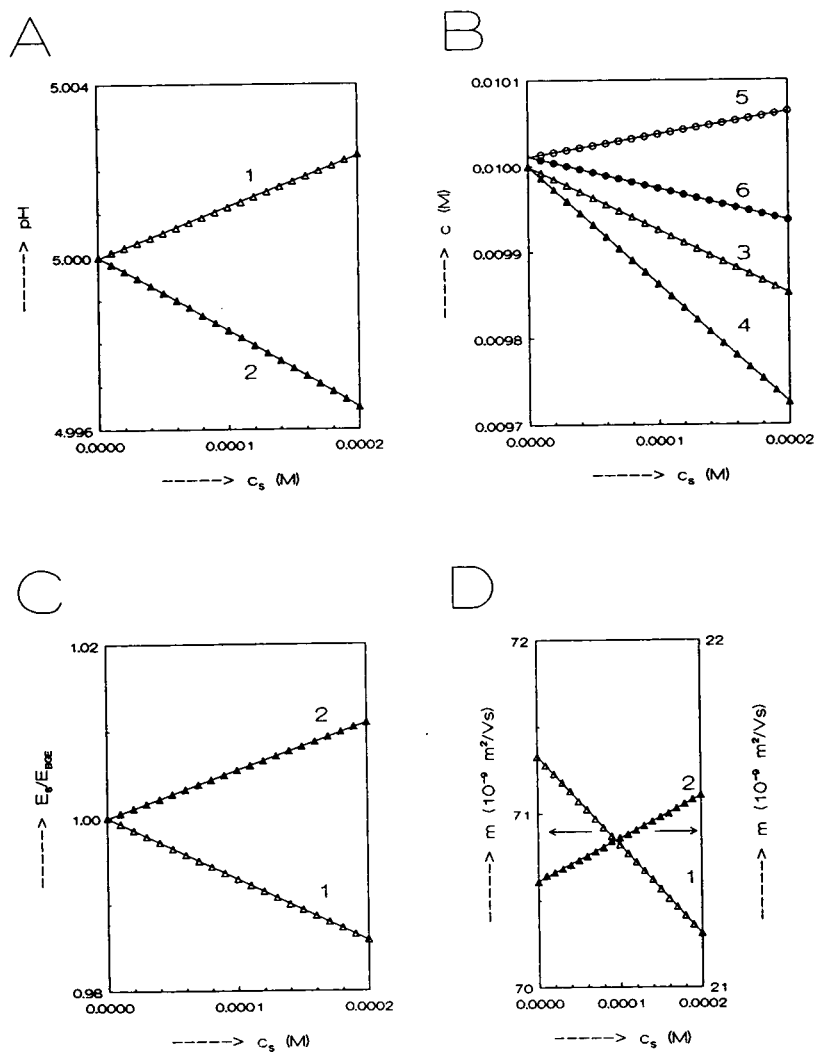


Fig. 5. Calculated relationships between the concentration of the sample component c_s and (A) pH, (B) ionic concentrations of counter and co-ions, (C) ratio E_s/E_{BGE} and (D) apparent mobility of the sample components in the sample zones applying a BGE consisting of 0.01 M lithium adjusted to pH 5 by adding acetic acid for (1) the sample component potassium with a mobility higher than that of the co-ions and (2) sample component TBA with a lower mobility. Ionic concentrations of the co-ions and counter ions are respectively (3, 5) for the sample component potassium and (4, 6) for the sample component TBA. For further explanation, see text.

sample components with a low mobility. Because the E gradient in the potassium zone decreases for higher concentrations of the sample component and because the ionic mobility of potassium is nearly constant, the apparent velocity of the potassium ions ($v = mE$) decreases. This results in the well known triangle-shaped peaks, because the higher concentrations of the sample

peak migrate at a lower velocity. This explains the diffuse fronting peaks for sample components with a mobility higher than that of the co-ions and sharp tailing peaks for sample components with a lower mobility. If the mobilities of sample components and co-ions are different, Gaussian peaks can only be obtained by applying very sensitive detectors and for sample com-

ponent zones at very low concentrations. In that case the variations in electric field strength are so small that the contribution of peak broadening by diffusion is larger than that by electrodispersion. In Fig. 5D the effect of varying E gradients in the zone is shown. In Fig. 5D the relationship between the product of ionic mobility and E_S/E_{BGE} ratio which can be considered to be the apparent mobility of a specific segment of the sample peak and correcting in this way for the effect of varying E , and the concentration of the sample component c_S is given (if an EOF is present the apparent mobility can be presented as $m_i E_S/E_{BGE} + m_{EOF}$). It can clearly be seen that if mobilities are calculated from the top of sample peaks, for components with a high mobility too low mobilities are obtained, whereas for "slow" components an overestimation of the mobilities will be obtained.

In Fig. 6 the same parameters as described in Fig. 5 for cations are given for the anionic sample components (1) chloride and (2) MES applying a BGE consisting of 0.01 M formic acid adjusted to pH 6 by adding histidine. As shown in Fig. 6A, the pH decreases in sample peaks for a sample component with a mobility higher than that of the co-ions of the BGE, whereas the pH increases for components with a mobility lower than that of the co-ions, just as in anionic ITP. In Fig. 6B the lines (3, 4) represent the calculated total concentrations of the co-ions (left-hand scale) and (5, 6) the total concentrations of the counter ions histidine (right-hand scale). Because the pK value of the component MES is about 6, and the pH in the sample zone varies the total concentrations are given. From Fig. 6B it can be seen that the concentrations of the co-ions decrease with increasing concentrations of the sample components. This effect is larger for sample components with a low mobility. The concentration of the counter ions can both increase and decrease. If the mobility of the sample components is high, the transfer ratio is low and the ionic strength increases, through which the total concentration of the counter ions increases. For sample components with a high mobility the ratio E_S/E_{BGE} decreases (see Fig. 6C), resulting in a decrease in the apparent

mobility ($m_i E_S/E_{BGE}$) at higher sample concentrations c_S (see Fig. 6D). With this model the typical triangle-shaped character of sample peaks can be understood. For the sample component MES an irregularity is observable in all graphs at a c_S of about 0.00016 M, probably connected with its pK value of about 6.1.

3. Discussion

The basis of the mathematical model described is that sample zones are divided into segments with a specific sample concentration and calculations show that these segments are characterized by a specific mobility. Because the apparent mobilities of these segments vary by a combined effect of a variation in effective mobility, due to a varying pH in the sample peak, and in the ratio E_S/E_{BGE} , the for CZE typical triangle-shaped sample peaks are obtained. According to this model, the apparent mobility depends on the local concentration of the sample component c_S , as already indicated by several workers [8,10]. The beginning of the diffuse side of a sample peak, calculated on a spatial basis, at time t is positioned at the point

$$x = vt = m_{app,BGE} E_{BGE} t \quad (6)$$

where $m_{app,BGE}$ is the apparent mobility of the sample component in the BGE ($c_S = 0$) and E_{BGE} is the electric field strength in the BGE. The position of a segment i with a specific concentration of the sample component can be calculated according to

$$x_i = v_i t = m_{app,i} E_{BGE} = m_{eff,i} E_i \quad (7)$$

where $m_{app,i}$ is the effective mobility of a segment i recalculated to the applied electric field strength of the BGE, E_{BGE} . The calculations of the positions of the segments i are repeated until the summation of all products of the concentrations of the sample component c_i , length of the corresponding segment Δx_i and capillary area $A = \sum c_i \Delta x_i$ A is equal to the total injected amount of the sample component. In this treatment the back and front sides of the component

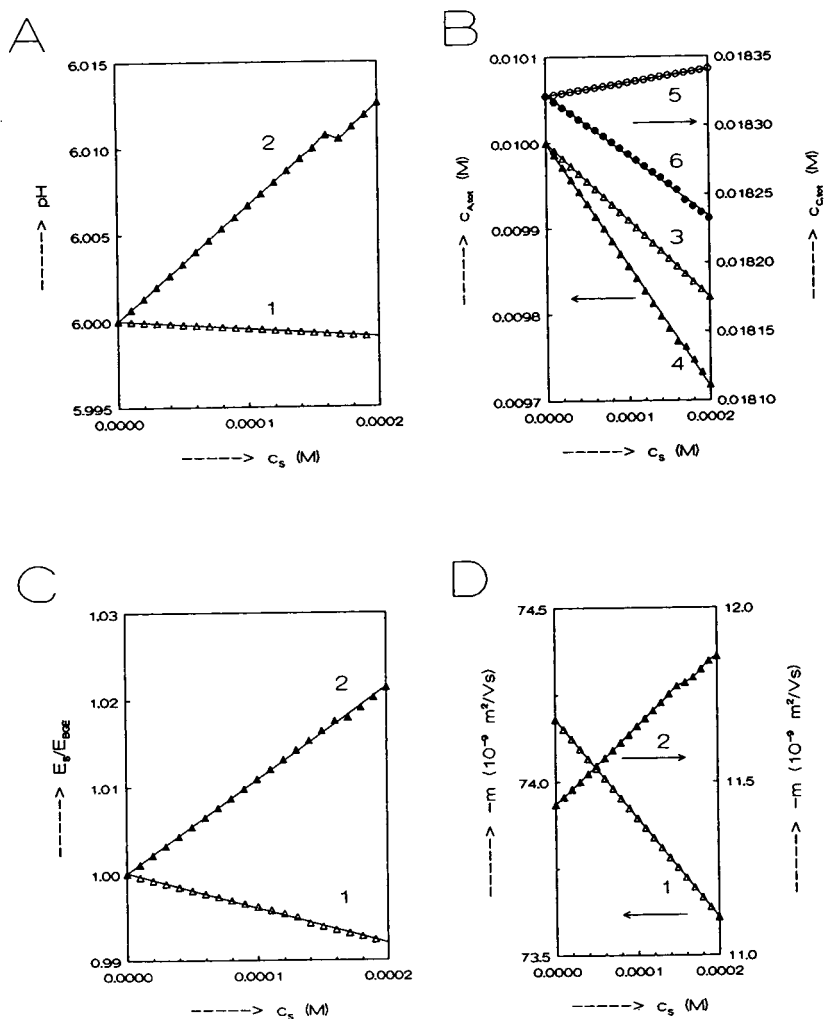


Fig. 6. Calculated relationships between the concentration of the sample component c_s and (A) pH, (B) total concentrations of counter and co-ions, (C) ratio E_s/E_{BGE} and (D) apparent mobility of the sample components in the sample zones applying a BGE consisting of 0.01 M formic acid adjusted to pH 6 by adding histidine for the sample component (1) chloride with a mobility higher than that of the co-ions and (2) MES with a lower mobility. Total concentrations of the co-ions and counter ions are respectively (3, 5) for the sample component chloride and (4, 6) for the sample component MES. For further explanation, see text.

peaks are assumed to be sharp and this model will only be valid if diffusion effects are negligible compared with the electrodispersive character of the sample peak. The electropherograms calculated in this way have a spatial character. As an example, sample peaks present in a capillary tube after a 300-s CZE separation, are calculated, for cations with mobilities of (1) 75, (2) 65, (3) 50, (4) 35 and (5) $25 \cdot 10^{-9}$

$\text{m}^2/\text{V} \cdot \text{s}$, respectively. All sample pK values are assumed to be 7. The BGE in the simulation was 0.01 M imidazole adjusted to pH 4.2 by adding benzoic acid. The results of the calculations are given in Fig. 7.

In Fig. 7A the concentrations of the sample components are given as function of the position of the peaks after a separation time of 300 s. It can be clearly seen that the calculated peaks are

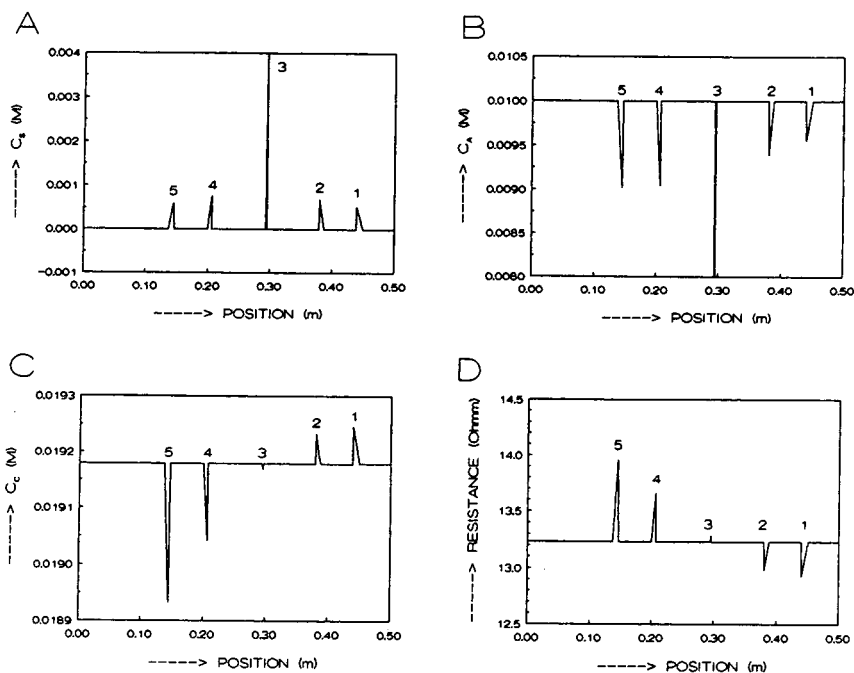


Fig. 7. Calculated (A) concentrations of the sample components, (B) concentrations of the co-ions A, (C) concentrations of the counter ions C and (D) zone resistances for sample peaks of cations with mobilities of (1) 75, (2) 65, (3) 50, (4) 35 and (5) $25 \cdot 10^{-9} \text{ m}^2/\text{V} \cdot \text{s}$ and a pK value of 7 as a function of the position in the separation capillary, applying a BGE consisting of 0.01 M imidazole adjusted to pH 4.2 by adding benzoic acid. The sample zones are calculated after a separation time of 300 s. Further simulation conditions: capillary diameter, 75 μm ; capillary length, 0.467 m; injection–detection distance, 0.4 m; applied voltage, 10 kV; amounts injected for all sample compounds, $1 \cdot 10^{-11}$ mol. For further explanation, see text.

fronting if the sample components have a mobility higher than that of the co-ions (peaks 1 and 2) and tailing if their mobilities are lower (peaks 4 and 5). For a component with a mobility nearly equal to that of the co-ions (peak 3), a very sharp sample zone is obtained, because in the mathematical model peak broadening due to diffusion is neglected. In fact, the calculated sample concentrations in Fig. 7A represent the simulated electropherogram obtained on applying the direct UV mode, if the effect of the molar absorptivities is included. In Fig. 7B the calculated concentrations of the co-ions A are given for the different sample peaks in the capillary tube after the 300-s separation. Peak 3 is sharp again, whereas peaks 1 and 2 are fronting and 4 and 5 are tailing. It is notable that peaks 4 and 5 are larger than peaks 1 and 2, because the transfer ratios of components 4 and 5 are larger

than those of components 1 and 2 [11]. All components are present as negative peaks, as can be expected because Fig. 7B represents the classical “indirect UV” mode [12].

In Fig. 7C, the concentrations of the counter ions C are given for the sample peaks after the 300-s separation. As explained earlier [12], the sample peaks for components with a mobility higher than that of the co-ions are positive, whereas those for lower mobilities are negative. The reason is simple. The transfer ratio for sample components with a mobility higher than that of the co-ions is smaller than unity, i.e., in the sample peak the ionic strength increases, as can be seen in Fig. 7C. If the counter ions C are the only UV-absorbing ions of the BGE in the electropherogram, negative and positive peaks are the result, as shown in Fig. 7C. For components with a mobility nearly equal to that of

the co-ions, the transfer ratio is unity, i.e. the concentration of the counter ions is constant. In Fig. 7D the specific zone resistances in the sample peaks are given for the 300-s separation. For sample components with a high mobility (peaks 1 and 2) the zone resistances decrease whereas for components with low mobilities the zone resistances increase (peak 4 and 5). It is satisfying that the results of this mathematical model, based on mass balances, correspond with the results of a total different model based on Kohlrausch's regulation function as described in Ref. [12].

4. Conclusions

All parameters of the sample zones in CZE can be calculated by a mathematical model, whereby non-steady-state processes in CZE can be estimated by repeated application of a steady-state model to sample zones divided into segments. The calculations are started from the diffuse side of the peak, where the composition of the sample peak differs only slightly from that of the BGE and it is assumed that Ohm's law, the electroneutrality and the mass balances of the co-ions and counter ions must be obeyed. Calculations with this model show that linear relationships are obtained between concentrations of the sample ions and parameters such as the pH, concentrations of co- and counter-ions, E gradients and specific resistance in the sample zone on a spatial basis. The combined effect of the change in pH, resulting in a changing effective mobility for weak acids and bases, and the change in the electric field strength E leads to a change in apparent mobility of the different segments of the sample peaks. For sample ions, both anions and cations, with a mobility higher than that of the co-ions of the BGE a diffuse

front-side results from the calculations whereas tailing peaks are obtained for sample components with low mobilities, as is known from experiments.

Applying this model, simulated electropherograms on a spatial basis can be calculated. The limitations of the described mathematical model are obvious. In this model, peak broadening effects due to the diffusion and differences in temperature in the radial and axial directions are neglected. In this model all sample peaks are considered apart, and initial effects connected with the co-migration of the different sample components and the effect of, e.g., sample stacking cannot be treated. In Part II this mathematical model will be used for the simulation of electropherograms on a temporal basis, through which simulated and measured electropherograms can be compared to check the model.

References

- [1] F. Foret, S. Fanali, L. Ossicini and P. Boček, *J. Chromatogr.*, 470 (1989) 299.
- [2] J.L. Beckers and F.M. Everaerts, *J. Chromatogr.*, 480 (1989) 69.
- [3] F.M. Everaerts, J.L. Beckers and Th.P.E.M. Verheggen, *Isotachophoresis – Theory, Instrumentation and Applications*, Elsevier, Amsterdam, 1976.
- [4] M. Bier, O.A. Palusinski, R.A. Mosher and D.A. Saville, *Science*, 219 (1983) 1281.
- [5] R.A. Mosher, D.A. Saville and W. Thormann, *The Dynamics of Electrophoresis*, VCH, Weinheim, 1992.
- [6] F.E.P. Mikkers, F.M. Everaerts and Th.P.E.M. Verheggen, *J. Chromatogr.*, 169 (1979) 1.
- [7] W. Thormann, *Electrophoresis*, 4 (1983) 383.
- [8] H. Poppe, *Anal. Chem.*, 64 (1992) 1908.
- [9] J.L. Beckers, *J. Chromatogr. A*, 662 (1994) 153.
- [10] F.E.P. Mikkers, *Thesis*, Eindhoven University of Technology, Eindhoven, 1980.
- [11] M.W.F. Nielen, *J. Chromatogr.*, 588 (1991) 321.
- [12] J.L. Beckers, *J. Chromatogr. A*, 679 (1994) 153.

Influence of buffer electrolyte pH on the migration behavior of phenolic compounds in co-electroosmotic capillary electrophoresis

Sonja M. Masselter, Andreas J. Zemann*

Institute for Analytical Chemistry and Radiochemistry, Leopold Franzens University Innsbruck, Innrain 52a, A-6020 Innsbruck, Austria

First received 18 August 1994; revised manuscript received 26 October 1994; accepted 10 November 1994

Abstract

The separation behavior of phenolic compounds with various substituents was investigated with co-electroosmotic capillary electrophoresis (migration of the analytes in the same direction as the electroosmotic flow). Co-electroosmotic flow conditions were set up when the electroosmotic flow direction was reversed by adding either a cationic surfactant (cetyltrimethylammonium bromide) or a polycation (1,5-dimethyl-1,5-diazaundecamethylene polymethobromide) to the buffer. An alkaline buffer electrolyte was chosen to ensure complete dissociation of the phenols (pH 10–12). It was shown that a separation of the chosen phenols was possible under co-electroosmotic conditions by optimizing the buffer pH.

1. Introduction

Capillary Electrophoresis (CE) has become a powerful tool for the separation of charged [1,2] and uncharged [3,4] compounds. Traditional CE methods, including micellar supported techniques like micellar electrokinetic (capillary) chromatography (MEKC, MECC) [5–7], make use of the fact, that anionic analytes migrate in the opposite direction of the electroosmotic flow (EOF). These methods may be called *counter-electroosmotic* methods. As a consequence, these techniques often cause rather long migration times of anions. Some early attempts have been made to change the ζ -potential of a silica surface by long-chained alkylammonium salts

which, at concentrations slightly below the critical micellar concentration, form dimeric hemimicelles. These are attached with the charged head groups arranged in opposite directions orthogonal to the negatively charged surface [8]. The coating takes place even at moderate pH values due to low pK_A value of the silanol groups of 7.1 [9] which causes a change of the sign of the ζ -potential. This concept was applied to coat a fused-silica capillary with cetyltrimethylammonium bromide (CTAB) to obtain a positively charged inner surface and a reversed EOF [10]. Detailed investigations of the separation behavior of inorganic anions in hemimicellar coated capillaries have been carried out recently [11–13]. Another possibility to dynamically coat the capillary is the usage of coating agents [14] and polycations with more than one positive

* Corresponding author.

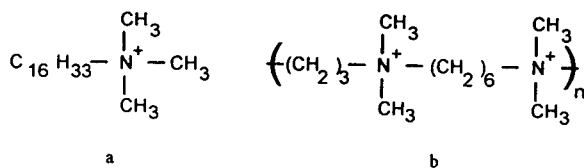


Fig. 1. Chemical structures of CTAB (a) and HDB (b).

functionality per molecule, e.g. 1,5-dimethyl-1,5-diazaundecamethylene polymethobromide (hexadimethrin bromide, HDB, Polybrene) [15]. This compound is also known to allow protein analysis by CE as it prevents cationic proteins from sticking to the wall. By using EOF modifiers, an EOF from the cathodic to the anodic side of the capillary is established. Using a power supply with reversed polarity (“negative power supply”), no hardware alterations of the CE system are required. As anionic species migrate into the same direction as the EOF this principle is called *co-electroosmotic CE* [16].

In this paper, CTAB and HDB are used as EOF modifiers. (Fig. 1).

We assumed that the application of co-electroosmotic methods on mixtures of organic acids (e.g. phenols) should result in fast separations of these compounds. In counter-electroosmotic CE run times can be shortened by applying higher voltages and using shorter capillaries. However, this reduction of run time results in a deterioration of resolution according to the Giddings–Jorgenson (see [1]) relation. Moreover, simple optimization of the buffer composition does not eliminate the problem of Joule’s heat, as for fast separations with counter-electroosmotic conditions a high electroosmotic flow mobility has to be established, which requires the application of high voltages.

2. Experimental

2.1. Apparatus

A Quanta 4000 CE system connected with a system interface module and a personal computer was used. Data processing was performed

with commercial chromatography software (Maxima 820). Uncoated, narrow-bore silica capillaries (AccuSep) with an inner diameter of 50 μm , a total length of 32 cm and an effective separation length of 24.5 cm each were used. All these devices and parts were obtained from Waters Chromatography, Division of Millipore, Milford, MA, USA.

2.2. Reagents

All reagents were of analytical grade. Phenol standard solutions were prepared by dissolving the various phenols (Sigma, Deisenhofen, Germany and Aldrich, Steinheim, Germany) in gradient-grade methanol (Fluka, Buchs, Switzerland). CTAB and HDB (Polybrene) were obtained from Sigma. Depending on the type of EOF modifier 0.7 mM CTAB or 0.001% (w/v) HDB were used. Buffer electrolyte mixtures with 15 mM of phosphate and 1.25 mM of tetraborate each and a pH of 10 to 12 were prepared from borax and disodium hydrogenphosphate (Merck, Darmstadt, Germany) by dissolving in ultrapure water from a Milli-Q system with a conductivity of 18 M Ω (Millipore, Bedford, MA, USA). The pH values were adjusted with 0.5 M NaOH. All buffer solutions were vacuum degassed with sonication prior to usage.

2.3. Procedure

Prior to usage the capillary was purged for approximately 15 min with a non-CTAB- or -HDB-containing buffer electrolyte with the same composition as the running buffer (purging buffer I). After this pretreatment the capillary was rinsed with the running buffer containing the EOF modifier (purging buffer II). Between the runs a purging sequence consisting of 1 min buffer I followed by 2 min buffer II was applied. The pre-conditioning of the capillary and the purging sequence between the runs were essential to obtain reproducible results. Injection was performed hydrostatically for 5 s. On-column UV detection was carried out at 254 nm.

3. Results and discussion

Phenols can be separated under neutral or moderately alkaline conditions with counter-electroosmotic methods [17–21]. As phenolic compounds can be considered to be weak acids, they dissociate at high pH values depending on their substituents. With co-electroosmotic flow conditions at high pH values a faster separation of these compounds should be possible.

In this investigation two different EOF modifiers were used (see Introduction). It appeared that alkylated phenols give rise to strong interactions with the aliphatic backbone of the EOF modifier. Likewise electrostatic interactions of the phenolates with the charged headgroups of the EOF modifier can be assumed. This causes peak zones to broaden and theoretical plate numbers to deteriorate. Thus, the separation of phenolic compounds at a high pH value above their pK_A values with CTAB as EOF modifier is limited to phenols with certain substituents.

The compounds for the standard mixture used in this paper were chosen with respect to their functional groups. Three phenolic acids, one phenolic aldehyde and eight alkylphenols were used (Table 1). The magnitude of the electrophoretic mobilities of phenolic compounds mainly depends on their pK_a values. Furthermore, the phenolic acids are doubly dissociated due to

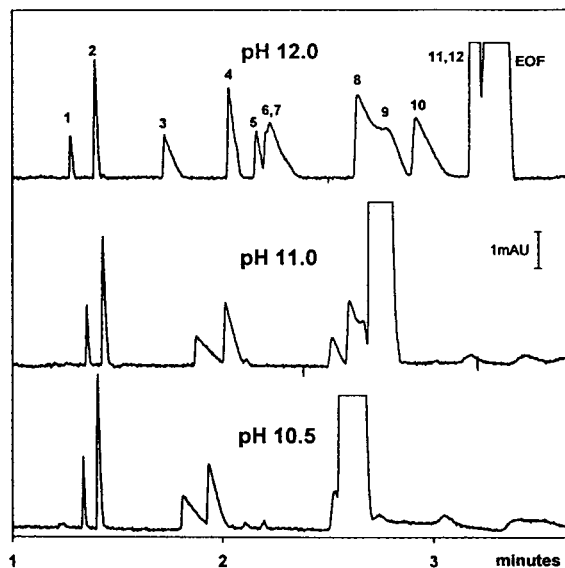


Fig. 2. Capillary electropherograms of a set of 12 phenols with 0.7 mM CTAB as EOF modifier at pH 10.5, 11.0 and 12.0. For conditions see Experimental section; for peak identification see Table 1. 10 kV.

their acidic and phenolic functional groups and thus elute first.

Fig. 2 shows capillary electropherograms of a mixture of these 12 phenolic compounds acquired in the pH range of 10.5 to 12.0 with CTAB as EOF modifier. The phenolic acids are

Table 1
Phenolic compounds used in this study and corresponding pK_a values

Class	No.	Compound (IUPAC)	Trivial name	pK_a
Phenolic acids	1	4-Hydroxybenzoic acid		4.61, 9.31
	2	4-Hydroxy-3,5-dimethoxybenzoic acid	Syringic acid	4.20, 9.10
	3	4-Hydroxy-3,5-cinnamic acid	Sinapic acid	Not available
Aldehyde	4	4-Hydroxy-3,5-dimethoxybenzaldehyde	Syringaldehyde	Not available
Alkylphenols	5	3-Methylphenol	<i>m</i> -Cresol	10.09
	6	4-Methylphenol	<i>p</i> -Cresol	10.27
	7	2-Methylphenol	<i>o</i> -Cresol	10.32
	8	3,4-Dimethylphenol	3,4-Xylenol	10.36
	9	2,3-Dimethylphenol	2,3-Xylenol	10.54
	10	2,6-Dimethylphenol	2,6-Xylenol	10.63
	11	2,3,5-Trimethylphenol		10.69
	12	2,4,6-Trimethylphenol		10.99

doubly dissociated at this pH value and migrate in front of the EOF as the species with the highest electrophoretic mobilities. In the case of 4-hydroxy-3,5-cinnamic acid (sinapic acid), hydrophobic interactions of substituents with CTAB become obvious: in contrast to HDB as EOF modifier, which will be discussed later, this particular phenolic acid is clearly retarded compared to the other acids and partly overlaps with 4-hydroxy-3,5-dimethoxybenzaldehyde (syringaldehyde). This is due to the aliphatic chain of the 4-hydroxy-3,5-cinnamic acid which strongly interacts with the cetyl core of the surfactant. The mobility of syringaldehyde is intermediate compared to the acids and the alkylphenols and is more or less independent on pH of the buffer electrolyte. Cresols, xylenols and trimethylphenols have the lowest mobility and cannot be separated under these conditions. Below pH 11 the dimethylphenols migrate only slightly in front of the EOF. Despite the fact that the pH value is above the respective pK_a value of the trimethylphenols, these compounds do not possess a net electrophoretic mobility large enough to separate at pH 11. Only at pH values above 12 the mono- and dimethylphenols show considerable electrophoretic mobilities. Nevertheless, no satisfactory separation of the isomers is possible. Moreover, high pH values above 12 are not desirable as they require high ionic strengths.

The observed low electrophoretic mobilities of the phenols, especially of the higher methylated species, are a result of mainly two effects: on the one hand the net electrophoretic velocities and on the other hand the formation of aggregates of free CTAB surfactant molecules and hemimicelles with the phenolic analytes in terms of hydrophobic interactions. This results in altered charge properties of the phenols and does significantly influence the migration behavior of the phenols. The poor peak shapes of the investigated methylphenols, which are observed with CTAB can be attributed to these interactions. In addition, the CTAB system is prone to changes in pH as the concentration of hemimicelles varies thus influencing the magnitude of the EOF.

A significant improvement in performance of the co-electroosmotic separation upon the

CTAB system is achieved with HDB as EOF modifier. This type of EOF modifier also reverses the EOF by a dynamic coating. However, this coating is more stable and insensitive to minor changes in buffer pH than the CTAB system. Although some interactions of the analytes with the aliphatic sections of the EOF modifier as well as electrostatic interactions are assumable even with this modifier, the results are much more promising.

The performance of the separation mainly depends on the pH value of the buffer (Fig. 3). At pH 10.5 some peak zones coincide. As in the case of CTAB, the phenolic acids migrate with the highest mobility, followed by the aldehyde and the alkylphenols, which appear as unseparated and broad peaks with low mobilities. This is due to the fact that the pH value of the buffer is in the range of the pK_a values of the alkylphenols (see Table 1). In the HDB system sinapic acid does not interact with the EOF modifier. This implies that with HDB solvophobic interactions do not seem to play an

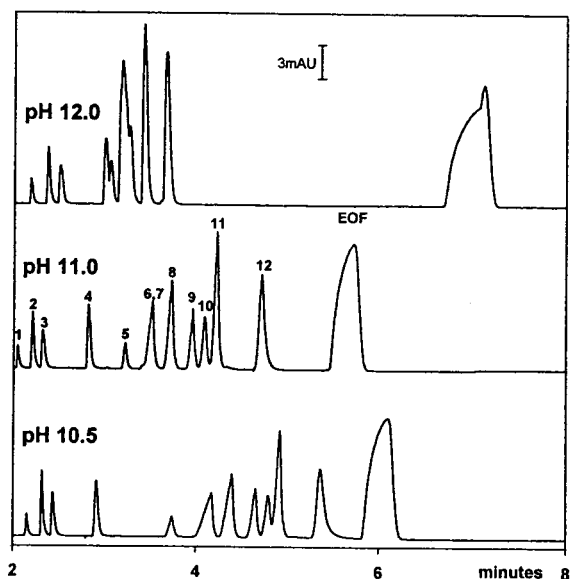


Fig. 3. Capillary electropherograms of a set of 12 phenols with 0.001% (w/v) HDB as EOF modifier at pH 10.5, 11.0 and 12.0. For conditions see Experimental section; for peak identification see Table 1. 10 kV.

important role. This becomes obvious when electropherograms, both acquired at pH 11, but with different EOF modifiers, are compared. Peak zones of the methylated phenols and separation efficiencies are improved dramatically as well as the electrophoretic mobilities of these analytes are also increased. This comparison proves the influence of the hydrophobic interactions in the surfactant based CTAB system on the migration behavior and the separation efficiency of the phenols. On the contrary, a satisfactory separation of the test mixture (except for *p*- and *o*-cresol) is possible at pH 11 and with HDB as EOF modifier. It is to mention that the migration order of the methyl phenols strictly coincides with the pK_a values of the specific isomeric class (mono-, di- and trimethylphenols), though a relation of migration order and pK_a value actually can only be drawn among the compounds of a single isomeric class as the mass-to-charge ratio is altered with additional substituents.

At pH 12 the separation deteriorates again as the electrophoretic mobilities of the methylated phenols become too high and some of these analytes coincide again. The dependence of the electrophoretic mobilities of the investigated phenols on the pH value of the buffer electrolyte take the expected course with both types of EOF modifier. In the CTAB system (Fig. 4) the mobilities of the cresols increase markedly above pH 11, corresponding to the pK_a , whereas the di- and trimethylphenols are retarded almost completely. Above pH 11.5 a measurable electrophoretic mobility occurs. The magnitude of the EOF steadily decreases over the investigated range. Anyway, even with this increased separation window the hydrophobic interactions of analytes and CTAB prevent a reasonable separation.

With HDB (Fig. 5), the effective electrophoretic mobilities of the phenolic acids slightly increase, whereas the mobility of the phenolic aldehyde remains constant until pH 11.5 is reached. Above this value an increased mobility is observed. The mobilities of the methylphenols steadily increase over the entire pH range 10.5–12. With the trimethylphenols this increase is

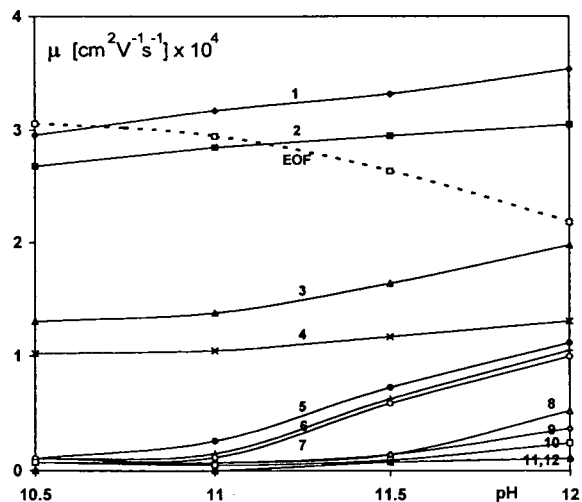


Fig. 4. Dependence of electroosmotic flow and effective electrophoretic mobilities (μ) of phenols on buffer pH. Conditions as in Fig. 2.

more dominant above pH 11. The EOF remains relatively stable over the pH range 10.5–12.

The dependence of the theoretical plate numbers of some selected phenols in the HDB system on the pH value is shown in Table 2. It proves that a pH value of approximately 11 is optimal for the co-electroosmotic separation of the selected phenols in terms of time of analysis, resolution and theoretical plate number.

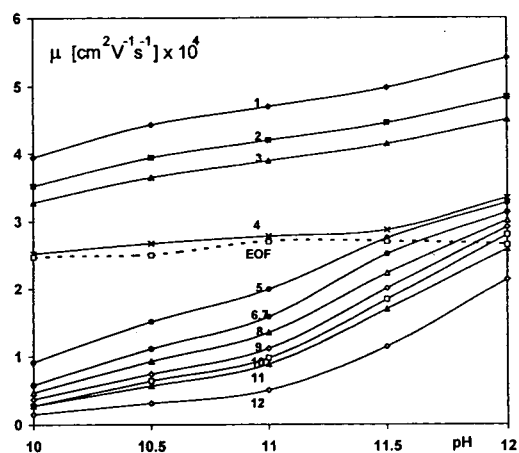


Fig. 5. Dependence of electroosmotic flow and effective electrophoretic mobilities of phenols on buffer pH. Conditions as in Fig. 3.

Table 2
pH dependence of theoretical plate numbers with HDB as EOF modifier

pH	Theoretical plate number				
	Syringic acid	Syringaldehyde	<i>m</i> -Cresol	2,3-Xylenol	2,4,6-Trimethylphenol
10.0	127 000	109 200	87 000	133 000	55 600
10.5	166 700	104 600	104 800	136 200	92 500
11.0	113 800	135 100	213 000	208 500	134 800
11.5	111 300	122 800	n.d.	161 200	104 000
12.0	109 900	101 000	104 900	n.d.	90 400

n.d. = Not determined.

4. Conclusions

As a general rule, a satisfactory co-electroosmotic separation of phenolic compounds is possible if the extent of interactions of anionic phenolates with the positively charged capillary wall and the cationic EOF modifiers molecules can be kept within certain limits. In this investigation electrostatic interactions of anionic phenolates with cationic species did not appear to be of a considerable disadvantageous effect. On the other hand, hydrophobic interactions of alkylated phenols with the aliphatic backbone of the EOF modifier had a significant influence on the separation. Especially in the case of CTAB as EOF modifier only selected species do not interact with the modifier. HDB does not have the disadvantageous effects of CTAB in terms of interactions with the analytes. This implies a different mechanism of the surface coating. It is conceivable that the polycation forms coils with the hydrophobic methylene groups directed to the inner side and the charged groups arranged on its surface. This may explain the low tendency to form hydrophobic aggregates of HDB with alkylated phenols. As run times are shorter and theoretical plate numbers are in the range or higher than comparable counter-electroosmotic methods, co-electroosmotic CE procedures should be used as suitable alternatives in special applications. Fig. 6 shows a fast co-electroosmotic separation of six selected phenols. Arising from this it may be stated that co-electroosmotic CE is a suitable method for the analysis of

phenols. Although the interactions of some of the analytes with the EOF modifier limits the application to certain phenols, the addition of organic solvents to the buffer electrolyte enables the separation of analyte mixtures which cannot be analyzed with the system described above [22]. This increases the separation window as well as selectivity and performance of the method.

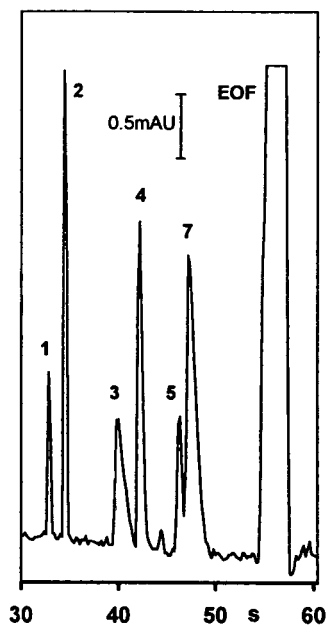


Fig. 6. Fast co-electroosmotic separation of six phenols with 0.7 mM CTAB as EOF modifier. Conditions as in Fig. 2. 25 kV, 90 μ A.

References

- [1] J.W. Jorgenson and K.D. Lukacs, *Anal. Chem.*, 53 (1981) 1298.
- [2] J.W. Jorgenson and K.D. Lukacs, *Science*, 222 (1983) 266.
- [3] S. Terabe, K. Otsuka, K. Ichikawa, A. Tsuchiya and T. Ando, *Anal. Chem.*, 56 (1984) 111.
- [4] K. Otsuka, S. Terabe and T. Ando, *J. Chromatogr.*, 396 (1987) 350.
- [5] J. Gorse, A.T. Balchunas, D.F. Swaile and M.J. Sepaniak, *J. High Resolut. Chromatogr. Chromatogr. Commun.*, 11 (1988) 554.
- [6] G.M. Janini and H.J. Issaq, *J. Liq. Chromatogr.*, 15 (1992) 961.
- [7] A.T. Balchunas and M.J. Sepaniak, *Anal. Chem.*, 60 (1988) 617.
- [8] D.W. Fuerstenau, *J. Phys. Chem.*, 60 (1956) 981.
- [9] M.L. Hair and W. Hertl, *J. Phys. Chem.*, 74 (1970) 91.
- [10] K.D. Altria and C.F. Simpson, *Anal. Proc.*, 23 (1986) 453.
- [11] P. Jandik, W.R. Jones, A. Weston and P.R. Brown, *LC·GC*, 9 (1991) 634.
- [12] J. Romano, P. Jandik, W.R. Jones and P.E. Jackson, *J. Chromatogr.*, 546 (1991) 411.
- [13] W.R. Jones, *J. Chromatogr.*, 640 (1993) 387.
- [14] J.E. Wiktorowicz and J.C. Colburn, *Electrophoresis*, 11 (1990) 769.
- [15] J.E. Wiktorowicz, *US Pat.*, 5 015 350 (1991).
- [16] P. Jandik and G.K. Bonn, *Capillary Electrophoresis of Small Molecules and Ions*, VCH, New York, 1993.
- [17] C.D. Gaitonde and P.V. Pathak, *J. Chromatogr.*, 514 (1990) 389.
- [18] M. Aguilar, A. Farran and V. Martí, *Sci. Tot. Environm.*, 132 (1993) 133.
- [19] M.F. Gonnord and J. Collet, *J. Chromatogr.*, 645 (1993) 327.
- [20] S. Masselter, A. Zemann and O. Bobleter, *Chromatographia*, in press.
- [21] C. Rony, J.C. Jacquier and P.L. Desbène, *J. Chromatogr. A*, 669 (1994) 195.
- [22] S.M. Masselter, A.J. Zemann and O. Bobleter, *Electrophoresis*, 14 (1993) 36.



ELSEVIER

Journal of Chromatography A, 693 (1995) 366–370

JOURNAL OF
CHROMATOGRAPHY A

Short communication

Chiral metal complexes
XLII[☆]. Reversed-phase high-performance liquid
chromatographic separation of racemic dipeptides as their
ternary Co(III) complexes with a chiral triamine

J.R. Aldrich-Wright^a, P.D. Newman^{b,1}, K.R.N. Rao^c, R.S. Vagg^d and
P.A. Williams^{e,*}

^aSchool of Chemistry and Technology, University of Western Sydney Macarthur, Campbelltown, New South Wales 2560, Australia

^bSchool of Chemistry and Applied Chemistry, University of Wales Cardiff, P.O. Box 912, Cardiff CF1 3TB, UK
^cJones Chromatography Ltd., Hengoed, South Wales, UK

^dSchool of Chemistry, Macquarie University, Kingswood, New South Wales 2109, Australia

^eDepartment of Chemistry, University of Western Sydney, Nepean, P.O. Box 10, Kingswood, NSW 2747, Australia

First received 24 May 1994; revised manuscript received 16 November 1994; accepted 17 November 1994

Abstract

The enantiomeric and diastereoisomeric dipeptides Gly-*R,S*-Val, Gly-*R,S*-Leu, Gly-*R,S*-Phe, *R,S*-Leu-Gly, *R,S*-Leu-*R,S*-Ala and *R,S*-Leu-*R,S*-Phe have been separated by RP-HPLC methods when coordinated in ternary Co(III) complexes [Co(*R,R*-benzet)(peptidato)]²⁺ [benzet = *N*-benzyl-*N'*-(2-picolyl-1,2-diaminocyclohexane)], on Amex Prepsil columns under a variety of conditions. A method is illustrated for the recovery of the pure peptides from the separated diastereoisomers. The method appears to be applicable for dipeptides, in general.

1. Introduction

Optically active α -amino acids are very important chiral reagents used in the preparation of a number of commercial pharmaceuticals. Twenty or so amino acids with the same relative configuration as *S*-alanine occur in free form in cellular tissues and fluids of living organisms and are the normal constituents of vegetable and

animal proteins. These natural amino acids may be isolated for synthetic use (including the preparation of dipeptides) from appropriate organisms. Several non-proteinogenic amino acids of opposite hand to the above occur in certain biological systems, but the majority have to be synthesised, as do all unnatural amino acids.

Enantiomerically pure α -amino acids (which are essential for peptide synthesis) may be obtained directly by asymmetric synthesis, or more commonly, by the resolution of racemic products from syntheses using achiral or prochiral reagents. Resolution may be achieved by microbiological or chemical methods [1,2]. Chemi-

* For Part XLI, see R.R. Fenton, F.S. Stephens, R.S. Vagg and P.A. Williams, *Inorg. Chim. Acta*, in press.

¹ Present address: Department of Chemistry, The University, Glasgow G12 8QQ, UK.

* Corresponding author.

cal resolution involves the formation of diastereoisomeric salts or adducts which may be separated by fractional crystallisation or, now more frequently, chromatographic methods.

Both free and derivatised racemic amino acid and dipeptide mixtures have been resolved in the presence of chiral ligands and metal ions by high-performance liquid chromatography (HPLC). The asymmetric secondary ligand, commonly an amino acid derivative or a chiral polyamine, can be a component of the mobile phase [3,4], or be attached covalently to the stationary phase [5–8]. The metal ion is usually a labile, divalent transition metal such as Cu^{2+} , Ni^{2+} or Zn^{2+} , present as a constituent of the mobile phase. Diastereoisomers of inert Co(III) complexes containing a chiral ligand(s) and/or an asymmetric metal centre have been resolved previously by reversed-phase (RP) HPLC [9]. Ion-pairing anions such as *p*-toluenesulphonate, camphorsulphonate and diantimony tartrate, capable of interaction with the complexes and the hydrophobic stationary phase, are commonly used as mobile phase additives to effect or enhance resolution.

The resolution of dipeptides would be of interest, since resolution of the amino acid constituents used for the synthesis would not always be necessary. In this note, the separation of racemic dipeptides as their $[\text{Co}(\text{R,R-benzet})\text{dipeptidato}]^+$ [where benzet = N-benzyl-N'-(2-

picolyl)-1,2-diaminocyclohexane, **I**] diastereoisomeric complexes by RP-HPLC is discussed. Baseline resolution has been achieved in short times without the need for any chiral additives.

2. Experimental

2.1. Preparation of racemic dipeptide complexes

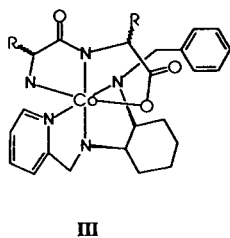
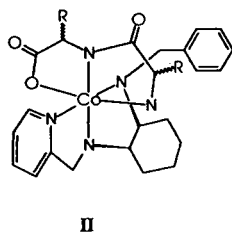
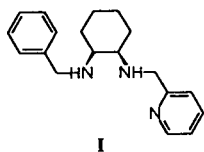
To a stirred suspension of $[\text{Co}(\text{R,R-benzet})\text{Cl}_3]$ [10] (0.15 g, 3.28×10^{-4} mol) in 5 cm³ of water was added 1 mol equivalent of the appropriate dipeptide (Sigma–Aldrich). The mixture was warmed gently with stirring for 15 min, whereupon 4 mol equivalents of triethylamine were added. A deep purple solution immediately resulted. After stirring and warming for a further 45 min, the mixture was cooled to room temperature and applied to a CM-Sephadex column (40 × 1.5 cm) in the Na^+ cycle. The single purple-red band formed upon elution with 0.1 M aqueous NaCl was collected in bulk, and taken to dryness in vacuo at 35°C. The dry residue obtained was desalted twice with methanol to give a deep-purple solid after removal of the solvent in vacuo. ¹H NMR analysis of the dry residue confirmed all solids to be isomeric mixtures of the species represented in **II** and **III** [10].

2.2. Columns

Apex Prepsil ODS 15M (100 × 4.5 mm) and 5M (150 × 4.5 mm) columns were obtained from Jones Chromatography.

2.3. Apparatus

For the chromatographic runs using the phosphate-based mobile phase, a Merck Hitachi L-6200 intelligent pump was used to provide constant mobile phase flow, and a Merck Hitachi L-4200 variable wavelength detector operating at 254 or 480 nm was employed to monitor column eluent. The chromatographic data were recorded and processed with a JCL 6000 computer package (purchased from Jones Chromatography) in conjunction with a Walters personal computer.



For the runs using the *p*-toluenesulphonate-based mobile phase, Gilson 303 dual pumps were employed to control mobile phase flow in combination with a Gilson holochrome variable-wavelength UV-Vis detector operating at 280 or 480 nm. A BBC Coerz Meterawatt SE 120 chart recorder was used to record all the chromatograms.

2.4. Chromatographic procedures

Phosphate buffer solutions were prepared by adjusting a stock solution of NaH_2PO_4 (0.01 M) to the required pH using concentrated H_3PO_4 , and an appropriate amount of HPLC grade acetonitrile and methanol was added thereto. The mixture was filtered through a micropore fibreglass filter paper, and degassed for 5 min under reduced pressure with constant stirring. All runs using this solvent system were performed under isocratic conditions.

p-Toluenesulphonate buffers were prepared in an analogous fashion to the phosphate buffer, but using a stock solution which was 25 mM in *p*-toluenesulphonic acid and adjusting to the required pH using sodium *p*-toluenesulphonate. Both isocratic and gradient elutions were performed using this mobile phase. The ternary Co(III) complexes were introduced by microsyringe as methanolic solutions.

2.5. Removal of glycylglycine from its ternary complex

$\text{C}[\text{Co}(\text{R,R-benzet})(\text{Gly-Gly})]\text{ClO}_4 \cdot 2\text{H}_2\text{O}$ (160 mg) was dissolved in dilute HCl (0.001 M, 150 cm^3) and a potential difference of -1 V was applied for 5 h using an EG & G Princeton Applied Research Model 363 potentiostat (using an Hg working electrode and a Pt counter electrode). During this time, the red colour of the Co(III) complex gradually faded until a very pale pink solution remained. The solution was then neutralised and applied to a CM-Sephadex column (15 \times 1.0 cm) in the Na^+ cycle. The dipeptide was eluted with water and shown to be present by ^1H NMR analysis of the residue remaining after removal of the water. Due to the

small scale of the reduction, no further attempts were made to purify the dipeptide. This method is known to yield enantiomerically pure peptides, quantitatively [11].

3. Results and discussion

It has previously been shown that enantiomerically pure dipeptides give a single diastereoisomer when coordinated to the $[\text{Co}(\text{R,R-benzet})]^{3+}$ nucleus [10]. Therefore, two isomers are to be expected for a racemic dipeptide containing a glycyl fragment, and four isomers for a dipeptide with two asymmetric centres. For Gly-Val, Gly-Leu, Gly-Phe, Leu-Gly, Leu-Ala and Leu-Phe, the diastereomeric products formed by

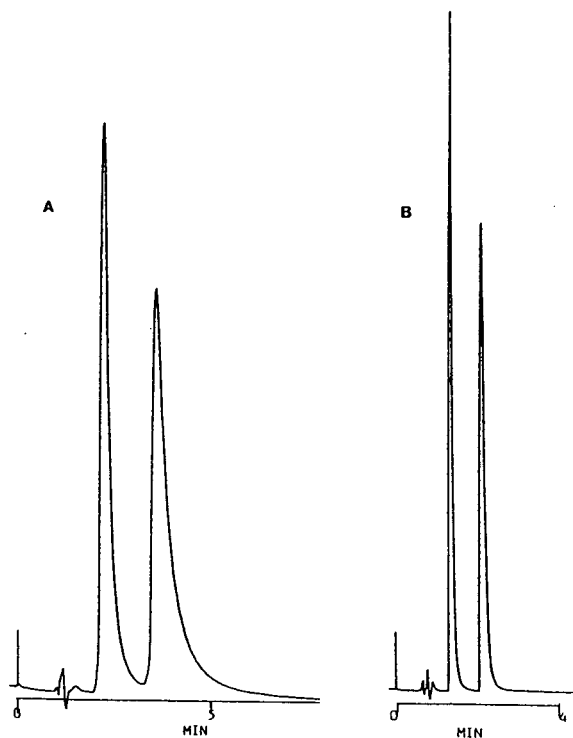


Fig. 1. Separation of the two diastereoisomers of (A) $[\text{Co}(\text{R,R-benzet})(\text{Gly-R,S-Leu})]^+$; 0.01 M phosphate-MeOH-MeCN (pH 4.5) mobile phase; 10 cm 15 μm C_{18} column, flow-rate 2.0 $\text{cm}^3 \text{min}^{-1}$ and (B) $[\text{Co}(\text{R,R-benzet})(\text{Gly-R,S-Val})]^+$; 0.01 M phosphate-MeOH-MeCN (pH 4.5) mobile phase; 10 cm 5 μm C_{18} column, flow-rate 2.0 $\text{cm}^3 \text{min}^{-1}$.

reaction of $[\text{Co}(\text{R,R-benzet})\text{Cl}_3]$ and the racemic dipeptides were not separated by chromatography on CM-Sephadex using aqueous NaCl as eluent. However, all the isomers formed with any particular dipeptide have been completely resolved by RP-HPLC.

The separation of the two diastereoisomers of Gly-*R,S*-Val and Gly-*R,S*-Leu using an aqueous phosphate-MeCN-MeOH mobile phase is shown in Fig. 1. Retention times for these and the other complexes using this solvent system are listed in Table 1. Baseline resolution has been achieved in all cases, with the sole exception of Leu-Gly, within a short time (order of minutes).

In the pH range 2.0–5.0, little change was observed in retention times for the complexes, although the quality of the separation was reduced at the upper limit as the peaks became broadened. Optimum resolution and peak shape was achieved at a pH of 3.0. In a series of runs employing $[\text{Co}(\text{R,R-benzet})(\text{Gly-}\text{R,S-Phe})]$, variation of retention times and separation factors with varying phosphate concentration and methanol proportion was assessed. Small de-

creases in retention times and separation were observed with increasing total PO_4^{3-} concentration, coinciding with improved peak shape and chromatographic profile. The slowest eluted diastereoisomer was observed as a broad hump at low MeOH proportion, but gradually sharpened as the ratio was increased.

For Gly-Val and Gly-Leu, the complex containing the dipeptide with the *R* stereochemistry is eluted first, an observation noted also for Leu-Gly. $[\text{Co}(\text{R,R-benzet})(\text{S-Leu-S-Ala})]^+$ has the longest retention time of the diastereoisomers containing this dipeptide. Although the order of elution is only known completely for Gly-Val, Gly-Leu and Leu-Gly, the above observations imply that complexes of dipeptides with *S* chiral centres are more efficiently retained on the ODS column than their counterparts with the *R* stereochemistry. A pattern such as this is not entirely surprising, when it is considered that all the complexes are believed to possess a common topology at the metal centre ($[\text{OC-6-64-C}]$) [10]. Similar interactions would be expected within the series of complexes with the *S* stereo-

Table 1
Retention times (t_n) and their ratios for the $[\text{Co}(\text{R,R-benzet})(\text{dipeptidato})]^+$ complexes

Peptide	t_n (min)	t_2/t_1	t_3/t_2	t_4/t_3
Gly- <i>R,S</i> -Val	1.10	2.00		
	2.20			
Gly- <i>R,S</i> -Leu	1.86	1.86		
	3.46			
Gly- <i>R,S</i> -Phe	2.22	2.06		
	4.58			
<i>R,S</i> -Leu-Gly	2.09	2.67		
	2.67			
<i>R,S</i> -Leu- <i>R,S</i> -Ala	2.36	1.29	1.26	1.38
	3.04			
	3.84			
	5.29			
<i>R,S</i> -Leu- <i>R,S</i> -Phe	6.48	1.23	1.66	1.66
	8.00			
	13.28			
	22.08			

All runs performed under isocratic conditions using a 10 cm, 15 μm C_{18} silica column and an MeOH-MeCN-aqueous phosphate buffer (10:30:60) mobile phase initially 25 mmol in total PO_4^{3-} adjusted to pH 4.5; flow-rate 2.0 $\text{cm}^3 \text{min}^{-1}$. n refers to the number of the peak.

chemistry, and likewise the complexes containing *R* peptides. It is, however, not possible to ascertain the exact nature of the interactions leading to the observed separation, but the pendant benzene ring of the triamine and the side-chain of the dipeptide would be expected to have an affinity for the octadecyl residues of the stationary phase. In addition, the amine hydrogens and the hydrogen phosphate anions could form ion-pairs in solution.

Baseline separation was not fully achieved for Leu–Gly, and to a lesser extent for Leu–Ala, using the isocratic phosphate mobile phase. Improved resolution resulted when an aqueous *p*-toluenesulphonate solvent system was employed. Long retention times and fairly broad, but well-separated peaks were observed with isocratic elution. Gradient elution gave baseline separation in shorter times with improved peak shape, but with reduced values for ratios of retention times.

The dipeptides are not readily released from their Co(III) complexes by treatment with H₂S or aqueous Na₂CO₃, but may be recovered by an electrolytic method as outlined in the Experimental section. The small scale of the syntheses made it impractical to perform the reduction on all the complexes; details concerning the complex containing Gly–Gly are given as being typical. However, the method is applicable to all the complexes isolated and may be used for the resolution of other dipeptides not examined in this study [11].

In conclusion, several racemic dipeptides have

been resolved by prior formation of ternary Co(III) complexes with the chiral triamine *R,R*-benzet and subsequent separation of resultant ternary species by RP-HPLC. Two aqueous mobile phases have been successfully employed, and conditions optimised in each case. Complete separation of the diastereoisomers has been achieved in all cases within minutes.

References

- [1] J.P. Greenstein and M. Winitz, *Chemistry of the Amino Acids*, Vol. 1, Wiley, New York, 1961.
- [2] J. Jacques, A. Collet and S.H. Wilen, *Enantiomers, Racemates and Resolutions*, Wiley-Interscience, New York, 1981; and references cited therein.
- [3] W. Linder, J.N. LePage, G. Davies, D.E. Seitz and B.L. Karger, *J. Chromatogr.*, 185 (1979) 323.
- [4] Y. Tapuhi, N. Miller and B.L. Karger, *J. Chromatogr.*, 205 (1981) 325.
- [5] A. Foucault, M. Caude and L. Oliveros, *J. Chromatogr.*, 185 (1979) 345.
- [6] Yu.A. Zolotarev, D.A. Zeitzov, V.I. Penkina, I.N. Dostavalov and N.F. Myasoyedov, *J. Radioanal. Nucl. Chem.*, 121 (1988) 469.
- [7] K. Sugden, C. Hunter and G. Lloyd-Jones, *J. Chromatogr.*, 192 (1980) 228.
- [8] K. Saito, Y. Yuchi, H. Kimoto, T. Hishida and M. Hasegawa, *Bull. Chem. Soc. Japan*, 61 (1988) 322.
- [9] D.A. Buckingham, *J. Chromatogr.*, 313 (1984) 93.
- [10] P.D. Newman, P.A. Williams, F.S. Stephens and R.S. Vagg, *Inorg. Chim. Acta*, 183 (1991) 145.
- [11] C.R. Clark, R.F. Tasker, D.A. Buckingham, D.R. Knighton, D.R.K. Harding and W.S. Hancock, *J. Am. Chem. Soc.*, 103 (1981) 7023.



ELSEVIER

Journal of Chromatography A, 693 (1995) 371–375

JOURNAL OF
CHROMATOGRAPHY A

Short communication

Determination of Methocel A15-LV cellulose ether in blends with microcrystalline cellulose

Sergio S. Cutié*, Charles. G. Smith

Analytical Sciences, Materials Science Characterization, 1897D Building, The Dow Chemical Company, Midland, MI 48667, USA

Received 21 September 1994; accepted 14 November 1994

Abstract

Methocel (trademark of Dow Chemical) A15-LV cellulose ether is mixed with microcrystalline cellulose and used in pharmaceutical formulations to coat slow release drugs. An analysis was needed to monitor the efficiency of the mixing of Methocel cellulose ether with the microcrystalline cellulose. The similarities in chemical structure of Methocel cellulose ether and cellulose made it extremely difficult for some spectroscopy techniques to distinguish between them. An extraction technique followed by separation in a size-exclusion chromatography column with refractive index detector was developed and validated and successfully used to monitor Methocel cellulose ether in cellulose. Also developed was a direct pyrolysis–capillary gas chromatography technique with flame ionization detector that generates equivalent results to the extraction–size-exclusion chromatographic technique. Due to limitations imposed by the requirement for small samples, the pyrolysis–GC approach is not as reproducible as the extraction–size-exclusion chromatographic procedure.

1. Introduction

Methocel (trademark of Dow Chemical) cellulose ethers are increasingly being used [1–3] in pharmaceutical applications. (Methocel A-15 LV, a low-molecular-mass polymer, is mixed with microcrystalline cellulose which is widely used in pharmaceutical applications [4–6] to make slow release drug formulations.) Microcrystalline cellulose is a non-fibrous form of cellulose in which the cell wall of plant fibers has been broken into fragments ranging in size from a few hundred micrometers to a few tenths of a micrometer in

length. Cellulose is insoluble in water while Methocel A15-LV cellulose ether is soluble. Microcrystalline cellulose acts like a pressure-sensitive adhesive and when tablets containing this material are placed in water, there is rapid disintegration, but no dissolution. Approximately 5% of Methocel cellulose ether is added to microcrystalline cellulose and there exists a need to determine how accurate the mixing process is. After some minor modifications, an extraction procedure followed by size-exclusion chromatography (SEC), previously used to determine concentrations of polyacrylic acid in water at the ppm level [7], was used to determine the Methocel cellulose ether content of a blended sample SG-955. Pyrolysis–gas chromatography

* Corresponding author.

(Py-GC) was evaluated as an alternate technique for this analysis.

2. Experimental

2.1. SEC

A series of standards containing from 1.7 to 7.4% Methocel A15-LV cellulose ether were prepared by shaking appropriate masses of this polymer and the microcrystalline cellulose overnight on a flatbed shaker. About 0.02 g of these standards and the blended sample were extracted for 2 h by placing samples vials with about 10 g of 0.05 M sodium chloride using a mechanical shaker for solution agitation. After removal from the shaker, the samples were held for about 10 min to allow for phase separation. Aliquots of each extract were filtered (0.45- μ m filter) before injection into the SEC apparatus. Instrumental parameters for this analysis are summarized in Table 1.

2.2. Py-GC

Portions of Methocel A15-LV cellulose ether, microcrystalline cellulose, a blended sample (SG-955), and the standard mixtures were weighed (52–562 μ g) into quartz tubes. These sample tubes were placed into a Pt coil and equilibrated 10 min in the 200°C interface connected to the injection port of an HP5890 gas chromatograph equipped with dual flame ionization detectors. The sample was subsequently pyrolyzed (CDS 120 Pyroprobe; ramp = Off, interval = 20 s) at a set temperature of 500°C. Pyrolysis products were split between a 60 m \times

0.2 mm) capillary column (J & W DB WAX; 0.25 μ m film) and a 6 ft. \times 1/8 in. stainless-steel column (1 ft. = 30.48 cm; 1 in. = 2.54 cm), packed with 0.1% SP1000 on Carbopack C (80–100 mesh). These columns were simultaneously programmed from 50°C (4 min) to 220°C at 6°C/min and the dual column separations were monitored with PE Nelson Turbochrom 3.3 software.

3. Results and discussion

3.1. SEC

The response of the refractive index detector was found to be linear for Methocel A15-LV cellulose ether from 30 to 340 ppm as shown in the plot of Fig. 1. Fig. 2 compares the SEC chromatograms for extracts from the microcrystalline cellulose blend, microcrystalline cellulose, and the Methocel A15-LV cellulose ether. The cellulose ether is distinctly apparent as a positive peak response at a retention time of about 5.3 min.

3.2. Accuracy study

To determine the recovery of known amounts of Methocel A15-LV cellulose ether from blends with microcrystalline cellulose, fourteen replicate portions of the blended standards were extracted and the extracts were analyzed by SEC. Results

Table 1
Instrument parameters for SEC analysis

Column	1 TSK G1000 PW
Detector	Refractive index; Waters Model 410
Eluent	0.05 M Sodium chloride
Integration	PE Nelson Turbochrom 3.3
Flow	1 ml/min
Injection	100 μ l

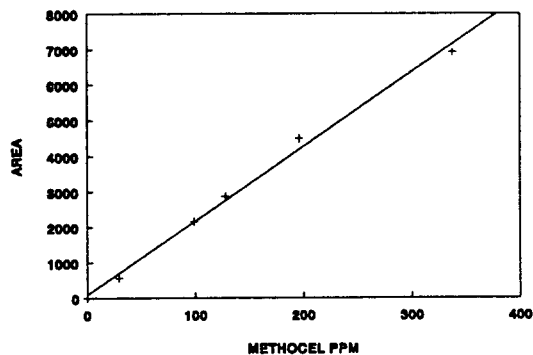


Fig. 1. Linearity curve for the refractive index detector. $y = 20.8791x + 88.0173$.

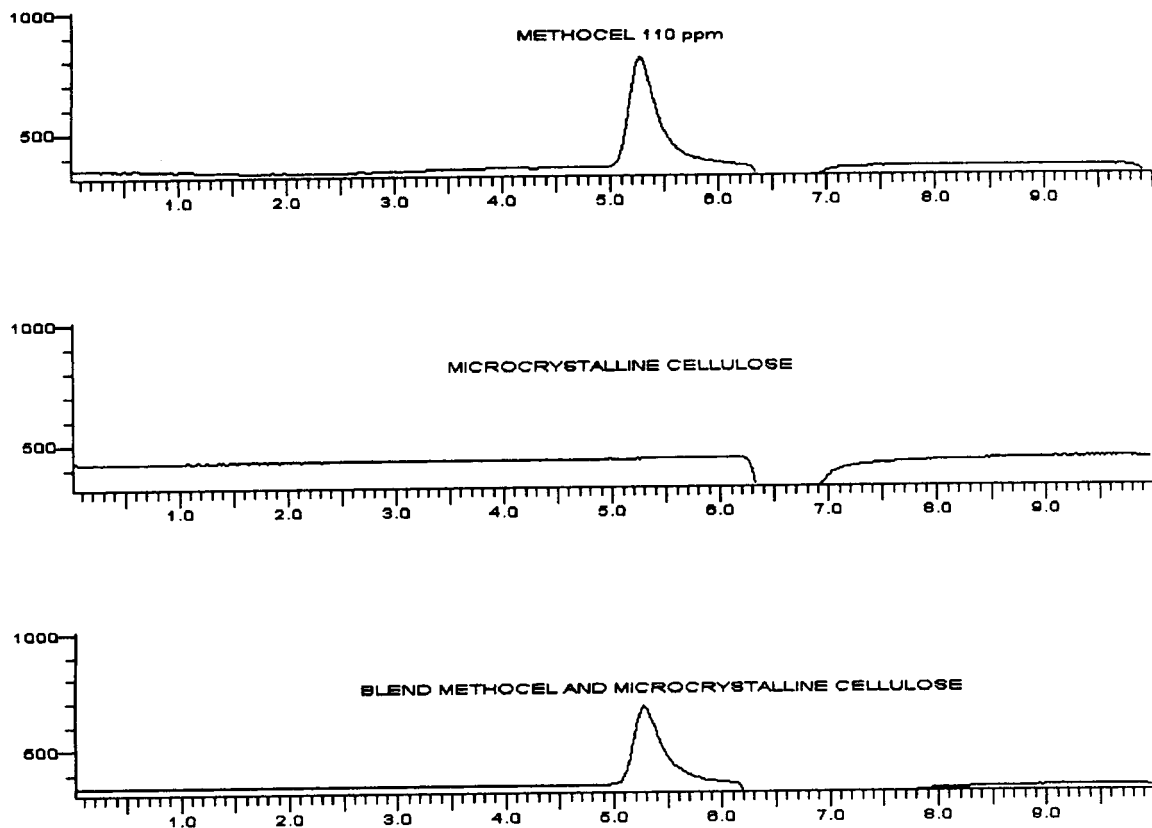


Fig. 2. Comparison of size-exclusion chromatograms.

showed average recoveries of 96% with a standard deviation of 6.9% and a range of 88 to 110%.

3.3. Precision study

To estimate the precision of the extraction-SEC procedure, eleven portions of a standard blend (5.9% Methocel A15-LV cellulose ether) were extracted and analyzed over a two day period. Results showed a relative standard deviation of $\pm 14.2\%$ at the 95% confidence level.

3.4. Py-GC

Initially, samples of the Methocel A15-LV cellulose ether, microcrystalline cellulose, and blended standards were pyrolyzed at a set tem-

perature of 700°C. Pyrograms for these runs contained several peaks from the microcrystalline cellulose that interfered with the major peak from pyrolysis of the cellulose ether. Using a lower set pyrolysis temperature (500°C), however, resulted in pyrograms with fewer interferences from the microcrystalline cellulose as shown in the comparison of Fig. 3.

Portions (454–562 μg) of the powdered standard blends (1.7–7.4% Methocel A15-LV cellulose ether) and microcrystalline cellulose, were pyrolyzed at a set temperature of 500°C. Pyrolysis products were split and separated using the dual-column system, then the area of a unique Methocel A15-LV cellulose ether pyrolysis product (9.1 min on the capillary DB WAX column) was plotted against the mass of cellulose ether pyrolyzed for each standard blend. The resulting curve (Fig. 4) showed a linear correla-

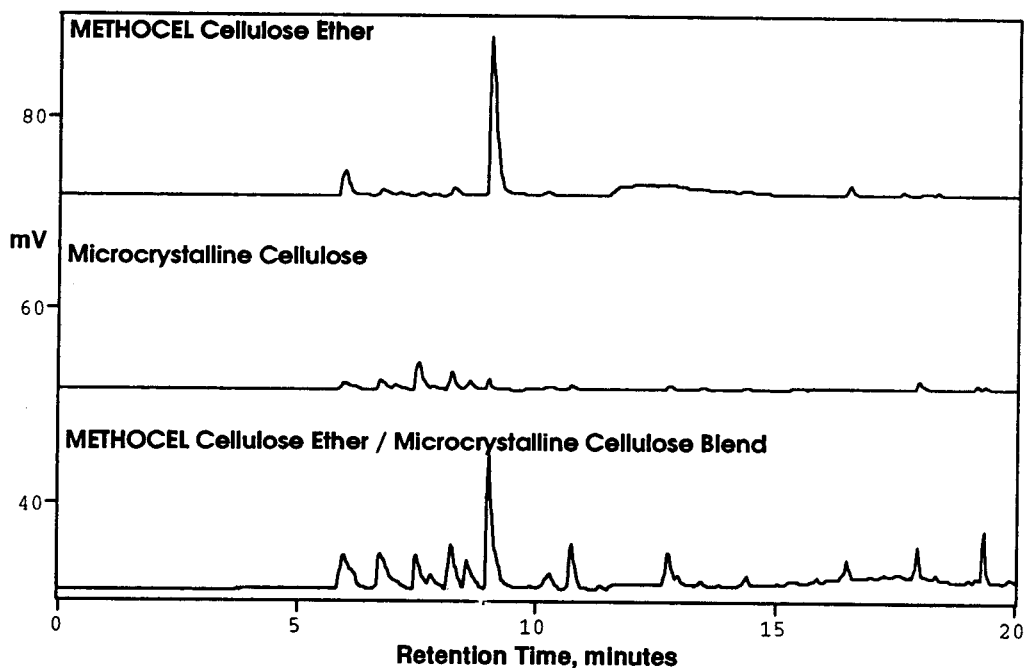


Fig. 3. Comparison of partial 500°C pyrograms for Methocel A15-LV, microcrystalline cellulose, and a blended sample.

tion over the range of the prepared standard blends.

To estimate the reproducibility of pyrolysis data, duplicate portions of the 5.9% Methocel cellulose ether standard blend and three portions

of the SG-955 blend, were weighed, pyrolyzed and chromatographed using the dual-column system. Using the average response factor (μg Methocel cellulose ether per area at 9.1 min) from capillary chromatography of the standard

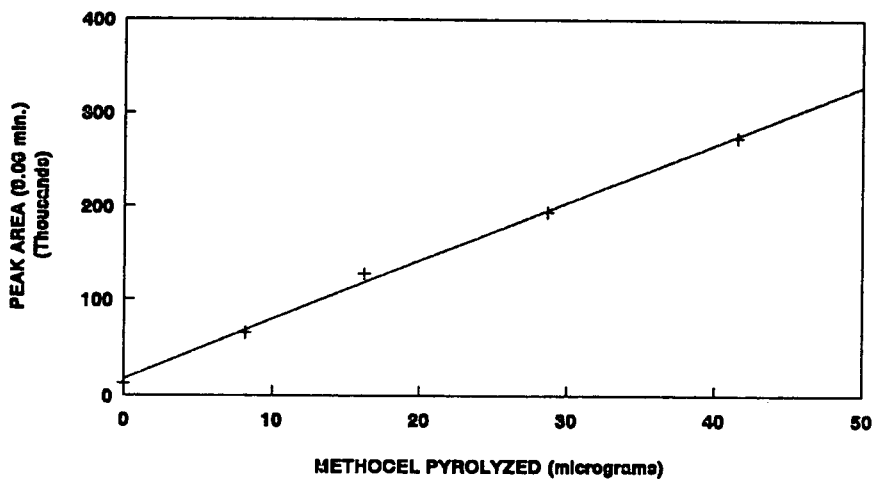


Fig. 4. Correlation curve for Methocel A15-LV cellulose ether concentration and pyrolysis response at 9.1 min. $y = 6245.836x + 16430.2497$.

blend, the Methocel cellulose ether content of the SG-955 blend was calculated at 4.0, 5.4, 5.8% (average = 5.1%). These data highlight a flaw in the Py-GC technique for quantitative analysis of this type of insoluble sample. The technique is not as reproducible as the extraction-SEC approach because of (1) errors in weighing small samples and (2) possible non-uniform distribution of components in the sample. Consequently, the extraction-SEC procedure is preferred for the determination of Methocel A15-LV cellulose ether in blends with microcrystalline cellulose.

References

- [1] I. Lichnerov, J. Heinrich and J. Rak, *Ceska Slov. Farm.*, 43 (1994) 22–25.
- [2] K. Mitchell, J.L. Ford, D.J. Armstrong, P.N. Elliott, C. Rostron and J.E. Hogan, *Int. J. Pharm.*, 100 (1993) 155–163.
- [3] G. Agoes, U. Maru and R. Setiadi, *Acta Pharm. Indones.*, 14 (1989) 1–10.
- [4] H. Miyamoto, *Pharm. Tech. Jpn.*, 10 (1994) 321–330.
- [5] L.S. Wan, Prasad and P.P. Kanneganti, *Int. J. Pharm.*, 41 (1988) 159–167.
- [6] M. Landin, R. Martinez-Pacheco, J.L. Gomez-Amoza, C. Souto, A. Concheiro and R.C. Rowe, *Int. J. Pharm.*, 91 (1993) 143–149.
- [7] S.S. Cutié, W.C. Buzanowski and J.W. Berdasco, *J. Chromatogr.*, 513 (1990) 93–105.

Short communication

Quantitative analysis by gas chromatography of volatile carbonyl compounds in cigarette smoke

Takashi Miyake, Takayuki Shibamoto*

Department of Environmental Toxicology, University of California, Davis, CA 95616, USA

First received 26 May 1994; revised manuscript received 28 November 1994; accepted 29 November 1994

Abstract

The cigarette smoke from 26 commercial brands was drawn into a separatory funnel containing an aqueous cysteamine solution. Almost the entire smoke from a cigarette was trapped as mainstream cigarette smoke. The carbonyl compounds in the smoke were derivatized to thiazolidines and were then quantitatively analyzed by gas chromatography with nitrogen–phosphorus detection. Total carbonyl compounds recovered ranged from 2.37 to 5.14 mg/cigarette. The general decreasing order of the carbonyl compounds yielded was acetaldehyde, butanal, hexanal, propanal, acetone, octanal, 2-methylpropanal and formaldehyde. Acetaldehyde was the major aldehyde in the smoke sample from 26 brands and it made up 46–72% of the total carbonyl compounds in the sample. Amounts of formaldehyde ranged from 73.8 to 283.8 $\mu\text{g}/\text{cigarette}$. It is hypothesized that these carbonyl compounds form from lipid and wax constituents in tobacco leaves.

1. Introduction

In the last three decades, tremendous numbers of chemicals have been isolated and identified in cigarette smoke as a result of the refinement of advanced analytical instruments such as the gas chromatograph–mass spectrometer. Consequently, the presence of many toxic chemicals such as polynuclear aromatic hydrocarbons [1], N-nitrosamines [2] and volatile aldehydes [3,4] have been identified in cigarette smoke. These chemicals in smoke are deposited directly into the blood following inhalation. In contrast to benzo[*a*]pyrene and N-nitrosornicotine which require enzyme activation to be toxic [5], reactive

aldehydes such as formaldehyde and acetaldehyde can directly cross-link to proteins and bind covalently to nucleic acids [6–8], and consequently cause biological complications including carcinogenesis [9–12]. For example, formaldehyde reportedly induced squamous cell carcinoma in the nasal cavity of rats upon repeated inhalation [13]. Acetaldehyde is also capable of inducing nasal carcinomas in experimental animals [14].

The quantitation of these toxic aldehydes in cigarette smoke is of great importance because tobacco smoking is one of the major causes of aldehyde contamination of indoor air [15]. For example, formaldehyde in sidestream cigarette smoke can mean considerable exposure for the non-smoker through passive smoking [16]. According to the technical support document pre-

* Corresponding author.

pared by the California Environmental Protection Agency/Air Resources Board [17], ambient acetaldehyde is an air pollutant which may cause or contribute to an increase in mortality or an increase in serious illness, or which may pose a present or potential hazard to human health based on the findings of carcinogenicity and the results of the risk assessment.

Some highly volatile or reactive compounds such as formaldehyde, acetaldehyde and acrolein are still extremely difficult to analyze. There are, therefore, only a few reports on direct analysis of these reactive carbonyls in cigarette smoke [18]. There are also very few reports on accurate quantitative analysis of volatile carbonyl compounds in cigarette smoke. Most commonly used analytical methods for volatile carbonyl compounds involve derivatization with 2,4-dinitrophenylhydrazine (2,4-DNP) and the resulting derivatives are determined by GC or HPLC. After the 2,4-DNP method was used to determine formaldehyde in cigarette smoke in the 1960s [19], many volatile carbonyl compounds have been identified in cigarette smoke using this method. For example, formaldehyde (25–69 $\mu\text{g}/\text{cigarette}$) and acetaldehyde (752–1234 $\mu\text{g}/\text{cigarette}$) were reported in mainstream cigarette smoke [20].

We recently developed a simple and sensitive analytical method to identify volatile carbonyl compounds in foods and beverages [21,22]. This method involves derivatization of carbonyl compounds with cysteamine to yield stable thiazolidines. The resulting thiazolidines are determined by GC with a fused-silica capillary column and nitrogen–phosphorus detection (NPD). Cysteamine readily reacts with carbonyl compounds at room temperature and neutral pH. The only drawback of this method is that cysteamine does not react with α,β -unsaturated aldehydes such as acrolein. Vapor-phase formaldehyde was satisfactorily analyzed using this derivatization method [23]. In the present study, vapor-phase carbonyl compounds formed in the cigarette smoke from various commercial brands were quantitatively analyzed using the above method.

2. Experimental

2.1. Materials

All cigarette samples were bought from local markets and stored in sealed packages until used. Cysteamine hydrochloride, thiazolidine and 2,4,5-trimethylthiazole were purchased from Aldrich, Milwaukee, WI, USA. The standard stock solution of 2,4,5-trimethylthiazole was prepared by adding 10 mg of 2,4,5-trimethylthiazole to 1 ml of chloroform; it was stored at 5°C. The authentic thiazolidines were synthesized according to the method reported previously [22,24].

2.2. Sample preparations

Cysteamine hydrochloride (0.8 g) was dissolved in 200 ml of deionized water and the pH of the solution was adjusted to 8 with a 6 M NaOH solution. The cysteamine solution (approximately 200 ml) was placed in a 1000-ml separatory funnel whose headspace was evacuated at 8.4 mmHg (1 mmHg = 133.322 Pa) for 10 min. Immediately after a cigarette was lit, about 1 mm of the other end of the cigarette was inserted in the tip of the separatory funnel. Most cigarettes were fitted into the tip of the funnel. Cigarettes with a diameter smaller than the inside diameter of the tip of the funnel were wrapped with masking tape in order to fit. The cock of the separatory funnel was opened gradually to draw the smoke into the separatory funnel. It took 20 s to completely smoke one cigarette. After smoke was sucked into the separatory funnel, the funnel was shaken for 5 min in order to let the carbonyl compounds in the smoke react thoroughly with the cysteamine. After the pH of the reaction mixture was adjusted to 7 with a 1 M HCl solution, it was extracted with 50 ml of chloroform using a liquid–liquid continuous extractor for 3 h. The extract was dried over anhydrous sodium sulfate for 12 h. After removal of the sodium sulfate, the volume of the extract was adjusted to exactly 50 ml with chloroform. A standard solution of 2,4,5-trimethylthiazole (100 μl) was added as an

internal standard prior to GC analysis. An aqueous solution (200 ml) containing 0.8 g of cysteamine was extracted with 50 ml chloroform at pH 8, the same as for the smoke samples, and the extract was used as a blank sample.

2.3. Instrumental analysis

A Hewlett-Packard (HP) Model 5890A GC system equipped with a NPD system and a 30 m × 0.25 mm I.D. (film thickness, $d_f = 1 \mu\text{m}$) DB-1 bonded phase fused-silica capillary column was used for quantitative analysis of thiazolidines. The oven temperature was programmed from 60 to 180°C at 4°C/min and held for 10 min. Peak areas were integrated with a Tsp SP 4400 series integrator. The injector and detector temperatures were 250°C. The linear velocity of helium carrier gas was 30 cm/s. The quantitative analysis was conducted according to the internal standard method previously reported [25].

A HP Model 5890 series II GC system interfaced to a HP 5971 mass spectrometer was used to confirm the thiazolidine derivatives in the samples. The GC conditions were as above. The mass spectra were obtained by electron impact ionization at 70 eV and an ion source temperature of 250°C.

3. Results and discussion

The optimum yield of each thiazolidine from the reaction of a corresponding aldehyde and cysteamine was previously obtained at pH 8 in our laboratory [26]. In the present study, the recovery efficiencies of the carbonyl compounds from an aqueous solution were 92.8% for formaldehyde, 96.0% for acetaldehyde, 98.2% for acetone, 95.3% for propanal, 93.0% for 2-methylpropanal, 92.3% for butanal, 88.0% for hexanal and 99.8% for octanal (the values are the mean of four replications). The NPD detection limits of each aldehyde were 5.8 pg for formaldehyde, 6.9 pg for acetone, 7.1 pg for acetaldehyde, 10.0 pg for propanal, 12.5 pg for

2-methylpropanal, 14.4 pg for butanal, 24.7 pg for hexanal and 36.5 pg for octanal.

As mentioned above, the most commonly used derivative for analysis of volatile carbonyl compounds is 2,4-DNP. There are several HPLC methods for the separation of 2,4-DNP derivatives obtained from carbonyl compounds present in cigarette smoke [20,27,28]. However, HPLC analysis of the 2,4-DNP derivatives is difficult because they produce *syn*- and *anti*-forms except in the case of formaldehyde. Moreover, preparation of 2,4-DNP derivatives requires a strong acidic condition which may alter the chemicals of interest. In contrast to 2,4-DNP preparation, carbonyl compounds readily react with cysteamine at neutral pH and room temperature.

Many different kinds of smoking machines which are constructed to simulate human smoking have been used for the study of cigarette smoke [29]. The amounts of smoke collected in the present study are not similar to those inhaled

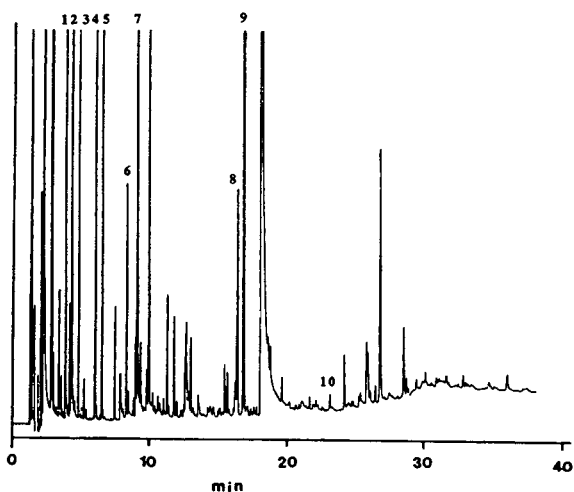


Fig. 1. A typical gas chromatogram of the extract from cigarette smoke (cigarette N) trapped in a cysteamine solution. Peaks: 1 = thiazolidine (formaldehyde); 2 = 2-methylthiazolidine (acetaldehyde); 3 = 2,2-dimethylthiazolidine (acetone); 4 = 2,4,5-trimethylthiazole (internal standard); 5 = 2-ethylthiazolidine (propanal); 6 = 2-isopropylthiazolidine (2-methylpropanal); 7 = 2-propylthiazolidine (butanal); 8 = 2-pentylthiazolidine (hexanal); 9 = (*S*)-(-)-nicotine; 10 = 2-heptylthiazolidine (octylaldehyde).

by a smoker because a smoking machine was not used. All of the smoke trapped in the present study might be classified as mainstream cigarette smoke.

Fig. 1 shows a typical GC–NPD separation of the chloroform extract from the cigarette smoke trapped in a cysteamine solution. All peaks in this chromatogram contain one or more nitrogen atoms. Table 1 presents the results of quantitative analysis of volatile carbonyl compounds. The greatest and the least amounts of total carbonyl compounds obtained were 5.135 and 2.365 mg/cigarette, respectively. There was no

significant difference in aldehyde formation in menthol and non-menthol cigarettes. With a few exceptions, the general decreasing order of each aldehyde yielded was acetaldehyde, butanal, hexanal, propanal, acetone, octanal, 2-methylpropanal and formaldehyde. For example, the amount of formaldehyde (237.5 μg) recovered was the second largest (after acetaldehyde) in the case of one cigarette.

Acetaldehyde was the major aldehyde in the smoke from all brands analyzed in the present study. Acetaldehyde as a percentage of the total carbonyl compounds ranged from 49.1 to 72.1.

Table 1

Amounts of formaldehyde (FA), acetaldehyde (AA), acetone, propanal (PA), 2-methylpropanal (2-MPA), butanal (BA), hexanal (HA) and octanal (OA) yielded in the smoke from various brands of cigarettes

Cigarette brand	Amounts ($\mu\text{g}/\text{cigarette}$)							
	FA	AA	Acetone	PA	2-MPA	BA	HA	OA
A ^{a,b}	101.4 \pm 10.0	2154 \pm 280.7	206.7 \pm 70.5	245.5 \pm 53.4	111.6 \pm 18.5	441.0 \pm 66.4	234.0 \pm 51.8	166.7 \pm 47.8
B ^{a,b}	265.7 \pm 33.9	2109 \pm 119.7	188.9 \pm 31.4	256.6 \pm 36.5	100.2 \pm 17.8	374.2 \pm 43.6	331.1 \pm 52.8	288.3 \pm 56.5
C ^{a,b}	109.2 \pm 12.0	2024 \pm 105.1	239.3 \pm 41.7	250.0 \pm 33.1	122.3 \pm 16.6	462.4 \pm 66.7	380.9 \pm 45.0	194.2 \pm 53.2
D ^a	176.7 \pm 23.7	2274 \pm 62.6	206.7 \pm 46.3	245.6 \pm 23.1	92.4 \pm 9.1	175.4 \pm 31.1	112.2 \pm 55.4	82.0 \pm 38.4
E ^a	157.5 \pm 5.4	2815 \pm 11.9	559.0 \pm 21.9	349.3 \pm 17.4	147.7 \pm 5.2	601.9 \pm 40.7	289.5 \pm 48.5	177.3 \pm 42.4
F ^a	79.1 \pm 6.9	1722 \pm 34.0	154.4 \pm 39.9	198.0 \pm 24.8	80.2 \pm 6.8	166.7 \pm 41.9	157.1 \pm 42.8	87.4 \pm 45.1
G ^a	237.5 \pm 7.8	1924 \pm 28.1	203.3 \pm 29.9	228.3 \pm 21.7	90.8 \pm 7.3	319.6 \pm 29.7	180.1 \pm 61.2	148.9 \pm 64.3
H ^a	138.8 \pm 11.5	2221 \pm 253.4	236.6 \pm 45.5	236.1 \pm 48.5	97.4 \pm 16.6	539.5 \pm 1.9	165.0 \pm 67.1	165.3 \pm 46.1
I ^a	73.8 \pm 5.0	2030 \pm 130.6	191.3 \pm 41.0	233.8 \pm 42.2	105.0 \pm 20.5	155.3 \pm 49.4	180.5 \pm 64.0	101.7 \pm 51.5
J ^a	87.6 \pm 8.0	2245 \pm 46.4	395.3 \pm 7.7	257.1 \pm 18.2	110.3 \pm 5.0	296.5 \pm 24.0	179.1 \pm 49.4	97.6 \pm 30.6
K ^a	123.9 \pm 18.5	2166 \pm 107.0	233.4 \pm 34.5	253.0 \pm 37.0	103.0 \pm 17.5	395.1 \pm 32.1	190.7 \pm 48.5	76.1 \pm 35.7
L ^a	84.6 \pm 15.8	1706 \pm 15.6	132.7 \pm 23.9	186.0 \pm 27.1	68.5 \pm 10.8	88.6 \pm 13.0	102.1 \pm 56.9	–
M ^a	118.6 \pm 10.2	2099 \pm 12.7	136.8 \pm 46.7	207.0 \pm 59.8	77.9 \pm 19.3	236.5 \pm 39.4	144.2 \pm 75.5	55.2 \pm 39.1
N ^{a,c}	143.8 \pm 20.5	2377 \pm 35.2	249.2 \pm 110.5	226.7 \pm 89.7	81.5 \pm 32.3	433.0 \pm 145.1	209.4 \pm 74.5	76.0 \pm 39.6
O ^{a,c}	115.7 \pm 9.6	2015 \pm 103.1	246.7 \pm 35.4	242.0 \pm 41.8	98.2 \pm 12.2	287.8 \pm 47.0	225.8 \pm 62.2	120.4 \pm 28.3
P ^d	119.4 \pm 9.5	2902 \pm 12.0	278.5 \pm 30.0	316.3 \pm 21.2	133.1 \pm 5.5	429.2 \pm 28.1	314.0 \pm 48.9	157.0 \pm 32.8
Q ^d	206.1 \pm 17.3	2706 \pm 63.8	283.4 \pm 75.0	298.3 \pm 50.3	132.2 \pm 17.3	553.8 \pm 161.6	297.4 \pm 84.4	217.3 \pm 34.0
R ^d	183.3 \pm 5.6	2591 \pm 30.6	255.9 \pm 18.1	304.6 \pm 18.0	122.2 \pm 3.7	787.7 \pm 12.1	368.1 \pm 42.0	258.2 \pm 93.4
S ^d	107.2 \pm 16.7	1990 \pm 43.5	202.3 \pm 17.9	230.8 \pm 17.6	92.8 \pm 4.0	119.9 \pm 17.8	133.6 \pm 42.7	–
T ^d	125.2 \pm 6.2	2705 \pm 33.9	619.4 \pm 17.6	336.2 \pm 34.4	140.9 \pm 12.1	514.1 \pm 25.8	144.2 \pm 35.9	124.5 \pm 31.9
U ^d	125.7 \pm 13.2	2356 \pm 174.6	210.4 \pm 32.8	275.9 \pm 31.7	114.2 \pm 5.9	440.8 \pm 100.2	300.5 \pm 67.4	187.1 \pm 67.0
V ^d	122.8 \pm 7.4	1909 \pm 52.9	153.7 \pm 19.2	217.6 \pm 28.0	87.5 \pm 7.6	142.8 \pm 13.9	124.9 \pm 32.7	–
W ^{d,c}	123.3 \pm 10.1	2403 \pm 46.5	220.8 \pm 17.4	268.6 \pm 16.2	105.9 \pm 3.9	115.6 \pm 16.8	137.4 \pm 47.5	98.5 \pm 44.1
X ^c	205.6 \pm 8.7	2315 \pm 59.1	312.8 \pm 20.9	284.7 \pm 20.9	115.9 \pm 3.1	519.0 \pm 43.7	261.9 \pm 55.8	197.0 \pm 70.6
Y ^c	151.3 \pm 10.1	1491 \pm 177.1	142.1 \pm 42.1	171.1 \pm 41.3	76.3 \pm 15.7	413.7 \pm 60.1	212.1 \pm 58.5	128.2 \pm 35.6
Z ^c	283.8 \pm 26.2	2521 \pm 78.6	312.7 \pm 61.9	302.0 \pm 22.8	115.0 \pm 10.9	928.3 \pm 149.5	369.9 \pm 74.4	308.3 \pm 103.3

^a Regular size.

^b No filter.

^c Menthol.

^d King size.

^e Super king size.

The amounts of acetaldehyde recovered ranged from 1.5 to 2.9 mg. Butanal was found in large amounts in the smoke from some cigarettes. For example, it composed 18% of the smoke in the case of one cigarette.

The precursors and formation mechanisms of these volatile carbonyl compounds in the cigarette smoke are not yet well understood. However, it is well known that these carbonyl compounds are formed from lipids by heat treatment [30–33]. Tobacco contains certain amounts of lipids [34] and waxes [35] which may be precursors of these carbonyl compounds. Aldehydes and ketones have been reportedly formed from heat treatment of various lipids via oxidative cleavage of the double bond; examples include beef fats [3,31], pork fat [32] and corn oil [33]. Oxidative degradation of squalene isolated from tobacco smoke [36] also yielded formaldehyde, acetaldehyde, and acetone [37]. It was proposed that many low-molecular-mass radicals such as $\cdot\text{OH}$, $\cdot\text{CHO}$, $\cdot\text{CH}_2\text{CHO}$, $\cdot\text{CH}_3$, and $\cdot\text{COCH}_3$ were formed from lipids upon oxidative degradation and that these radicals combine to form low-molecular-mass aldehydes [38]. Presence of radicals has been recognized in the cigarette smoke by using an electron spin resonance spectrometer [39].

4. Conclusions

The sample collection method developed in the present study does not require a large, heavy trapping device. Once flasks are vacuumed, they can be carried to any place to collect smoke samples in order to monitor toxic carbonyl compounds contamination in the ambient air. The analytical method used for volatile carbonyl compounds in cigarette smoke in the present study is simple, highly sensitive, and specific. Also, baseline separation of all thiazolidine derivatives was obtained with a high resolution fused-silica capillary column. The cigarette smoke trapped in the present study is not comparable to that trapped using a cigarette machine. Comparison of the levels of carbonyl compounds found in the present study to the

previous studies is not within the scope of this study.

References

- [1] *The Evaluation of the Carcinogenic Risk to Humans: Tobacco Smoking (IARC Monographs, Vol. 38)*, International Agency for Research on Cancer, Lyon, 1986, pp. 168–170.
- [2] S.S. Hecht, C.-H.B. Chen, G.D. McCoy and D. Hoffmann, in J.-P. Anselme (Editor), *N-Nitrosamines (ACS Symposium Series, No. 101)*, American Chemical Society, Washington, DC, 1986, pp. 125–152.
- [3] *Environmental Health Criteria 89*, World Health Organization, Geneva, 1989.
- [4] E.J. Bardana, Jr. and A. Montanaro, *Ann. Allergy*, 66 (1991) 441.
- [5] T. Sugimura, *Cancer*, 49 (1982) 1970.
- [6] C. Auerbach, M. Moutschen-Dahman and J. Moutschen, *Mutat. Res.*, 39 (1977) 317.
- [7] A.J. Fornace, Jr., J.F. Lechner, R.C. Graftstrom and C.C. Harris, *Carcinogenesis*, 3 (1982) 1373.
- [8] C.W. Lam, M. Casanova and H.D. Heck, *Fundam. Appl. Toxicol.*, 6 (1986) 541.
- [9] A.K. Basu, L.J. Marnett and L.J. Romano, *Mutat. Res.*, 129 (1984) 39.
- [10] R.C. Graftstrom, A. Fornace, Jr. and C.C. Harris, *Cancer Res.*, 44 (1984) 4323.
- [11] B.M. Goldschmidt, *J. Environ. Sci. Health*, C2 (1984) 231.
- [12] V. Nair, C.S. Cooper, D.E. Vietti and G.A. Turner, *Lipids*, 21 (1986) 6.
- [13] R.E. Albert, A.R. Sellakumar, S. Laskin, M. Juschner, N. Nelson and C.A. Snyder, *J. Natl. Cancer Inst.*, 68 (1982) 597.
- [14] Y.J. Feron, A. Krusysse and R.A. Woutersen, *Eur. J. Cancer Clin. Oncol.*, 18 (1982) 13.
- [15] S.E. Feinman (Editor), *Formaldehyde Sensitivity and Toxicity*. CRC Press, Boca Raton, FL, 1988.
- [16] *Formaldehyde and Other Aldehydes*. National Research Council, National Academy of Sciences, Washington, DC, 1980.
- [17] *Acetaldehyde as a Toxic Air Contaminant*, California Environmental Protection Agency, Air Resources Board, Stationary Source Division, Sacramento, CA, 1993.
- [18] K.D. Brunneemann, M.R. Kagan, J.E. Cox and D. Hoffmann, *Carcinogenesis*, 11 (1990) 1863.
- [19] R.E. Leonard and J.E. Kiefer, *J. Gas Chromatogr.*, 4 (1966) 142.
- [20] P.R. Houlgate, K.S. Dhingra, S.J. Nash and W.H. Evans, *Analyst*, 114 (1989) 355.
- [21] T. Hayashi, C.A. Reece and T. Shibamoto, *J. Assoc. Off. Anal. Chem.*, 69 (1986) 101.

- [22] T. Miyake and T. Shibamoto, *J. Agric. Food Chem.*, 41 (1993) 1968.
- [23] A. Yasuhara and T. Shibamoto, *J. Assoc. Off. Anal. Chem.* 72 (1989) 899.
- [24] A. Yasuhara and T. Shibamoto, *Agric. Biol. Chem.*, 53 (1989) 2273.
- [25] L.S. Ettre, in L.S. Ettre and A. Zlatkis (Editors), *The Practice of Gas Chromatography*. Interscience, New York, 1967, p. 402.
- [26] A. Yasuhara and T. Shibamoto, *J. Chromatogr.*, 547 (1991) 291.
- [27] D.L. Manning, M.P. Maskarinec, R.A. Jenkins and A.H. Marshall, *J. Assoc. Off. Anal. Chem.*, 66 (1983) 8.
- [28] C.T. Mansfield, B.T. Hodge, R.B. Hege and W.C. Hamlin, *J. Chromatogr. Sci.*, 15 (1977) 301.
- [29] E.L. Wynder and D. Hoffmann, *Tobacco and Tobacco Smoke*, Academic Press, New York, 1967, pp. 1–2.
- [30] S. Ohnishi and T. Shibamoto, *J. Agric. Food Chem.*, 32 (1984) 987.
- [31] K. Umano and T. Shibamoto, *J. Agric. Food Chem.*, 35 (1987) 14.
- [32] A. Yasuhara and T. Shibamoto, *J. Food Sci.*, 54 (1989) 1471.
- [33] C. Macku and T. Shibamoto, *J. Agric. Food Chem.*, 39 (1991) 1265.
- [34] M.K. Wassef and J.W. Hendrix, in *Proceedings of the University of Kentucky Tobacco and Health Workshop Conference, March 1973*. Tobacco and Health Research Institute, University of Kentucky, Lexington, KY, 1973, pp. 768–773.
- [35] W. Carruthers and R.A.W. Johnstone, *Nature*, 184 (1959) 1131.
- [36] A. Rodgman, L.C. Cook and C.K. Chappell, *Tobacco Sci.*, 5 (1961) 1.
- [37] H.C.H. Yeo and T. Shibamoto, *Lipids*, 27 (1992) 50.
- [38] F. Niyati-Shirhodaee and T. Shibamoto, *J. Agric. Food Chem.*, 41 (1993) 227.
- [39] J.R. Wasson, H.E. Francis, G.L. Seebach and L. de Salles de Hys, in *Proceedings of the University of Kentucky Tobacco and Health Workshop Conference, March 1973*, Tobacco and Health Research Institute, University of Kentucky, Lexington, KY, 1973, pp. 474–484.

Short communication

Capillary electrophoresis of plant starches as the iodine complexes

Jeffrey D. Brewster*, Marshall L. Fishman

US Department of Agriculture, ARS, Eastern Regional Research Center, 600 East Mermaid Lane, Philadelphia, PA 19118, USA

First received 9 September 1994; revised manuscript received 15 November 1994; accepted 15 November 1994

Abstract

Much research is currently focused on the use of plant starch as an industrial raw material which can reduce dependence on non-renewable resources. Development of new starch-based products requires effective methods for analysis and characterization of starch and related biopolymers. Most separations methods are not suitable for this application due to the high molecular mass ($> 10^6$) of starch. We describe here the use of iodine complexation to impart charge and permit detection of starch components in capillary electrophoresis. Amylopectin and amylose are resolved in less than 10 min using iodine-containing buffers in unmodified capillaries. Partial resolution of an oligosaccharide mixture was also demonstrated, indicating potential utility of the method for analysis of smaller biopolymers. The primary basis for separation is shown to be iodine binding affinity, which can be manipulated through control of temperature and iodine concentration.

1. Introduction

Plant starches and other polysaccharides comprise the most abundant source of renewable natural products on the planet [1]. Starch consists primarily of two components, amylose and amylopectin. Amylose is a linear or very lightly branched polymer consisting of several thousand (1→4)- α -D-linked D-glucose units with molecular masses ranging from $2 \cdot 10^5$ to $2 \cdot 10^6$ [2]. Amylopectin is a much larger, highly branched polymer consisting of relatively short (25 residue) segments of (1→4)- α D-linked-glucan units connected by (1→6)- α -D-glucosidic linkages, with molecular masses ranging from 10^7 to $5 \cdot 10^8$ [2,3]. Native plant starches typically con-

tain 20–30% amylose, but the amylose content may range from 0 to 80% [2]. In potato and some other species a small fraction ($< 1\%$) of the glucose residues in amylopectin are phosphorylated [3].

The primary end-use of starch is in food products, with non-food uses accounting for approximately $2 \cdot 10^9$ kg of starch per year in the USA. Newer applications of starch in areas such as superabsorbent polymers [4] and biodegradable films [5] are emerging, but account for a small fraction of current starch production. There is great interest in expanding non-food uses of starch and other biopolymers, both to reduce dependence on non-renewable materials such as petroleum, and to provide new, high-value markets for agricultural products. Rapid and effective techniques for polysaccharide

* Corresponding author.

characterization are needed to support development of new starch applications, and to facilitate fundamental research on biopolymers. The tools currently used for characterization of polysaccharides include classical chemical techniques [6] and size-exclusion chromatography (SEC) [7]. The classical methods provide useful structural and chemical data, but can only determine average properties of the sample components. Chromatographic methods such as SEC can provide data on physical, chemical and structural properties of each component in a complex polysaccharide mixture [8]. Unfortunately, SEC separations provide limited resolution, and the high-resolution methods commonly used in carbohydrate analysis, such as reversed-phase HPLC [9], ion-exchange HPLC [10], and gel electrophoresis [11], are only useful for analytes with molecular masses much smaller than that of starch. High-molecular-mass polysaccharides have been separated using paper electrophoresis and related techniques [12], but this approach is less than ideal in terms of resolution, analysis time and detection capability.

Capillary electrophoresis (CE) has proven to be a very powerful tool for characterization of biomolecules [13]. Highly efficient separations of proteins [14] and nucleic acids [15] are now routinely obtained with CE. The application of CE to carbohydrate separations has not developed to the same degree, largely due to the lack of functional groups containing chromophores and charges. Simple sugars at relatively high concentrations have been separated as the anionic borate complexes [12,16,17] using CE with UV absorbance detection [18]. Oligosaccharide–borate complexes also have been separated, but derivatization with UV absorbing [19] or fluorescent [20,21] labels is required for detection. The derivatization procedures are lengthy (4–24 h), and detection of larger polysaccharides is problematic since only one label is typically introduced per molecule. Separations based on borate complexation appear to be limited to a maximum molecular mass of ca. 30 000 because borate complexes of larger molecules acquire a constant mass-to-charge ratio and are not resolved [22]. Only a few CE separations of larger

polysaccharides have been reported. Borate complexes of synthetic mixtures of monodisperse dextrans have been resolved through use of pulsed-field conditions and sieving media with laser-induced fluorescent detection [22]. Fluorescent labeling was required, and the generality of the approach is not yet known. Unlabeled polysaccharides have been separated by CE under constant field conditions using indirect fluorescence detection at pH 11.5 [23]. In this case different classes of polysaccharides (e.g. amylose, pectin, dextrin) could be resolved, but each class migrated as a single peak.

An alternative strategy for imparting charge and optical detection sensitivity to carbohydrates is through iodine complexation. The starch–iodine complex consists of a helix of sugar residues surrounding a linear I_5^- core [24,25]. Unlike borate complexation, iodine binding is a cooperative interaction which exhibits strong chain-length dependence in both complexation and optical properties. The iodine binding constant increases nearly exponentially with glucan chain length, reaching a plateau at ca. 125 residues [26]. The wavelength of maximum absorbance (λ_{max}) also increases with chain length, varying from 496 nm for degree of polymerization (DP) 22 to 642 nm for DP 1500 [27]. The binding constant for amylose is several orders of magnitude higher than that of amylopectin, reflecting the much shorter average segment length in amylopectin. At sufficiently high iodine concentrations, however, both polymers bind approximately 20% of their mass in iodine at 20°C. Iodine binding and λ_{max} are also temperature dependent, especially for shorter chains. For example, the iodine binding capacity for a glucan of DP 31 increases almost tenfold on changing the temperature from 20.4 to 1.4°C [28]. Although iodine complexation was used over 40 years ago for agar gel electrophoresis of oligosaccharides [29] and free solution zone electrophoresis of cyclodextrins [30], this approach has not been exploited for the separation of high-molecular-mass polysaccharides. We describe here experiments which indicate that this strategy is applicable to the separation by CE of a wide range of carbohydrates ranging from

maltooligosaccharides of DP < 40 to amylopectins with molecular masses in the tens of millions. These separations can be achieved without derivatization or capillary modification, and with the speed, flexibility and small sample volumes typical of CE.

2. Experimental

2.1. Apparatus

CE was conducted with a Spectra Phoresis 1000 instrument (Thermo-Separations, San Jose, CA, USA) equipped with an autosampler, column temperature control, and UV-visible detector. The detector was generally operated in the multi-wavelength mode (simultaneous acquisition of data at several wavelengths), and occasionally in the high-speed scanning mode (data acquisition over a wide wavelength range at 5-nm increments) for acquisition of spectra. The fused-silica capillaries used were 50 μm I.D. \times 340 μm O.D., with overall length of 36 cm and injector to detector length of 28 cm.

2.2. Reagents and solutions

All chemicals were used without further purification. Potato starch, amylose and amylopectin were from Sigma (St. Louis, MO, USA). Maltodextrin M-040, a mixture of maltodextrin oligomers with DP 1–40, was the gift of Dr. A. Hotchkiss, US Department of Agriculture, Philadelphia, PA, USA. Amaizo V (amylomaize V, apparent amylose content 50%) was obtained from American Maize Products (Chicago, IL, USA). Cornstarch was purchased at a local market. All other chemicals were reagent grade. Solutions were prepared with 18 M Ω water obtained from a Nanopure (Barnstead, Dubuque, IA, USA) water-purification system.

2.3. Procedures

Stock solutions of saccharides were prepared by magnetic stirring of a mixture containing 20 mg/ml of the analyte in dimethyl sulfoxide

(DMSO) at room temperature until gelatinization (dissolution) was complete. Iodine stock solution contained 10 mg/ml KI and 10 mg/ml I₂. The stock solutions were stored at room temperature until needed. Shortly before analysis, an aliquot of the sample stock solution was diluted with water and buffer stock (50 mM) solution to give a sample of the appropriate composition. Run buffers were prepared by mixing buffer stock solution (50 mM), water, and iodine stock solution in the appropriate amounts shortly before use. The capillary was rinsed with run buffer using the instrument vacuum system for 2 min (ca. 3 column volumes) prior to each run. Injections were made by applying vacuum to the detector end of the capillary using the instrument injection system. The capillary was cleaned daily by rinsing for 10 min each with 1 M NaOH, water and run buffer.

3. Results and discussion

Typical electropherograms of amylose, amylopectin and potato starch are shown in Fig. 1. Amylopectin and amylose are well resolved from each other, with amylose migrating as a broad peak with electrophoretic mobility about 5 times higher than amylopectin. The electrophoretic mobility (adjusted for electroosmotic flow) of amylopectin was dependent on iodine concentration, as shown in Table 1. This dependence reflects the iodine binding behavior of amylopectin determined by titrimetry [28], and results from the short average chain length of amylopectin segments. Amylopectin mobility was also dependent on temperature (Table 2), commensurate with the strong temperature dependence of iodine binding of shorter segments. The mobility of amylose was virtually independent of iodine concentration and temperature (except for a viscosity-related mobility increase with temperature) over the same range, reflecting the fact that the long chains of amylose are essentially saturated with iodine even at very low iodine concentrations.

The broad distribution of migration times of the amylose fraction was unexpected. Since the

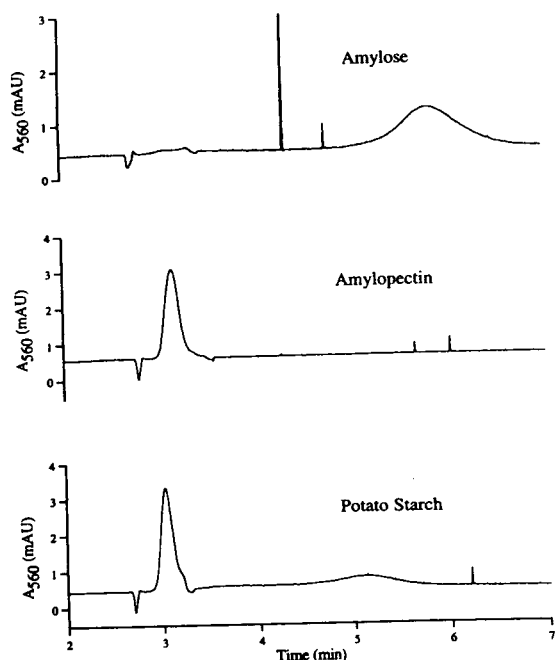


Fig. 1. Electropherograms of amylose, amylopectin and potato starch. Applied voltage: 20 kV; temperature: 25°C; injection: 5 s hydrodynamic; sample concentration: 1 mg/ml; run buffer: 20 mM citrate-phosphate, pH 6, 0.1 mg/ml KI, 0.1 mg/ml I₂.

iodine binding affinity of segments with DP > 100 is essentially constant, and the average segment length is ca. 200 for amylose, it was anticipated that all amylose molecules would

Table 1
Iodine concentration dependence of amylopectin and amylose mobility

[I ₂] (mg/ml)	Mobility (10 ⁻⁶ m ² V ⁻¹ s ⁻¹)		Ratio
	Amylopectin	Amylose	
0.05	2.5	13.7	5.5
0.2	6.4	14.9	2.3
0.5	8.4	14.8	1.8
1.0	8.5	14.2	1.7

Conditions: applied voltage, 20 kV; temperature, 25°C; injection, 5 s hydrodynamic; sample concentration, 1 mg/ml; run buffer, 20 mM pH 5 acetate buffer containing indicated concentration of iodine. (Apparent mobilities corrected for electroosmotic flow).

Table 2
Temperature dependence of amylopectin mobility

Column temperature (°C)	Amylopectin mobility (10 ⁻⁶ m ² V ⁻¹ s ⁻¹)
25	8.10
45	7.50
60	6.30

Conditions: applied voltage, 20 kV; injection, 5 s hydrodynamic; sample concentration, 1 mg/ml; run buffer, 20 mM pH 7 citrate-phosphate, 0.5 mg/ml I₂. (Apparent mobilities corrected for electroosmotic flow).

acquire a constant charge-to-mass ratio and migrate at a uniform velocity. Peak broadening due to wall interactions can not be ruled out, but seems unlikely since both the capillary wall and the amylose-iodine complex carry a negative charge. Addition of hydroxypropyl cellulose (0.1%) to the run buffer, an agent known to reduce analyte-wall interactions, did not alter the amylose peak width, nor was peak width markedly effected by pH in the range 4–7.5 (data not shown). This evidence suggests that the distribution in mobility is due to sample heterogeneity, and not wall interactions, but further investigation is required to elucidate the mechanism for the dispersion in amylose mobility.

Spectra acquired during the runs (not shown) exhibited absorbance maxima of 560 nm for the amylopectin peak and 640 nm for the amylose peak. Spectra acquired at various points between the half maxima of both peaks appeared identical. Spectra at points near the base of the major peaks have absorbance maxima differing from the peak maximum, but the low signal-to-noise ratio of these spectra made accurate determination of the maximum value difficult. The dependence of absorbance maximum on chain length proved to be very useful in identifying components and can be an effective aid in developing and interpreting separations using iodine complexation. However, variations in λ_{\max} and extinction coefficient with chain length must be born in mind when performing quantitative studies.

Separation of several starches and a mixture of

maltodextrin oligomers with a pH 7 citrate-phosphate buffer system are shown in Fig. 2. The partial separation of maltodextrin oligomers indicates the wide range of polymer molecular masses which can be studied by iodine complexation CE. The tall, narrow peaks migrating between amylopectin and amylose are observed in most amylose-containing samples, and to a lesser extent in amylopectin samples. The number and height of the peaks increase with sample age, while the exact number and location of the peaks varies from preparation to preparation and run to run. These peaks are believed to be associated with retrogradation (precipitation) of the amylose. Aqueous starch solutions are gener-

ally not stable, and tend to form crystalline solids or gels on standing. Relatively stable solutions of starch can be prepared in DMSO, and samples were prepared by dilution of the stock solutions in DMSO with aqueous electrolyte shortly before the separation to minimize retrogradation.

Separations have been conducted in a number of buffers (acetate, phosphate and citrate-phosphate) over the pH range 4–7.5. Results similar to those shown in Fig. 1 were observed with all buffers, but differences in electroosmotic flow and small changes in peak shape were observed with various buffers. Higher-pH buffers appeared to lose iodine rapidly and gave irreproducible results. Iodine concentrations from 0.05 to 5 mg/ml have been used, with 0.1–0.5 mg/ml appearing optimal. At lower iodine concentrations amylopectin is not resolved from the void peak, while Joule heating due the high conductivity of KI solutions prevented separations in 50 μm capillaries at higher concentrations.

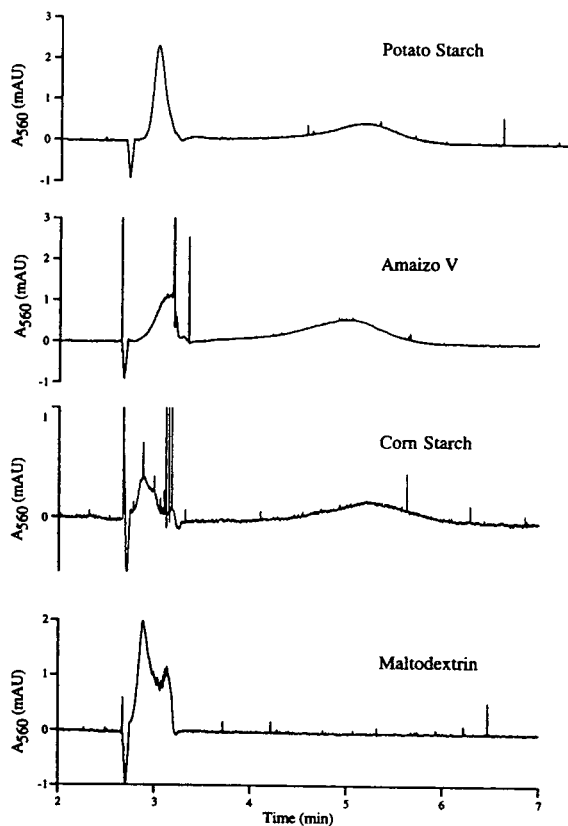


Fig. 2. Electropherograms of potato starch, Amaizo V, corn starch and maltodextrin M-040. Applied voltage: 20 kV; temperature: 25°C; injection: 5 s hydrodynamic; sample concentration: 1 mg/ml; run buffer: 20 mM citrate-phosphate, pH 7, 0.1 mg/ml KI, 0.1 mg/ml I_2 .

4. Conclusions

CE of starches using iodine-containing buffers provides a simple, rapid method for separation and detection of the principal starch components. In contrast to other approaches for CE of carbohydrates, lengthy (4–24 h) derivatization steps are avoided, and separations can be carried out in unmodified silica capillaries using commonly available detectors. The method can be used with relatively low-molecular-mass oligosaccharides as well as with high-molecular-mass polysaccharides which cannot be resolved using borate complexation [22]. The primary mechanism for selectivity is iodine binding affinity, and this can be manipulated by varying temperature and iodine concentration. Variations in iodine binding capacity and λ_{max} can reveal information on the size and structure of the analytes independent of their electrophoretic behavior. While much work is required to optimize separations and improve reproducibility, this approach appears very promising as a simple, rapid method for starch characterization.

References

- [1] W.M. Doane, in *New Crops, New Uses, New Markets, 1992 Yearbook of Agriculture*, Office of Publishing and Visual Communication, US Department of Agriculture, 1992, Ch. 22, pp. 149–153.
- [2] D. French, in R.L. Whistler, J.N. Bemiller and E.G. Paschall (Editors), *Starch: Chemistry and Technology*, Academic Press, Orlando, FL, 1984, p. 184.
- [3] D.J. Manners, *Carbohydr. Polym.*, 11 (1989) 87–112.
- [4] M.O. Weaver, R.R. Montgomery, L.D. Miller, V.E. Sohns, G.F. Fanta and W.M. Doane, *Stärke*, 29 (1977) 413–422.
- [5] H. Roper and H. Koch, *Starch/Stärke* 42 (1990) 123–130.
- [6] M.F. Chaplin and J.F. Kennedy, *Carbohydrate Analysis—A Practical Approach*, IRL Press, Oxford, 1986.
- [7] O. Mikeš, *High-Performance Liquid Chromatography of Biopolymers and Biooligomers*, Part B, Elsevier, Amsterdam, 1988, Ch 11, pp. 239–298.
- [8] M.L. Fishman and P.D. Hoagland, *Carbohydr. Polym.*, 23 (1994) 175–183.
- [9] P.C. Maes, L.J. Nagels and B.R. Spanoghe, *Chromatographia*, 37 (1993) 511–516.
- [10] K. Koizumi, Y. Kubota, T. Tanimoto and Y. Okada, *J. Chromatogr.*, 464 (1989) 365–371.
- [11] P. Jackson, *Anal. Biochem.*, 216 (1994) 243–252.
- [12] A.B. Foster, in R.L. Whistler and M.L. Wolfrom (Editors), *Methods in Carbohydrate Chemistry*, Vol. 1, Academic Press, New York, 1962, pp. 51–60.
- [13] B.L. Karger, A.S. Cohen and A. Guttman, *J. Chromatogr.*, 492 (1989) 585–614.
- [14] M. Gilges, M.H. Kleemiss and G. Schomburg, *Anal. Chem.*, 66 (1994) 2038–2046.
- [15] D.N. Heiger, A.S. Cohen and B.L. Karger, *J. Chromatogr.*, 516 (1990) 33–48.
- [16] B.A. Lewis and F. Smith, *J. Am. Chem. Soc.*, 79 (1957) 3929–3931.
- [17] Z. El Rassi, *Adv. Chromatogr.*, 34 (1994) 177–250.
- [18] S. Hoffstetter-Kuhn, A. Paulus, E. Gassmann and H.M. Widmer, *Anal. Chem.*, 63 (1991) 1541–1547.
- [19] S. Honda, A. Makino, S. Suzuki and K. Kakeki, *Anal. Biochem.*, 191 (1990) 176.
- [20] J. Liu, O. Shirota and M.N. Novotny, *J. Chromatogr.*, 559 (1991) 223.
- [21] M. Stefansson and M. Novotny, *Carbohydr. Res.*, 258 (1994) 1–9.
- [22] J. Sudor and M. Novotny, *Proc. Natl. Acad. Sci. U.S.A.*, 90 (1993) 9451–9455.
- [23] M.D. Richmond and E.S. Yeung, *Anal. Biochem.*, 210 (1993) 245–248.
- [24] R.E. Rundle and D. French, *J. Am. Chem. Soc.*, 65 (1943) 558.
- [25] R.C. Teitelbaum, S.L. Ruby and T.J. Marks, *J. Am. Chem. Soc.*, 100 (1978) 3215–3217.
- [26] A. Thoma and D. French, *J. Am. Chem. Soc.*, 65 (1961) 1825–1828.
- [27] W. Banks, C.T. Greenwood and K.M. Khan, *Carbohydr. Res.*, 17 (1971) 25–33.
- [28] W. Banks and C.T. Greenwood, *Starch and its Components*, Wiley, New York, 1975.
- [29] D.L. Mould and R.L.M. Synge, *Biochem. J.*, 58 (1954) 585–593.
- [30] E. Norberg and D. French, *J. Am. Chem. Soc.*, 72 (1950) 1202–1205.

Author Index

- Ahmad, F. and Roberts, D.J.
Use of narrow-bore high-performance liquid chromatography–diode array detection for the analysis of intermediates of the biological degradation of 2,4,6-trinitrotoluene 693(1995)167
- Aldrich-Wright, J.R., Newman, P.D., Rao, K.R.N., Vagg, R.S. and Williams, P.A.
Chiral metal complexes. XLII. Reversed-phase high-performance liquid chromatographic separation of racemic dipeptides as their ternary Co(III) complexes with a chiral triamine 693(1995)366
- Andersson, J.T. and Schmid, B.
Polycyclic aromatic sulfur heterocycles. IV. Determination of polycyclic aromatic compounds in a shale oil with the atomic emission detector 693(1995)325
- Awaka, I., see Saitoh, K. 693(1995)176
- Baltes, W., see Brinkmann, E. 693(1995)271
- Banks, P.R. and Paquette, D.M.
Monitoring of a conjugation reaction between fluorescein isothiocyanate and myoglobin by capillary zone electrophoresis 693(1995)145
- Beckers, J.L.
Calculation of the composition of sample zones in capillary zone electrophoresis. I. Mathematical model 693(1995)347
- Bello, M.S., Zhukov, M.Yu. and Righetti, P.G.
Combined effects of non-linear electrophoresis and non-linear chromatography on concentration profiles in capillary electrophoresis 693(1995)113
- Benson, L.M., Veverka, K.A., Mays, D.C., Nelson, A.N., Shriver, Z.H., Lipsky, J.J. and Naylor, S.
Simultaneous structure–activity determination of disulfiram photolysis products by on-line continuous-flow liquid secondary ion mass spectrometry and enzyme inhibition assay 693(1995)162
- Brewster, J.D. and Fishman, M.L.
Capillary electrophoresis of plant starches as the iodine complexes 693(1995)382
- Brinkmann, E., Dehne, L., Oei, H.B., Tiebach, R. and Baltes, W.
Separation of geometrical retinol isomers in food samples by using narrow-bore high-performance liquid chromatography 693(1995)271
- Brooks, C.A. and Cramer, S.M.
Investigation of displacer equilibrium properties and mobile phase operating conditions in ion-exchange displacement chromatography 693(1994)187
- Cai, C.-h., Romano, V.A. and Dubin, P.L.
Ionic strength dependence of protein retention on Superose 12 in SEC–IEC mixed mode chromatography 693(1995)251
- Camel, V., Tambuté, A. and Caude, M.
Influence of ageing on the supercritical fluid extraction of pollutants in soils 693(1995)101
- Cantwell, F.F., see Vermeulen, D.M. 693(1995)205
- Caude, M., see Camel, V. 693(1995)101
- Christie, W.W., see Nikolova-Damyanova, B. 693(1995)235
- Cramer, S.M., see Brooks, C.A. 693(1994)187
- Croes, K., McCarthy, P.T. and Flanagan, R.J.
HPLC of basic drugs and quaternary ammonium compounds on microparticulate strong cation-exchange materials using methanolic or aqueous methanol eluents containing an ionic modifier 693(1995)289
- Cutié, S.S. and Smith, C.G.
Determination of Methocel A15-LV cellulose ether in blends with microcrystalline cellulose 693(1995)371
- Dehne, L., see Brinkmann, E. 693(1995)271
- Dowd, V. and Yon, R.J.
Further examination of a “concerted cluster” model of multivalent affinity. Heterogeneous adsorption of lactate dehydrogenase to Cibacron Blue immobilised on cellulose 693(1995)15
- Dubin, P.L., see Cai, C.-h. 693(1995)251
- Dubin, P.L., see Shah, G. 693(1995)197
- Edholm, L.-E., see Palmarsdóttir, S. 693(1995)131
- Eyer, P., see Spöhrer, U. 693(1995)55
- Farkas, G., see Quintero, G. 693(1995)1
- Fishman, M.L., see Brewster, J.D. 693(1995)382
- Fischella, S., Foti, S., Maccarrone, G. and Saletti, R.
Tryptic peptide mapping of sequence 299–585 of human serum albumin by high-performance liquid chromatography and fast atom bombardment mass spectrometry 693(1995)33
- Flanagan, R.J., see Croes, K. 693(1995)289
- Font, G., see Picó, Y. 693(1994)339
- Foti, S., see Fischella, S. 693(1995)33
- Geissler, H., see Wachholz, S. 693(1995)89
- Gelencsér, A., Kiss, G., Krivácsy, Z., Varga-Puchony, Z. and Hlavay, J.
A simple method for the determination of capacity factor on solid-phase extraction cartridges. I 693(1995)217
- Gelencsér, A., Kiss, G., Krivácsy, Z., Varga-Puchony, Z. and Hlavay, J.
The role of capacity factor in method development for solid-phase extraction of phenolic compounds. II 693(1995)227
- Görgényi, M., Van Langenhove, H. and Király, Z.
Prediction of gas chromatographic retention indices of 2,4-dinitrophenylhydrazones 693(1995)181
- Goto, H., see Murata, H. 693(1995)263
- Hage, D.S., Noctor, T.A.G. and Wainer, I.W.
Characterization of the protein binding of chiral drugs by high-performance affinity chromatography. Interactions of R- and S-ibuprofen with human serum albumin 693(1995)23
- Harada, K.-I., see Murata, H. 693(1995)263
- Herslöf, B., see Nikolova-Damyanova, B. 693(1995)235
- Hlavay, J., see Gelencsér, A. 693(1995)217
- Hlavay, J., see Gelencsér, A. 693(1995)227
- Jackson, P.E.
Analysis of oxalate in Bayer liquors: a comparison of ion chromatography and capillary electrophoresis 693(1995)155
- Janas, J., see Voelkel, A. 693(1995)315

- Just, U., see Wachholz, S. 693(1995)89
- Käppler, K., see Wachholz, S. 693(1995)89
- Keidel, F., see Wachholz, S. 693(1995)89
- Khalaf, H., see Steinert, J. 693(1995)281
- Kim, J.-H., Nishida, Y., Ohru, H. and Meguro, H.
Simple and highly sensitive high-performance liquid chromatographic method for separating enantiomeric diacylglycerols by direct derivatization with a fluorescent chiral agent, (*S*)-(+)-2-*tert*-butyl-2-methyl-1,3-benzodioxole-4-carboxylic acid 693(1994)241
- Király, Z., see Görgényi, M. 693(1995)181
- Kiss, G., see Gelencsér, A. 693(1995)217
- Kiss, G., see Gelencsér, A. 693(1995)227
- Kondo, F., see Murata, H. 693(1995)263
- Krivácsy, Z., see Gelencsér, A. 693(1995)217
- Krivácsy, Z., see Gelencsér, A. 693(1995)227
- Lau, O.-W. and Mok, C.-S.
High-performance liquid chromatographic determination of active ingredients in cough-cold syrups with indirect conductometric detection 693(1995)45
- Lipsky, J.J., see Benson, L.M. 693(1995)162
- Liu, H., see Ruan, Z. 693(1995)79
- Maccarrone, G., see Fisichella, S. 693(1995)33
- Mañes, J., see Picó, Y. 693(1994)339
- Masselter, S.M. and Zemany, A.J.
Influence of buffer electrolyte pH on the migration behavior of phenolic compounds in co-electroosmotic capillary electrophoresis 693(1995)359
- Mays, D.C., see Benson, L.M. 693(1995)162
- McCarthy, P.T., see Croes, K. 693(1995)289
- Meguro, H., see Kim, J.-H. 693(1994)241
- Miyake, T. and Shibamoto, T.
Quantitative analysis by gas chromatography of volatile carbonyl compounds in cigarette smoke 693(1995)376
- Mok, C.-S., see Lau, O.-W. 693(1995)45
- Murata, H., Shoji, H., Oshikata, M., Harada, K.-I., Suzuki, M., Kondo, F. and Goto, H.
High-performance liquid chromatography with chemiluminescence detection of derivatized microcystins 693(1995)263
- Naylor, S., see Benson, L.M. 693(1995)162
- Nelson, A.N., see Benson, L.M. 693(1995)162
- Newman, P.D., see Aldrich-Wright, J.R. 693(1995)366
- Nikolova-Damyanova, B., Christie, W.W. and Herslöf, B.
Silver ion high-performance liquid chromatography of esters of isomeric octadecenoic fatty acids with short-chain monounsaturated alcohols 693(1995)235
- Nishida, Y., see Kim, J.-H. 693(1994)241
- Noctor, T.A.G., see Hage, D.S. 693(1995)23
- Oei, H.B., see Brinkmann, E. 693(1995)271
- Ohru, H., see Kim, J.-H. 693(1994)241
- Ojanperä, I., see Rasanen, I. 693(1995)69
- Oshikata, M., see Murata, H. 693(1995)263
- Pálmarsdóttir, S. and Edholm, L.-E.
Enhancement of selectivity and concentration sensitivity in capillary zone electrophoresis by on-line coupling with column liquid chromatography and utilizing a double stacking procedure allowing for microliter injections 693(1995)131
- Paquette, D.M., see Banks, P.R. 693(1995)145
- Picó, Y., Redondo, M.J., Font, G. and Mañes, J.
Solid-phase extraction on C₁₈ in the trace determination of selected polychlorinated biphenyls in milk 693(1994)339
- Pirkle, W.H., see Villani, C. 693(1995)63
- Quintero, G., Vo, M., Farkas, G. and Vigh, G.
Series of homologous displacers for preparative chiral displacement chromatographic separations on Cyclobond-II columns 693(1995)1
- Rao, K.R.N., see Aldrich-Wright, J.R. 693(1995)366
- Rasanen, I., Ojanperä, I. and Vuori, E.
Comparison of four homologous retention index standard series for gas chromatography of basic drugs 693(1995)69
- Redondo, M.J., see Picó, Y. 693(1994)339
- Righetti, P.G., see Bello, M.S. 693(1995)113
- Rimpler, M., see Steinert, J. 693(1995)281
- Roberts, D.J., see Ahmad, F. 693(1995)167
- Romano, V.A., see Cai, C.-h. 693(1995)251
- Ruan, Z. and Liu, H.
Preparation of 4-vinylpyridine and divinylbenzene porous-layer open tubular columns by in situ copolymerization 693(1995)79
- Saitoh, K., Awaka, I. and Suzuki, N.
Determination of chlorophylls by reversed-phase high-performance liquid chromatography with isocratic elution and the column-switching technique 693(1995)176
- Saletti, R., see Fisichella, S. 693(1995)33
- Schenk, T., Schuphan, I. and Schmidt, B.
High-performance liquid chromatographic determination of the rhamnolipids produced by *Pseudomonas aeruginosa* 693(1995)7
- Schmid, B., see Andersson, J.T. 693(1995)325
- Schmidt, B., see Schenk, T. 693(1995)7
- Schuphan, I., see Schenk, T. 693(1995)7
- Shah, G. and Dubin, P.L.
Adsorptive interaction of Ficoll standards with porous glass size-exclusion chromatography columns 693(1995)197
- Shibamoto, T., see Miyake, T. 693(1995)376
- Shoji, H., see Murata, H. 693(1995)263
- Shriver, Z.H., see Benson, L.M. 693(1995)162
- Smith, C.G., see Cutié, S.S. 693(1995)371
- Spöhrer, U. and Eyer, P.
Separation of geometrical *syn* and *anti* isomers of obidoxime by ion-pair high-performance liquid chromatography 693(1995)55
- Steinert, J., Khalaf, H. and Rimpler, M.
HPLC separation and determination of naphtho[2,3-*b*]-furan-4,9-diones and related compounds in extracts of *Tabebuia avellanedae* (Bignoniaceae) 693(1995)281
- Suzuki, M., see Murata, H. 693(1995)263
- Suzuki, N., see Saitoh, K. 693(1995)176
- Tambuté, A., see Camel, V. 693(1995)101
- Tan, H.S.I., Xu, J. and Zheng, Y.
Cation-exchange high-performance liquid chromatographic assay of piperazine in some pharmaceutical formulations 693(1994)307
- Tiebach, R., see Brinkmann, E. 693(1995)271
- Vagg, R.S., see Aldrich-Wright, J.R. 693(1995)366

- Van Langenhove, H., see Görgényi, M. 693(1995)181
- Varga-Puchony, Z., see Gelencsér, A. 693(1995)217
- Varga-Puchony, Z., see Gelencsér, A. 693(1995)227
- Vermeulen, D.M. and Cantwell, F.F.
Slow change in the electrical potential at glass and silica surfaces due to Na⁺ sorption in the hydrated layer 693(1995)205
- Veverka, K.A., see Benson, L.M. 693(1995)162
- Vigh, G., see Quintero, G. 693(1995)1
- Villani, C. and Pirkle, W.H.
Direct high-performance liquid chromatographic resolution of planar chiral tricarbonyl (η^6 -arene)-chromium(0) complexes 693(1995)63
- Vo, M., see Quintero, G. 693(1995)1
- Voelkel, A. and Janas, J.
Elimination of adsorption effects of polarity parameters determined by inverse gas chromatography 693(1995)315
- Vuori, E., see Rasanen, I. 693(1995)69
- Wachholz, S., Keidel, F., Just, U., Geissler, H. and Káppler, K.
Analysis of a mixture of linear and cyclic siloxanes by cryo-gas chromatography-Fourier transform infrared spectroscopy and gas chromatography-mass spectrometry 693(1995)89
- Wainer, I.W., see Hage, D.S. 693(1995)23
- Williams, P.A., see Aldrich-Wright, J.R. 693(1995)366
- Xu, J., see Tan, H.S.I. 693(1994)307
- Yon, R.J., see Dowd, V. 693(1995)15
- Zemann, A.J., see Masselter, S.M. 693(1995)359
- Zheng, Y., see Tan, H.S.I. 693(1994)307
- Zhukov, M.Yu., see Bello, M.S. 693(1995)113

Carbohydrate Analysis

High Performance Liquid Chromatography and Capillary Electrophoresis

Edited by Z. El Rassi

Journal of Chromatography Library, Volume 58

The objective of the present book is to provide a comprehensive review of carbohydrate analysis by HPLC and HPCE by covering analytical and preparative separation techniques for all classes of carbohydrates including mono- and disaccharides; linear and cyclic oligosaccharides; branched heterooligosaccharides (e.g., glycans, plant-derived oligosaccharides); glycoconjugates (e.g., glycolipids, glycoproteins); carbohydrates in food and beverage; compositional carbohydrates of polysaccharides; carbohydrates in biomass degradation; etc.

The book will be of interest to a wide audience, including analytical chemists and biochemists, carbohydrate, glycoprotein and glycolipid chemists, molecular biologists, biotechnologists, etc. It will also be a useful reference work for both the experienced analyst and the newcomer as well as for users of HPLC and HPCE, graduates and postdoctoral students.

Contents: Part I. The Solute.

1. Preparation of carbohydrates for analysis by HPLC and HPCE (A.J. Mort, M.L. Pierce).

Part II. Analytical and Preparative Separations.

2. Reversed-phase and hydrophobic interaction chromatography of carbohydrates and glycoconjugates (Z. El Rassi).
3. High performance hydrophilic interaction chromatography of carbohydrates with

polar solvents (S.C. Churms).
4. HPLC of carbohydrates with cation- and anion-exchange silica and resin-based stationary phases (C.G. Huber, G.K. Bonn).
5. Analysis of glycoconjugates using high-pH anion-exchange chromatography (R.R. Townsend).
6. Basic studies on carbohydrate - protein interaction by high performance affinity chromatography and high performance capillary affinity electrophoresis using lectins as protein models (S. Honda).
7. Modern size exclusion chromatography of carbohydrates and glycoconjugates (S.C. Churms).
8. High performance capillary electrophoresis of carbohydrates and glycoconjugates (Z. El Rassi, W. Nashabeh).
9. Preparative HPLC of carbohydrates (K.B. Hicks).

Part III. The Detection.

10. Pulsed electrochemical detection of carbohydrates at gold electrodes following liquid chromatographic separation (D.C. Johnson,

W.R. LaCourse).
11. On-column refractive index detection of carbohydrates separated by HPLC and CE (A.E. Bruno, B. Krattiger).
12. Mass spectrometry of carbohydrates and glycoconjugates (C.A. Settineri, A.L. Burlingame).
13. Evaporative light scattering detection of carbohydrates in HPLC (M. Dreux, M. Lafosse).
14. Chiroptical detectors for HPLC of carbohydrates (N. Purdie).
15. Pre- and post-column detection-oriented derivatization techniques in HPLC of carbohydrates (S. Hase).
16. Post-column enzyme reactors for the HPLC determination of carbohydrates (L.J. Nagels, P.C. Maes).
17. Other direct and indirect detection methods of carbohydrates in HPLC and HPCE (Z. El Rassi, J.T. Smith).
Subject index.

©1995 692 pages Hardbound
Price: Dfl. 425.00 (US\$250.00)
ISBN 0-444-89981-2

ORDER INFORMATION

ELSEVIER SCIENCE B.V.
P.O. Box 330
1000 AH Amsterdam
The Netherlands
Fax: +31 (20) 485 2845

For USA and Canada:
P.O. Box 945, New York
NY 10159-0945
Fax: +1 (212) 633 3680

US\$ prices are valid only for the USA & Canada and are subject to exchange rate fluctuations; in all other countries the Dutch guilder price (Dfl.) is definitive. Customers in the European Union should add the appropriate VAT rate applicable in their country to the price(s). Books are sent postfree if prepaid.



ELSEVIER

An imprint of Elsevier Science

Chromatography of Mycotoxins

Techniques and Applications

edited by V. Betina

Journal of Chromatography Library Volume 54

This work comprises two parts, Part A: Techniques and Part B: Applications. In Part A the most important principles of sample preparation, extraction, clean-up, and of established and prospective chromatographic techniques are discussed in relation to mycotoxins. In Part B the most important data, scattered in the literature, on thin-layer, liquid, and gas chromatography of mycotoxins have been compiled. Mycotoxins are mostly arranged according to families, such as aflatoxins, trichothecenes, lactones etc. Chromatography of individual important mycotoxins and multi-mycotoxin chromatographic analyses are also included. Applications are presented in three chapters devoted to thin-layer, liquid, and gas chromatography of mycotoxins.

Contents: PART A. TECHNIQUES.

1. Sampling, Sample Preparation, Extraction and Clean-up

(*V. Betina*). Introduction. Sampling and Sample Preparation. Sample Extraction and Clean-up. Illustrative Example. Conclusions.

2. Techniques of Thin Layer Chromatography

(*R.D. Coker, A.E. John, J.A. Gibbs*). Introduction. Clean-up Methods. Normal Phase TLC. Reverse-phase TLC (RPTLC). High Performance Thin Layer Chromatography (HPTLC). Preparative TLC. Detection. Quantitative and Semi-Quantitative Evaluation. Illustrative Examples. Conclusions.

3. Techniques of Liquid Column Chromatography.

(*P. Kuronen*). Introduction. Sample Pretreatment. Column Chromatography. Mini-Column Chromatography. High-Performance Liquid Chromatography. Conclusions.

4. Techniques of Gas

Chromatography (*R.W. Beaver*).

Introduction. Resolution in Gas Chromatography. Extracolumn Resolution. Conclusions.

5. Emerging Techniques:

Immunoaffinity Chromatography

(*A.A.G. Candlish, W.H. Stimson*).

Introduction. Immunoaffinity Chromatography Theory. Practical Aspects and Instrumentation. Sample Preparation. Illustrative Examples.

6. Emerging Techniques:

Enzyme-Linked Immunosorbent Assay (ELISA) as Alternatives to Chromatographic Methods

(*C.M. Ward, A.P. Wilkinson, M.R.A.*

Morgan). Introduction. Principles of ELISA. Sample Preparation. Instrumentation and Practice.

Illustrative Examples. Conclusions.

PART B. APPLICATIONS.

7. Thin-Layer Chromatography of Mycotoxins

(*V. Betina*). Introduction. Aflatoxins. Sterigmatocystin and Related Compounds. Trichothecenes. Small Lactones. Macrocyclic Lactones. Ochratoxins. Rubratoxins. Hydroxyanthraquinones.

Epipolythiopiperazine-3,6-diones. Tremorgenic Mycotoxins. Alternaria Toxins. Citrinin. α -Cyclopiazonic Acid. PR Toxin and Roquefortine.



**ELSEVIER
SCIENCE** B.V.

Xanthomegnin, Viomellein and Vioxanthin. Naphtho- γ -pyrones. Secalonic Acids. TLC of Miscellaneous Toxins.

Multi-Mycotoxin TLC. TLC in Chemotaxonomic Studies of Toxigenic Fungi. Conclusions.

8. Liquid Column Chromatography of Mycotoxins

(*J.C. Frisvad, U. Thrane*).

Introduction. Column Chromatography. Mini-Column Chromatography. High Performance Liquid Chromatography. Informative On-line Detection Methods. Conclusions.

9. Gas Chromatography of Mycotoxins

(*P.M. Scott*).

Introduction. Trichothecenes. Zearalenone. Moniliformin. Alternaria Toxins. Slaframine and Swainsonine. Patulin. Penicillic Acid. Sterigmatocystin. Aflatoxins. Ergot Alkaloids. Miscellaneous Mycotoxins. Conclusions.

Subject Index.

1993 xiv + 440 pages

Price: US \$ 180.00 / Dfl. 315.00

ISBN 0-444-81521-X

ORDER INFORMATION

For USA and Canada
ELSEVIER SCIENCE INC.

P.O. Box 945
Madison Square Station
New York, NY 10160-0757
Fax: (212) 633 3880

In all other countries
ELSEVIER SCIENCE B.V.

P.O. Box 330
1000 AH Amsterdam
The Netherlands
Fax: (+31-20) 5862 845

US\$ prices are valid only for the USA & Canada and are subject to exchange rate fluctuations; in all other countries the Dutch guilder price (Dfl.) is definitive. Customers in the European Union should add the appropriate VAT rate applicable in their country to the price(s). Books are sent postfree if prepaid.

PUBLICATION SCHEDULE FOR THE 1995 SUBSCRIPTION

Journal of Chromatography A and *Journal of Chromatography B: Biomedical Applications*

MONTH	O 1994	N 1994	D 1994	J 1995	
Journal of Chromatography A	683/1 683/2 684/1	684/2 685/1 685/2 686/1	686/2 687/1 687/2 688/1 + 2	689/1 689/2 690/1 690/2	The publication schedule for further issues will be published later.
Bibliography Section					
Journal of Chromatography B: Biomedical Applications				663/1 663/2	

INFORMATION FOR AUTHORS

(Detailed *Instructions to Authors* were published in *J. Chromatogr. A*, Vol. 657, pp. 463–469. A free reprint can be obtained by application to the publisher, Elsevier Science B.V., P.O. Box 330, 1000 AH Amsterdam, Netherlands.)

Types of Contributions. The following types of papers are published: Regular research papers (full-length papers), Review articles, Short Communications and Discussions. Short Communications are usually descriptions of short investigations, or they can report minor technical improvements of previously published procedures; they reflect the same quality of research as full-length papers, but should preferably not exceed five printed pages. Discussions (one or two pages) should explain, amplify, correct or otherwise comment substantively upon an article recently published in the journal. For Review articles, see inside front cover under Submission of Papers.

Submission. Every paper must be accompanied by a letter from the senior author, stating that he/she is submitting the paper for publication in the *Journal of Chromatography A* or *B*.

Manuscripts. Manuscripts should be typed in **double spacing** on consecutively numbered pages of uniform size. The manuscript should be preceded by a sheet of manuscript paper carrying the title of the paper and the name and full postal address of the person to whom the proofs are to be sent. As a rule, papers should be divided into sections, headed by a caption (e.g., Abstract, Introduction, Experimental, Results, Discussion, etc.). All illustrations, photographs, tables, etc., should be on separate sheets.

Abstract. All articles should have an abstract of 50–100 words which clearly and briefly indicates what is new, different and significant. No references should be given.

Introduction. Every paper must have a concise introduction mentioning what has been done before on the topic described, and stating clearly what is new in the paper now submitted.

Experimental conditions should preferably be given on a *separate* sheet, headed "Conditions". These conditions will, if appropriate, be printed in a block, directly following the heading "Experimental".

Illustrations. The figures should be submitted in a form suitable for reproduction, drawn in Indian ink on drawing or tracing paper. Each illustration should have a caption, all the *captions* being typed (with double spacing) together on a *separate sheet*. If structures are given in the text, the original drawings should be provided. Coloured illustrations are reproduced at the author's expense, the cost being determined by the number of pages and by the number of colours needed. The written permission of the author and publisher must be obtained for the use of any figure already published. Its source must be indicated in the legend.

References. References should be numbered in the order in which they are cited in the text, and listed in numerical sequence on a separate sheet at the end of the article. Please check a recent issue for the layout of the reference list. Abbreviations for the titles of journals should follow the system used by *Chemical Abstracts*. Articles not yet published should be given as "in press" (journal should be specified), "submitted for publication" (journal should be specified), "in preparation" or "personal communication".

Vols. 1–651 of the *Journal of Chromatography*; *Journal of Chromatography, Biomedical Applications* and *Journal of Chromatography, Symposium Volumes* should be cited as *J. Chromatogr.* From Vol. 652 on, *Journal of Chromatography A* (incl. Symposium Volumes) should be cited as *J. Chromatogr. A* and *Journal of Chromatography B: Biomedical Applications* as *J. Chromatogr. B*.

Dispatch. Before sending the manuscript to the Editor please check that the envelope contains four copies of the paper complete with references, captions and figures. One of the sets of figures must be the originals suitable for direct reproduction. Please also ensure that permission to publish has been obtained from your institute.

Proofs. One set of proofs will be sent to the author to be carefully checked for printer's errors. Corrections must be restricted to instances in which the proof is at variance with the manuscript.

Reprints. Fifty reprints will be supplied free of charge. Additional reprints can be ordered by the authors. An order form containing price quotations will be sent to the authors together with the proofs of their article.

Advertisements. The Editors of the journal accept no responsibility for the contents of the advertisements. Advertisement rates are available on request. Advertising orders and enquiries can be sent to the Advertising Manager, Elsevier Science B.V., Advertising Department, P.O. Box 211, 1000 AE Amsterdam, Netherlands; Tel: 31 (20) 485 3796; Fax: 31 (20) 485 3810. Courier shipments to street address: Molenwerf 1, 1014 AG Amsterdam, Netherlands. *UK:* T.G. Scott & Son Ltd., Tim Blake, Portland House, 21 Narborough Road, Cosby, Leics. LE9 5TA, UK; Tel: (0116) 2750 521/2753 333; Fax: (0116) 2750 522. *USA and Canada:* Weston Media Associates, Daniel S. Lipner, P.O. Box 1110, Greens Farms, CT 06436-1110, USA; Tel: (203) 261 2500, Fax: (203) 261 0101.

1995 International Symposium & Exhibit on
PREPARATIVE CHROMATOGRAPHY

June 11-14, 1995
Washington, DC, USA

*Organized by Professor Georges Guiochon
University of Tennessee and Oak Ridge National Laboratory*

**LECTURE & POSTER PRESENTATIONS
WORKSHOPS
SEMINARS
ROUNDTABLE DISCUSSIONS
CASE STUDIES
INSTRUMENTATION EXHIBIT**

Sponsored by the Washington Chromatography Discussion Group

For more information contact: Janet Cunningham, c/o Barr Enterprises
P.O. Box 279, Walkersville, Maryland 21793 USA
(tele. 301-898-3772, fax 301-898-5596)



0021-9673(19950224)693:2;1-J